STATISTICAL MECHANICS OF HIGH DIMENSIONAL DYNAMICAL SYSTEMS

by

JÉRÔME LOSSON

Department of Physics
McGill University
Montréal, Québec, Canada

September 1994

A Thesis submitted to the
Faculty of Graduate Studies and Research
in partial fulfillment
of the requirements for the degree of
Doctor of Philosophy.

A mes parents

De même que par une seule boule d'argile on connait tout ce qui est fait d'argile, et que toute modification n'en est qu'un nom qui a la parole pour support, tandis que seul ce que l'on appelle argile *est réel; de même que par un seul morceau de cuivre on connait tout ce qui est fait de cuivre, et que toute modification n'en est qu'un nom qui a la parole pour support, tandis que seul ce que l'on appelle* cuivre *est réel;*
de même est ce *dont je te parle.*

Chandogya Upanishad

Abstract

The statistical properties of high dimensional dynamical systems modeled by coupled map lattices (CML's) and differential delay equations (DDE's) are considered in this thesis. First, the properties of the simplest lattices, containing only two elements are described. We highlight the presence of coupling induced statistical cycling. Similar phenomena observed in arbitrarily large (but finite) systems are explained by studying the Perron-Frobenius operator induced by deterministic nonsingular CML's using functions of bounded variation techniques. Analytic phase diagrams are given for coupled tent map lattices, when the coupling is either diffusive or global, as well as for a piecewise linear bimodal map. This approach is extended to permit a similar investigation of lattices perturbed stochastically, and we derive the transfer operators for these systems in the presence of additive and multiplicative noise. Various results concerning the spectral decomposition of these operators are proven. The formalism developed is then applied to coupled map lattices designed to approximate differential delay equations, both with and without noise. Continuous time statistical cycling at equilibrium is reported in these equations, and we describe the phenomenon of noise-induced cycling. The results on the Perron Frobenius and transfer operators induced by coupled maps are invoked to describe the statistical properties of delay equations analytically. Finally, the functional, continuous time transfer operator for these hereditary models is derived, and reduced, *via* functional expansions, to an infinite chain of integrable hyperbolic partial differential equations.

Résumé

Cette thèse porte sur les propriétés thermodynamiques (ou macroscopiques) de systèmes possèdant un nombre élevé de degrés de liberté. Les classes de modèles étudiées ici sont utilisées dans des champs de recherches qui vont de la théorie des réseaux neuronaux à l'optique nonlinéaire et à la dynamique des fluides, en passant par la description d'algorithmes de reconnaissance d'images et par la modélisation des fluctuations de certains marchés boursiers. Les opérateurs de transfert qui décrivent les évolutions d'ensembles statistiques pour certaines classes de treillis d'itérations nonlinéaires couplées sont définis, et l'on exploite le lien conceptuel entre leurs propriétés spectrales et la thermodynamique des treillis pour élaborer de façon rigoureuse une description thermodynamique de ces systèmes. Notre approche est basée sur l'utilisation des fonctions à variations bornées pour characteriser le spectre des opérateurs de Markov, et nous permet d'obtenir des diagrammes de phases exacts pour certains réseaux. Nous démontrons que les transitions de phases observées dans ces systèmes ont pour origines certains changements qualitatifs du spectre desdits opérateurs. L'influence de perturbations stochastiques dans de nombreux modèles est également étudiée analytiquement. Nous prouvons plusieurs théorèmes qui établissent que les opérateurs intégraux qui sont définis grâce à des noyaux aléatoires sont des opérateurs constrictifs. On démontre également que les opérateurs qui régissent le tranfert de probabilité dans les réseaux aléatoires sont définis grâce à de tels noyaux, et l'on déduit de cette analyse leurs propriétés spectrales, comme dans le cas déterministe. Ce formalisme, que nous développons en vue d'étudier des réseaux (qui ont une structure dans l'espace, par opposition aux modèles qui décrivent l'évolution d'un seul point dans le temps), est, et celà de manière surprenante, directement applicable à la description de systèmes qui possèdent une mémoire (sans avoir de structure spatiale). On introduit pour ces derniers un opérateur de transfert de dimension infinie, qui se réduit, grâce aux techniques de la théorie des perturbations fonctionelles à une chaine hierarchique d'équations différentielles partielles hyperboliques intégrables.

Acknowledgements

It is no easy task to express within the confines of a few lines my gratitude to Michael Mackey, my thesis supervisor, professor of physiology, physics, and mathematics. His scientific versatility, and the energy he spends training his students provide constant sources of inspiration. His willingness to let them follow their own leads, and develop their perpectives while providing encouraging support and critical advice make him the quintessential *mentor*. His teachings have extended far beyond the realm of scientific research, and I hope they will continue to do so.

I also would like to express my gratitude to Professor Abraham Boyarski for a series of fruitful conversations, as a result of which I undertook the work which forms most of Chapter 3. At about the same time, I benefited from several insightful comments from Professor David Ruelle whom I would like to thank for subsequently sending me a copy of J. Loviscach's thesis on related issues; it turned out to be most useful. Professor Frank Moss encouraged me to pursue the work on noise and DDE's and I am very thankful for the several weeks he spent in Montreal sharing his insights. In addition, Professor Marek Capiński provided critical comments and made important suggestions to improve the early versions of the work presented in Chapter 6. I would like to acknowledge Professor John Milton's collaboration, his kindness in providing unlimited access to his computing facilities, and his many invitations to go to conferences as well as a most enjoyable stay at the University of Chicago. I am indebted to John Outerbridge for his dedication to set up a transparent and efficient computer system which was not administered for his comfort, but for ours. More generally, I thank the faculty members at the Center for Nonlinear Dynamics, Professors Jacques Bélair, Anne Beuter, Leon Glass and Michael Guevarra, for sharing numerous insights at various stages of my research. I would also like to thank (now Professor) André Longtin, for getting me here in the first place, and for setting the standards.

I have had a wonderful experience with the members old and new of the Center for Nonlinear Dynamics and its many visitors. Danny Kaplan (now also Professor), Marc Courte-

manche, Ira Nechaeva and Hiro Ito made room 1125 a great place to imitate all sorts of accents, and I could have not hoped for a better environment to enjoy work in. The other students of the center, Arkady, Andrew, Claude, Kosta and Gil are all equally responsible for making the CNLD a fun place to be... Add the physiology crowd, Andrew and Misha, Paul, Brigitte and the molecular biology freaks Joan and Sherry and you start to get an idea of what the atmosphere was like on the eleventh floor of the McIntyre.

On the home front, I have found my strength in the constant encouragements of the friends without whom most of this would not mean much... they know who they are, and even though this is probably the only part of the thesis they will read (I don't blame them), I also wrote some of it for them. Last but not least, I want to thank my parents, to whom I dedicate the fruits of my efforts; Caroline, Thomas and Luca/Naomi for being there always, and Coleen for her sweet, sweet support.

I acknowledege the Fonds FCAR of the Government of Québec for financial support in the form of a post-graduate fellowship.

Contributions to Original Knowledge

The Faculty of Graduate Studies and Research of McGill University requires that all Ph.D. theses contain an explicit list of original contributions included in the thesis. With the exception of the introductory chapter, most of the material presented in this thesis is original. We therefore list the specific contributions by chapter.

Chapter 2:

1. First published report of coupling induced statistical cycling in two-dimensional maps.
2. The derivation of the two-dimensional Perron-Frobenius operator for coupled logistic maps has not been published elsewhere.
3. First published analytic phase diagrams for coupled tent maps. The geometrical methods of Sections 2.3 are all novel.

Most of this material has appeared in

• J. Losson and M.C. Mackey, "Coupling induced statistical cycling in two coupled maps", *Physica D* **72**:324-342 (1994)

Chapter 3:

1. This chapter contains the first extensive numerical investigations of asymptotic periodicity in coupled map lattices.
2. Section 3.3 introduces and describes a new biologically motivated model, which is relevant to the description of N species competing for shared resources.
3. This chapter contains the first analytic description of locally coupled CML's, which includes the proof of the existence of phase transitions, and the sufficient conditions for their presence at a location of parameter space (in the case of various piecewise linear map lattices).

4. The phase diagrams of Sections 3.5 and 3.6 are the first such diagrams analytically obtained for any large coupled map lattice.

5. The calculation of the quantity $\sin\theta(\tilde{\pi})$ for nonrectangular partition is given explicitly for the first time.

Most of this material has appeared (or will appear) in

• J. Losson and M.C. Mackey, "Statistical cycling in coupled map lattices", *Physical Review E* **50**:843-856 (1994)

• J. Losson and J.G. Milton and M.C. Mackey, "Phase transitions in networks of chaotic elements with short and long range interactions", *Physica D* (in press)

Chapter 4:

1. All numerical observations concerning the influence of noise on the CML's described in Section 4.3 are original.

2. The transfer operator for CML's perturbed by multiplicative noise is derived for the first time.

3. The spectral properties of the transfer operator in the presence of additive and multiplicative perturbations are described for the first time.

4. Explicit conditions on the local dynamics and on the characteristics of the noise which guarantee asymptotic periodicity in stochastic CML's are given. These conditions are surprisingly mild.

Most of this material has been submitted as

• J. Losson and M.C. Mackey, "The evolution of probability densities in stochastic coupled map lattices", submitted *Physical Review E* (July 1994).

Chapter 5:

1. We derive an approximation scheme for a class of differential delay equations which is framed as a coupled map lattice, in both the deterministic, and the stochastic case (when the noise is δ-correlated).

2. Continuous time statistical cycling is described numerically for the first time in a deterministic delay differential equation.

3. Noise-induced statistical cycling in a DDE is also discovered.

4. The CML approximation is used to analytically understand (in both the stochastic case and the deterministic one), the origin of this statistical cycling behavior. For an equation with a piecewise linear forcing term, we can give exact conditions on the parameters which guarantee asymptotic periodicity in the CML approximation of the DDE.

Most of this material has been submitted as

• J. Losson and M.C. Mackey, "Coupled map lattices as models of delay differential equations", submitted to *Physical Review E* (August 1994).

Chapter 6:

1. The two-interval generating functional $\mathcal{Z}_t$ for deterministic DDE's is introduced.
2. The evolution equation for this functional is derived, and reduced, using perturbation theory, to a set of hyperbolic PDE's for the moments.
3. Necessary conditions satisfied by the invariant functional measures generated by DDE's are given.
4. The connection between the evolution equation for $\mathcal{Z}_t$ and the functional version of the Kramers-Moyal equation is explicitly described.

Most of this material has appeared in

• J. Losson and M.C. Mackey, "A Hopf-like equation and perturbation theory for delay differential equations", *Journal of Statistical Physics* **69**:1025-1046 (1992).

Contents

List of figures

List of Tables

Chapter 1

Introduction

Choses rares ou choses belles,
Ici patiemment assemblées
Instruisent l'oeil à regarder
Comme jamais encore vues
Toutes choses qui sont au monde.

Paul Valéry, *Inscription, Musée de L'Homme*

One of the great inventions of modern physical thought is the point particle. This theoretical construct allows the investigator to discard all internal structures of a system, and focus exclusively on the few degrees of freedom which evolve in time under the action of external stimuli. This mechanistic approach is justified in some areas of research (celestial mechanics comes to mind), but it fails to bear fruit when the systems under consideration possess a nontrivial internal structure, so their global evolution is due to external stimuli as well as nontrivial interactions between some parts of the whole.

Systems which possess internal structure are ubiquitous in nature. In fact, it is arguable that *all* physical entities possess internal structure (with the possible exception of some elementary particles). Depending on the situation under consideration, this structure can be thought of as being continuous, in which case the appropriate mathematical models are usually framed as partial differential equations (PDE's), or it can be discrete in which case one views the system as a "network" of connected elements. The evolution of such networks is typically described mathematically by coupled ordinary differential equations (if time is continuous), or by coupled iterative maps (if time is discrete). Our work focuses on the macroscopic properties of the latter.

The term "macroscopic", is used to denote those properties which are the result of interaction between the constitutive parts, and which are devoid of meaning when one describes the dynamics of a single element, though they must generally depend on the dynamics of the element. For example, the brain is a collection of anatomically distinct regions, each of which is a large collection of neurons, each of which is made of molecules, made of atoms, made of the elementary constituents of matter. Depending on which property of brain function is considered, the appropriate structure must be studied. The issue of whether the function at one level of organization (*eg.* the recognition of visual inputs, resulting from the joint operation of the visual cortex with other centers associated with memory) can be understood from investigations of a different level (*eg.* the organization of atoms in the molecules which make-up all neural tissue) is beyond the scope of our presentation, and will undoubtedly remain the subject of intense debate for many generations to come. However, it is clear that a single atom does not recognize a face, and at some level, function results from interaction.

Describing "systems with internal structure" is a rather vague research program. We restrict our attention more specifically to systems which are networks of chaotic, interacting elements, whose evolution in time is discrete. Such systems can be profitably modeled by networks of coupled iterative maps, usually referred to as coupled map lattices (CML's for short). The research in this thesis uses novel analytical techniques to investigate the statistical properties of CML's, and discusses their thermodynamic behavior.

The description of CML's has been the subject of intense scrutiny in the past decade, and most (though by no means *all*) investigations have been primarily numerical rather than analytical. Investigators have often been concerned with the statistical properties of CML's, because a deterministic description of the motion of all the individual elements of the lattice is either out of reach or uninteresting, unless the behavior can somehow be described with a few degrees of freedom. However there is still no consistent framework, analogous to equilibrium statistical mechanics, within which one can describe the probabilistic properties of CML's possessing a large but finite number of elements. For analytic insight, one is usually forced to reduce the model to a small lattice (as is done in Chapter 2 and the references cited therein, for example), or take the so-called thermodynamic limit in which the number of elements goes to infinity. As explained in Section 1.4.4, the thermodynamic limit is a useful conceptual tool of statistical mechanics when the systems under study possess simple local dynamics. It is often unnecessary when the models possess locally chaotic elements. More generally, the framework of classical statistical mechanics is not entirely appropriate

for the description of the probabilistic behavior of dissipative dynamical systems, and in this thesis we use some of the techniques developped in ergodic theory to describe dissipative systems in the spirit of statistical mechanics.

1.1 Coupled map lattices: Initial presentation

Models framed as coupled discrete time maps are not a novelty. Caianiello [23] proposed his "neuronic equations", which are coupled iterative maps, as generalizations of the McCulloch and Pitts neural networks more than three decades ago. Similarly, the work of Denman [45], trying to characterize the dynamics of interacting pressure and electromagnetic waves in plasmas, made use of coupled discrete maps, and related models were used in the early theory of transmission lines [179]. However, the modern body of work dealing with coupled map lattices can be traced back to the beginning of the eighties (*cf.* work by Kaneko [95], Waller and Kapral [214, 215] and Deissler [43]) as phenomenological models to study the behavior of large collections of coupled chaotic elements (we will come back below on more precise descriptions of these and more recent investigations of CML dynamics).

In their most general form, deterministic coupled map lattices are mappings $\Phi : \mathbb{R}^N \longmapsto \mathbb{R}^N$ governing the evolution of a state vector $\mathbf{x}_t$,

$$\mathbf{x}_{t+1} = \Phi(\mathbf{x}_t) \quad t = 0, 1, \cdots. \tag{1.1}$$

More specifically, the evolution of a component $x_t^{(i)}$ of the state vector $\mathbf{x}_t$ is governed by the difference equation

$$x_{t+1}^{(i)} = \Phi_{\text{local}}^{(i)}(x_t^{(i)}) + \Phi_{\text{neighbours}}^{(i)}(\cdots, x_t^{i-1}, x_t^{i+1}, \cdots)$$

where $\Phi_{\text{local}}^{(i)}$ models the local dynamics at site i, and $\Phi_{\text{neighbours}}^{(i)}$ denotes the mechanisms acting on i from a specified neighbourhood. If those mechanisms are the same for all sites on the lattice, and if they are locally modeled by the map $S : \mathbb{R} \longmapsto \mathbb{R}$, and in the neighbourhood by the map $T : \mathbb{R} \longmapsto \mathbb{R}$ one can write

$$x_{t+1}^{(i)} = S(x_t^{(i)}) + \sum_{\substack{\text{some} \\ \text{neighbourhood}}} T(x_t^j).$$

In many situations of interest, it is possible to further simplify the formulation of the models

by letting $T \equiv S$, and using a linear coupling scheme between the elements[1]. In these circumstances, we have

$$x_{t+1}^{(i)} = (1-\varepsilon)S(x_t^{(i)}) + \frac{\varepsilon}{p} \sum_{\substack{p \\ \text{neighbours}}} S(x_t^j) \tag{1.2}$$

where $\varepsilon \in [0,1]$ is the coupling term. Again, i denotes a discrete space index (of arbitrary finite dimension), and t denotes discrete time.

In our description of CML's, we view the sites of the lattice as being located on the nodes of a regular body centered cubic lattice, and we will always assume periodic boundary conditions, except where the contrary is stated explicitly (as in Chapter 5 for example). There are investigations of coupled map lattices in which the underlying lattice is not as simple as the body-centered-cubic example chosen here, and possesses intrinsically "complex" (sometimes called hierarchical) structure. In these cases, it was demonstrated [39, 40] that the bifurcation structure of the CML can depend on the topology of the lattice, but we will not dwell on this point, since most of the analytical tools introduced in this thesis do not depend on the properties of the underlying lattice topology. Finally, we will discuss in Chapters 4 and 6 the properties of systems of the form (1.2) which are perturbed by noise, but the formal presentation of stochastic CML's is delayed until then.

The developments which followed the introduction of CML's have established the usefulness of these models to investigate the dynamics of a wide variety of systems in various areas of research ranging from population dynamics to solid state physics. Our own research was motivated in part by this flurry of activity, and we therefore review the literature briefly before proceeding to a description of CML thermodynamics.

1.2 Overview of models framed as CML's

Two collections of papers on the subject, both edited by K. Kaneko [94, 50] are available. Some of the material discussed in the present section is taken from these collections, but we also mention many of the more recent published works on coupled map lattice dynamics.

[1]The coupling scheme of equation (1.2) is called *linear* because $x_{t+1}^{(i)}$ is linearly proportional to $S(x_t^{(i)})$. Some authors [103] would call such architectures nonlinear, but we will adhere to this convention for reasons which will be clear in Chapter 3.

1.2.1 Biological applications

There are many biological systems which can be thought of as collections of interacting elements with intrinsic nontrivial dynamics. When this is case, and if the local dynamics can reasonnably be modeled by discrete time maps, it is feasible to introduce models framed as CML's.

This approach has been fruitful in population dynamics, in which the discrete time occurs naturally if generations do not overlap (insect populations are possible examples). The investigations of Solé *et al.* [198, 199] have led these authors to conclude that CML's provided the simplest models for discrete ecological models. Franke and Yakubu [58] have recently proposed a CML to investigate the inter-species competition of large bird population which we consider in more detail in Chapter 3. These CML's are crude models for the evolution of species competing for shared resources, which are obtained by straightforward (albeit not very realistic) multidimensional generalizations of proposed one-dimensional maps [153, 209]. They open the way for more realistic population competition models which could be framed as CML's in which the underlying lattice is not regular, perhaps taking into account some of the spatial features observed in the field. Cosenza and Kapral [39, 40] showed that complex spatial architectures can have a nontrivial influence on the bifurcation structures of the CML. Ikegami and Kaneko [102] have also proposed a model for host-parasitoid networks, and their study of the corresponding CML have led them to introduce a generalization of the idea of homeostasis. The proposed alternative, "homeochaos" describes an asymptotic state reached by networks of evolving and mutating host-parasitoid populations in which chaotic fluctuations in the numbers of hosts and parasitoids are observed at equilibrium.

Beyond population dynamics, the mathematical description of neural behavior has also benefited from discrete time, discrete space models. The foundations of the modeling of cortical function were laid in two seminal papers by Wilson and Cowan [218, 219]. However, the original models presented by these authors are computationally costly, and are not easily amenable to analytic investigations. As a result, there have been attempts to reduce the original networks of integro-differential equations to simpler spatially extended models. Reduction to CML's are presently being considered by some of the same authors [151]. In its methodology, this work [*ibid*] is typical of investigations in which the CML is proposed as a discrete-time version of previously considered continuous-time systems. For example, Molgedey *et al.* [155] made use of coupled map lattices to examine the effects of noise on spatiotemporal chaotic behavior in a neural network which was originally proposed (in its

continuous-time version) by Sompolinsky *et al.* [200]. Following a similar path, Nozawa [161] has presented a CML model, obtained by using the Euler approximation in the original Hopfield equations.

One of the outstanding problems motivating this neural oriented research is the identification of organizing principles to explain the synchronization of large populations of neurons possessing individually complex dynamics. Such synchronizations are thought to take place in pathological situations (*eg.* epileptic seizures) as well as in the normal brain. For example, Andersen and Andersson [4], and later Steriade and Deschênes [201] have hypothesized that such a synchronized activity of the reticular thalamic nucleus (RTN) acted as a pacemaker for the so-called "spindle oscillations" observed during various sleep stages. Models of the RTN framed as networks of coupled differential delay equations have been proposed by Destexhe [46], and these can be reduced, by a straightforward singular perturbation procedure [88], to CML's. Models of the RTN framed as coupled ODE's have also been considered recently, and provide a motivation for the theoretical description of globally coupled arrays of oscillators [65]. An interesting review of the mathematical description of cortical behavior in terms of coupled nonlinear units is given in [221]. A less recent, but somewhat broader view of the contemporary efforts to mathematically describe the behavior of neural networks using the conceptual tools of nonlinear dynamics is presented in [191]. For the sake of completeness, we also refer the reader to the review by Herz [77], which describes some of the earlier neural modeling attempts which made use of CML's, as well as some of the models based on delay differential equations.

At the molecular level, Cocho *et al.* [34] proposed a CML model to describe the evolution of genetic sequences. A comprehensive account of the development of this idea can be found in [35]. In this simplified formalism, each genetic sequence is made up of m nucleotides, which come in four flavors. The latter is determined by which of four possible bases (guanine, cytosine, adenine, thymine) complements the phosphate and deoxyribose groups which make-up the nucleotide. The building block of a genetic sequence is then a triplet of nucleotides, called a codon (which codes for an amino acid). Cocho *et al.* established that for certain viruses, it is relevant to restrict attention to sequences containing only two types of codons, denoted type I and II. Hence a sequence of length $L = m/3$ codons is uniquely characterized by the number i_I of type I codons it possesses. i_I can also be thought of as a position index in a configuration space, and in this case two sequences are "close" if they differ by a small number of codons. Under specified fitness constraints (whose meaningful definition

imposes the most important limits on this approach), sequences can mutate: a type I codon becomes type II, or *vice-versa.* The CML model for genetic sequence evolution describes the evolution of the number of sequences at location i_I in the configuration space, and therefore, local interactions are due to mutations, whereas ecological constraints (*i.e* coming from limited food supplies) generate long range coupling. Recently [36], the same authors have extended this approach to study the mutations of the HIV1 AIDS virus, and their predictions concerning the regularity of the chemical compositions of this virus' RNA sequences agree with statistical analyses of gene data banks.

The use of CML's, though interesting from the mathematical biologist's point of view, is not restricted to biological models. Contemporary developments in the theory of image processing have led to the introduction of various algorithms which are in fact coupled map lattices.

1.2.2 Image processing applications

One of the basic challenges in image processing is the so-called "shape from shading" problem [20], which surfaces both in computer graphics, where shading is used to enhance realism, and computer vision, where the study of shading is crucial for the proper interpretation of a pattern's two dimensional projection (its picture). In computer vision, a typical task is the classification of patterns into classes (*eg.* faces *vs.* landscapes), where the input patterns possess underlying "shapes" describing their essential features (nose, eyes, *vs.* trees or clouds) which are immersed in secondary information due to the shading of the image.

Several approaches to this problem [20, 204, 210] make use of algorithms which are coupled map lattices, although there are no explicit acknowledgements in this literature of the link between the structure of the algorithms and their formulation as CML's. We illustrate this link with a frequently encountered model used to approach shape from shading, which was introduced by Brooks and Horn and is known as the B-H algorithm [19]. To derive the model, the shape of an object is thought of as a function which minimizes a given functional. After minimization of the proper errors [210], the B-H algorithm is written

$$x_{t+1}^{(ij)} = \bar{x}_t^{(ij)} + \frac{\varepsilon^2}{4\lambda}\left(E^{(ij)} - x_t^{(ij)} \cdot \mathbf{S}\right)\mathbf{S} \tag{1.3}$$

where $E^{(ij)}$ is the shading, $x_t^{(ij)}$ is the surface normal at site (i,j) of the image, λ and ε describe the role of a smoothness constraint, and $\mathbf{S}$ is the light source vector (the light

source being responsible for the presence of shade), and $\bar{x}_t^{(ij)}$ is the average of the normals in a neighbourhood of site (i, j). The local coupling comes from this latter term, and as a result, the evolution of the initial image under the action of the B-H shade from shading algorithm is akin to the evolution of an initial vector under the action of a CML. There are more recent descriptions of this problem which do not make use of the variational techniques used to derive (1.3), and which lead to different CML's (one example is given in [210]).

The treatment of fuzzy images is not limited to the shape from shading problem. In fact, prior to this analysis, "dirty" images, possibly obtained with remote sensing equipment must be "cleaned". This procedure, known as the segmentation of an image, is an attempt t0 highlight edges while smoothing the noise in regions devoid of edges. A "physicist-friendly" presentation of the segmentation problem is given by Price *et al.* [171]. They introduce a coupled map lattice designed as an alternative to the costlier and more unstable segmentation algorithms obtained by the minimization of a cost function. Their work is an additional illustration of the potential benefits to the image-processing community which could follow from an increased awareness of the wealth of dynamics displayed by high-dimensional nonlinear discrete time maps: the stability properties of the algorithms, and their possible pathological treatments of real images can often be determined beforehand by an indepth investigation of the corresponding CML.

At a more formal level, CML's are also encountered by computer scientists interested in computation theory. The CML's presented in Section 1.1 are discrete time, discrete space continuous state dynamical systems. In that sense, they are a generalization of digital computers which are discrete in all three respects.

The results presented by Price *et al.* [78] indicate that CML's considered as parallel deterministic computers probably cannot perform computations which cannot be performed by digital computers. However, it is likely that task specific analogue computers modelled accurately by CML's will be more *efficient* than digital computers in solving various classes of problems (such examples could result from the hardware implementation of the image processing algorithms discussed above using analogue rather than digital chips).

In spite of the obvious interest generated by CML's for their many potential applications, the main motivation for their investigation from a physicist's point of view undoubtedly lies in their use as phenomenological models for the study of more general spatially extended systems

1.3 Phenomenological models framed as CML's

The modern body of theoretical and experimental work on the behavior of low dimensional chaotic dynamical systems goes back to the classical paper of Lorenz [130], which describes the reduction of the Navier-Stokes equation to a now famous system of three coupled ordinary differential equations. The rationale for this work was to gain insight into the mechanisms which underly the development of turbulence in fluids. This endeavor is ongoing, and although some progress has been made since the early work of Lorenz, a complete understanding of the fully developped turbulent regime is still lacking. The traditional description of turbulence, known as the Landau interpretation, views fully turbulent motion as resulting from the superposition of infinitely many periodic modes of incommensurate frequencies. This superposition of modes provides one mechanism for the observed complexity, but it fails to explain the mixing behavior typically associated with fluid turbulence. Furthermore, the intuitive notion underlying Landau's description, that complexity is a consequence of the interactions between many degrees of freedom, has been shattered by the developments of nonlinear dynamics since Lorenz' work. It is now clearly established that a single degree of freedom, if it evolves according to a discrete time nonlinear law can possess unpredictable complex behavior: it can display deterministic chaos [190]. The introduction by Ruelle and Takens [186, 185, 184] of nonlinear dynamical systems to describe fluid turbulence also provides mechanisms for the observed mixing which cannot be dealt with in the Landau picture (we will come back to this point in Section 1.4.5).

The link between low dimensional deterministic chaotic dynamical systems and fluid dynamics is well documented, both theoretically and experimentally [147], and it provides a useful framework for the description of various non-turbulent regimes [110, 190]. In order to extend the understanding of more irregular fluid motion, coupled map lattices were proposed as natural extensions to low dimensional nonlinear models.

1.3.1 Spatiotemporal intermittency and weak turbulence

An example of the fruitful application of CML's to study fluid dynamics is given by the work of Chaté and Manneville, concerning the transition to turbulence *via* spatio-temporal intermittency [27, 28]. In this work, the CML's are constructed to reflect what are thought to be the essential features of a fluid undergoing the transition from laminar flow to turbulent flow *via* the so-called intermittency scenario, according to which a laminar flow gradually

becomes turbulent by the growth of regions in the laminar regime in which the flow is turbulent. Hence, the essential features of the Chaté-Manneville models are the partition of the local phase space into two regimes: one laminar, and the other turbulent. Their analysis of the corresponding CML's lead to the identification of universality classes describing the "contamination process" of the laminar flows by turbulent "islands" [27, 29, 28]. The usefulness of the CML approach is that these models capture much of the phenomenology while remaining amenable to extensive numerical simulations.

The destabilization of laminar flows does not always occur *via* spatiotemporal intermittency. Various convective instabilities can result in alternate destabilizing mechanisms, and some of the recent work on CML's focuses on the dynamics of these instabilities in so-called "open flow" models [44]. Convective instabilities grow as they are transported downstream, and they are localized in the sense that a laboratory observer sees them pass by from upstream to downstream as localized defects [147]. Such situations are encountered, for example, in the modeling of shear flows and boundary layers, and they provide situations in which spatial order can be coexistent with temporal chaos. Given the complexity of the full equations of motion, it has been helpful to consider reduced models framed as CML's. In [12], Biferale *et al.* describe the convective instabilities of a unidirectionally coupled CML by focusing on the tangent vector associated with a trajectory of the CML. This analysis could not have been carried out on the original PDE's governing the fluid motion, and it resulted in a relatively simple description of the localization of temporal chaos around the defects of the lattice. Other descriptions of asymmetrically coupled CML's include the works of Jensen [92, 91], Aranson *et al.* [5], and Willeboordse [217]. In all these, the coupling between the elements of the CML is not isotropic, and there is a preferred spatial direction in the lattice along which information is more easily transmitted. In Chapter 5 we will explore the dynamics of such a CML, introduced as a model for a class of differential delay equations.

In addition to these fluid-dynamical motivations, the quest for organizing principles of morphogenesis has led to the use of CML models to investigate the appearance of macroscopic patterns in spatially extended systems. It is not possible to give an exhaustive review of the vast literature dealing with the problem of classifying and understanding the development of patterns in nonlinear spatially extended models. This problem arises in fields of research as varied as mathematical biology (for extensive reviews, consult [159, 220]), chemical engineering [103], and the dynamics of diffusion limited aggregation [211]. Cross and Hohenberg give an authoritative review of this literature related to physical applications

in [41]. The specific applications of CML's to the discussion of macroscopic pattern formation have mostly focused on models of reaction diffusion systems, and on models of globally coupled elements.

1.3.2 Reaction diffusion models

Reaction-diffusion models play an important role in the description of real spatially extended systems because the competition between these two general mechanisms is ubiquitous in nature. In one dimension, they are modeled by the generic PDE

$$\frac{du(x,t)}{dt} = D\nabla^2 u(x,t) + F(u(x,t)), \tag{1.4}$$

where F is the reaction term. In a seminal work, Turing [207] established that this competition was at the origin of many pattern-forming instabilities. Reaction diffusion systems have been the subject of many descriptions in terms of CML's because diffusion is approximated by a nearest neighbour coupling in CML's of the form (1.2) (examples of this reduction are given by Puri *et al.* [175] for the one dimensional Cahn-Hilliard equation, and by some of the same authors for the Fischer equation [163]). We note that the reduction of models framed as PDE's to their CML counterparts is usually not a rigorous procedure, although there are special circumstances (for some externally forced models) in which the CML provides a close approximation to the PDE [107]. As mentioned in [127], the benefits of using CML's in the majority of investigations stem from the fact that they reproduce most of the interesting phenomenology, without requiring the prohibitively large computing resources associated with PDE simulations. In addition, it is likely that as those resources increase with technological breakthroughs, so will the complexity of the problems considered by the modeling community, so that there is some intrinsic virtue in trying to understand reduced systems, such as CML's, to help in the study of more complicated ones.

Because of their computational efficiency, CML's are well-suited for the introduction of new quantifiers of spatiotemporal dynamics, or for the multidimensional generalizations of one-dimensional concepts [205] (this was an important motivation for the early discussions [43, 214, 215]). In this spirit, Kaneko has introduced such concepts as the "comoving mutual information flow" [96], and various "pattern entropies" and "pattern distribution functions" [97], to mention a few of the frequently encountered statistical descriptors of the motion. Reaction diffusion CML's are then usually of the form (1.2) with $p = 2$ in one spatial

dimension, or $p = 4$ in two dimensions, and used to explore in great detail the behavior of the quantifiers of spatio-temporal motion more efficiently than if PDE's were considered.

Similar lattices have been used to simulate interfacial phenomena in reaction diffusion systems [127]. In these investigations, the CML's usually arise from the phenomenological simplification of PDE's of the form (1.4), and they provide the simplest models which retain the disparate length and time scales necessary for the appearance of rich interfacial dynamics. Other typical examples of this approach are given for crystal growth by Oono and Puri [162] and for chemical waves by Barkley [7]. A phenomenological description of interfacial phenomena was recently given by Kapral *et al.* [105], using a piecewise linear CML (with a branch with slope zero in the local map) which displays some of the interfacial structures associated with continuous time, continuous space models. In a similar spirit, the behavior of liquids at the boiling transition was studied by Yanagita [223] with another reaction-diffusion CML. To conclude, we refer the intertested reader to the comprehensive review of the applications of CML's to capture the essential features of pattern formation in chemically reacting systems given by Kapral in [103]

1.3.3 Arrays of globally coupled oscillators

In this section, we do not give an extensive review of the burgeoning literature dealing with the behavior of globally coupled oscillators. We focus instead on those works which have made profitable use of phenomenological models framed as CML's.

The introduction of all-to-all (or mean-field, or global) coupling in theoretical physics to investigate the dynamics of spatially extended systems is not novel; it has always been one of the standard techniques used to describe the magnetic properties of spin systems. As experimentalists probe ever deeper into the behavior of systems with a large number of degrees of freedom, new models of globally coupled oscillator arrays are introduced, in which the individual oscillators are either continuous or discrete in time. Some of the experimental situations in which global coupling arises naturally are related to nonlinear optics, with examples ranging from solid-state laser arrays [225], to multimode lasers [90]. In electronics, a number of experiments on Josephson junction arrays coupled in series or in parallel have indicated the presence of very rich dynamics, often related to the multiplicity of attractors, or the linear stability properties of fully synchronized states (*cf.* [160] and references therein). The majority of models proposed to describe these dynamics are framed as globally coupled sets of ordinary differential equations [73, 194, 202]. The ODE's are usually not rigorously re-

duced to CML's, and the introduction of the discrete-time map lattices is often motivated by the desire to improve the phenomenological insight into the evolution of the continuous-time oscillators. For example, Wiesenfeld and Hadley [216] found that CML's provided useful reduced systems to investigate the effects of low levels of noise on large globally coupled arrays which possess an even larger number of attractors. More recently, discrete maps were used to describe the dynamical properties of periodic attractors in arrays of $p-n$ diode junctions [54], and the stability regions of various solution types for the CML's agreed qualitatively with the experimental data obtained from two coupled diode junctions. We close this admittedly incomplete presentation of some contemporary discussions of global coupling in the physical sciences, by mentioning that CML's have recently been used to study theoretically the remarkable phenomenon of mutually destructive fluctuations in which the activity of the mean field is observed to have a much *smaller* variance than the individual trajectories [160]. This phenomenon is extremely interesting for researchers trying to understand the role of noise in the transmission of information in spatially extended processing systems. For example, it is well known that the behavior of individual neurons can sometimes be more erratic than that of the average behavior of a population of neurons [152]. This leads us to the description of all-to-all coupling in biological networks.

Global coupling arises in the description of certain populations of insects [154], and in the modeling of neural activity. In this last field of investigation, global coupling is the simplest approximation to the highly complex inter-neuronal coupling which is anatomically observed. As an example, globally coupled ODE's have been introduced to model the clustering behavior of a population of inhibitory neurons [65]. Although this model is not framed as a CML, our investigation of excitable CML's with long range inhibitory coupling (*cf.* Chapter 3) confirms the qualitative description of the behavior which is given in [65].

1.3.4 Additional comments on CML phenomenology

To conclude this introduction, we briefly review other works whose themes do not neatly fall into the various sections enumerated above. Most report novel behavior which extends the zoology of spatiotemporal dynamics, therefore posing interesting theoretical problems.

Crutchfield and Kaneko [42], Politi *et al.* [168] have reported the counterintuitive presence of long-lived erratic behavior, observed even when the Lyapunov exponents in the system are negative. Although the exact dependence of the transient length on the system size was initially misunderstood (and thought to grow hyperexponentially with system size),

this phenomenon is interesting because it highlights the importance of transient behavior in spatially extended dynamical systems in which nonlinearities play an important role. The question of transient length in CML's has also been discussed in papers by Qu and Hu [176] and more recently by Kapral *et al.* [105].

Qu and Hu [*ibid*] also discuss the bifurcation structure in locally coupled lattices, and their description of CML's brings us to a broad class of investigations which tend to focus on the identification in these spatially extended models of behaviors which are well-understood in lower dimensional chaotic systems. Another example is the discussion of the extreme dependence on both parameters and initial conditions in spatio-temporal systems given by Lai and Winslow [119], which generalizes to high dimensions previous descriptions of similar behavior in low dimensional models [57, 69]. A third example is the theoretical description of universal behavior in the bifurcation structure of a large class of CML's, given by Kook *et al.* [114], using renormalization group transformations to obtain the scaling exponents of the period-doubling cascade. This work, and similar studies due to Alstrøm and Stassinopoulos [2] and Kuznetsov [115, 116, 118] are a first step towards a classification of universality classes in spatiotemporal phenomena, and they complement the strong numerical evidence for parameter scaling in the bifurcation diagram of various lattices of coupled maps [49, 106, 92]. The investigations of the possible presence of universality classes in the behavior of CML's is largely motivated by the desire to classify the various scenarios which are followed by spatially extended systems bifurcating from synchronized states to spatio-temporally chaotic ones. The work of Chaté and Manneville, mentioned previously, was partly inspired by a desire to verify a conjecture of Pomeau's that the spatio-temporal intermittency transition in fluids was in the same universality class as the directed percolation transition. Extensive numerical studies of CML's lead to the contrary conclusion.

Sometimes, the investigation of CML's can also point the way to the misunderstanding of results of a fundamental nature. For example, observations of the coherent behavior of globally coupled and some locally coupled CML's reported by Kaneko [99, 101], Perez *et al.* [164], and Chaté and Maneville [31] have led to a controversy in the recent literature concerning an apparent violation of the law of large numbers in these models. Recently, Pikovsky and Kurths [165] have given a partial explanation of the phenomenon, although these considerations are not well grounded theoretically, because they do not make use of the proper tools to describe the evolution of thermodynamic ensembles of CML's. We come back to this discussion in Section 1.4.5.1, which illustrates that considering simple models

(CML's) can go a long way towards the consistent extension of classical results, *e.g.* the law of large numbers, to the study of previously exotic situations (modeled by high dimensional nonlinear dynamical systems for example).

The ongoing discussion of the violation of the law of large numbers is resolved by a careful consideration of the statistical mechanics of coupled map lattices. Until now, there have been only a few attempts at a systematic construction of this formalism for high dimensional chaotic dynamical systems. These investigations follow two broad and intersecting paths: One is the extension of the so-called *thermodynamic formalism* of Ruelle [183], Bowen [16] and Sinai [195], and has led to various proofs of existence for Gibbs measures describing spatiotemporal chaos [21, 22, 72] in hyperbolic systems. This approach rests on the symbolic representation of dynamical systems, and will be briefly described in Section 1.4.4.3. The other path is the one we follow, and it rests on the study of so-called transfer operators. It was pioneered by Keller and Künzle [109], Gorá and Boyarski [66], and it is powerful for the investigation of finite (but high) dimensional dynamical systems.

Our work complements these presentations, and we will, in the next section, discuss exactly what is meant by "the thermodynamics of chaotic systems".

1.4 Statistical mechanics of dynamical systems

In the first part of this section, we consider the thermodynamics of crystals, and briefly describe the theoretical steps which lead to the expressions for experimentally measurable thermodynamic quantities. This schematic presentation is helpful to introduce the statistical mechanics of dynamical systems.

1.4.1 The thermodynamics of crystals: A brief digression

The purpose of this short digression is to introduce in a natural fashion a description of dynamical systems which is analogous to the description of materials given by classical statistical mechanics. We consider silicates because for these minerals, small amplitude motions are well-described by phonons (*cf.* the collection of articles in [189]), but we could have equally well discussed oscillations of magnetic moment in certain magnetic materials using magnons or spin waves. Our presentation is based on a paper by Price and Parker [171], in which the thermodynamics of silicates are examined by focusing on the vibrational properties of the atomic lattice. No claim is made here concerning the validity of this

approach, and we concentrate on the methodology of the presentation, rather than the relation between the ensuing results and experimental evidence.

First, it is necessary to determine the free energy of the material. In silicates, as in many other minerals, it is "stored" partly in the phonons, the quantum vibrational modes of the atomic lattice. We now briefly illustrate how a given material is characterized, in this picture, by the distribution $\mathbf{f}(\omega)$ of these phonons.

For the purpose of our discussion, a phonon is essentially a quantum harmonic oscillator, and the mineral is therefore thought to be a regular lattice whose normal modes of oscillation are described by a collection of phonons. As is well-known [61], the energy of a linear harmonic oscillator can assume the values

$$E_z = \left(z + \frac{1}{2}\right)\hbar\omega, \quad z = 0, 1, 2, \cdots.$$

From maximal entropy principles, it is straightforward to show [142] (see also the more traditional presentation given by Cochran [37]) that at equilibrium, the probability that a harmonic oscillator has energy E_z is given by

$$p(E_z) = \frac{e^{-E_z/kT}}{\sum_{i=0}^{\infty} e^{-E_i/kT}}$$

so that the mean energy is

$$\langle E \rangle = \sum_{z=0}^{\infty} E_z p(E_z).$$

Recalling the identities

$$\sum_{k=0}^{\infty} e^{-kx} = (1 - e^{-x})^{-1} \quad \text{and} \quad \sum_{k=0}^{\infty} k e^{-kx} = e^x (e^x - 1)^{-2},$$

the mean energy is of s single mode is shown to be

$$\langle E \rangle = \hbar\omega \left[\frac{1}{2} + \frac{1}{e^{\hbar\omega/kT} - 1}\right].$$

Hence, the overall energy of the crystal is given by [172]

$$E_{Tot} = U + \int_0^{\omega_{max}} \hbar\omega \left[\frac{1}{2} + \frac{1}{e^{\hbar\omega/kT} - 1}\right] \mathbf{f}(\omega)\, d\omega$$

where U is the static lattice energy, and ω_{max} is the maximum vibrational frequency of the crystal. From this expression, one obtains the heat capacity of the crystal at constant volume

$$C_V = \frac{\partial E_{Tot}}{\partial T}.$$

In order to calculate the other important thermodynamic functions of the crystal, it is necessary to measure the molar volume M_V, the isothermal bulk modulus K_T, and the Gruneisen parameter g_r, which is related to the average change in the frequency of one normal mode as a function of change in molar volume (a precise definition is given in Section 5 of [172]). With these measured quantities, one can then obtain the heat capacity at constant pressure, C_P, the entropy S, the enthalpy H, the Gibbs free energy G, and other thermodynamic functions by making use of their basic definitions:

$$\begin{aligned} C_P &= C_V + \frac{g_r^2 C_V^2 T}{K_T M_V} \\ S &= \int \frac{C_P}{T}\, dT \\ G &= E_{Tot} - TS \\ H &= E_{Tot} + PM_V. \end{aligned}$$

It is clear from this brief overview that the subtleties of the modeling of crystals from a thermodynamics point of view lie in the determination of the density of normal mode excitations $\mathbf{f}(\omega)$. Such subtleties are beyond the scope of this presentation, and we only note in passing that determining $\mathbf{f}(\omega)$ is related to the study of the phonon dispersion relations in crystals (the interested reader is referred to [178] in which $\mathbf{f}(\omega)$ is calculated for Forsterite).

This description of the macroscopic properties of crystals illustrates the essential connection between the thermodynamics of these systems and the density $\mathbf{f}(\omega)$. In this interpretation, the crystal itself is thought of as a large collection of independent normal modes, each of which describes a time-independent excitation property of the mineral (this description of crystals is not always appropriate, since phonons sometimes interact, but we focus here on those cases in which independence of the phonons is a valid approximation). Suppose now that the symbol ω is stripped of its interpretation as a lattice normal mode, that it becomes time-dependent, and that it starts evolving under the action of a dynamical system $\mathcal{T}$ (either continuous or discrete in time). Obviously, ω no longer bears any relevance to the description of crystals, and the function $\mathbf{f}$ now describes the probability of occupation of the phase space of $\mathcal{T}$ (the exact meaning of $\mathbf{f}$ is described in more detail in the next section). Thus we are lead rather naturally to the conclusion that the thermodynamic description of the dynamical system $\mathcal{T}$ must primarily focus on the probability of occupation of its phase space.

1.4.2 The thermodynamics of dynamical systems

Suppose that the dynamics of a physical system are modeled by a (deterministic or stochastic) dynamical system denoted by $\mathcal{T} : \mathbb{X} \longmapsto \mathbb{X}$ (many examples of such situations are described in Sections 1.2 and 1.3). Suppose further that some observable $\mathcal{O}(\mathbf{x}_n)$, which depends on the state $\mathbf{x}_n$ of $\mathcal{T}$, is being measured at time n (The observable $\mathcal{O}$ is arbitrary, though it must be a bounded measurable function). The expectation value of this observable, denoted by $E(\mathcal{O}_n)$, is the mean value of $\mathcal{O}(\mathbf{x}_n)$ when the measurement is repeated a large (ideally infinite) number of times. Mathematically it is given by

$$E(\mathcal{O}_n) = \int_{\mathbb{X}} \mathbf{f}_n(\mathbf{y})\mathcal{O}(\mathbf{y})\, d\mathbf{y}, \tag{1.5}$$

where $\mathbf{f}_n(\mathbf{x})$ is the density of the variable $\mathbf{x}_n$, *i.e.* the probability $p(\mathbf{x}'_n)$ of finding $\mathbf{x}_n$ between $\mathbf{x}'_n$ and $\mathbf{x}'_n + \delta\mathbf{x}'_n$ is

$$p(\mathbf{x}'_n) = \int_{\mathbf{x}'_n}^{\mathbf{x}'_n+\delta\mathbf{x}'_n} \mathbf{f}_n(\mathbf{y})\, d\mathbf{y}.$$

All thermodynamic functions which characterize the ensemble properties of a system are observables whose expectation values are defined by (1.5) since $\mathcal{O}$ was arbitrary. Therefore, the thermodynamic state of the CML $\mathcal{T}$ at time n is completely characterized by the density function $\mathbf{f}_n$. Hence a complete description of the thermodynamics of $\mathcal{T}$ must focus on the behavior and properties of $\mathbf{f}_n$. To this end, we introduce the transfer operator associated with $\mathcal{T}$, denoted by $\mathcal{P}_\mathcal{T}$, which governs the time evolution of $\mathbf{f}_n$

$$\mathbf{f}_{n+1}(\mathbf{x}) = \mathcal{P}_\mathcal{T}\mathbf{f}_n(\mathbf{x}), \quad n = 0, 1, \cdots. \tag{1.6}$$

To draw an analogy with more familiar physical systems, the transfer operators discussed here describe the arbitrary dynamical system $\mathcal{T}$ much as the Liouville equation describes the ensemble dynamics of ODE's, the Fokker Planck equation those of the Langevin equation (which is a stochastic ODE), or the Perron-Frobenius operator (defined in Section 1.4.3) those of deterministic maps (*cf.* Table 1.1).

For the sake of completeness we mention that there are dynamical systems which are not associated with probability density functions. In those cases, the thermodynamic description is given by a measure, which for the purpose of this discussion, allows the generalization of the notion of density (precise measure-theoretic definitions are given in the preliminaries of Chapter 6). In general, the thermodynamic state of the (semi)dynamical system $\mathcal{T} : \mathbb{X} \longmapsto \mathbb{X}$ is then the measure space $(\mathbb{X}, \mathcal{B}, \mu_t)$ where $\mathcal{B}$ is a finite σ-algebra and μ_n is a measure defined

on $\mathcal{B}$ at time n. In the cases described above, the measure μ_n is absolutely continuous with respect to the Lebesgue measure, and, therefore, is associated with a density function $\mathbf{f}_t(\mathbf{x})$ by the relation $\mu_n(A) = \int_A \mathbf{f}_n(\mathbf{x})d\mathbf{x}$ for all $A \in \mathcal{B}$. Hence, the evolution of the thermodynamic state of $\mathcal{T}$ is described by the evolution of the phase space densities $\mathbf{f}_n$ associated with the measures μ_n. The state of thermodynamic equilibrium for a nonsingular[2] dynamical system $\mathcal{T}$ is therefore described by the fixed point $\mathbf{f}_*$ of the transfer operator $\mathcal{P}_\mathcal{T}$ governing density evolution, when such a fixed point exists (*i.e.* when there exists $\mathbf{f}_*$ such that $\mathcal{P}_\mathcal{T}\mathbf{f}_* = \mathbf{f}_*$).

Description of the model	*Description of ensemble dynamics*
Deterministic maps	The Perron-Frobenius operator
Stochastic maps	The transfer operator
Deterministic ODE's	The generalized Liouville equation
Stochastic ODE's (white noise)	The Fokker Planck equation
Stochastic ODE's (non-white noise)	The Kramers- Moyal equation
Differential delay equations	The Hopf equation for the characteristic functional

TABLE 1.1:
Brief summary of the probabilistic descriptions associated with various types of discrete and continuous-time models.

Our presentation of the statistical mechanics of CML's focuses for the first part of the thesis on deterministic models. We derive in Chapter 4 the expressions for the transfer operators for stochastic systems, and we therefore delay until then a discussion of CML's perturbed by noise. In the absence of noise, the CML's induce, under mild conditions, a transfer operator known as the Perron-Frobenius operator, which is described in the next section.

1.4.3 The Perron-Frobenius operator $\mathcal{P}_\Phi$

A discrete-time nonsingular transformation $\Phi : \mathbb{X} \longmapsto \mathbb{X}$ $(\mathbb{X} \subset \mathbb{R}^N)$ induces an operator denoted $\mathcal{P}_\Phi$ which acts on probability densities, and which is defined implicitly by the relation

$$\int_{\mathbb{A}} \mathcal{P}_\Phi \mathbf{f}(\mathbf{x})\, d\mathbf{x} = \int_{\Phi^{-1}(\mathbb{A})} \mathbf{f}(\mathbf{x})\, d\mathbf{x}, \quad \text{for all } \mathbb{A} \subset \mathbb{X}, \tag{1.7}$$

[2]Nonsingular means in this case that $\mu_{\mathbb{X}}^L(\mathcal{T}^{-1}(\cdot))$ is absolutely continuous w.r.t Lebesgue measure $\mu_{\mathbb{X}}^L$ on $\mathbb{X}$.

and all probability densities $\mathbf{f}$. $\mathcal{P}_\Phi$ is called the Perron-Frobenius operator induced by Φ, and a study of its properties will be the cornerstone of our probabilistic description of deterministic CML's. If the transformation Φ is piecewise monotone, it is possible to give a more explicit definition of $\mathcal{P}_\Phi$, by performing a change of variable in the above definition.

Define Π to be a partition of the phase space $\mathbb{X}$ which contains $s(\Pi)$ elements denoted $\pi_1, \pi_2, \cdots, \pi_{s(\Pi)}$. Let $\Phi_{|i}$ be the monotone restriction of Φ to the set $\pi_i \subset \mathbb{X}$, $i = 1, \cdots, s(\Pi)$ (with $\bigcup_{i=1}^{M} \pi_i = \mathbb{X}$). Let $\tilde{\pi}_i$ denote the image of the set π_i: $\tilde{\pi}_i \equiv \Phi_{|i}(\pi_i)$. The Perron-Frobenius operator induced by Φ can be written

$$\mathbf{f}_{n+1}(\mathbf{x}) \equiv \mathcal{P}_\Phi \mathbf{f}_n(\mathbf{x}) = \sum_{i=1}^{s(\Pi)} \frac{\mathbf{f}_n(\Phi_{|i}^{-1}(\mathbf{x}))}{\mathcal{J}(\Phi_{|i}^{-1}(\mathbf{x}))} \chi_{\tilde{\pi}_i}(\mathbf{x}), \tag{1.8}$$

where $\chi_{\tilde{\pi}_i}(\mathbf{x}) \equiv 1$ iff $\mathbf{x} \in \tilde{\pi}_i$, and 0 otherwise, and $\mathcal{J}(Z)$ is the absolute value of the Jacobian of Z. A more intuitive version of (1.8) is

$$\mathcal{P}_\Phi \mathbf{f}_n(\mathbf{x}) = \sum_{\mathbf{y} \in \Phi^{-1}(\mathbf{x})} \frac{\mathbf{f}_n(\mathbf{y})}{\mathcal{J}(\Phi(\mathbf{y}))}.$$

It should be clear from our presentation that the asymptotic properties of the sequence $\{\mathbf{f}_n\}$ of the iterates of an initial density $\mathbf{f}_0$ under the action of $\mathcal{P}_\Phi$ determine the thermodynamic behavior of the dynamical system Φ. These asymptotic properties of $\{\mathbf{f}_n\}$ themselves dependent on the spectral characteristics of the operator $\mathcal{P}_\Phi$, and our investigations of CML thermodynamics will in fact focus on the spectral properties of $\mathcal{P}_\Phi$.

There have been several attempts at using the Perron-Frobenius operator to describe the dynamics of CML's [82, 83, 98, 166], but these have all concentrated on the properties of an operator acting on one-dimensional densities. The "proper", or complete description is given instead by the N-dimensional operator, and it will be the object of our attention.

Remark 1: WHEN discussing the thermodynamics of dynamical systems, and more precisely to clarify the link between the notion of *temperature* and the control parameters of the model under study, it is useful to generalize the definition of the Perron-Frobenius operator and introduce the following alternative [183, 203]:

$$\mathcal{P}_{\Phi,\beta} \mathbf{f}_n(\mathbf{x}) = \sum_{i=1}^{s(\Pi)} \frac{\mathbf{f}_n(\Phi_i^{-1}(\mathbf{x}))}{\left[\mathcal{J}(\Phi_i^{-1}(\mathbf{x}))\right]^\beta} \chi_{A_i}(\mathbf{x}), \ \beta > 0, \tag{1.9}$$

which reduces to our previous definition when $\beta = 1$. Changing β allows us to determine which of the preimages dominate the transfer of mass from $\mathbf{f}_n(\mathbf{x})$ to $\mathbf{f}_{n+1}(\mathbf{x})$ (*i.e.* which

microstates contribute to the density most). To illustrate the connection with classical statistical mechanics, apply $\mathcal{P}_{\Phi,\beta}$ T times to the uniform initial density $\mathbf{f}_0(\mathbf{x}) = \chi_{\mathbf{X}}(\mathbf{x})$. Using the identity

$$u^v \equiv e^{v \ln u}, \quad u > 0,$$

and replacing $\mathbf{f}_0(\mathbf{x}) = \chi_{\mathbf{X}}(\mathbf{x})$ in (1.9), one obtains

$$\begin{aligned} \mathbf{f}_T(\mathbf{x}) &= \sum_{\mathbf{y}^{(i)} \in \Phi_i^{-T}(\mathbf{x})} \left[\det \mathcal{J}(\Phi_i^{-N}(\mathbf{y}^{(i)}))\right]^{-\beta} \\ &= \sum_{\mathbf{y}^{(i)} \in \Phi_i^{-T}(\mathbf{x})} \exp\left[-\beta \sum_{t=0}^{T-1} \log |\Phi_i'(\mathbf{y}^{(i)})|\right] \\ &\equiv Z_T^{\text{top}}(\beta), \end{aligned}$$

where the simplified notation $\mathcal{J}(\cdot) \longrightarrow |\cdot'|$ is used. The sum over the $\Phi_i^{-T}(\mathbf{x})$ is over the set of preimages (of order T) of $\mathbf{x}$ (which is a sum over i), whereas the sum in the exponent runs over iterates of initial values x_0 (distributed according to $\mathbf{f}_0$). $Z_T^{\text{top}}(\beta)$ is known as the *topological partition function* [8] which is instrumental in the definition of meaningful thermodynamic quantities for dynamical systems (such as the topological pressure which plays the role of the free energy for hyperbolic systems since it satisfies a variational principle, like the free energy in classical statistical mechanics). The interested reader is referred to the clear discussion of the topological partition function and its relation to various other thermodynamic functions of chaotic systems which is given in Chapter 16 of [8]. We will see below that if the transformation Φ is Markov, then its topological partition function is exactly the partition function of an N^{th} order Potts model, where N is the number of elements of the Markov partition. Hence, changing β is akin to changing the temperature. But suppose that some parameter in transformation Φ is varied. The resulting effect on the partition function will be qualitatively similar to a change in β. This somewhat convoluted argument helps to precisely define what the meaning of the notion of temperature is in dynamical systems. ■

Remark 2: THE invariant density $\mathbf{f}_*$ is implicitly defined by the relation

$$\mathbf{f}_* = \mathcal{P}_\Phi \mathbf{f}_*,$$

and it plays a special role in the thermodynamic description of any dynamical system, since it describes the state(s) of thermodynamic equilibrium(ia). Uniqueness of the invariant

density implies uniqueness of the state of thermodynamic equilibrium for the system, and the approach of the sequence $\{\mathbf{f}_n\}$ to $\mathbf{f}_*$ describes the non-equilibrium behavior of the dynamical system. ■

We will come back in Section 1.4.5 to the various convergence properties of the sequence of functions $\{\mathbf{f}_n\}$, and their relation to thermodynamics, but we first proceed to explore the strong link between the transfer operator methods used in this thesis and the more frequently described transfer matrix formalism of statistical mechanics.

1.4.4 The operator $\mathcal{P}_\Phi$ and transfer matrices

There is a strong conceptual link between our description of CML statistical mechanics and the formalism of transfer matrices. Beck and Schlögl [8] have described the connection between $\mathcal{P}_\Phi$ and the statistical mechanics of spin systems in a comprehensive manner, and our presentation closely adheres to their *exposé*. The interested reader is referred to Chapters 8, 16 and 17 of [8] for a more extensive discussion.

We begin by describing the matrix representation of the Perron-Frobenius operator for the simplest possible transformation: A one-dimensional piecewise linear Markov map[3].

1.4.4.1 $\mathcal{P}_\Phi$ for a piecewise linear, Markov, expanding map

Consider the one dimensional map Φ displayed in Figure 1.1. We are now going to illustrate that the Perron-Frobenius operator $\mathcal{P}_\Phi$ induced by this transformation can, in some circumtances, be represented by a 5×5 matrix. The actual dimension of the matrix representation of $\mathcal{P}_\Phi$ depends on the density $\mathbf{f}$ on which $\mathcal{P}_\Phi$ operates, but the all-important invariant density $\mathbf{f}_*$ which describes the thermodynamic equilibrium of the map can be determined from the 5×5 matrix representation given below.. This is a consequence of a result due to Boyarsky and Scarowsky [17] which states that the unique absolutely continuous invariant measures (absolute continuity implies that measures are associated with well-behaved probability densities) are piecewise constant on the Markov partition.

[3] A map Φ is said to be *Markov*, if it is piecewise monotone on a partition of the phase space, and if the set of all edges of this partition is Φ-invariant [8, 17].

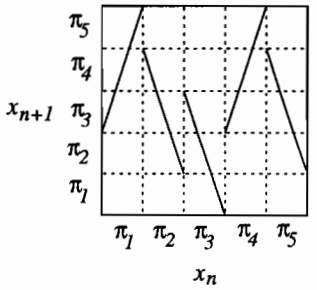

FIGURE 1.1:

The Markov map Φ for which the Perron-Frobenius operator is explicitly given in (1.14).

Suppose that the probability density $\mathbf{f}$ can be written

$$\begin{aligned} \mathbf{f}(x) &= \sum_{k=1}^{5} c_k \chi_{\pi_k}(x), \quad \text{for all } x \in [0,1] \\ &\equiv (c_1, \cdots, c_5)^{\text{trans}}, \end{aligned} \tag{1.10}$$

where the superscript denotes matrix transposition. This restriction is not as stringent as it might seem at first, since, as explained above, the invariant density satisfies the decomposition (1.10).

Now, since $\mathcal{P}_\Phi$ is a linear operator, we have

$$\mathcal{P}_\Phi \mathbf{f}(x) = \sum_{k=1}^{5} c_k \mathcal{P}_\Phi \chi_{\pi_k}(x) \tag{1.11}$$

$$= \sum_{k=1}^{5} \frac{c_k}{|\Phi_k'^{-1}|} \chi_{\Phi_k(\pi_k)}(x) \tag{1.12}$$

$$\equiv (d_1, \cdots, d_5)^{\text{trans}}.$$

We are now in a position to derive a matrix which governs the "transfer of probability" as the map is iterated. We have $\mathcal{P}_\Phi \mathbf{f}(x) = d_j$. By considering Figure 1.1, it is straightforward to check that the mass[4] of the set π_1 at time $t+1$ comes from that which was in set π_3 at time t, and that the mass in set π_2 comes from π_2, π_3 and π_5. Suppose that the matrix equation of this transfer of mass is written

$$(d_1, \cdots, d_5)^{\text{trans}} = M_\Phi (c_1, \cdots, c_5)^{\text{trans}}. \tag{1.13}$$

[4]The measure-theoretic mass of a set is equivalent in this discussion to the integral of the probability density over that set.

From (1.12) and Figure 1.1, the only term contributing to the first term d_1 is the third term c_3, weighted by the reciprocal of the derivative, and similarly for the other d_k's, hence define

$$\begin{aligned} \Delta_{jk} &= 1 \quad \text{if } x_{t+1} \in \pi_j \text{ and } x_t \in \pi_k \\ \Delta_{jk} &= 0 \quad \text{otherwise,} \end{aligned}$$

and $(m_{jk}) = \Delta_{jk}|\Phi_k'|^{-1}$. Then the entries of the matrix M_Φ are the m_{jk}'s. For the example of Figure 1.1, the matrix M_Φ is given by

$$M_\Phi = \begin{pmatrix} 0 & 0 & \frac{1}{|\Phi_3'^{-1}|} & 0 & 0 \\ 0 & \frac{1}{|\Phi_2'^{-1}|} & \frac{1}{|\Phi_3'^{-1}|} & 0 & \frac{1}{|\Phi_5'^{-1}|} \\ \frac{1}{|\Phi_1'^{-1}|} & \frac{1}{|\Phi_2'^{-1}|} & \frac{1}{|\Phi_3'^{-1}|} & \frac{1}{|\Phi_4'^{-1}|} & \frac{1}{|\Phi_5'^{-1}|} \\ \frac{1}{|\Phi_1'^{-1}|} & \frac{1}{|\Phi_2'^{-1}|} & 0 & \frac{1}{|\Phi_4'^{-1}|} & \frac{1}{|\Phi_5'^{-1}|} \\ \frac{1}{|\Phi_1'^{-1}|} & 0 & 0 & \frac{1}{|\Phi_4'^{-1}|} & 0 \end{pmatrix}. \tag{1.14}$$

In other words, $(d_1, \cdots, d_n) = (c_1, \cdots, c_n)M_\Phi^{\text{trans}}$, and M_Φ^{trans} is the matrix representation of the Perron-Frobenius operator $\mathcal{P}_\Phi$ acting on densities which can be written as in (1.10). Obviously, for arbitrary functions, the matrix M_Φ is infinite dimensional, since the number of terms in the series in (1.10) is in general infinite. However, from the results in [17] the matrix (1.14) can be used to *exactly* determine the invariant density, since that problem is then reduced to finding the solution of 5 linear equations.

In addition to being instrumental in determining $\mathbf{f}_*$, the matrix M_Φ is also useful to calculate the "transfer of probabilities" in the system. Let $q(i)$ denote the probability for the trajectory of the map to be in π_i at some time, and let $q(j,i)$ denote the joint probability to find the trajectory in π_j at some time, and then in π_i at the next time. Higher order probabilities can be defined similarly: $q(i_0, i_1, \cdots, i_{T-1})$ is the probability that the system trajectory will visit sequentially the corresponding π_i's. Note that if the map is Markov, it is possible to factor this function:

$$q(i_0, i_1, \cdots, i_T) = q(i_0)q(i_1|i_0)q(i_2|i_1)\cdots q(i_{T-1}|i_{T-2}) \tag{1.15}$$

where the conditional probabilities $q(i|j)$ are the entries of the matrix M_Φ.

Now we recall the definition of the topological partition function described in Remark 1 of Section 1.4.3. The definition given there makes explicit use of the transformation Φ, and an alternate definition [8] is:

$$Z_T^{\text{top}}(\beta) = \sum_{y^{(i)} \in \Phi_i^{-T}(x)} \exp\left[-\beta \sum_{t=0}^{T-1} \log|\Phi_i'(y^{(i)})|\right]$$

$$= \sum_{i_0,\cdots,i_{T-1}} q^{\beta}(i_0, i_1, \cdots, i_{T-1}). \tag{1.16}$$

If the map is Markov, so that (1.15) holds, we have

$$Z_T^{\text{top}}(\beta) = q(i_0)q(i_1|i_0)q(i_2|i_1)\cdots q(i_{T-1}|i_{T-2}). \tag{1.17}$$

To establish the connection between $Z_T^{\text{top}}(\beta)$ for a general dynamical system, and the partition function for a spin system, we recall some basic results on the statistical mechanics of the one-dimensional Ising model with nearest-neighbour interactions and periodic boundary conditions.

1.4.4.2 The transfer matrix formalism

This section is based on the presentation of Section 8.4 in [8]. The partition function of an Ising model in the presence of a magnetic field B is, when the interaction between spins is limited to the nearest neighbours, given by

$$Z_T = \sum_{s_1,\cdots,s_T}^{T} \exp\left[\tilde{\beta}J\sum_{j=1}^{N} s_j s_{j+1} + \tilde{\beta}B\sum_{j=1}^{N} s_j\right] \tag{1.18}$$

where $\tilde{\beta}$ is the reciprocal of the product (Temperature×Boltzmann's constant), not to be confused with the parameter β of equation (1.16). Define the generic interaction term

$$m(x, y) = \exp\left[\tilde{\beta}Jxy + \frac{1}{2}\tilde{\beta}B(x + y)\right]$$

so that (1.18) can be written

$$Z_T = \sum_{s_1,\cdots,s_T}^{T} m(s_1, s_2)m(s_2, s_3)\cdots m(s_T, s_1). \tag{1.19}$$

Now construct a matrix which contains the four possible values assumed by $m(x, y)$:

$$M = \begin{pmatrix} m(1,1) & m(1,-1) \\ m(-1,1) & m(-1,-1) \end{pmatrix}. \tag{1.20}$$

With this definition, the sum over $s_2, \cdots, s_N$ in (1.18) becomes a matrix multiplication, while the sum over s_1 is analogous to taking the trace of the matrix M^T. Hence, it is customary to write

$$Z_T = \text{trace } M^T.$$

The matrix elements $m(x,y)$ are of the form $e^{\tilde{\beta}E_{xy}}$, and E_{xy} is an interaction energy between x and y. One of the basic results of equilibrium statistical mechanics states that the probability associated with a state of energy E is proportional to $e^{\tilde{\beta}E}$, hence it is natural to give a probabilistic interpretation to the matrix elements $m(x,y)$: they describe the conditional probability that on our Ising chain, two neighbouring spins take on the values x and y. The expression (1.16) can then be recovered from (1.19) if we let

$$m(s_1, s_2) = q^{\beta}(s_2|s_1),$$

thus demonstrating the link between transfer matrices and the Perron-Frobenius (or more generally the operator of Remark 1).

1.4.4.3 Symbolic Dynamics

The similarities between the formalisms describing the probabilistic properties of dynamical systems and the statistical mechanics of spin systems are a consequence of the correspondance between the trajectories of these dynamical systems and symbolic sequences. In a seminal work, Badii [6] has proposed a general framework for the construction of the statistical mechanics of high dimensional dynamical systems which is based on this correspondance. Badii's work extends the pioneering descriptions of low-dimensional hyperbolic dynamical systems given by Ruelle, Bowen and Sinai which form the theoretical edifice commonly referred to as the thermodynamic formalism. A detailed discussion of that field of research lies beyond the scope of this introduction, and we refer the interested reader to Ruelle's classic presentation [183]. However, it is instructive to understand the basic premises of the theory, so we illustrate them with the map of Figure 1.1.

A trajectory of the map of Figure 1.1 can be represented by a sequence of symbols which take on five discrete values $(1, \cdots, 5)$:

$$x_n \longmapsto i, \quad \text{if } x_n \in \pi_i, \quad i = 1, 2, 3, 4, 5.$$

Since the map is Markov, there is a one-to-one mapping between the trajectory and the symbolic sequence (in this case, the partition $\Pi = \bigcup_i \pi_i$ is said to be a *generating partition* [6]). Once this is done, the trajectory of the one-dimensional map is viewed as an infinitely long chain of spins, which can take five different values. Hence, our dynamical system has been mapped to a fifth order Potts model. Since the map is Markov, the factorization (1.15) is possible, and hence the interaction between the spins in the Potts model are only

nearest neighbour. In general, this is clearly not the case, and the spin-spin interactions can extend to infinity. This presentation illustrates the fact that phase transitions in the sense of satistical mechanics, which are only rigorously defined in spin systems of infinite extent, can also be defined in one-dimensional maps. We will discuss the presence of phase transitions in CML's with a finite number of elements. The connection with symbolic dynamics discussed here clearly shows that if such transitions are possible in one-dimensional maps, they are *a fortiori* possible in CML's.

If the map is multi-dimensional, the corresponding Potts model becomes cumbersome to work with, and the resulting analysis using the theory of Gibbs random fields is not welcoming to the non-specialist. This avenue is explored for certain CML's by Bunimovich and Sinai [21], but this aproach suffers from many short-comings. The main problem with these techniques is that they break down in practice when the map is no longer Markov, and the Markov assumption is exceedingly restrictive. Hence, we will concentrate on the properties of the tranfer operator in the remainder of the thesis, and proceed with our description of the most frequently encountered thermodynamic properties.

1.4.5 Ergodicity, mixing and asymptotic periodicity

Here we discuss the behavior of the sequence of densities $\{\mathbf{f}_n\}$ which is intimately linked to the equilibrium and nonequilibrium properties of the CML. For example, $\mathcal{T}$ is ergodic if and only if the sequence is *weak Cesàro convergent* to the invariant density $\mathbf{f}_*(\mathbf{x})$,

$$\lim_{n\to\infty} \frac{1}{n} \sum_{k=0}^{n-1} \int_{\mathbf{X}} \mathbf{f}_k(\mathbf{x})\mathbf{q}(\mathbf{x})\, d\mathbf{x} = \int_{\mathbf{X}} \mathbf{f}_*(\mathbf{x})\mathbf{q}(\mathbf{x})\, d\mathbf{x}, \quad \text{for all } \mathbf{q} \in L_1(\mathbb{X}),$$

and all initial probability densities $\mathbf{f}_0(\mathbf{x})$. A stronger (but familiar) property, mixing, is equivalent to the *weak convergence* of the sequence to $\mathbf{f}_*$:

$$\lim_{n\to\infty} \int_{\mathbf{X}} \mathbf{f}_n(\mathbf{x})\mathbf{q}(\mathbf{x})\, d\mathbf{x} = \int_{\mathbf{X}} \mathbf{f}_*(\mathbf{x})\mathbf{q}(\mathbf{x})\, d\mathbf{x}, \quad \text{for all } \mathbf{q} \in L_1(\mathbb{X})$$

and all initial probability densities $\mathbf{f}_0(\mathbf{x})$. An even stronger type of chaotic behavior, known as *exactness* (or asymptotic stability) is reflected by the *strong convergence* of the sequence $\{\mathbf{f}_n\}$ to the invariant density $\mathbf{f}_*$:

$$\lim_{n\to\infty} \|\mathcal{P}_{\mathcal{T}}\mathbf{f}_n - \mathbf{f}_*\|_{L^1} = 0$$

for all initial probability densities $\mathbf{f}_0(\mathbf{x})$. Exactness implies mixing and is interesting from a physical point of view because it is the only one of the properties discussed so far which guarantees the evolution of the thermodynamic entropy of $\mathcal{T}$ to a global maximum, irrespective of the initial condition $\mathbf{f}_0$ [142].

The hierarchy of chaotic behaviors

$$\text{Exactness} \implies \text{Mixing} \implies \text{Ergodicity}$$

is discussed here because it is shown in Chapters 3 and 4 that many deterministic and stochastic CML's are either exact, or possess a another dynamical property, known as *asymptotic periodicity*, of which exactness is a special case.

Asymptotic periodicity is a property of certain Markov operators which ensures that the density sequence $\{\mathbf{f}_n\}$ converges strongly to a periodic cycle [recall that $\mathcal{P}$ is a Markov operator if it is linear, and if for all probability densities f it satisfies (1) $\mathcal{P}f \geq 0$ for $f \geq 0$, (2) $\|\mathcal{P}f\|_{L^1} = \|f\|_{L^1}$].

Definition 1: Asymptotic Periodicity

A Markov operator $\mathcal{P}$ is asymptotically periodic if there exist finitely many distinct probability density functions $v_1, \cdots, v_r$ with disjoint supports, a unique permutation γ of the set $\{1, \cdots, r\}$ and positive linear continuous functionals $\Gamma_1, \cdots, \Gamma_r$, on $L_1(\mathbb{X})$ such that, for almost all initial densities $\mathbf{f}_0$,

$$\lim_{n\to\infty} \left\| \mathcal{P}^n \left(\mathbf{f}_0 - \sum_{i=1}^{r} \Gamma_i[\mathbf{f}_0] v_i \right) \right\|_{L^1} = 0 \tag{1.21}$$

and

$$\mathcal{P}v_i = v_{\gamma(i)}, \quad i = 1, \cdots, r.$$

Clearly, if $\mathcal{P}$ satisfies these conditions with $r = 1$, it is exact (or *asymptotically stable*). If $r > 1$ and the permutation γ is cyclical, asymptotic periodicity also implies ergodicity [142]. The early papers discussing asymptotically periodic Markov operators are [113, 112, 124, 125, 121]. A somewhat more intuitive presentation is given in [122]. ■

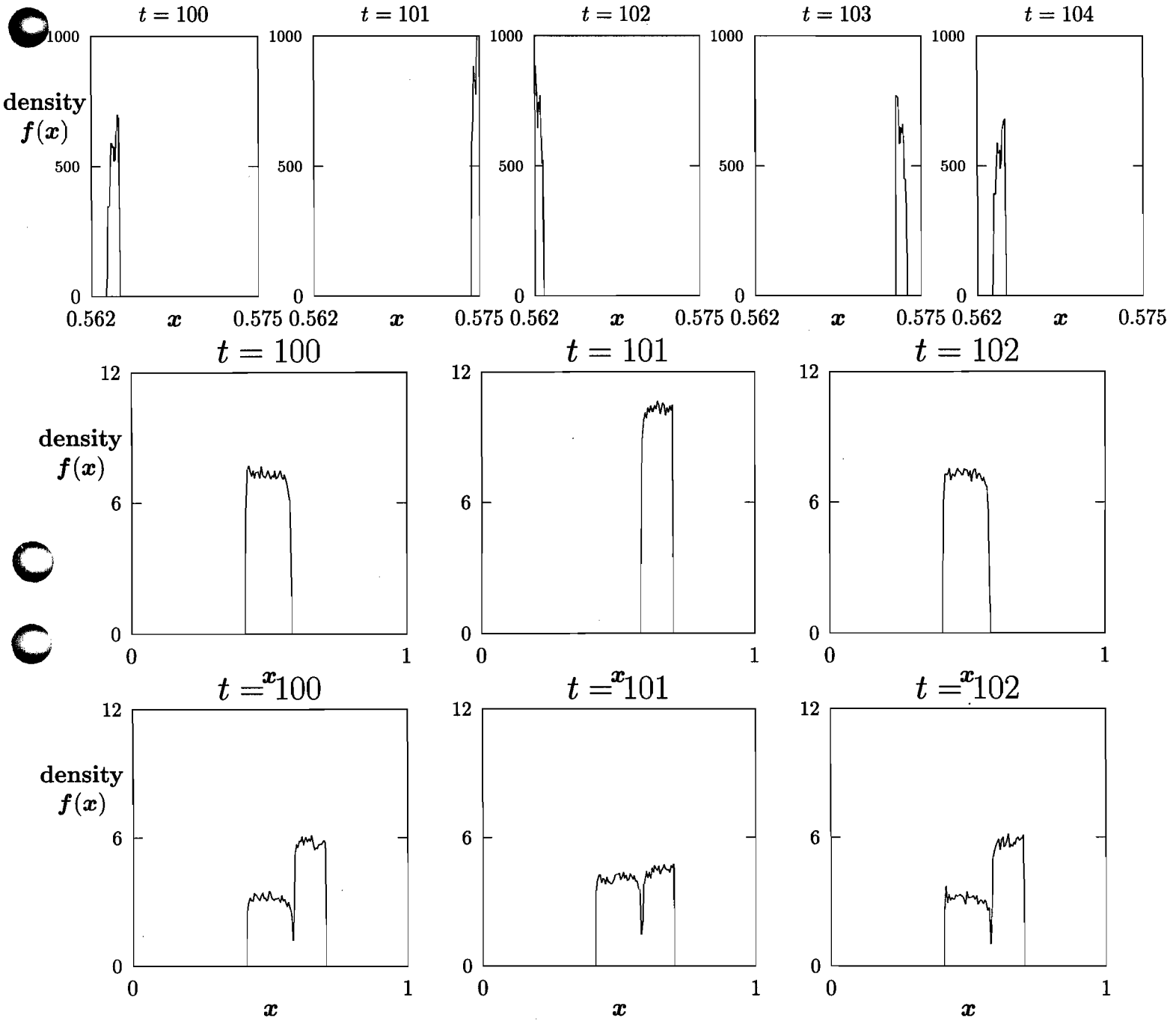

FIGURE 1.2

Illustration of asymptotic periodicity in the tent map (2.2). *Top row* When it is asymptotically periodic (AP) with period 4 ($a = 1.15$); the initial density is uniformly distributed on $[0.562 : 0.565]$. *Middle row* When it is AP with period 2, ($a = 1.4$). The initial density was uniform on

$[0.3 : 0.4]$. *Bottom row* Same parameters as in **b)** except the initial density is now uniform on $[0 : 1]$. This illustrates a generic property of asymptotically periodic systems: The density cycle depends sensitively on the initial ensemble density.

Remark 3: As illustrated in Figure 1.2 for the tent map, the phase space density $\mathbf{f}_n$ of an AP system at any (large) time n is a linear combination of "basis states" (denoted v_i above) with disjoint supports, and at every time step the coefficients (Γ_i) of this linear combination are permuted by γ. Therefore, the density evolution in such systems is periodic, with a period bounded above by $r!$, but with the exact cycle depending on the initial preparation since the Γ_i's are functionals of the initial density (*cf.* (1.21)). A direct consequence of asymptotic periodicity is that the thermodynamic equilibrium of the system consists in a sequence of metastable states which are visited periodically. It was shown in [122] that AP systems are ergodic if and only if the permutation γ is cyclical. We will see in Chapters 3 and 4 that most systems of interest fall into this category. ■

Suppose that an asymptotically periodic dynamical system, for which the permutation γ in (1.21) is cyclical, generates a sequence $\mathbf{x}_1, \cdots, \mathbf{x}_N$. If the distribution $\mathbf{f}$ of these variables is determined from a long time trajectory, it will, because the system is ergodic (by Theorem 5.5.1 of [122]), converge in the weak Cesáro sense to the invariant (or equilibrium) distribution of the system. If, on the other hand, $\mathbf{f}$ is constructed as an ensemble density, it will, for almost all initial ensemble distributions, be time-dependent.This is a straightforward consequence of the spectral decomposition (1.21).

Some of the usual misconceptions concerning the true meaning of ergodicity are exacerbated when supposed consequences of ergodicity are violated by systems which turn out to be asymptotically periodic. We illustrate this statement with the next Section, motivated by a recent controversy, mentioned at end of Section 1.3.4 concerning the verification of the law of large numbers as it applies to CML's.

1.4.5.1 Asymptotic periodicity and the law of large numbers

Kaneko [99], and later Perez *et al.* [164] have reported that "globally coupled chaos violates the law of large numbers, but not the central limit theorem". This claim was based on a numerical description of the CML:

$$x_{n+1}^{(i)} = (1-\varepsilon)S(x_n^{(i)}) + \frac{\varepsilon}{N}\sum_{j=1,\, j\neq i}^{N} S(x_n^j), \quad n = 0, 1, 2, \cdots,$$

where $i = 1, \cdots, N$ and S is the logistic nonlinearity

$$S(x) = 1 - ax^2. \tag{1.22}$$

Before describing the "violation", a few definitions are necessary. The mean field of the lattice is defined by these authors to be

$$h_n \equiv \frac{1}{N} \sum_j S(x_n^j).$$

The density f of the variable h is then constructed over different times, for some fixed value of a and ε, following a trajectory of the lattice. Numerically, this density is seen to converge, with increasing N to a Gaussian. Thus, by the central limit theorem, one concludes that if N is large, the value of h at one time is essentially independent of the value of h at the next time. Kaneko states that the law of large numbers is violated by the n variables h because $E((h-\bar{h})^2)$ does not behave like $1/N$ as N is increased, where the mean square displacement is calculated with

$$E((h - \bar{h})^2) = \int h^2 f(h) dh - \left[\int h f(h) dh \right]^2. \tag{1.23}$$

We claim that the law of large numbers does not refer to the behavior of $E((h - \bar{h})^2)$ if f is constructed from a single trajectory of the CML, and therefore, that the investigations of Kaneko [*ibid*] and Perez [*ibid*] are inconclusive. The density which should be used for the determination of E is the ensemble density, which would be obtained by starting many CML's with many initial conditions, and letting each realization evolve for some fixed number of time steps. Ergodicity is not quite enough to guarantee the equivalence of both constructions (*i.e.* single trajectory, and ensemble), if the system under consideration is AP. Before discussing the possible presence of AP in the logistic CML, we recall precisely the statement of the law of large numbers.

This law comes in two flavors, weak and strong [18], which differ in the notion of convergence which is used for their definition. The *weak* form is associated with the notion of *stochastic convergence*, whereas the *strong* form refers to *almost sure convergence.* Concise definitions of these types of convergence can be found in Chapter 10 of Lasota and Mackey [122].

Definition 2: The weak law of large numbers:

Let $\xi_1, \xi_2, \cdots, \xi_N$, denote a sequence of *independent* random variables, each distributed according to the function $f(\xi)$. Denote also the mathematical expectation of the variable ξ_i

by e_i:

$$E(\xi_i) = \int_\Omega \xi_i f(\xi_i) d\xi_i = e_i, \quad (\Omega \text{ denoting the space of events})$$

and let the variance of the sequence of random variables be finite:

$$M = \sup_i E((\xi_i - e_i)^2) < \infty.$$

Then,

$$\text{prob} \left\{ \left| \frac{1}{n} \sum_{i=1}^{n} (\xi_i - e_i) \right| \geq \varepsilon \right\} < \frac{M}{n\varepsilon^2}, \qquad \text{(The weak form)}$$

for every $\varepsilon > 0$. If, in particular, $e_1 = e_2 = \cdots = e_n = e$, then we have the "stochastic-limit"

$$\text{st-lim} \frac{1}{n} \sum_{i=1}^{n} \xi_i = e.$$

[This notation indicates the stochastic convergence of the left hand side of the equation to the right hand side. Stochastic convergence is described explicitly in the penultimate relation]. ■

The other version of this law is due to Kolmogorov:

Definition 3: The strong law of large numbers:

Let $\xi_1, \xi_2, \cdots, \xi_N$, denote a sequence of *independent* random variables with f, e_i, and M defined as above, then

$$\lim_{n\to\infty} \frac{1}{n} \sum_{i=1}^{n} (\xi_i - e_i) = 0 \qquad \text{(The strong form)}$$

with probability 1. ■

In the above definitions, the ξ_i's are independent. Hence the density function f which must be used to calculate (1.23) should be the distribution of mean fields obtained from an ensemble of realizations. Ergodicity guarantees the equivalence of both methods *if the system is at equilibrium.* If it is not, and if the system is AP, trajectory statistics and ensemble statistics are not equivalent.

Hence for an AP system, the e_i's of Definitions 2 and 3 will cycle in time.

There is strong analytical and numerical evidence that the logistic map defined above is asymptotically periodic for a spectrum of values of the parameter a [173]. For such parameter values, the law of large numbers would predict a time-dependent fluctuation of the mean e_i (and therefore of the variable h). This is indeed observed by Kaneko [*ibid.*] and Perez *et al.* [*ibid*] in globally coupled maps. If the globally coupled logistic CML acts as an array

of independent AP maps, one can (see [166]) explain the supposed violations of the law of large numbers by pointing out that ensemble densities and single trajectory densities are not equivalent, since the system converges (in weak Cesáro sense) to equilibrium, but at the same time converging strongly to a limit cycle (in density space).

But the globally coupled map lattice is *not* always an array of uncoupled maps. The argument of Pikovsky and Kurths is based on the reduction of the CML to an effectively one-dimensional dynamical system. This is sometimes justifiable, and sometimes it is not. For example, when local, instead of global coupling is discussed, the reduction to a single map is no longer realistic. Chaté and Manneville [31], and Binder and Privman [13] discuss "quasi-periodicity" in locally coupled CML's, so the question is then "how do we study the eventual ergodicity, mixing or asymptotic periodicity of the *whole* lattice, viewed in all its glory as an N-dimensional mapping, and not necessarily as a reduced system?"

In the absence of noise, the answer lies in the investigation of the N-dimensional Perron-Frobenius operator. In the presence of noise, the answer lies with the similar study of the N-dimensional transfer operator.

1.5 Some outstanding problems

The broad overview of the current literature presented in the first part of this introduction highlights the importance of CML's for the modeling of varied biological, computational and physical systems, as well as the crucial role they are playing as "toy models" to further our understanding of the phenomenology of many complex systems.

The second part of this introduction was a brief presentation of the concepts which must be referred to in order to examine the statistical mechanics of coupled map lattices. The rest of this thesis is a detailed examination of the collective behavior of CML's, described from a statistical perspective. There are very few such descriptions of CML's (the exceptions are the works of Keller [109], Bunimovich and Sinai [21, 22] and Rand and Gundlach [72]), and these place the emphasis on formal situations which are not relevant to the modeling community. The main unaddressed problems of this field of research can be summarized as follows:

1) Establish explicit criteria on the control parameters of a given model, which guarantee the existence of a state of thermodynamic equilibrium.

2) Examine the non-equilibrium properties of the systems to determine whether or not a

system prepared out of equilibrium will relax to equilibrium, and how this relaxation process will take place.

3) Determine the uniqueness of the equilibrium.

Although these questions seem to be somewhat formal, they must be addressed before any serious discussion of the extensive properties of high dimensional dynamical systems can begin.

The next Chapter examines these questions in the simplest possible CML: a network of two elements. Chapter 3 extends the results of Chapter 2 to arbitrarily large but finite deterministic lattices. Chapter 4 examines the statistical behavior of large lattices in the presence of stochastic perturbations: we derive the transfer operators, and examine their spectral properties to answer the questions mentioned above. Chapter 5 examines the strong connection between differential delay equations and coupled map lattices, and we apply the methods developed in Chapters 3 and 4 to these hereditary models. Finally Chapter 6 is a presentation of the functional transfer operator which generalizes the presentation of the previous chapters to infinite dimensional spaces.

Chapter 2

Coupling induced statistical cycling in two coupled maps

ABSTRACT

This chapter discusses the effects of "diffusively" coupling two identical one dimensional maps. Attention is focused on situations where the local (isolated) maps are statistically stable, but where the coupled system is not. A biologically motivated map and the logistic map are numerically shown to display this behavior. The piecewise linear tent map is then investigated analytically, and we give a phase diagram of this system which displays the location of nonequilibrium phase transitions. It is conjectured that the diffusive coupling of two chaotic but statistically stable maps (*i.e.* with asymptotically stable Perron-Frobenius operators) can yield a two dimensional system which is not statistically stable, whose associated Perron-Frobenius operator is asymptotically periodic.

Rien au monde ne dure qu'un éternel changement

Honorat de Bueil, *Odes, La venue du printemps*

2.1 Introduction.

The proper understanding of statistical cycling in large CML's is greatly facilitated by a discussion of this behavior in the simplest possible CML (with two elements). This chapter examines the statistical behavior of two dimensional maps obtained by coupling two identical one-dimensional chaotic maps.

We discuss situations in which the statistical behavior of the decoupled maps is qualitatively different than that of the coupled system: the local maps are statistically stable, they possess an absolutely continuous invariant measure, and physical observables converge to a constant value in the asymptotic regime; the coupled maps however, cycle statistically: The invariant measure is not reached asymptotically for almost all initial preparations, but instead a periodic cycle in density-space is reached, indicating that the Perron-Frobenius operator satistifies the spectral decomposition (1.21). Physical observables in the latter situation are also seen to cycle periodically in the asymptotic regime, so that the thermodynamic "equilibrium" for the two maps is in fact a sequence of metastable states visited periodically.

Statistical cycling has been numerically reported in cellular automata schemes [27, 60], as well as in coupled map lattices [31, 99, 164]. Houlrik's investigation of periodic symbolic orbits in two coupled Chaté-Manneville maps [84] indicates that there is underlying statistical periodicity. Previous investigations of two coupled maps, from different perspectives, include the works of Yamada and Fujisaka [222], Yuan *et al.* [226], Froyland [59], Fabiny and Wiesenfeld [54], and Chapeau-Blondeau and Chauvet [26] but these do not address the periodic statistical behavior reported here. The recent description of two coupled maps given by Kuznetsov [117] describes the scaling properties of the "2^n" chaotic windows, but without mentioning that the underlying property responsible for this behavior is in fact asymptotic periodicity (incidentally, asymptotic periodicity also explains the "phase multistability" described by Kuznetsov, which is a reflection of the dependence of the Γ_i's of (1.21) on $\mathbf{f}_0$).

There has been speculation in the literature concerning the possibility that such behavior might not be asymptotically observable in physical systems [60, 169]. The results presented here show that statistical cycling can be explained analytically in a simplistic model, an be

expected in more general settings: they clearly indicate the existence of complicated states of thermodynamic equilibria in the simplest CML (*i.e.* two elements).

In Section 2.1.1, we introduce the three systems which will be discussed in this paper, as well as some of the ideas concerning the relation between phase space densities and thermodynamic states. In Section 2.1.2, we recall a useful definition of the two-dimensional Perron-Frobenius operator, and describe some properties of the Boltzmann-Gibbs entropy.

In Section 2.2, we relate discrete time maps to differential delay equations, and numerically describe the phenomenon of coupling-induced statistical cycling in two smooth maps: one is obtained from the reduction of a differential delay equation used in biomathematical modeling, and the other is the celebrated logistic map.

In Section 2.3, a detailed analytic and numerical investigation of the dynamics of two coupled generalized tent maps is presented. A phase diagram giving the *loci* in parameter space where phase transitions occur is described analytically in Section 2.3.1, while Section 2.3.2 illustrates the temporal evolution of a statistical quantifier, the Boltzmann-Gibbs entropy, when the underlying system is statistically periodic.

Section 2.4 presents a brief summary, and several conjectures concerning the Perron-Frobenius operator associated with the two-dimensional map are put forward.

2.1.1 Three simple maps

The two dimensional maps considered here are constructed by diffusively coupling two one-dimensional maps:

$$\Phi \circ (x,y) = (x_1, y_1), \text{ with } \left\{ \begin{array}{rcl} x_1 & = & (1-\varepsilon)S(x) + \varepsilon S(y) \\ y_1 & = & (1-\varepsilon)S(y) + \varepsilon S(x), \end{array} \right. \quad \varepsilon \in [0,1], \tag{2.1}$$

where S denotes the local map. In this paper, we focus on three systems: One is the tent map rescaled so that it is onto $[0,1]$ independent of the parameter a:

$$S(z) = \left\{ \begin{array}{ll} az + 2 - a & \text{if } z \in [0,(a-1)/a] \\ a(1-z) & \text{if } z \in [(a-1)/a, 1] \end{array} \right. \quad \text{and } a \in (1,2]. \tag{2.2}$$

Another is obtained in Section 2.1 by taking a singular perturbation limit on a differential delay equation to obtain:

$$S(z) = \frac{az}{1+z^n}, \qquad a,\ n \in \mathbb{R}. \tag{2.3}$$

The third map is the celebrated logistic map

$$S(z) = az(1-z), \quad a \in (1,4], \tag{2.4}$$

whose behavior reproduces that of the more realistic system (2.3), suggesting that the behavior discussed here may be generic in systems with a locally logistic maximum.

Depending on the system's location in parameter space, the map (2.1) with nonlinearities (2.2), (2.3) or (2.4) transforms the unit square into a simply connected set (as shown in Figures 2.1a, 2.2a, 2.4b for example) or a collection of disconnected sets (as in Figures 2.1b, 2.2b, 2.5b or 2.7). Here, we investigate the boundaries between regions in the (a, ε) plane[1] in which the number of these sets differ. When the attractor is a simply connected set, ensemble statistics can be computed from a numerically obtained invariant measure to which almost all initial preparations evolve; we conjecture that this reflects the asymptotic stability of the associated Perron-Frobenius operator. When the attractor is a collection of disconnected sets, almost all numerical initial conditions eventually reach a cycle in density space, and statistical quantities like the Boltzmann-Gibbs entropy, the temporal correlation function and more generally all ensemble averages are seen to cycle in the asymptotic regime with a period related to the number of disconnected sets forming the attractor. Such cyclical statistical behavior is well described for certain one dimensional maps, where it reflects the asymptotic periodicity of the Perron-Frobenius operator [113, 143], but it has not been described in two (or higher) dimensional systems. We propose strong circumstancial evidence that it reflects the asymptotic periodicity of the two dimensional Perron-Frobenius operator.

Before proceeding, let us clarify the link between phase transitions (*i.e* qualitative changes in the thermodynamic state of a system) and qualitative changes in statistical behavior (reflected by transitions in the number of disconnected sets forming the attractor). Consider the system $\Phi_{\{\alpha\}} : \mathbb{X} \longmapsto \mathbb{X}$, parametrized by $\{\alpha\}$, a set of real parameters. $\Phi_{\{\alpha\}}$ could be a map, a set of ordinary differential equation, or more generally any (semi)dynamical system.

In Section 1.4 we discussed in some detail the connection between the thermodynamic state of $\Phi_{\{\alpha\}}$ and the phase space density function $\mathbf{f}_{\{\alpha\}}$, which gives the probability that the system is at a given state $\mathbf{x} \in \mathbb{X}$. When $\mathbf{f}_{\{\alpha\}}$ changes qualitatively as a result of changing the parameters $\{\alpha\}$, so does the thermodynamic state of $\Phi_{\{\alpha\}}$ and the system undergoes a phase transition. The problem of identifying phase transitions is therefore reduced to that of finding the *loci* in parameter space where $\mathbf{f}_{\{\alpha\}}$ changes abruptly. Such an abrupt change necessarily occurs when the number of sets on which $\mathbf{f}_{\{\alpha\}}$ is nonzero changes (the union of these sets is called the *support* of $\mathbf{f}_{\{\alpha\}}$). In the tent map example discussed below, the analytic

[1]Note that the system is symmetric under the transformation $\varepsilon \leftrightarrow (1-\varepsilon)$, $S(x) \leftrightarrow S(y)$ so that we only consider the region of parameter space $0 \leq \varepsilon \leq 1/2$.

criteria given for phase transitions are criteria for abrupt changes in the support structure of $\mathbf{f}_{\{\alpha\}}$. The abruptness of this process indicates that the transitions are first order.

There are fundamental differences between the approach discussed here, and the usual discussion of the thermodynamics of dissipative dynamical systems. As discussed in Chapter 1, the thermodynamic formalism introduced by Bowen [16], Ruelle [183], Sinai [195] and others, which is the inspiration behind the existing studies of the thermodynamics of coupled map systems [21, 22, 72], rests on the introduction of meaningful symbolic representations of trajectories, so that ensemble statistics are constructed as they would be for generalized interacting spin systems.

The existence of such symbolic representations for the trajectories, and consequently the link with interacting spins is not the underlying premise here.

2.1.2 Definitions

Recall from Section 1.4.3 that the Perron-Frobenius operator $\mathcal{P}_\Phi$ induced by a nonsingular measurable transformations Φ is given by $\mathbb{X}$ is

$$\int_A \mathcal{P}_\Phi \mathbf{f}(\mathbf{x})\, d\mathbf{x} = \int_{\Phi^{-1}(A)} \mathbf{f}(\mathbf{x}) d\mathbf{x} \tag{2.5}$$

where $A \subset \mathbb{X}$. If the transformation Φ is the two dimensional mapping defined in (2.1) and operating on $[0,1] \times [0,1]$, (2.5) can be written

$$\mathcal{P}_\Phi \mathbf{f} = \frac{\partial^2}{\partial x \partial y} \iint_{\Phi^{-1}([0,x]\times[0,y])} \mathbf{f}(u,v)\, dvdu. \tag{2.6}$$

It is not always straightforward to numerically illustrate the the behavior of phase space densities under the action of (2.6). To simplify the task, we introduce a quantifier of density evolution which plays an important role in thermodynamics: the Boltzmann-Gibbs entropy. For a historical presentation of the concept, we refer the interested reader to Grandy [68]. It is important to note that the Boltzmann-Gibbs entropy is not necessarily the "thermodynamic entropy" of the system under consideration. By "thermodynamic entropy" we mean here that function which evolves to a maximum as a result of the second law of thermodynamics. If the density at equilibrium is uniform over the phase space, then the thermodynamic entropy is the Boltzmann-Gibbs construct (and this is the case for many of the classical systems discussed by Boltzmann and Gibbs a century ago), but in general, the thermodynamic entropy is the *conditional entropy* with respect to the invariant density [142, 173].

The Boltzmann-Gibbs entropy $H_{BG}(\mathbf{f})$ is defined by

$$H_{BG}(\mathbf{f}) = -\int_{\mathbb{X}} \mathbf{f}(\mathbf{x}) \ln \mathbf{f}(\mathbf{x})\, d\mathbf{x}, \tag{2.7}$$

where $\mathbf{f}$ is a probability density normalized over $\mathbb{X}$. When the system is in thermodynamic equilibrium, the Boltzmann-Gibbs entropy is usually thought of as being stationary at a local maximum (the internal energy being in a local minimum). The phase space density describing this equilibrium is a fixed point of the operator giving the evolution of densities [*i.e.* the Perron-Frobenius operator for discrete time maps, the Liouville (or Fokker-Planck) operator for deterministic (or stochastic) ODE's, *etc...*]. In contrast to the situation in which extensive quantities can be determined from the density of the invariant measure, the (most probable) state of thermodynamic equilibrium for an asymptotically periodic map is, as discussed inSection 1.4.5 a collection of metastable states which are visited in alternation. Thus, the Boltzmann-Gibbs entropy in this metastable equilibrium oscillates periodically for almost all initial preparations:

$$\lim_{t^*\to\infty} H_{BG}(\mathbf{f}_{t^*}) = \lim_{t^*\to\infty} H_{BG}(\mathbf{f}_{t^*+\kappa}) \Longleftrightarrow \alpha^\kappa(i) = i,\ (i = 1, \cdots, r), \text{ and } \gamma^j(i) \neq \gamma^\kappa(i),\ j < \kappa. \tag{2.8}$$

To see this, note that $v_i = v_j$ a.e. $\Leftrightarrow i = j$ since two different v_i's in equation (1.21) have disjoint supports. In addition, recall that $\mathcal{P}v_i = v_{\gamma(i)}$ (with $i = 1, \cdots, r$ and γ a permutation of the set $\{1, \cdots, r\}$), and therefore $\mathbf{f}_{t^*} = \mathcal{P}^\kappa \mathbf{f}_{t^*} \Leftrightarrow \alpha^\kappa(i) = i$. As a consequence, from (2.8), $\mathbf{f}_{t_1} = \mathbf{f}_{t_1+\nu}$ a.e. $\Leftrightarrow \nu = 0$ or $\alpha^\nu(i) = i$. Furthermore it is easy to show that if $\mathbf{f}(\mathbf{x}) = \mathbf{g}(\mathbf{x})$ a.e., $H_{BG}(\mathbf{f}) = H_{BG}(\mathbf{g})$ and hence

$$\lim_{t\to\infty} H_{BG}(\mathbf{f}_t) = \lim_{t\to\infty} H_{BG}(\mathbf{f}_{t+\nu}) \Longleftrightarrow \mathbf{f}_t = \mathbf{f}_{t+\nu},$$

with either $\nu = 0$ or ν such that $\gamma^\nu(i) = i$ which proves (2.8).

This cycling behavior of H_{BG} is numerically illustrated in Section 2.3.2 for the tent map, but is also observed in the sigmoidal map and the logistic map.

2.2 Statistical cycling in the coupled maps

We now turn to a study of coupling induced statistical cycling in three systems. The first of these is obtained as the singular perturbation limit of a first order differential delay equation (DDE).

2.2.1 Delayed feedback control loops and one dimensional maps

In this section we first quickly review the connection between continuous time models of delayed feedback control loops framed as DDE's and one-dimensional maps. We then discuss situations where coupling induced statistical cycling is observed in the two-dimensional system.

There are several connections between differential delay equations and one dimensional maps (see for example [132, 76], but the one making use of the singular perturbation method is by far the most general, because it is essentially independent of the details in the equation. The DDE's considered are of the form:

$$\frac{dx}{dt} = -\zeta x(t) + F(x(t-1)), \;\; \zeta \in \mathbb{R}^+, \; t \geq 0, \tag{2.9}$$

with initial function $x(t) \equiv \varphi(t)$ for $t \in [-1, 0]$ (the delay is, without loss of generality, rescaled to 1). Dividing by ζ and taking the limit $\zeta \to \infty$, $F/\zeta \to S$, one obtains from the DDE the difference equation

$$x(t) = S(x(t-1)), \; t \geq 0,$$

with $x(t) \equiv \varphi(t)$, $t \in [-1, 0)$. Confining our attention to integer values of time instead of a continuum, one obtains the one-dimensional map

$$x_{n+1} = S(x_n), \; n \in \mathbb{N},$$

with x_0 given. The procedure outlined here is known as a *singular perturbation* of the map, and it has been extensively studied by Ivanov and Sharkovskiĭ [88], who have been able to show that certain dynamical properties of the map can be extended to the infinite dimensional continuous time DDE. We follow this procedure to obtain the nonlinearity (2.3) from a DDE known in the literature as the Mackey-Glass equation, proposed as an attempt to model the oscillations in neutrophil numbers observed in certain patients suffering from chronic granulocytic leukemia [144]:

$$\frac{dx}{dt} = -\zeta x(t) + \frac{\tilde{a}x(t-1)}{1 + x^n(t-1)}. \tag{2.10}$$

Performing the singular perturbation procedure on (2.10) and setting $a = \lim_{\zeta \to \infty} \tilde{a}/\zeta$ yields the nonlinearity (2.3).

2.2.2 The sigmoidal map

Figure 2.1 displays two projections of the phase space density on the $x - y$ plane which numerically illustrates the phenomenon we conjecture to be coupling-induced asymptotic periodicity.

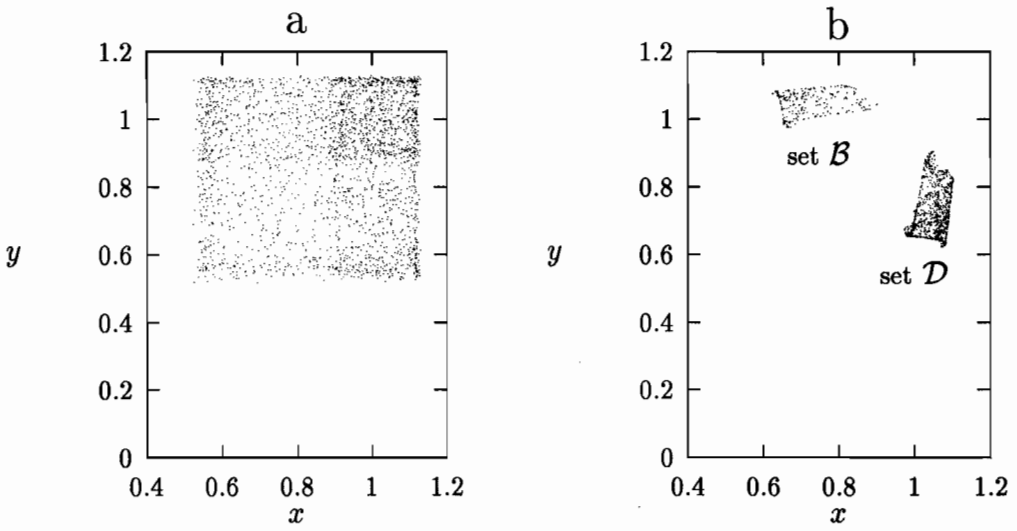

FIGURE 2.1:
Two dimensional projection of the phase space density for the map (2.1) with nonlinearity (2.3) with $a = 1.65$ and $n = 8$ in both panels. Time $t = 6000$, the figure was made with 3500 points and the initial density was supported uniformly on $[0:1] \times [0:1]$. a) $\varepsilon = 0.05$ and each map "fills" a simply connected subset of $\mathbb{R}^+$. The maps are conjectured to be asymptotically stable. b) $\varepsilon = 0.05$ and for all initial $(x, y) \in \mathcal{B}$, we numerically observe that $\Phi(x, y) \in \mathcal{D}$ and points in $\mathcal{D}$ are mapped into $\mathcal{B}$. This is an example of coupling induced statistical cycling.

The behavior displayed in Figure 2.1 can be summarized as follows: There are regions in the parameter space of system (2.1) with S given by (2.3) in which the individual maps are (numerically seen to be) statistically stable when they are decoupled (Figure 2.1a). When the coupling is turned on, ($\varepsilon > 0$), phase space densities cycle periodically, and they are supported on disjoint subsets of the phase space (as shown in Figure 2.1b). Points belonging to one subset are mapped into another at the next time step and so on. The period of the cycle depends on the parameters a, n and ε, while the details of the asymptotic cycle (*i.e.* the fraction of points belonging to various subsets) depend on the initial distribution of (x, y) pairs (the support of the initial density). This behavior should be interpreted in light of our discussion on asymptotically periodic Perron-Frobenius operators (*cf.* Section 1.4.5). We conjecture that Figure 2.1 illustrates coupling induced asymptotic periodicity of the Perron-Frobenius operator of Φ. If the coupling ε is increased further, the sets $\mathcal{B}$ and $\mathcal{D}$ of Figure 2.1 "break-up" (*i.e.* give rise to disconnected subsets) and the period of the density cycles increases. The dependence of this period on ε is complicated, and has not been studied in detail. We mention in passing that a recent publication by He and Li [74] explains the symmetry of the sets on Figure 2.1 using elegant group theoretic arguments which are also valid for larger lattices.

Before examining the analytically tractable tent map, we show that similar behavior is observed in coupled logistic maps. This is interesting since it suggests that the behavior presented above is probably generic in maps with a locally logistic maximum.

2.2.3 The logistic map

The logistic map is one of the most studied systems in the nonlinear dynamics literature. Here, we only review those aspects of its behavior connected with the presence of phase transitions. The main motivation for including this system in our discussion is that it reproduces the behavior displayed by the biologically motivated map of the previous example, while being much simpler analytically. The logistic map is defined in (2.4) and its Perron-Frobenius operator $\mathcal{P}_q$ is

$$\mathcal{P}_{\text{quad}} f(x) = \frac{1}{\sqrt{1-\frac{4x}{a}}} \left[f\left(\frac{1}{2} + \frac{1}{2}\sqrt{1-\frac{4x}{a}}\right) + f\left(\frac{1}{2} - \frac{1}{2}\sqrt{1-\frac{4x}{a}}\right) \right]. \qquad (2.11)$$

When $a = 4$, the Perron-Frobenius operator is asymptotically stable, and the density of the invariant measure is

$$f^*(x) = \frac{1}{\pi\sqrt{x(1-x)}}.$$

This is the only value of a for which the invariant density is known, although the existence of absolutely continuous invariant measures has been proven for a belonging to sets of positive Lebesgue measure [89]. There is, in addition, a spectrum of values labeled a_n, $n = 1, 2, \cdots$, where so-called banded chaos has been reported numerically [131]. At these values, the behavior of the iterates of the map is very similar to those of the tent map when it is asymptotically periodic: The phase space densities oscillate periodically in time. At the value $a = a_n$, the period of the density cycle is 2^n. The recipe for finding the a_n's is given in [71]. A proof of the asymptotic periodicity of $\mathcal{P}_{\text{quad}}$ at these values is not available yet, but the numerics clearly indicate that the so called "banded chaos" behavior in the logistic map is in fact asymptotic periodicity [173].

From (2.6) the expression for the Perron-Frobenius operator is

$$\mathcal{P}\mathbf{f}(x^1,x^2) = \frac{\partial^2}{\partial x^1 \partial x^2}\left\{\int_0^{\alpha^1(x^1,x^2)} du^1 + \int_{\beta^1(x^1,x^2)}^1 du^1\right\}\times\left\{\int_0^{\alpha^2(x^1,x^2)} \mathbf{f}(u^1,u^2)du^2 + \int_{\beta^2(x^1,x^2)}^1 \mathbf{f}(u^1 \tag{2.12}$$

where, by inverting (2.1) with S given by (2.4), we have

$$\alpha^i(x^1,x^2) = \frac{r(1-\varepsilon) - \sqrt{r^2(1-\varepsilon)^2 + 4r(1-\varepsilon)(\varepsilon\eta^i(x^j) - x^i)}}{2r(1-\varepsilon)} \tag{2.13}$$

$$\beta^i(x^1,x^2) = \frac{r(1-\varepsilon) + \sqrt{r^2(1-\varepsilon)^2 + 4r(1-\varepsilon)(\varepsilon\eta^i(x^j) - x^i)}}{2r(1-\varepsilon)} \tag{2.14}$$

$$\eta^i(x^j) = rx^j(1-x^j). \tag{2.15}$$

The two-dimensional version of Leibnitz's rule is

$$\frac{\partial^2}{\partial x^1\partial x^2}\int_0^a\int_0^b \mathbf{f}(u^1,u^2)du^2du^1 = \mathbf{f}(a,b)\left[\frac{\partial a}{\partial x^1}\frac{\partial b}{\partial x^2} + \frac{\partial a}{\partial x^2}\frac{\partial b}{\partial x^1}\right] + \frac{\partial^2}{\partial x^1\partial x^2}\int_0^a \mathbf{f}(u^1,b)du^1 + \frac{\partial^2}{\partial x^1\partial x^2}\int_0^b \mathbf{f}(a,u^2)du^2 \tag{2.16}$$

Expanding (2.12) yields

$$\mathcal{P}\mathbf{f}(x^1,x^2) = \frac{\partial^2}{\partial x^1\partial x^2}\int_0^{\alpha^1}\int_0^{\alpha^2} \mathbf{f}(u^1,u^2)du^2du^1$$

$$+\frac{\partial^2}{\partial x^1 \partial x^2}\int_1^{\beta^1}\int_1^{\beta^2}\mathbf{f}(u^1,u^2)du^2du^1$$
$$-\frac{\partial^2}{\partial x^1 \partial x^2}\int_0^{\alpha^1}\int_1^{\beta^2}\mathbf{f}(u^1,u^2)du^2du^1$$
$$-\frac{\partial^2}{\partial x^1 \partial x^2}\int_1^{\beta^1}\int_0^{\alpha^2}\mathbf{f}(u^1,u^2)du^2du^1. \qquad (2.17)$$

Applying (2.16) using (2.13-2.15), (2.17) becomes

$$\begin{aligned}
\mathcal{P}\mathbf{f}(x^1,x^2) \;=\; & \frac{1+\varepsilon^2 r^2(2x^2-1)(2x^1-1)}{\sqrt{r^2(1-\varepsilon)^2+4r(1-\varepsilon)(\varepsilon\eta^1(x^2)-x^1)}\sqrt{r^2(1-\varepsilon)^2+4r(1-\varepsilon)(\varepsilon\eta^2(x^1)-x^2)}} \\
& \times\left[\mathbf{f}(\alpha^1,\alpha^2)+\mathbf{f}(\beta^1,\beta^2)+\mathbf{f}(\alpha^1,\beta^2)+\mathbf{f}(\beta^1,\alpha^2)\right] \\
& +\frac{2r^2\varepsilon(1-\varepsilon)(2x^2-1)}{\{\sqrt{r^2(1-\varepsilon)^2+4r(1-\varepsilon)(\varepsilon\eta^1(x^2)-x^1)}\}^{3/2}}\left[\int_0^{\alpha^1}\mathbf{f}(u^1,\alpha^2)du^1-\int_0^{\alpha^1}\mathbf{f}(u^1,\beta^2\right. \\
& \left.+\int_1^{\beta^1}\mathbf{f}(u^1,\alpha^2)du^1-\int_1^{\beta^1}\mathbf{f}(u^1,\beta^2)du^1\right] \\
& +\frac{2r^2\varepsilon(1-\varepsilon)(2x^1-1)}{\{\sqrt{r^2(1-\varepsilon)^2+4r(1-\varepsilon)(\varepsilon\eta^2(x^1)-x^2)}\}^{3/2}}\left[\int_0^{\alpha^2}\mathbf{f}(\alpha^1,u^2)du^2-\int_0^{\alpha^2}\mathbf{f}(\beta^1,u^2\right. \\
& \left.+\int_1^{\beta^2}\mathbf{f}(\alpha^1,u^2)du^2-\int_1^{\beta^2}\mathbf{f}(\beta^1,u^2)du^2\right].
\end{aligned}$$

Checking for consistency, when $\varepsilon = 0$ and $r = 4$, this expression reduces to

$$\mathcal{P}\mathbf{f}(x^1,x^2)=\frac{1}{4\sqrt{1-x^1}}\frac{1}{4\sqrt{1-x^2}}\left[\mathbf{f}(\alpha^1,\alpha^2)+\mathbf{f}(\beta^1,\beta^2)+\mathbf{f}(\alpha^1,\beta^2)+\mathbf{f}(\beta^1,\alpha^2)\right], \qquad (2.19)$$

where

$$\begin{aligned}
\alpha^i &= \frac{1}{2}-\frac{1}{2}\sqrt{1-x^i} \\
\beta^i &= \frac{1}{2}+\frac{1}{2}\sqrt{1-x^i}.
\end{aligned}$$

As expected, the operator defined by (2.19) possesses an invariant density $f^*(x^1,x^2)$ given by

$$f^*(x^1,x^2)=\frac{1}{\pi\sqrt{x^1(1-x^1)}}\times\frac{1}{\pi\sqrt{x^2(1-x^2)}}. \qquad (2.20)$$

Although we have the exact expression for the Perron-Frobenius operator for two coupled logistic maps, a proof for asymptotic periodicity in this operator has remained out of reach. Hence we proceed with a numerical description of satistical cycling in the system.

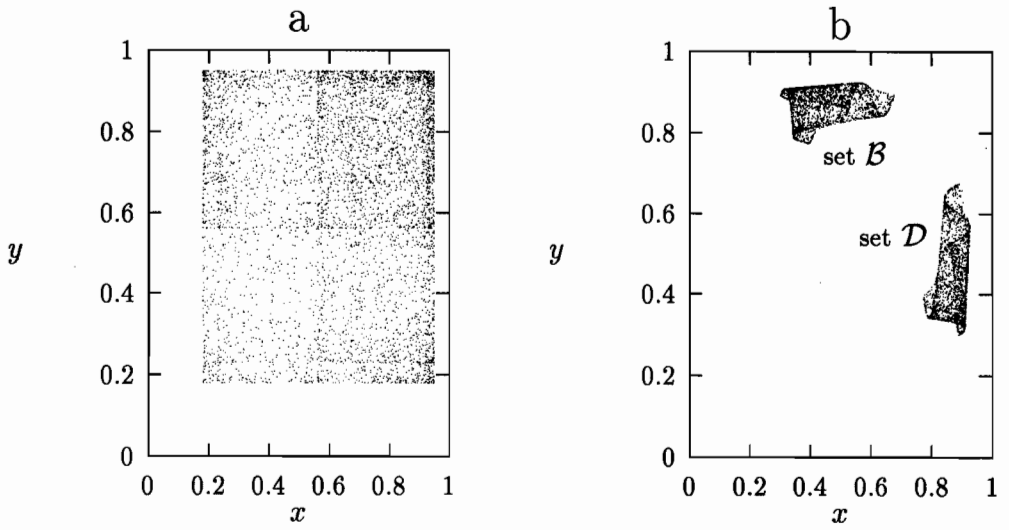

FIGURE 2.2:
Projection of the phase space density on the (x, y) plane for system (2.1) with the quadratic nonlinearity (2.4). In both panels, $a = 3.8$, time is $t = 6000$, the figure is made with 5000 pairs and the initial density was supported uniformly on $[0:1] \times [0:1]$. In a) the maps are decoupled: $\varepsilon = 0$; numerical simulations indicate that the system is asymptotically stable. b) $\varepsilon = 0.06$; the points in set $\mathcal{B}$ are mapped into set $\mathcal{D}$ and *vice versa* at every time step. This is clearly very similar to the behavior discussed in connection with the previous figure and is conjectured to reflect the underlying asymptotic periodicity of the Perron-Frobenius operator.

The behavior shown in Figure 2.2 is the same as that found in the sigmoidal map. It is presented here to highlight the fact that coupling induced statistical cycling is probably a generic property of maps with a logistic maximum. In fact, it also observed in a simpler system, the generalized tent map, which is topologically conjugate to the logistic map when $a = 2$, and which is analytically tractable.

2.3 Analytic investigation of two coupled tent maps

The one dimensional semidynamical system known as the tent map:

$$x_{n+1} = \begin{cases} ax_n & \text{if } x_n \in [0, 1/2] \\ a(1 - x_n) & \text{if } x_n \in [1/2, 1] \end{cases}$$

where $a \in (1, 2]$ has been extensively studied during the past decade, in part because the Perron-Frobenius equation can be solved explicitly at different values of the parameter a [224, 173]. The results which concern us here deal with the existence of critical values of the parameter a at which the thermodynamic state of (2.2) qualitatively changes. The Perron-Frobenius equation for the tent map (2.2) is

$$\mathcal{P}_{\text{tent}} f(x) = \frac{1}{a}\left[f\left(\frac{x}{a}\right) + f\left(1 - \frac{x}{a}\right)\right], \tag{2.21}$$

where $f(x)$ is a phase space density for the system. Depending on the value of the parameter a, $\mathcal{P}_{\text{tent}}$ can be proven to be either asymptotically stable or asymptotically periodic. To summarize its properties:

1) $a = 2$:

In this case $\mathcal{P}_{\text{tent}}$ is asymptotically stable and the invariant density is the uniform density on the phase space $[0, 1]$. [It is easy to check that $1_{[0,1]}(x)$ satisfies (2.21)].

2) $a \in (\sqrt{2}, 2)$:

$\mathcal{P}_{\text{tent}}$ is asymptotically stable, and the invariant density is supported on a simply connected subset of $[0, 1]$.

3) $a \in (2^{1/2^{n+1}}, 2^{1/2^n})$, $n = 1, \cdots$:

$\mathcal{P}_{\text{tent}}$ is asymptotically periodic, and the period of the density cycle is 2^n. The activity is supported on the union of 2^n disjoint subsets $J_1, \cdots, J_{2^n}$ each J_i being the support of one of the v_i's of Definition 1 (*cf.* (1.21) in Section 1.4.5).

We want to investigate to what extent this structure of the dynamics of the tent map survives diffusive coupling. To that effect, the phase diagram in (a, ε)-space is discussed in Section 2.3.1.

2.3.1 The phase diagram

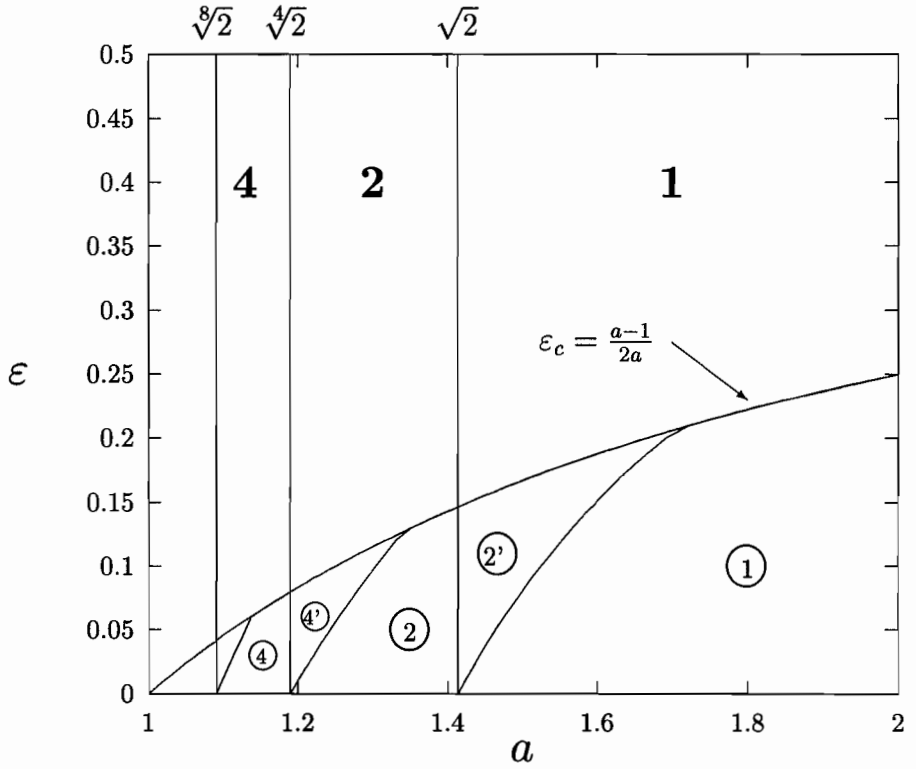

FIGURE 2.3:
Phase portrait of the map (2.1) with nonlinearity (2.2). In the upper regions labeled 1, 2 and 4 the map is one dimensional and respectively asymptotically stable (AS), asymptotically periodic with period 2 (AP-2) and period 4 (AP-4) (see Figures 2.4a,2.5a). In region (1) (2.1) is AS but now both λ_1 and λ_2 are > 1 (see Figure 2.4b). In region (2') Φ is AP-2, but x and y are *out of phase* (see Figure 2.2e and the text for details). In region (2) the map is AP-2, and x and y are either in phase or out of phase (see Figure 2.6a and the text for details).
In regions (4) and (4') the map is AP-4. Details concerning these regions are described in the section entitled AP-4 (see Figure 2.7). In regions (2') and (4') , the dynamics are not a trivial two dimensional generalization of one dimensional asymptotic periodicity, but rather *coupling induced.*

The phase diagram of the two dimensional system (2.1) with nonlinearity (2.2) naturally

separates into two major regions: In the first, which corresponds in Figure 2.3 to those areas labeled with non circled numbers, the behavior of Φ is effectively one dimensional since the flow is contracted along one of the eigendirections. In the second, which encompasses the areas of Figure 2.3 labeled with circled numbers, the behavior is truly two dimensional, since both eigendirections are unstable. The eigenvalues of the absolute value of the Jacobian of (2.1) with (2.2) satisfy the characteristic equation

$$((1-\varepsilon)a - \lambda)^2 - a^2 = 0 \tag{2.22}$$

which has 2 solutions

$$\lambda_1 = a \qquad \text{and} \qquad \lambda_2 = a(1-2\varepsilon). \tag{2.23}$$

When $\varepsilon \in ((a-1)/2a, (a+1)/2a)$, the dynamics are one dimensional since in this case $|\lambda_1| > 1$ and $|\lambda_2| < 1$. The behavior of (2.1) matches that of a single map and the upper portion of the phase diagram (Figure 2.3) describes the dynamics of (2.1).

We therefore focus on the regions such that $\lambda_2 > 1$. These regions are below the critical line $\varepsilon_c = (a-1)/2a$ in Figure 2.3. The solid lines on Figure 2.3 bound regions in which the the number of supports for the invariant density are fixed. We now describe each of these regions in detail.

2.3.1.1 Asymptotic stability.

Regions in which Φ is AS are labeled with a (1) and a "**1**" in Figure 2.3. In the region **1**, the dynamics are one dimensional since one of the eigendirections is contracting (*i.e.* $|\lambda_2| < 1$) and the other is expanding ($\lambda_1 > 1$). In this region, Φ is asymptotically stable, and $x = y$: The behavior is that of a single asymptotically stable tent map. Figure 2.4a displays the y *vs.* x plot for 8×10^3 points after 50 time steps. Initially, these points were uniformly distributed on $[0:1] \times [0:1]$. The boundary between **1** and (2') is the line $\varepsilon_c = (a-1)/2a$. The boundary between **1** and **2** is the value $a = \sqrt{2}$ (as in the one dimensional map). In the area labeled (1), the map is also AS, but now it is no longer effectively one dimensional. The plot y *vs.* x is given in Figure 2.4b, with the same initial conditions as in Figure 2.4a, but different ε. The coordinates of the vertices of the rhomboid are

$$\begin{aligned} V_0 &= (0,0) \\ V_1 &= \left([1 - \varepsilon + \frac{\varepsilon^2}{1-\varepsilon}](2-a), 2\varepsilon(2-a) \right) \end{aligned}$$

$$
\begin{aligned}
V_2 &= (1,1) \\
V_3 &= \left(2\varepsilon(2-a), [1-\varepsilon+\frac{\varepsilon^2}{1-\varepsilon}](2-a)\right).
\end{aligned} \tag{2.24}
$$

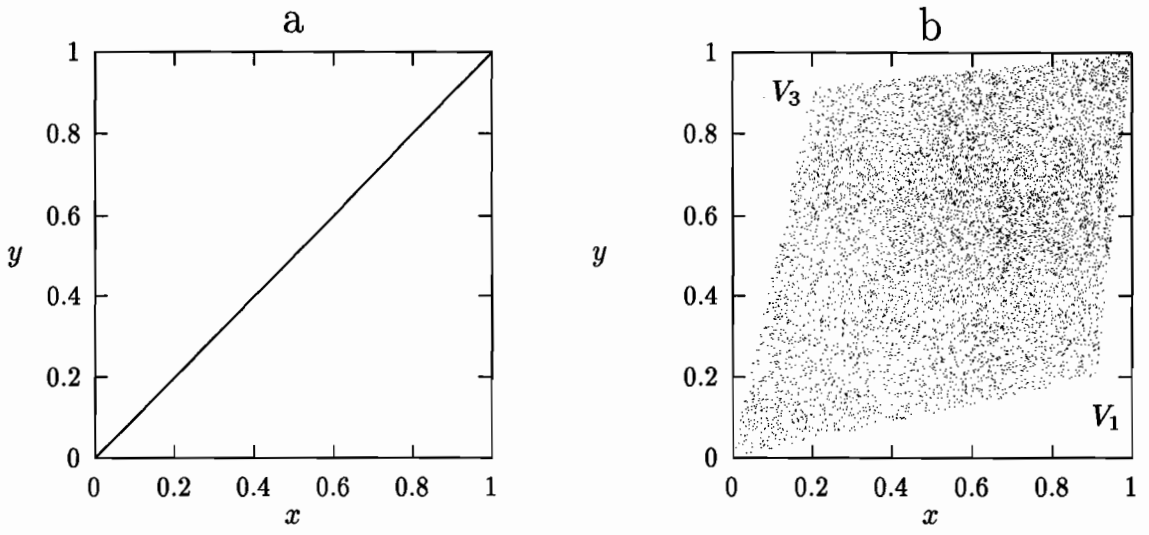

FIGURE 2.4:
Activity of the map Φ on the unit square. In a), $a = 1.6$ and $\varepsilon = 0.35$ (system is in region 1), hence $x = y$ eventually. In b), $a = 1.7$, $\varepsilon = 0.1$ so the parameters are such that the map is in region (1) . The vertices of the rhomboid are $V_0, \cdots, V_3$ given in (2.24). Both a) and b) were obtained numerically, using an ensemble of 8×10^3 initial conditions initially uniformly distributed on $[0,1] \times [0,1]$.

2.3.1.2 Asymptotic periodicity: period 2.

This behavior is observed in the three regions labeled **2**, (2) and (2') . In **2**, the behavior is again one-dimensional. The activity on $[0,1] \times [0,1]$ is plotted in Figure 2.5a, and is supported on two disjoint subsets of the diagonal $x = y$. The boundaries of this region are: The value $a = \sqrt{2}$, the value $a = 2^{1/4}$ and the line $\varepsilon_c = (a-1)/2a$.

Region (2)

The boundaries of region (2) are the line $\varepsilon_c = (a-1)/2a$, the value $a = \sqrt{2}$ and the line separating it from region (4') which will be discussed in Section 2.3.1.3. For parameter values in (2) , the behavior is statistically periodic with period 2: all points belonging to set $\mathcal{A}$ (in Figure 2.5b) at time t^* map into points belonging to $\mathcal{C}$ at time $t^* + 1$ and *vice versa*. This "flipping" behavior between two sets with disjoint supports, characteristic of

asymptotic periodicity, is also observed for sets $\mathcal{B}$ and $\mathcal{D}$. Every point belonging initially to the unit square is asymptotically attracted to one of these four sets. Furthermore, the images of a point belong to $\mathcal{A} \bigcup \mathcal{C}$ or $\mathcal{B} \bigcup \mathcal{D}$, but do not flip between these. Schematically

$$\cdots \longmapsto \mathcal{A} \longmapsto \mathcal{C} \longmapsto \mathcal{A} \longmapsto \cdots$$
$$\cdots \longmapsto \mathcal{B} \longmapsto \mathcal{D} \longmapsto \mathcal{B} \longmapsto \cdots$$

The behavior observed in region (2) is easily understood by noting that for such values of a the tent map is itself AP-2. The period 2 flipping described above therefore arises from the underlying asymptotic periodicity of the tent map. In other words, if ε were 0, one would obtain a picture rather close to that illustrated by Figure 2.5b (in fact, in that case, a y *vs.*x plot yields four square projection sets instead of the four rhomboids of Figure 2.5b). Cycle $(\mathcal{ACA})$ can be called the *in phase* cycle, and the other, $(\mathcal{BDB})$, *out of phase.* We will see later that the out of phase cycles can be stable in regions of parameter space where the in phase cycle is not. This is the origin of the coupling induced statistical periodicity observed in regions (2') and (4') . The activity observed in Figure 2.5b is sensitive to the initial distribution of points in the sense that if all initial points were included in the preimage of $\mathcal{A}$, all points would "flip" from set $\mathcal{A}$ to set $\mathcal{C}$ and back. Thus, the proportion of points which at time t^* are in set $\mathcal{A}$ depends in a sensitive way on the initial preparation. It is straightforward to derive analytic expressions for the edges of the four sets. For clarity, only the out of phase cycle is considered, and the expression for the coordinates of the edges of sets $\mathcal{B}$ and $\mathcal{D}$ are given in Appendix 2A (see also Figure 2.6b).

The region (2')

We now turn to the description of a novel type of dynamics, which is not a trivial two-dimensional generalization of the asymptotic periodicity well studied in 1-d maps.

In region (2') the activity of the pair (x, y) can be described as asymptotic periodicity (although again this is an observation which does not stem from an investigation of the spectral decomposition of the 2-d Perron-Frobenius operator). The supports of the 2-d density on $[0{:}1]^2$ are disjoint as demonstrated in Figure 2.6a. These supports are symmetrical with respect to the $x = y$ line, and every point belonging to one support at time t^* belongs to the other at time $t^* + 1$ and *vice versa.* These supports form the *out of phase* cycle $\mathcal{BDB}$ discussed previously, the *in phase* cycle $\mathcal{ACA}$ now being unstable. Coordinates of the vertices of set $\mathcal{B}$ displayed in Figure 2.6b are given in Appendix 2A.

These vertices of $\mathcal{B}$ map onto the boundary of the set $\mathcal{D}$. When $\varepsilon = (a-1)/2a$, the critical value for which $\lambda_2 = 1$, the points β_0 through β_7 (and all the points in $\mathcal{B}$) collapse

onto the single point with coordinates

$$\left(\frac{(a^2+1)}{a(a+1)}, \frac{(a-1)}{a}\right).$$

[similarly, the points in $\mathcal{D}$ collapse onto its mirror image with respect to the $x = y$ axis, and the activity on $[0,1] \times [0,1]$ is then concentrated on the diagonal, as illustrated in Figure 2.5a.]

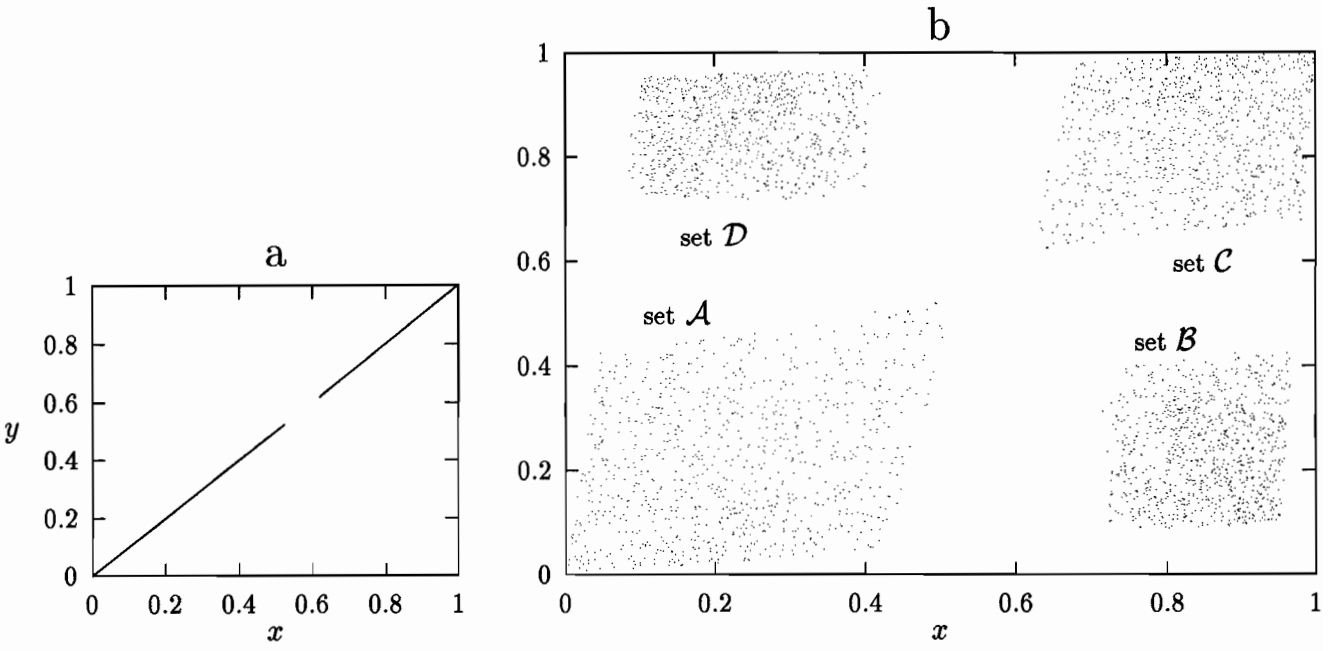

FIGURE 2.5:
Two dimensional projection of the phase space density for two coupled tent maps at time $t = 6000$. The figure was made with 5000 points. In a), $a = 1.38$ and $\varepsilon = 0.35$ (so (a, ε) is in region 2). All points on the left of the gap at time t^* are mapped into points on the right of the gap at time $t^* + 1$ and *vice versa*. In b) $a = 1.38$ and $\varepsilon = 0.05$ (again (a, ε) is in region 2). All points in $\mathcal{A}$ at time t^* map into points belonging to $\mathcal{C}$ at time $t^* + 1$ and *vice versa*. This flipping also occurs for sets $\mathcal{B}$ and $\mathcal{D}$ (see text for details).

The condition on the parameters a and ε such that the set $\mathcal{B}$ maps into $\mathcal{D}$ and *vice versa* is obtained by performing a two dimensional version of the calculation which yields the value $a = \sqrt{2}$ separating AP-2 and AP-4 in the one dimensional tent map, given for example in [224, 173]. The point whose image under Φ is the closest to the diagonal $x = y$ is β_1 (see Figure 2.6b). We call this image β_1^1. Its image under Φ, $\beta_1^2 = \Phi^2(\beta_1)$, lies within set $\mathcal{B}$

when the map is in region (2') *i.e.* when $\mathcal{B} \longmapsto \mathcal{D} \longmapsto \mathcal{B}$. When the map is in region (1) , β_1^2 does not lie within set $\mathcal{B}$ but above the line segment $[\beta_5, \beta_6]$ (Figure 2.6 should prove useful to follow this geometrical digression). In other words, points which are in $\mathcal{B}$ do not necessarily return to $\mathcal{B}$ after two iterations under Φ in (2) . Instead, they "fill up" the rhomboid displayed in Figure 2.4b. At the boundary between (1) and (2') , β_1^2 crosses the line segment $[\beta_5, \beta_6]$. Mathematically, this gives the following relation:

$$\Phi^2(\beta_1)^y = \beta_5^y,$$

or, explicitly,

$$(a(2\varepsilon - 1) + 1)\left[a^3(4\varepsilon(\varepsilon - 1) + 1) + a^2(2\varepsilon(1 - 2\varepsilon)) - 2a((1 - 2\varepsilon) + 1)\right] = 0 \qquad (2.25)$$

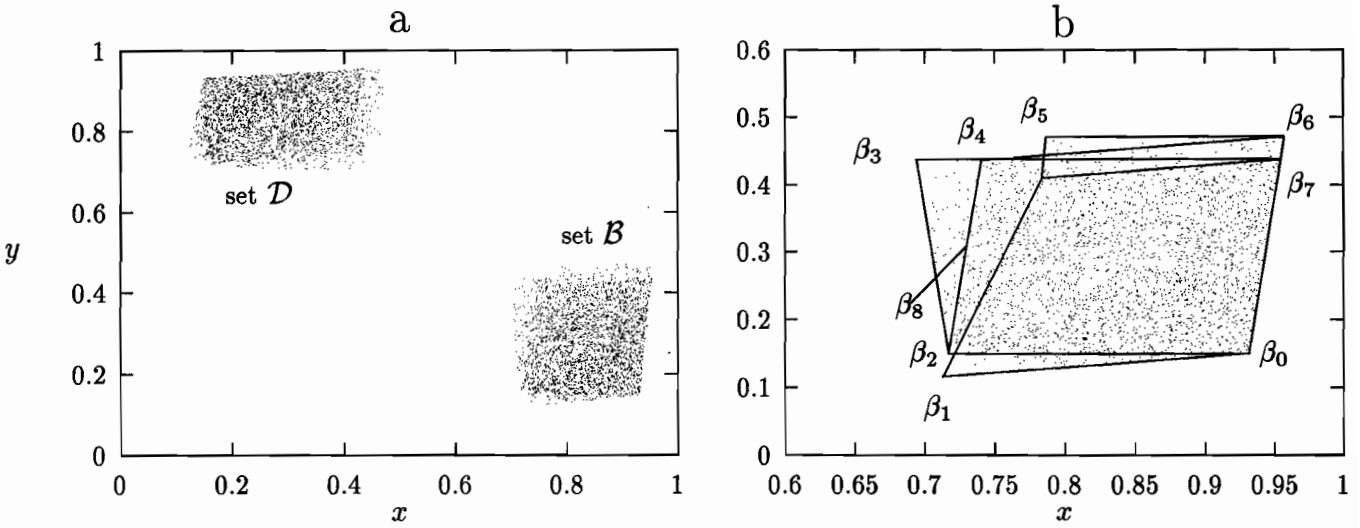

FIGURE 2.6:
Two dimensional projection of the phase space density for two coupled tent maps at time $t = 6000$. The figure was obtained with 5000 points. a) $a = 1.45$ and $\varepsilon = 0.075$ so the system is in region (2') , with initial conditions uniformly distributed on $[0, 1] \times [0, 1]$. b) The lines link the vertices given in Appendix 2A, plotted for $a = 1.45$ and $\varepsilon = 0.075$ superimposed with the data of panel a).

Equation (2.25) can be solved for a as a function of ε analytically since it is a fourth order polynomial in a. We do not give the solution, but note that when $\varepsilon = 0$, the four solutions $a_{c,1\cdots,4}$ are

$$a_{c,1} = 0,\ a_{c,2} = 1,\ a_{c,3,4} = \pm\sqrt{2}.$$

The root $a_{c,3} \equiv \sqrt{2}$ corresponds to the condition given by Provatas and Mackey for the one dimensional case [173]. In addition, when $a \in [1,2]$ all the roots are real. Two of these are irrelevant since they correspond to $\varepsilon \notin [0,1]$ and the other two delimit the region (2') of Figure 2.3. Note that one of the roots coincides with the previously obtained condition $\varepsilon_c = (a-1)/2a$ since

$$a_{c,2} = \frac{1}{1-2\varepsilon} \tag{2.26}$$

is one of the solutions of (2.25) for all a and ε.

The behavior illustrated in Figure 2.6 can be described as *coupling induced statistical cycling* since the individual maps are asymptotically stable when $(a,\varepsilon) \in$ (2') . We conjecture that it reflects the asymptotic periodicity of the Perron-Frobenius operator for this system. A "period 4 version" of this phenomenon is observed numerically in (4') , and is discussed in Section 2.3.1.3.

2.3.1.3 Asymptotic periodicity: period 4

As in the one dimensional case, there is period 4 statistical cycling in the coupled map system. The behavior in region (4) is illustrated in Figure 2.7.

It is possible to give an analytic expression for the boundary separating regions (2) and (4') There are many different equivalent ways to obtain this expression, but each of these involves determining the conditions on a and ε such that points belonging to an element of a cycle (an "element" being one of the four disjoint sets forming a cycle) return to that element after 4 iterations under Φ. One point whose trajectory yields the desired critical condition has coordinates

$$\begin{aligned} \beta_8^x &= \frac{\varepsilon(a-1)}{a(1-\varepsilon)} - \frac{4\varepsilon(1-a(1-\varepsilon^2)) - 2 + a}{1-\varepsilon} \\ \beta_8^y &= \frac{a-1}{a}. \end{aligned} \tag{2.27}$$

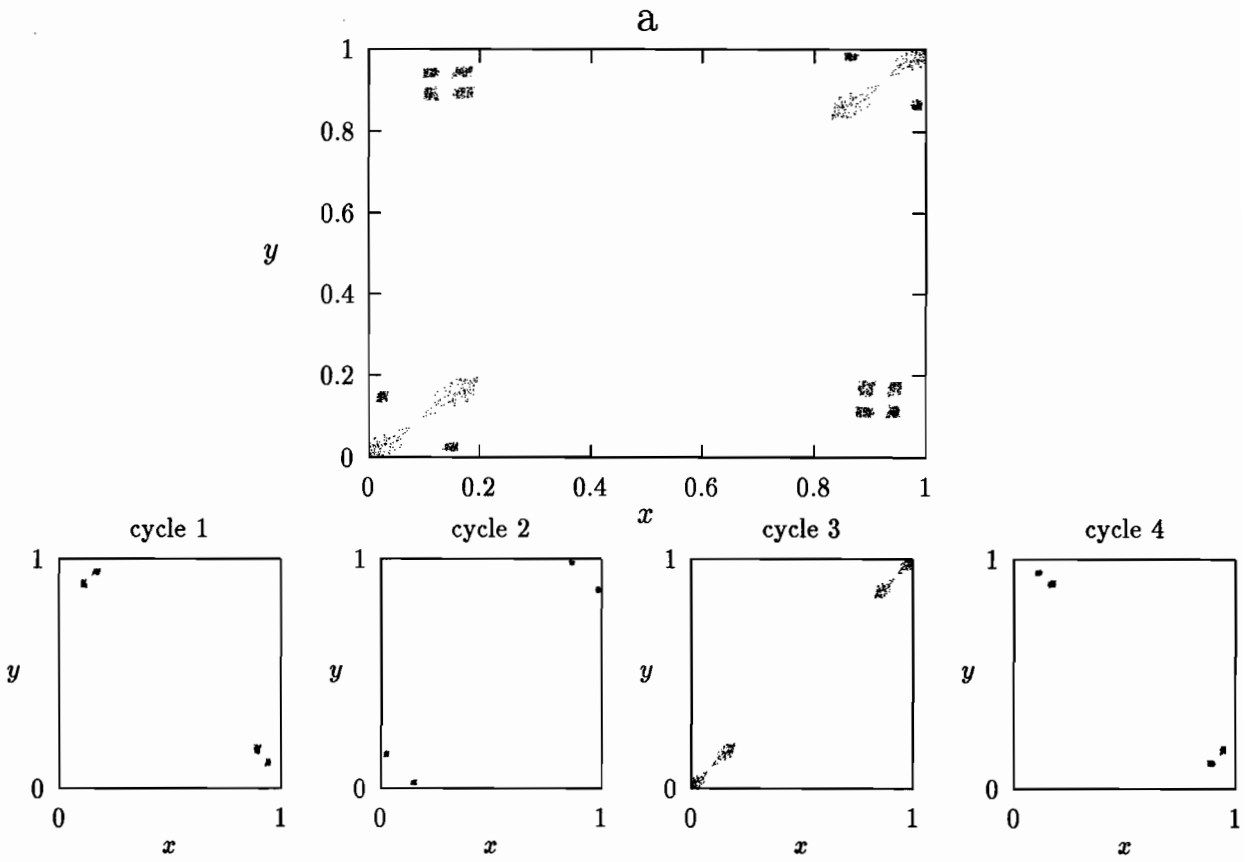

FIGURE 2.7:
Two dimensional projection of the phase space density for two coupled tent maps. $a = 1.17$ and $\varepsilon = 0.05$ (*i.e.* the system is in region (4)). The 16 disjoint supports shown in panel a) can be grouped into the four separate cycles of period 4 shown in the bottom panels. Points belonging to one cycle remain in this cycle. All points of the unit square eventually settle onto one of the cycles. The top panel was produced with 5000 pairs initially uniformly distributed in $[0,1]\times[0,1]$, and shows a snapshot of the activity at time $t = 200$. To obtain each of the four bottom panels, the initial points were uniformly distributed in a set belonging to one cycle, and each panel is the superimposition of four snapshots taken at four consecutive time steps $t = 200, \cdots, 203$.

Following the images of this point under Φ, it can be shown geometrically that the condition analogous to (2.25) is given by

$$\Phi^3(\beta_8)^x = \Phi^8(\beta_8)^y \tag{2.28}$$

which explicitly yields

$$a(2\varepsilon-1)\left[a(2\varepsilon-1)+1\right] \times \left[a^7(16\varepsilon^4+12\varepsilon^2(1-2\varepsilon)-2\varepsilon)\right.$$

$$+a^5(-8\varepsilon^2(1-\varepsilon)+2\varepsilon)+a^4(4\varepsilon(1-\varepsilon)-1)+2\Big] = 0 \quad (2.29)$$

The above is a ninth order polynomial in a. One of its roots is, as for condition (2.25)

$$a_{c,2} = \frac{1}{1-2\varepsilon}. \quad (2.30)$$

It is not possible to give the expression for the other roots but we note that at $\varepsilon = 0$, (2.29) becomes a sixth order polynomial with roots

$$a_{c,1,3} = \pm 2^{1/4},\ a_{c,4,5} = \pm i 2^{1/4},\ a_{c,5} = 1,\ a_{c,6} = 0.$$

The root $2^{1/4}$ corresponds to the condition given in [173] for the one dimensional transition between period 2 and period 4 asymptotic periodicity. The boundary between regions (2) and (4'), plotted in Figure 2.3, is the analytic curve $a_{c,1}(\varepsilon)$, determined from (2.29), for $\epsilon \in [0, 1/4]$.

In region (4') the in phase cycle (cycle 3 of Figure 2.7) disappears: this is analogous to the disappearance of the sets $\mathcal{A}$ and $\mathcal{C}$ (displayed in Figure 2.5) in region (2'). The "period 8 version" of this phenomenon, as well as the boundary between period 4 and period 8 statistical cycling is discussed in Appendix 2B.

2.3.1.4 Asymptotic periodicity of higher period:

We conclude the investigation of the phase diagram of the map Φ (Figure 2.3), by noting that one can numerically observe higher order bifurcations which correspond to the transitions from AP-8 to AP-16, and by conjecturing that transitions from asymptotic periodicity of period 2^n to asymptotic periodicity of period 2^{n+1} can probably be observed for all n. In other words, numerical studies strongly suggest that the one dimensional picture given in [173] essentially survives diffusive coupling, in the sense that there is a period doubling of the density cycles as the slope of the tent map is lowered from 2 to 1, but that it is modified by the appearance of coupling induced regions in which the behavior is not a straightforward generalization of the one dimensional behavior (two of which, labeled (2') and (4') are shown on Figure 2.3.

2.3.2 On the evolution of statistical quantifiers

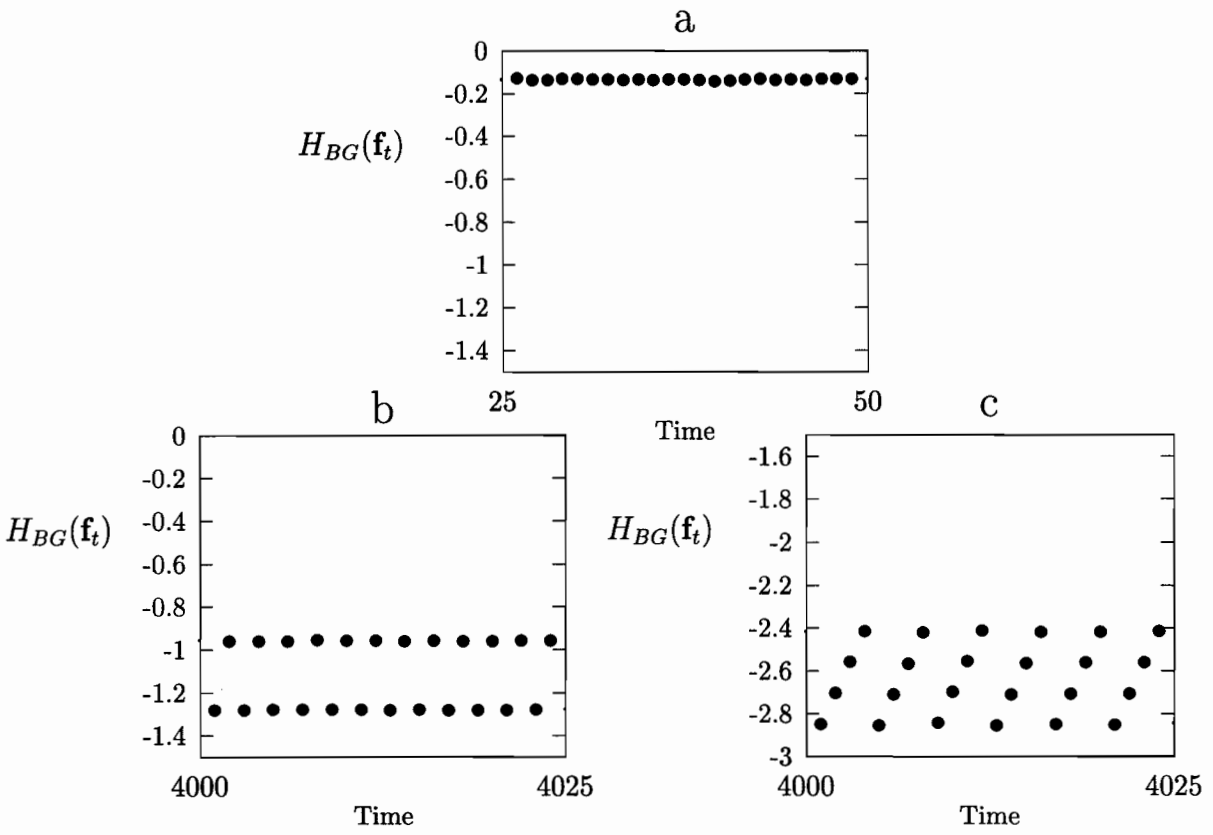

FIGURE 2.8

Three types of asymptotic behavior of the Boltzmann-Gibbs entropy (2.7). a) The map Φ is in region (1) : $a = 1.85$, $\varepsilon = 0.1$. b) The map Φ is in region (2) : $a = 1.45$, $\varepsilon = 0.075$. c) The map Φ is in region (4) : $a = 1.16$, $\varepsilon = 0.05$. In all three cases, the initial values of x_1 and x_2 were uniformly distributed on the set $[0.3, 0.4] \times [0.8, 0.9]$.

In this section, the evolution of the Boltzmann-Gibbs entropy for the tent map is discussed in the various regions of parameter space. The purpose of this discussion is to illustrate the oscillatory behavior of statistical quantifiers usually computed with the respect to an invariant density for equilibrium systems, in the presence of asymptotic periodicity[2].

The cycling displayed in Figure 2.8 is observed after transients were appropriately discarded: If the entropy behavior is seen to be the same for 10^4 time steps, then it is assumed that the asymptotic regime has been reached. In Figure 2.8a, the level reached by the en-

[2]The two coupled tent maps are not rigorously proven to be asymptotically periodic, but the analytical evidence provided in this chapter strongly indicates that they are.

tropy after about 10 iterations (for this particular initial condition) was the level at which the entropy was found after 10^4 iterations. The asymptotic cycling of H_{BG} in Figures 2.8b and 2.8c, reflects the fact that the Boltzmann-Gibbs entropy is not the quantity to which the Second Law of Thermodynamics applies for most asymptotically periodic system (or, more generally, for most dynamical systems).

2.4 Discussion

In this chapter, we have numerically observed that for the sigmoidal map, and the logistic map, the diffusive coupling of two chaotic but statistically stable elements can yield a system which shows periodic cycling of phase space densities, which we call "coupling induced statistical cycling". We conjecture that this behavior is a generic property of maps with a logistic maximum.

Using geometrical considerations, the analytic phase diagram for two diffusively coupled tent maps is constructed, and it is seen that the one dimensional bifurcation structure of the Perron-Frobenius operator essentially survives diffusive coupling, modulo the appearance of regions in parameter space in which the behavior is not a straightforward two dimensional generalization of the one dimensional behavior. We conjecture that the two dimensional Perron-Frobenius operator is asymptotically periodic when the one dimensional operator is, *but* that there are regions in parameter space in which the one dimensional systems have asymptotic periods differing from the coupled system.

This leads us to trace the origin of phase transitions in the coupled map system to qualitative changes in the spectral properties of the transfer operator. The techniques used in this paper to describe asymptotic periodicity are not easily extendable to larger systems, because the geometrical insight is rapidly lost as the number of maps coupled together increases.

Hence, when considering large CML's, it is necessary to introduce specific conceptual tools to describe the spectral properties of the N-dimensional Perron-Frobenius operator. This is the program of the next chapter, where we use general results from ergodic theory in higher dimensions to describe asymptotic periodicity (and phase transitions) in large coupled map lattices.

Appendix 2B

There is a region in parameter space in which the behavior is the period 8 analogue of that already described in regions (2') and (4') : The attractor on the unit square is a collection of 56 disjoint sets, forming 7 independent cycles of period 8 each[3]. The boundary between region (8') and region (4) is given by the following criterion:

$$\Phi^{13}(\beta_8)^x = \Phi^9(\beta_8)^x. \tag{2B-1}$$

Mathematically, the condition is

$$\begin{aligned}\left[a^2(2\varepsilon-1)+1\right]\left[a(2\varepsilon-1)+1\right] \times \; & \Big[a^{11}(256\varepsilon^8-896\varepsilon^7+1408\varepsilon^6-1280\varepsilon^5+736\varepsilon^4 \\ & -280\varepsilon^3+72\varepsilon^2-12\varepsilon+1) \\ & +a^8(-64\varepsilon^6+160\varepsilon^5-176\varepsilon^4+104\varepsilon^3-32\varepsilon^2+4\varepsilon) \\ & +a^3(8\varepsilon^3-12\varepsilon^2+8\varepsilon-2)-2\varepsilon\Big]=0. \end{aligned} \tag{2B-2}$$

It is possible to factor the above polynomial into an eighth degree polynomial in ε and two monomials, so that two of the roots can be written explicitly:

$$a_{c,1}=\frac{1}{1-2\varepsilon},\quad a_{c,2}=\frac{1}{\sqrt{1-2\varepsilon}}. \tag{2B-3}$$

The boundary drawn in Figure 2.3 between regions (8) and (8') shows $a_{\max}(\varepsilon)$ where $a_{\max}$ is the largest of the 12 other roots. When the coupling $\varepsilon = 0$, the 14 roots of the polynomial are:

$$\text{roots}: \pm 1, 1, 0, 0, 0, \pm 2^{1/8}, 2^{1/8}\left(\frac{1}{2}2^{1/2} \pm i\frac{1}{2}2^{1/2}\right), 2^{1/8}\left(-\frac{1}{2}2^{1/2} \pm i\frac{1}{2}2^{1/2}\right), \pm i2^{1/8}.$$

The root $2^{1/8}$ corresponds to the condition given in [173] for the transition from period 4 to period 8 AP in the one dimensional map.

[3]Since the behavior is period 8, one would expect 8 independent cycles yielding 64 disjoint supports, but one of these, the in-phase cycle is not observed, an observation already made in the period 2 and period 4 regimes.

Chapter 3

Statistical properties of deterministic coupled map lattices.

ABSTRACT

This chapter describes the statistical properties of large coupled map lattices. Transitions separating statistically stable and periodic phases are numerically observed in generic models of reaction-diffusion systems and excitable media. The transitions are studied in lattices of piecewise linear expanding maps by considering the spectral properties of the Perron-Frobenius operator acting on functions of bounded variation in $\mathbb{R}^n$, and using basic results from the theory of linear operators. Analytic phase diagrams for various models studied in the literature are presented.

Evolution... is a change from an indefinite incoherent homogeneity to a definite coherent inhomogeneity.

Herbert Spencer, *First Principles*

3.1 Introduction

Having studied in some detail the properties of the smallest CML's in Chapter 2, it is now natural to focus our attention on the larger lattices presented in the introduction. One of the conclusions of the previous chapter was that a class of phase transitions in the two-dimensional maps could be explained in terms of qualitative changes in the spectral properties of the Perron-Frobenius operator. The numerical evidence presented here will lead us to the conclusion that this is also the case in larger lattices. To butress this conclusion theoretically, it is necessary to introduce some techniques to deal with the Perron-Frobenius operator in high dimensions. We develop these techniques and apply them to a variety of systems discussed in the literature.

As mentioned in the introduction of the thesis, the presence of statistical cycling in coupled map lattices has been studied in some detail by Chaté and Manneville (*cf.* Section 3.2.2 of [31], and [32]), and by Binder and Privman [13]. Similar phenomena have also been observed by Gallas *et al.* [60], and Chaté and Manneville [30] in various cellular automata. In these references, the statistical cycling is referred to as "noisy periodicity", "quasiperiodicity" or "periodicity in the mean". This chapter contains the first analytical description of this phenomenology.

The variety of models framed as CML's precludes a general description of *all* these systems. Some are chaotic in time and space, others only in one of these dimensions, while others are periodic in one or both. Finally, and these are the most troublesome from our point of view, some models possess stable fixed point solutions (*i.e.* for which the activity of the lattice is time-invariant). These can be of interest from a modeling perspective, but they are not amenable to simple statistical treatment, because stable steady states tend to give rise to pathological probability densities. To avoid these difficulties, we restrict our attention in the remainder of this chapter to finite dimensional models which possess bounded nonstationnary solutions.

The transitions described here occur between statistically different regimes, which are referred to as "phases": a spatiotemporally chaotic phase in which the statistical quantifiers can be computed with respect to a unique absolutely continuous invariant measure, and another phase characterized by the cyclical evolution of phase space densities. The former regime is never associated with the evolution of large scale patterns, but in the statistically cycling phase, one can often observe the appearance of clusters of strongly correlated activity. The relation between the formation of these clusters and the presence of statistical cycling has been noted by some investigators [74], but it is not fully understood. We discuss some preliminary conclusions at the end of the chapter (*cf.* Section 3.8).

We motivate our analysis with a numerical description of the collective behavior of lattices of coupled tent and logistic maps in Section 3.2. Section 3.3 extends this numerical work to a class of biologically motivated CML's which are models of excitable media. In Section 3.5, we present the notion of variation in $\mathbb{R}^n$, and use it to discuss a classic result on the spectral properties of linear operators acting on embedded Banach spaces. Sections 3.6-3.7 present applications of this analysis to various models.

3.2 Lattices of logistic and tent maps

We begin our description of CML phenomenology by focusing on systems of the form (1.2) with periodic boundary conditions. When $p = 4$, the coupling in (1.2) is said to be diffusive, whereas when the p-neighbourhood encompasses all sites of the lattice, the coupling is referred to as mean field. In this section, we restrict our attention to two maps already discussed in the previous chapter, namely the logistic map, and the generalized tent map.

The tent map

$$S(x) = \begin{cases} ax & \text{if } x \in [0, 1/2) \\ a(1-x) & \text{if } x \in [1/2, 1] \end{cases} \quad 1 < a \leq 2. \tag{3.1}$$

is considered here because there is strong numerical evidence of asymptotic periodicity in large regions of the (a, ε) plane when it is coupled as in (1.2). Finally, the piecewise linear nature of the CML allows one to explicitly compute the eigenvalues of the absolute value of the derivative transformation, and carry out calculations efficiently in Section 3.6. In addition, the Perron-Frobenius operator induced by (3.1) was described by Shigematsu and Mori [224] and Provatas and Mackey [173] and the following results on asymptotic periodicity

are available:

$$2^{1/2^{n+1}} < a \leq 2^{1/2^n} \iff \begin{array}{c}\text{asymptotic periodicity}\\ \text{of}\\ \text{period } 2^n,\end{array} \quad n = 0, 1, 2, \cdots. \tag{3.2}$$

The results of Chapter 2 showed that this structure essentially survived intact in two coupled maps, and we are interested in studying its analogue in N coupled maps.

The other system which will be considered here is the CML (1.2) with the local nonlinearity given by the logistic map:

$$S(x) = ax(1-x), \quad r \in (3, 4]. \tag{3.3}$$

When $a < a_\infty \simeq 3.5699...$, and the map is locally periodic, the CML possesses stable spatiotemporal orbits (*i.e.* like the "coherent structures" discussed in [3, 177]). Each lattice site then eventually settles onto a periodic cycle, and the lattices reach frozen spatial structures consisting of domains which contain different phases in the cycles (this behavior was first reported by Kaneko [95]). We do not focus on this kind of evolution because it does not require the introduction of probabilistic tools for its discussion. At $a_c \simeq 3.57\cdots$, the bifurcation to chaos occurs beyond the period doubling scenario, and there are values of $a \in (a_c, 4]$ such that the local map possesses various types of chaotic behavior. The motivation for including the chaotic logistic map in this discussion is that when it is locally chaotic it is shown to display much of the behavior displayed by the simpler tent map, therefore leading us to the conjecture that the phase transitions explored here are to be expected generically in large classes of systems which are not necessarily everywhere expanding.

For fixed lattice sizes, the parameters describing the evolution are a, related to the local nonlinearity, and the coupling parameter ε. Two different sets of numerical experiments can therefore be carried out. The first involves changing a while keeping the coupling ε constant, and the second involves changing the coupling ε while the local nonlinearity parameter remains fixed.

3.2.1 Numerical investigations

Figure 3.1 displays nine panels, each of which is a snapshot of the activity of the tent map lattice after a transient of 10^5 iterations has been discarded. The coupling is constant in the figure and the parameter which is being changed is the slope a. Two qualitatively different types of behaviors are observed. The first is characterized by the evolution of large

scale patterns from the random initial conditions; this is the clustered, or ordered state $a = 1.1, \cdots, 1.5$. The panel $a = 1.3$ presents an interesting limiting case for which the "cluster" covers the entire area of the lattice; different initial conditions for such parameter values evolve to the more usual large scale patterns. We should mention here that the lattices are not at equilibrium in the panels displayed in this figure. It is not possible to observe the true equilibrium because of the astronomically large transients typical of a lattice of 40000 elements. The point of our investigation is not to describe explicitly the presence, stability and asymptotic behavior of the patterns presented here, but to understand how the thermodynamics of these lattices should be investigated. Although the problem of pattern formation in CML's is fascinating, it is not the focus of our investigation, and we will therefore not spend more time discussing the pattern dynamics *per se*. The interesting observation from our point of view is that the pattern-forming behavior associated with small values of a is also accompanied by statistical cycling in the lattice. This is illustrated by the behavior of various statistical quantifiers of the motion discussed below, rather than by the snapshots of Figure 3.1.

The second phase is characterized by the absence of discernable patterns, but more importantly, it is described statistically by a unique invariant measure generated by almost all initial conditions (again, more on this below). This corresponds to the spatiotemporally chaotic state described rigorously by Bunimovich and Sinai [21] in infinite lattices. Figure 3.2 displays the activity of a lattice of 200×200 logistic maps coupled diffusively. The top three panels illustrate the behavior of the lattice in the statistically cycling region, while the bottom three illustrate the fully turbulent and statistically stable regions. Note the absence of large scale patterns even in the asymptotically periodic regime, in marked contrast to the tent map lattice.

LEGEND FOR FIGURE 3.1(next page):

Snapshots of the activity at the surface of a 200×200 lattice of diffusively coupled tent maps when the coupling is constant ($\varepsilon = 0.45$) but the local slope is increased from $a = 1.1$ to $a = 1.9$. For all panels, the transient discarded is of length 10^5. The 256 grey scales range from black when $x^{i,j} = x_{min}$ to white when $x^{i,j} = x_{max}$ where x_{min} and x_{max} are the lower and upper bounds of the attracting subinterval of $[0, 1]$ respectively. The initial values on the lattice were in all cases given by a random number generator yielding uniform distributions on the unit interval. The transition from statistical cycling to statistical equilibrium occurs between $a = 1.5$ and $a = 1.6$ for this value of the coupling. This observation is not made from Figure 3.1 but with the help of the statistical quantifiers of the motion described below (*cf.* Figures 3.4, 3.5 and 3.6). The time evolution for the $a = 1.3$ case looks very much like the evolution of the top three panels in Figure 3.2 for the logistic map. For other statistically cycling cases, the light shades of grey are mapped into darker shades and *vice versa* at each time step. The bottom three panels display fully developped turbulence. They have reached their asymptotic state.

LATTICE OF 200^2 TENT MAPS. COUPLING IS $\varepsilon = 0.45$ 256 GREY SCALES: WHITE $\Longleftrightarrow$ 1; BLACK $\Longleftrightarrow$ 0

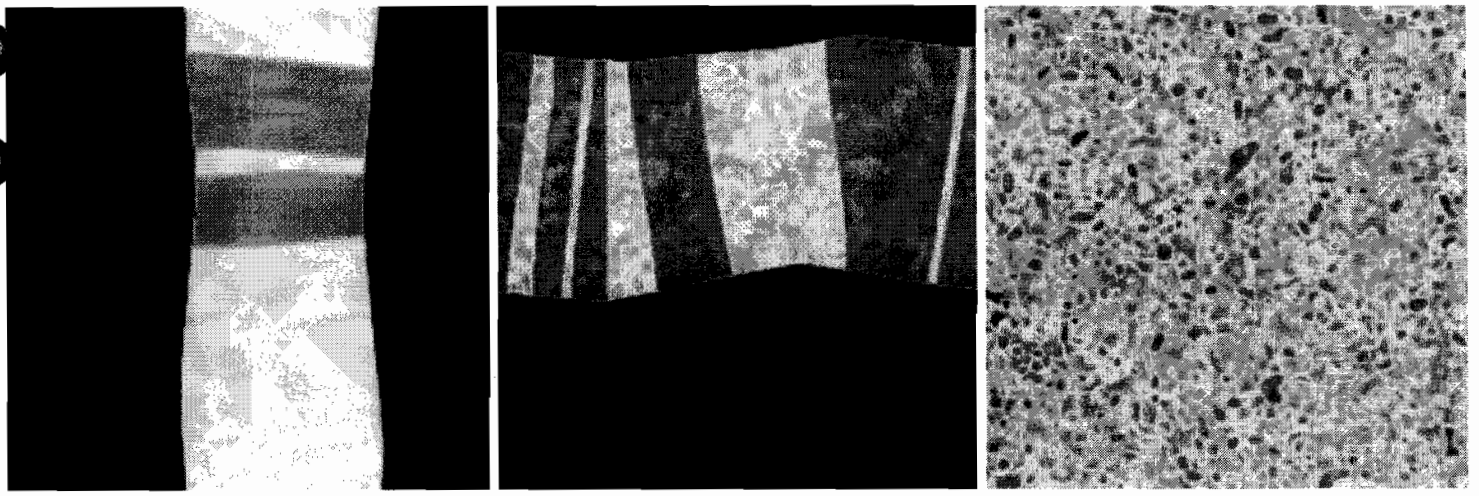

FROM LEFT TO RIGHT: $a = 1.1$, $a = 1.2$, $a = 1.3$

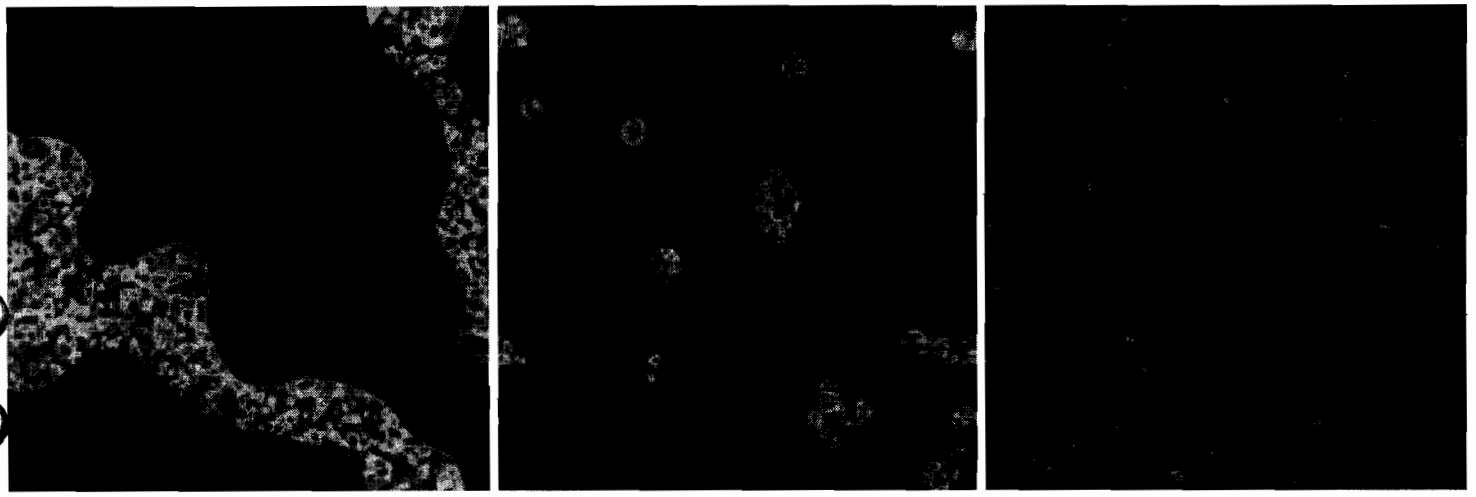

FROM LEFT TO RIGHT: $a = 1.4$, $a = 1.5$, $a = 1.6$

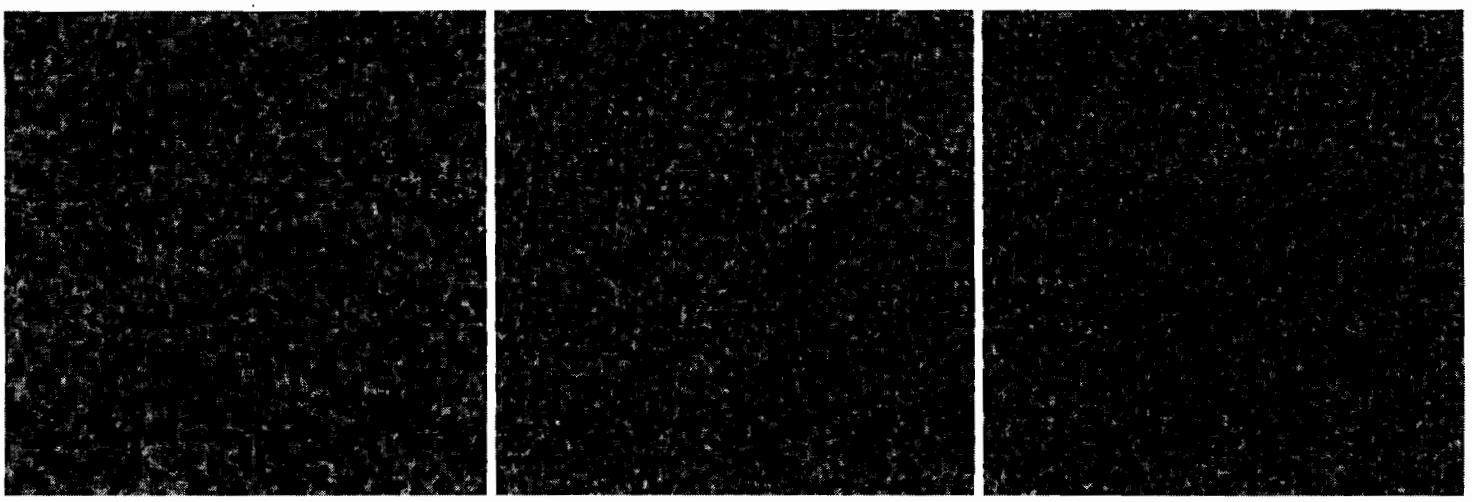

FROM LEFT TO RIGHT: $a = 1.7$, $a = 1.8$, $a = 1.9$

FIGURE 3.1

LEGEND FOR FIGURE 3.2(next page):

The six panels display two phases of a 200×200 lattice of coupled logistic maps with $\varepsilon = 0.45$. 10^5 transient iterations are discarded. *Top:* the system is statistically periodic with period 2, and $r = 3.678$. The evolution is reminiscent of that already observed in the tent map lattice with $a = 1.3$ and $\varepsilon = 0.45$. It is of interest to note that logistic map lattices were not observed numerically to form large scale patterns in the AP region, when the initial preparations did not contain any spatial information. This is in contrast with the pattern forming behavior of the tent map lattices. *Bottom:* the system is fully turbulent, and the parameter $r = 3.9$. For other parameter value, cycles of period 3 can also be observed in the lattice. In all cases, the exact asymptotic cycle depends on the initial preparation of the system, a property expected in an asymptotically periodic dynamical system.

LATTICE OF 200^2 LOGISTIC MAPS. 256 GREY SCALES: WHITE $\Longleftrightarrow$ 1; BLACK $\Longleftrightarrow$ 0

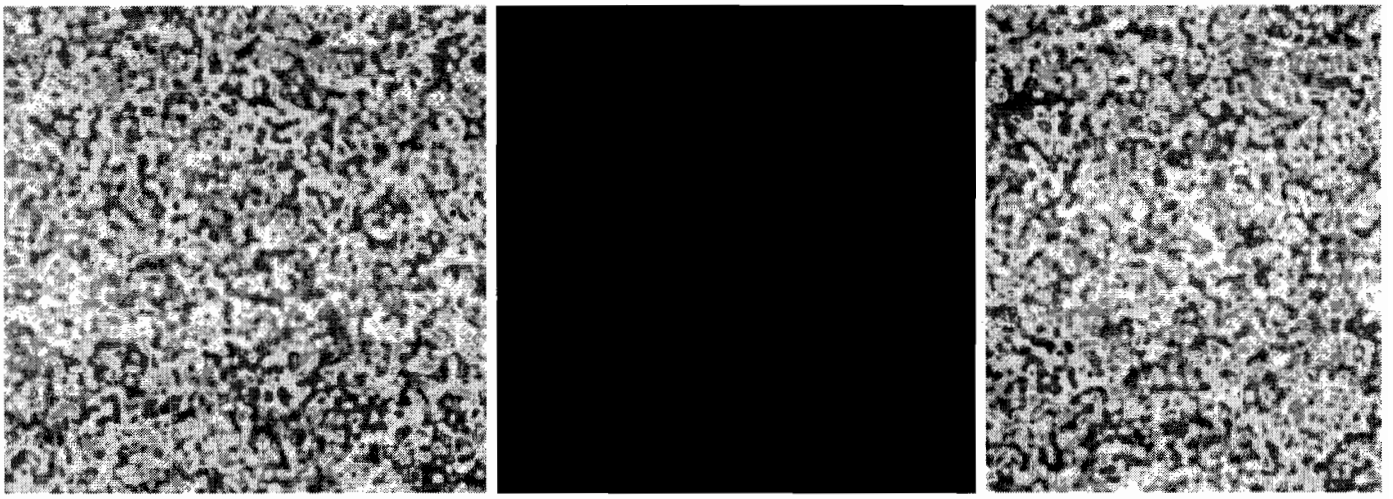

FROM LEFT TO RIGHT: $t = 10^5$, $t = 10^5 + 1$, $t = 10^5 + 2$

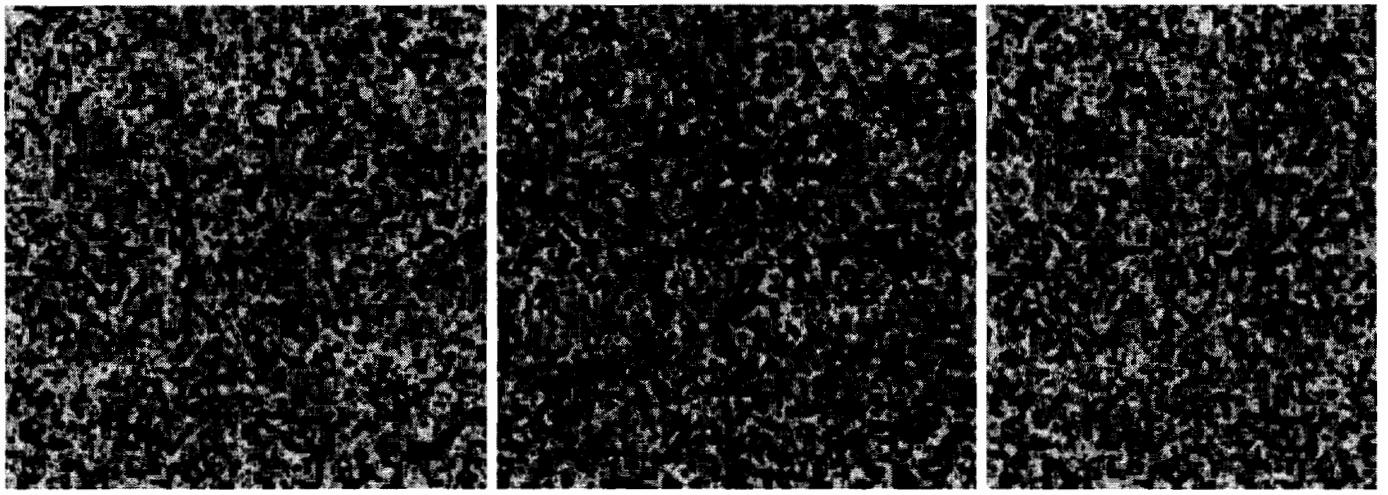

FROM LEFT TO RIGHT: $t = 10^5$, $t = 10^5 + 1$, $t = 10^5 + 2$

FIGURE 3.2

We now discuss the second set of numerical experiments which involves studying the evolution of the lattice when the slope is fixed but the coupling is varied. Figure 3.3 displays a transition from statistical stability to statistical cycling in the tent map CML when the slope is $a = 1.5$ as the coupling is increased from 0 to 1. When the coupling is 0, it follows from the results in [173] that the lattice will possess a unique invariant measure which will be reached for almost all initial preparations, because the local map possesses this property. For low values of the coupling, an invariant measure is also reached numerically, and this result is consistent with the analytical investigations of Keller and Künzle [109] and Rand and Gundlach [72]. When the coupling is increased (for $a = 1.5$), there is a critical value ε_c above which the lattice no longer reaches statistical equilibrium. Rather it reaches the "ordered" phase, characterized by cyclical statistical behavior. This statistical cycling is therefore coupling-induced, and it is the generalization to higher dimensions of the phenomenon described in the previous chapter in two dimensional maps.

Sometimes it is a nontrivial task to decide to which state a particular panel belongs to by simply looking at the activity of the lattice. To this end, we characterize the two phases with the help of statistical quantifiers which behave qualitatively differently depending on the phase of the lattice.

LEGEND FOR FIGURE 3.3(next page):
Snapshots of the activity of a 200×200 lattice of tent maps with a slope $a = 1.5$. The transients discarded are of length 10^5 in each panel. At low values of the coupling, the lattice generates an invariant measure for almost all initial preparations, and displays fully developped spatiotemporal chaos. At values of $\varepsilon > \varepsilon_c$, the lattice possesses an invariant measure, but it is almost never observed numerically. Instead, the phase space densities evolve to a periodic cycle which depends on the initial density. This reflects the coupling-induced asymptotic periodicity of the Perron-Frobenius operator for the lattice. The critical value of the coupling, is $\varepsilon_c \simeq 0.2$ when $a = 1.5$. The time evolution of the lattice in the bottom three panels is similar to the "flipping" shown at the top of Figure 3.2

LATTICE OF 200^2 TENT MAPS. SLOPE IS $\varepsilon = 1.5$ 256 GREY SCALES: WHITE $\Longleftrightarrow$ 1; BLACK $\Longleftrightarrow$ 0

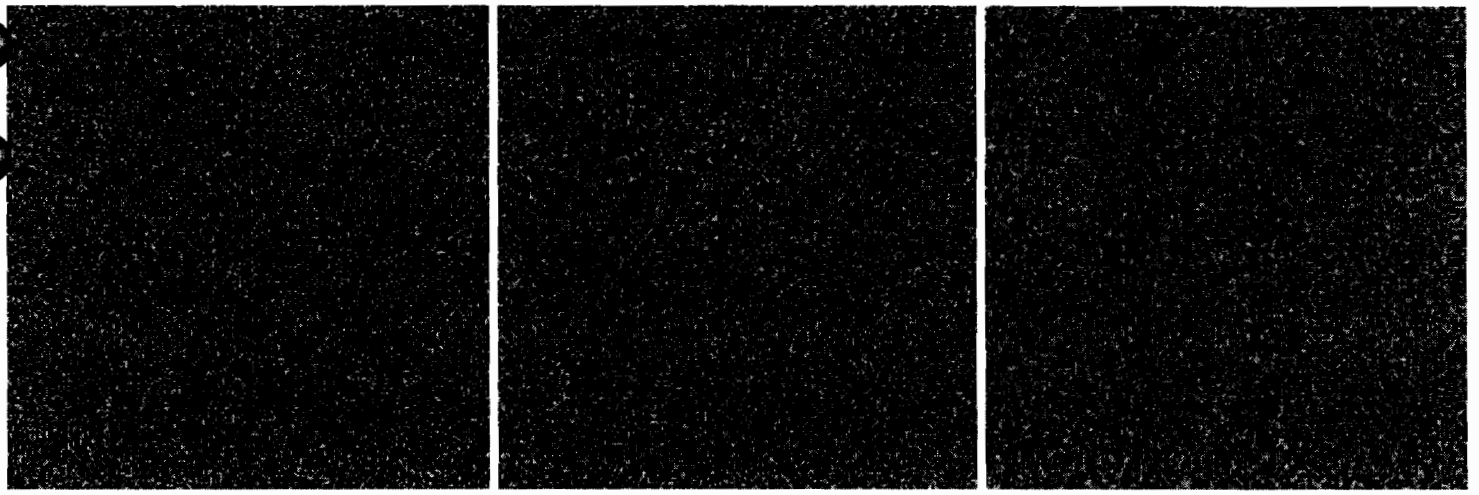

FROM LEFT TO RIGHT: $\varepsilon = 0.05$, $\varepsilon = 0.1$, $\varepsilon = 0.15$

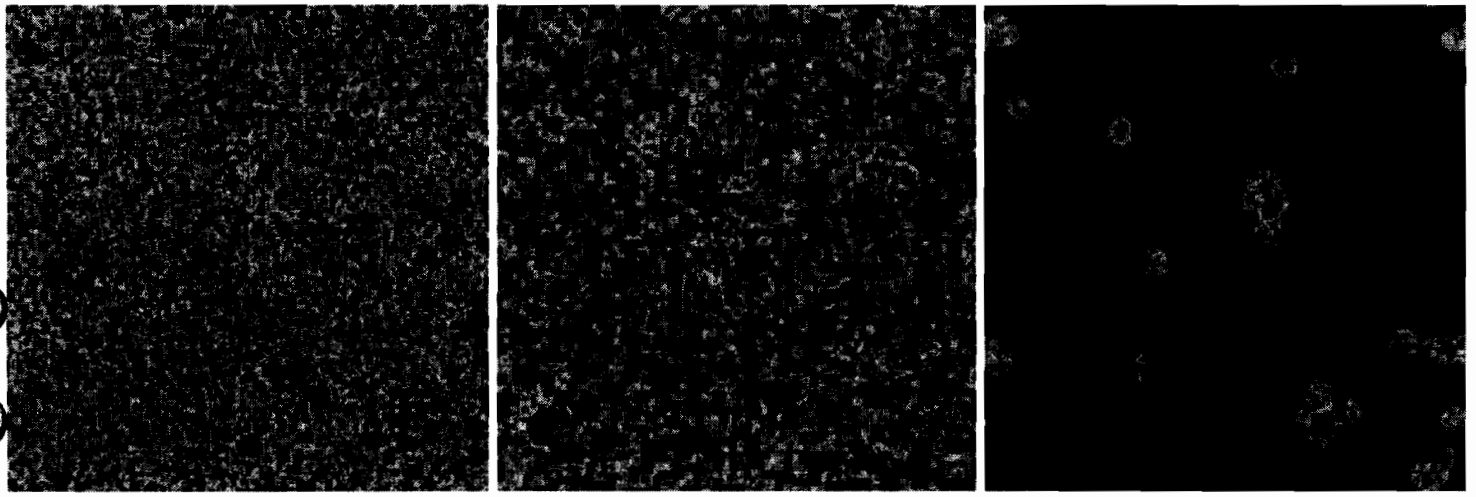

FROM LEFT TO RIGHT: $\varepsilon = 0.25$, $\varepsilon = 0.35$, $\varepsilon = 0.45$

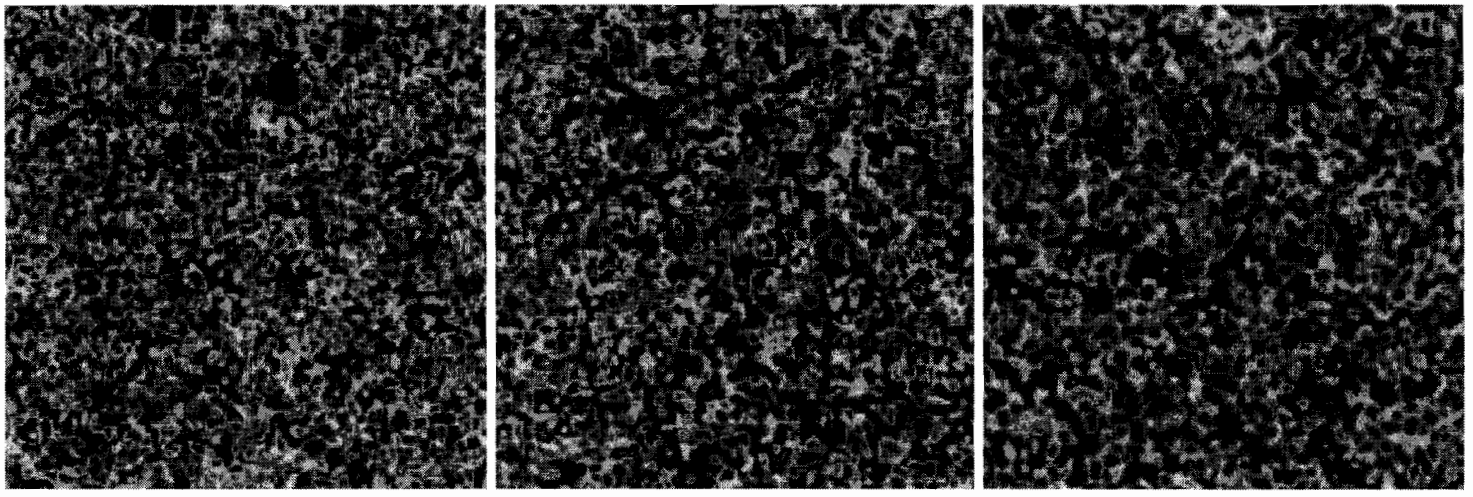

FROM LEFT TO RIGHT: $\varepsilon = 0.55$, $\varepsilon = 0.65$, $\varepsilon = 0.85$

FIGURE 3.3

3.2.1.1 The "collapsed density"

The collapsed density is the density of activity on a lattice at time t. Let $\mathbf{f}(\mathbf{x}_t)$ denote the phase space density for the lattice (1.2), where $\mathbf{x}_t = (x_t^{0,0}, \cdots, x_t^{N,N})$ is the state of the lattice. This density clearly cannot be represented graphically, and it is numerically expensive to obtain when working with large lattices. We therefore approximate its "collapsed version"

$$\mathbf{f}_t^c(z) = \int \cdots \int \mathbf{f}(\mathbf{x}) \prod_{i,j} \delta(x_t^{i,j} - z) dx^{i,j} \tag{3.4}$$

with the density f_t^c of activity across a single lattice defined implicitly by

$$\langle x_t \rangle = \frac{1}{N^2} \sum_{i,j} x_t^{i,j} \times f_t^c(x_t^{i,j}), \tag{3.5}$$

where $\langle \cdot \rangle$ denotes the average of the quantity inside the brackets. The purpose of this reduction is to characterize the two phases of the CML efficiently and unambiguously, and f_t^c is appropriate for this task. In addition, it is easy to show that if f_t^c is stationary in time, then $\mathbf{f}$ is *almost surely* stationary, while if f_t^c cycles, $\mathbf{f}$ must cycle. By *almost surely*, we simply mean that it is possible to initialize a lattice such that the cyclical behaviors of groups of sites on the lattice (a group consisting in a number of sites not necessarily spatially close) cancel each other's cycling on average, so that f_t^c does not reflect the behavior of $\mathbf{f}$. This situation is not expected to be observed for typical preparations of finite size lattices, because it is not "robust": A slight statistical perturbation of the initial preparation will almost surely (in the space of initial densities) yield a preparation such that the groups of sites do not cancel anymore, and therefore $\mathbf{f}$ and f_t^c will both be time periodic. Therefore f_t^c gives an efficient tool for studying certain properties of $\mathbf{f}$, and its behavior is illustrated in Figures 3.4 and 3.5.

LEGEND FOR FIGURE 3.4(next page):
The collapsed density f_t^c for a 200×200 lattice of diffusively coupled tent maps with $\varepsilon = 0.45$. The first 10^5 iterations are discarded as transients. In a) the cycle is of period 4, and $a = 1.3$. The initial density was uniformly distributed on $[0.3 : 0.4]$. In b) the cycle is of period 2, $a = 1.4$ and the initial density was uniformly distributed on $[0, 1]$. In c) the parameters are as in b) with an initial density supported on $[0.39 : 0.43]$. Note, as in Figure 3.1 the dependence of the asymptotic cycle on the initial density. d) The slope of the map is $a = 1.99$ and the initial density is $[0, 1]$. This density is numerically reached for all initial densities. Here the system is "fully turbulent", or "spatio-temporally chaotic".

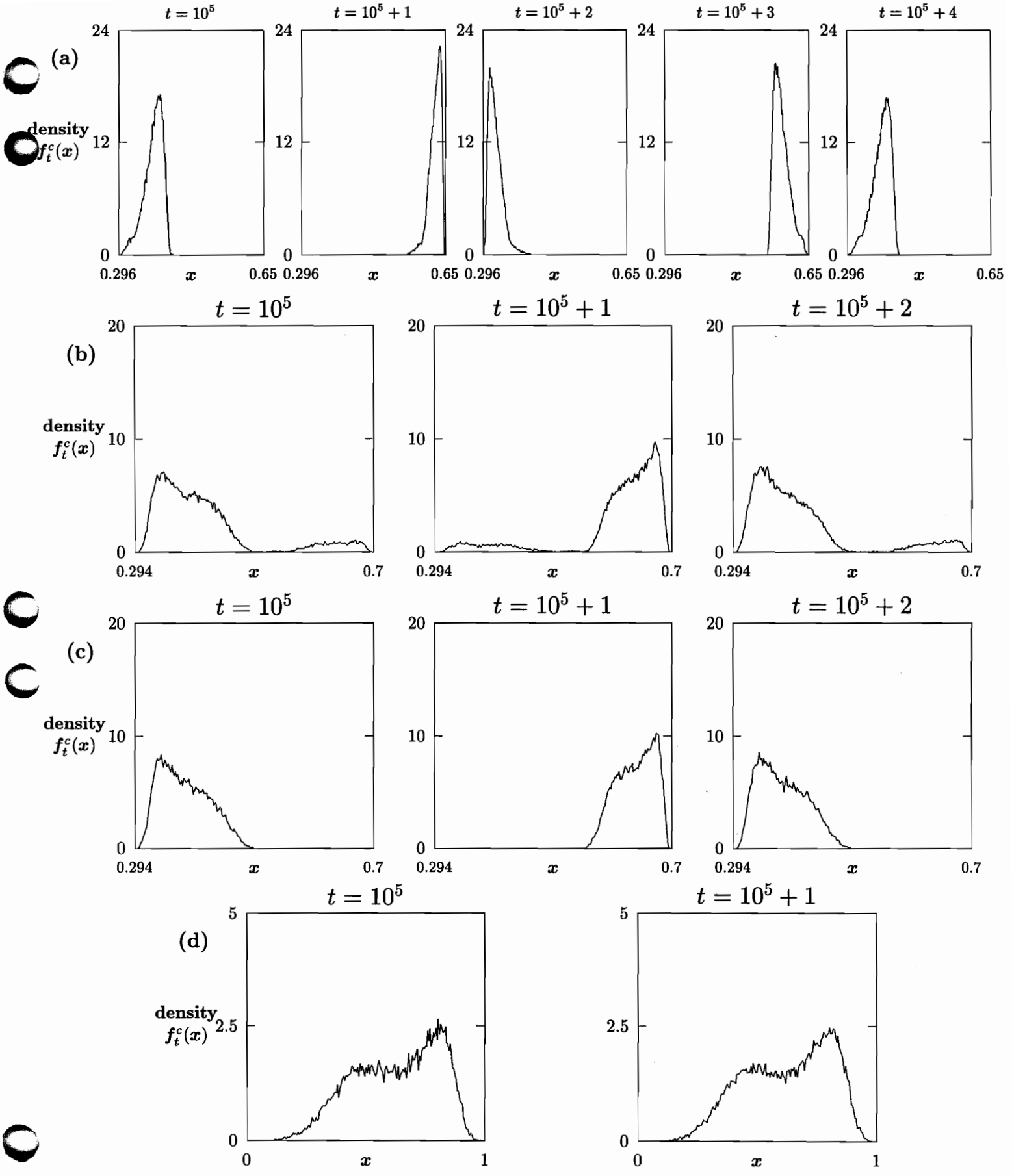
(a)
$t = 10^5$
$t = 10^5 + 1$
$t = 10^5 + 2$
$t = 10^5 + 3$
$t = 10^5 + 4$
density $f_t^c(x)$
24
12
0
0.296
x
0.65
(b)
$t = 10^5$
$t = 10^5 + 1$
$t = 10^5 + 2$
density $f_t^c(x)$
20
10
0
0.294
x
0.7
(c)
$t = 10^5$
$t = 10^5 + 1$
$t = 10^5 + 2$
density $f_t^c(x)$
20
10
0
0.294
x
0.7
(d)
$t = 10^5$
$t = 10^5 + 1$
density $f_t^c(x)$
5
2.5
0
0
x
1

FIGURE 3.4

LEGEND FOR FIGURE 3.5(next page):

The collapsed density f_t^c for a 200×200 lattice of logistic maps. In a) a cycle of period 2, obtained with $r = 3.678$ and an initial density uniformly supported on $[0, 1]$. In b) same parameters but an initial density uniformly supported on $[0.2 : 0.4]$. It should be noted that the cycle reached is, for both of these initial conditions the same one, modulo a phase difference. The fact that at each time the density is supported on a simply connected set reflects the absence of patterns on the logistic map lattice. Compare this "flipping" of densities with the behavior shown in the top panels of Figure 3.2. In c), $r = 3.99$ and the system numerically reaches the invariant density for all initial densities.

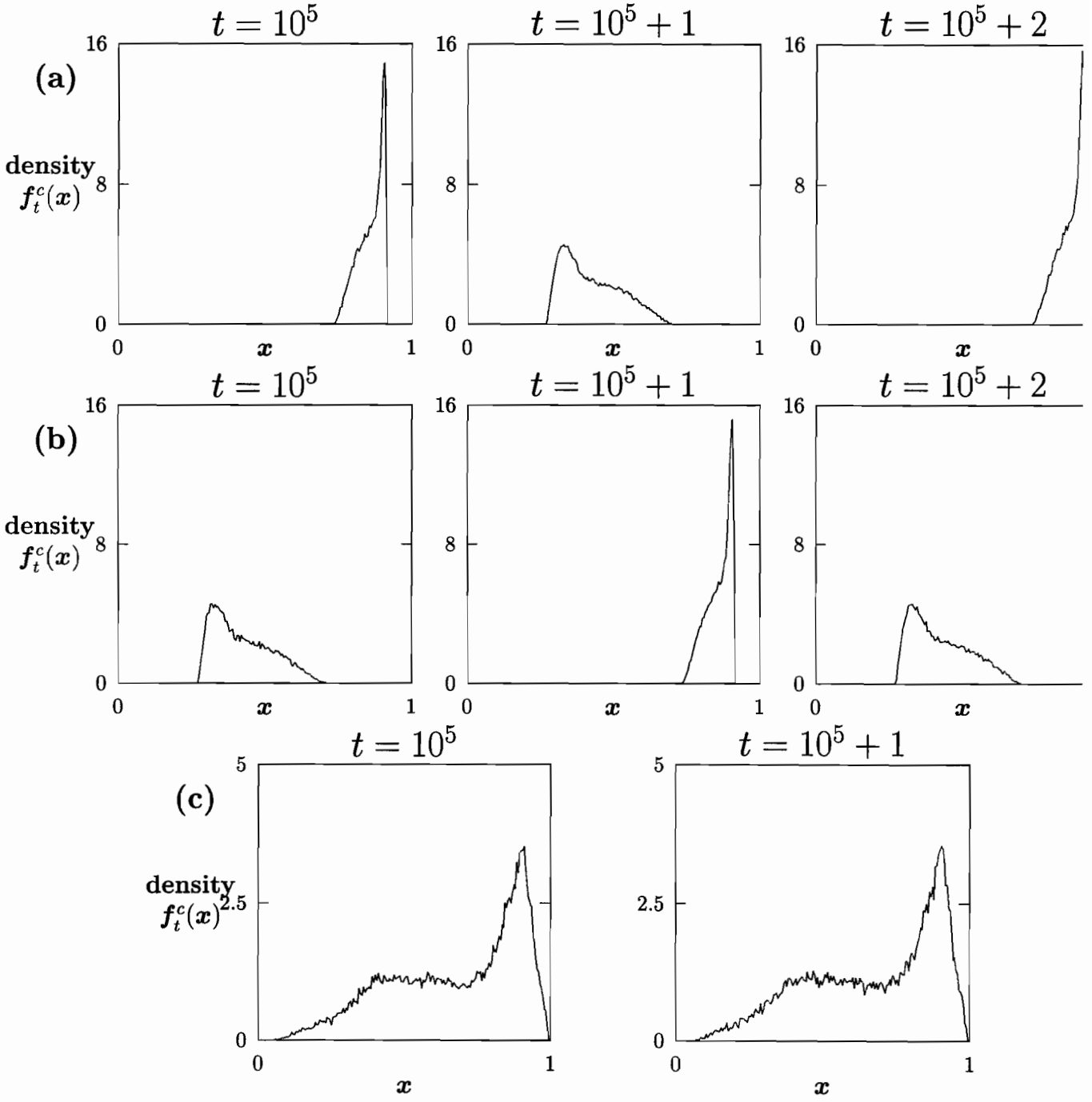
(a)
$t = 10^5$
$t = 10^5 + 1$
$t = 10^5 + 2$
density $f_t^c(x)$
16
8
0
0
1
x
(b)
$t = 10^5$
$t = 10^5 + 1$
$t = 10^5 + 2$
density $f_t^c(x)$
16
8
0
0
1
x
(c)
$t = 10^5$
$t = 10^5 + 1$
density $f_t^c(x)$
5
2.5
0
0
1
x

FIGURE 3.5

The previous figures display the evolution of f_t^c when the lattices are either in the statistically periodic or in the statistically stable regimes. As mentioned above, the temporal behavior of f_t^c reflects that of **f**. Hence the previous figures lead us to the conclusion that **f** cycles in time. This conclusion is corroborated by the analysis of Section 3.6, where we conditions on a and ε which are sufficient to guarantee the cycling of **f**.

When the cycling in the collapsed density is difficult to discern visually, studying the Boltzmann-Gibbs entropy of f_t^c (defined in Chapter 2) highlights either stationary behavior or cycling behavior, as illustrated by Figure 3.6.

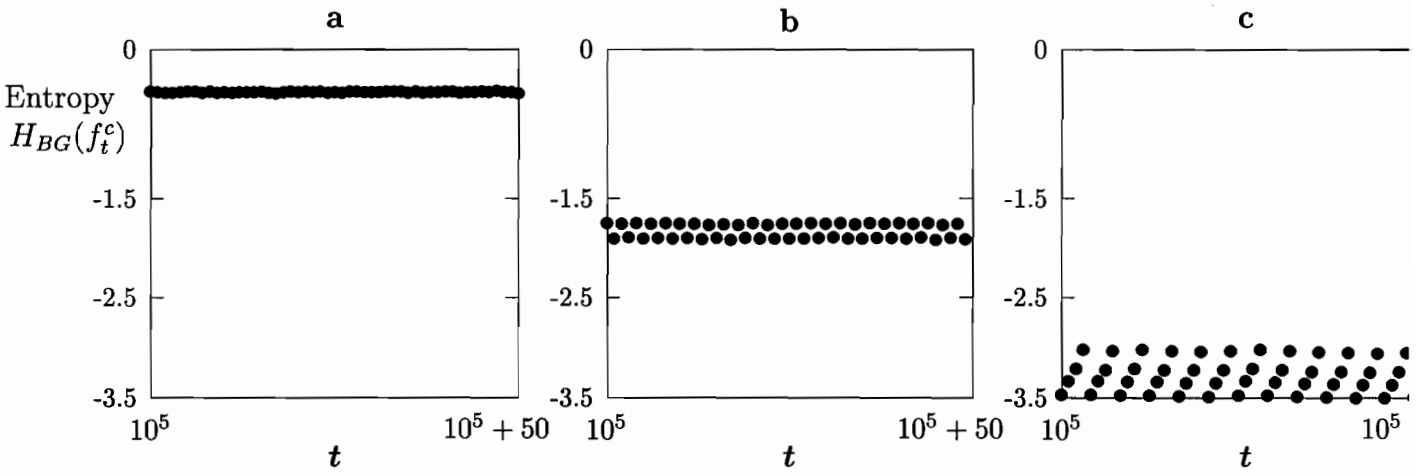

FIGURE 3.6
The Boltzmann-Gibbs entropy for the collapsed density of a lattice of 200×200 diffusively coupled tent maps. $\varepsilon = 0.45$ in all three panels. In a) $a = 1.99$, the CML is spatiotemporally chaotic. In b) $a = 1.4$, the CML is AP period 2. In c) $a = 1.3$ and the CML is period 4. The initial density was uniformly distributed on $[0, 1]$ for all three panels.

Finally, the auto- and cross-correlation functions were used to confirm the statistical oscillations observed in the "ordered phase". In the tent map lattice, the oscillations of the temporal autocorrelation functions

$$\rho^{i,j}(k) = \frac{c_k}{c_0}, \quad c_k = \frac{1}{N} \sum_{t=1}^{N-k} (x_t^{i,j} - \langle x^{i,j} \rangle)(x_{t+k}^{i,j} - \langle x^{i,j} \rangle) \tag{3.6}$$

shown in Figure 3.7 coexist with slow oscillations in the spatial cross-correlation of Figure 3.8, which reflect the presence of large clusters of synchronized activity.

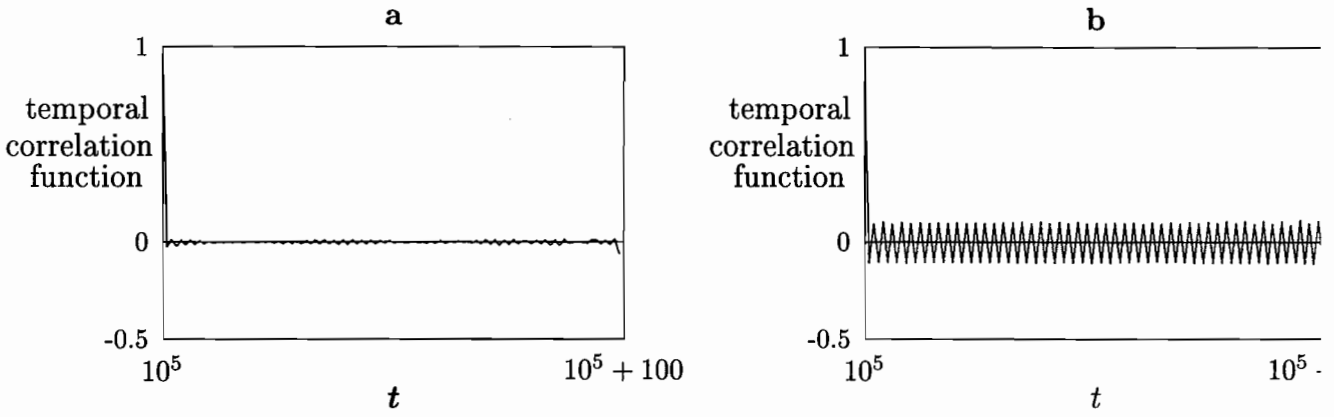

FIGURE 3.7

Temporal autocorrelation function (3.6) of the activity at site $(36, 156)$ (chosen for no particular reason) on a lattice of tent maps diffusively coupled with $\varepsilon = 0.45$ with the first 10^5 iterations discarded as transients, and the initial activity of the lattice uniformly distributed on $[0, 1]$. In a) the lattice is fully turbulent with $a = 1.99$. In b) the slope is $a = 1.4$ and the cyclical behavior of $\rho^{36,156}(k)$ reflects the statistical cycling in the lattice [k denotes time in this expression, as in (3.6)].

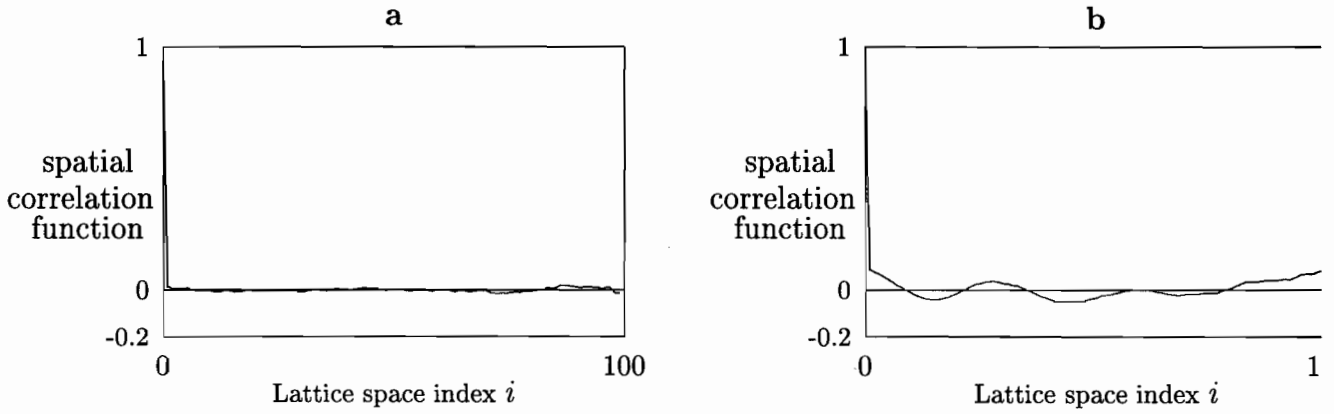

FIGURE 3.8

Spatial correlation function across a lattice of 200×200 tent maps diffusively coupled with $\varepsilon = 0.45$. The first 10^5 iterations are discarded as transients. In a) the slope is $a = 1.99$ and the system is spatially turbulent. In b) the slope is $a = 1.4$ and the slow oscillations reflect the presence of large scale patterns in Figure 3.1. The expression for this correlation function is (3.6) with k in this case denoting spatial position on the lattice.

The numerical results presented in this section clearly indicate that in the CML's considered, there are two easily identifiable "phases". In one, the statistical quantifiers of the motion reach a unique equilibrium, while in the other, the same quantifiers reach a periodic cycle. These two phases reflect qualitatively different properties of the operator which evolves densities in the CML's: the Perron-Frobenius operator.

Before proceeding to a theoretical discussion of this phenomenology, we describe very similar dynamics in a CML based on a model proposed by Franke and Yakubu [58] to describe the evolution of bob-white quail populations.

3.3 Excitable CML's

A biologically motivated map which has surprisingly received relatively little attention in the study of coupled map lattices is the asymmetric bimodal map

$$x_{t+1} = \left(a + \frac{b}{G(x_t)}\right) x_t \tag{3.7}$$

where $G(x) = 1 + x^n$ and $a + b > 1 > a > 0$. These maps arise in the description of the growth of ecological populations [9, 33, 153], neural networks [161], in the analysis of cardiac arrhythmias [193], and the study of the Belousov-Zhabotinsky chemical reaction [166]. They describe systems in which the dynamics depend on a threshold: rapid growth, or excitation, occurs when the variable crosses the threshold and is followed by a relatively long period of decline or decay. In this sense, these maps can be regarded as simple analogues for locally excitable dynamics. The bifurcation diagrams for these maps are quite complex and include stable limit cycles as well as regions of "banded" chaos [153].

3.3.1 A model for competing species

To construct a CML from (3.7), which is appropriate for the description of competing species, it is necessary to derive the appropriate form of the coupling architecture. The coupling is most easily obtained by considering an ecosystem composed of k territories in which the local dynamics of the k-th territory is described by (3.7). Equation (3.7) has been used to describe the growth of certain territorial animal populations, such as the bobwhite quail [58, 153], and describes a population which grows at rate $\sim (a+b)$ when $x < 1$ and declines at rate $\sim a$ when $x > 1$. The decrease in growth rate for large population densities arises

because of competition between individuals once the population exceeds the number which can be accommodated in preferred habitats. It follows that the influence of individuals in the $i \neq j$-th territory on the j-th territory must be through the term G, and hence the coupled map lattice is of the form

$$x_{t+1}^{(i)} = \left(a + \frac{b}{G^{(i)}(\mathbf{x}_t)}\right) x_t^{(i)}, \tag{3.8}$$

where $i = 1, \cdots, k$ is a space index which again need not be a scalar, and $\mathbf{x}_t = (x_t^{(i)}, \cdots, x_t^{(k)})$ denotes the state of the lattice at time t. Franke and Yakubu [58] introduced a coupling scheme given by

$$G^{(i)}(\mathbf{x}_t) = 1 + \sum_{j=1}^{k} \left[x_t^{(j)}\right]^n$$

to describe globally coupled species of bobwhite quail competing for shared resources and showed that for sufficiently large n, the species in all territories except one became extinct.

More realistically the coupling should reflect the fact that the greater the distance between two territories, the smaller the interaction between them. We therefore define

$$G^{(i)}(\mathbf{x}_t) = 1 + \left[x_t^{(i)} + \sum_{j=1,\neq i}^{k} w_{ij} x_t^{(j)}\right]^n \tag{3.9}$$

where w_{ij} denotes the weight of the connection between $x_t^{(j)}$ and $x_t^{(i)}$. This weight should decrease as the distance $\text{dist}(x^{(i)}, x^{(j)})$ between sites $x^{(i)}$ and $x^{(j)}$ increases. The distance between sites is calculated using the Euclidean metric:

$$\begin{aligned} \text{dist}(x^{(i)}, x^{(j)}) &= |i - j| \text{ for dimensionality 1} \\ \text{dist}(x^{(i_1 i_2)}, x^{(j_1 j_2)}) &= \sqrt{(j_1 - i_1)^2 + (j_2 - i_2)^2} \text{ for dimensionality 2, } \textit{etc....} \end{aligned}$$

The simplest coupling architecture decreasing with distance is piecewise constant:

$$w_{ij} = \begin{cases} 1/\mathcal{N} & \text{if } \text{dist}(x^{(i)}, x^{(j)}) \leq R \\ 0 & \text{if } \text{dist}(x^{(i)}, x^{(j)}) > R \end{cases} \tag{3.10}$$

where $\mathcal{N}$ denotes the number of territories located within euclidean distance R of $x_t^{(i)}$. In other words, the evolution of the local territory $x^{(i)}$ is influenced in an inhibitory fashion by the mean activity in a surrounding sphere of radius R.

The inhibitory effect of the coupling in (3.10) is illustrated by the behavior of the map

$$S^{\xi}(z) = \left(a + \frac{b}{1 + (z + \xi)^n}\right) z \tag{3.11}$$

which is another way of writing (3.8) with coupling (3.9) [*i.e.* the sum in (3.9) is replaced by the constant factor ξ]. Figure 3.9 illustrates the fact that if ξ is large, which represents a large mean activity in the neighbourhood of any lattice site $x_t^{(i)}$, the value $x_{t+1}^{(i)}$ tends to be smaller than $x_t^{(i)}$. The growth of $x_t^{(i)}$ is therefore inhibited locally by the activity of its neighbors.

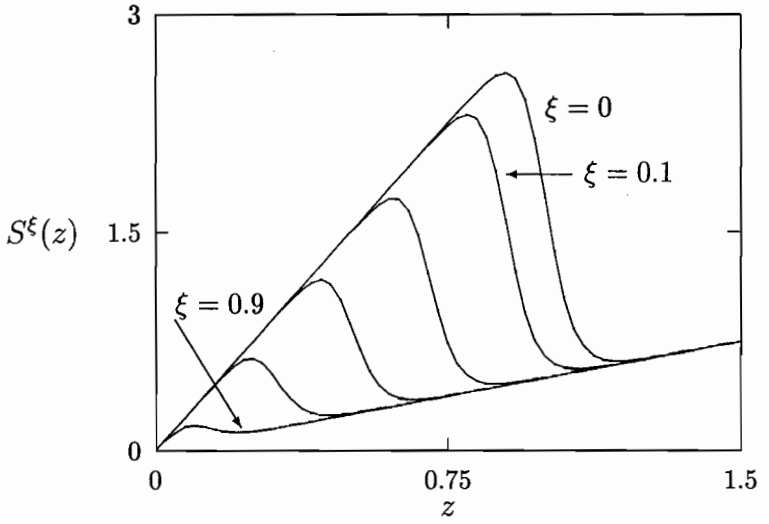

FIGURE 3.9:
Superimposition of several curves of the map (3.11) with $a = 0.5$, $b = 2.5$, $n = 29$ and $\xi = 0, \cdots, 0.9$.

The system (3.8) with (3.9) and (3.10) can now be investigated when the lattice extends in two spatial directions for various coupling ranges R and control parameters. When the parameters are such that the local maps possess stable limit cycles, the whole lattice synchronizes and forms "coherent structures" whose stability properties have been discussed previously in the context of diffusively coupled maps [3]. We do not consider these dynamics further here, but instead focus on the nontrivial statistical properties of the CML which arise when the local maps are chaotic.

When the local map is chaotic, numerical studies indicate that two distinct types of statistical evolutions are possible. Varying one (or several) control parameters can result in a transition from one phase to another.

3.3.2 Numerical investigations

Each phase is characterized by the behavior of the various statistical quantifiers of the motion presented in the previous section. Again, these evolve in qualitatively differing ways depending on the phase of the CML. There are many such quantifiers which have been developed to investigate spatiotemporal dynamics, and highlight nonlinear correlations between the elements (*e.g.* the mutual information), various stretching rates (*e.g.* the Lyapunov spectrum) or other information theoretic quantities of interest (*e.g.* the Rényi dimensions). In this section, we use the same simple quantifiers as before to characterize unambiguously the equilibrium statistical properties of system (3.8) with (3.9) and (3.10).

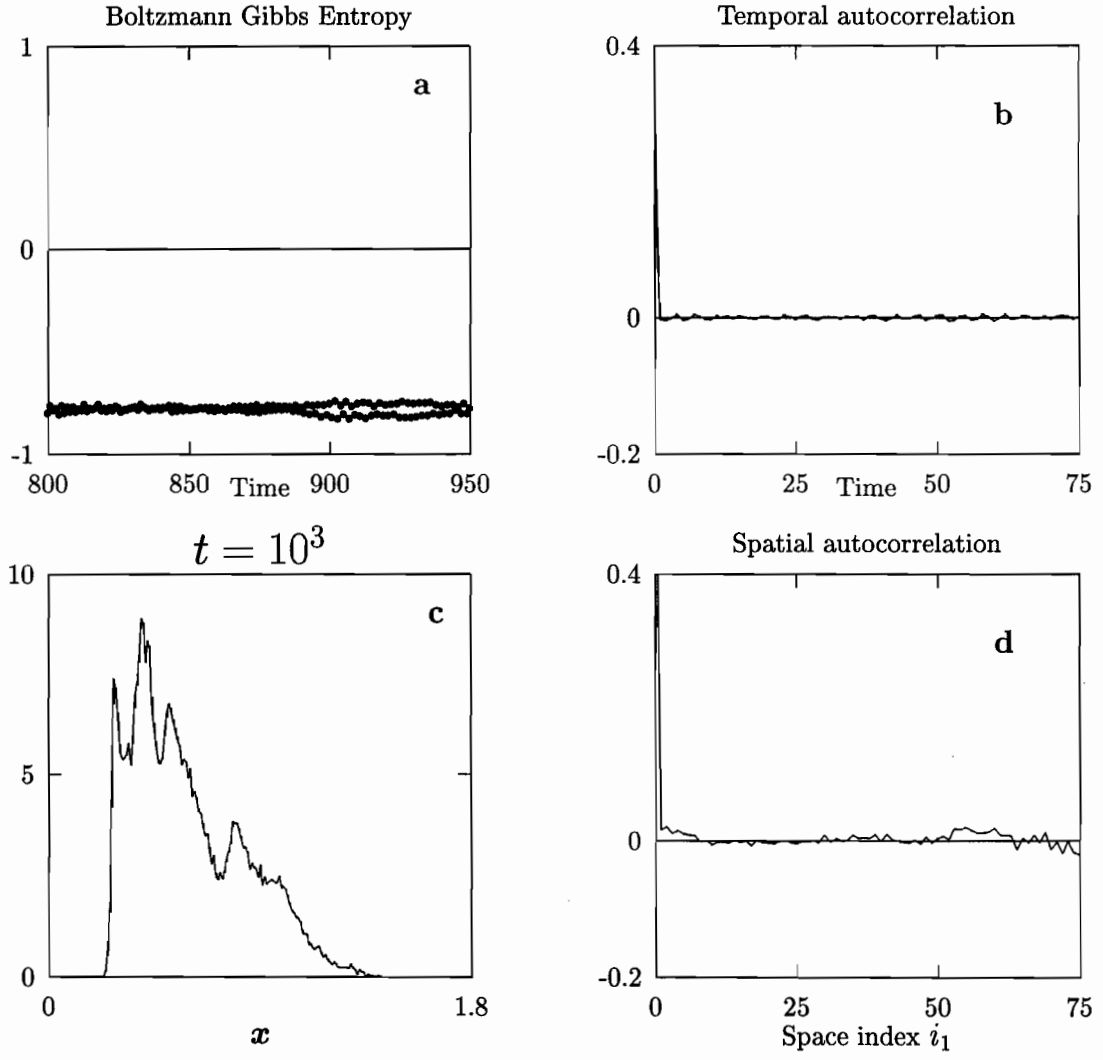

FIGURE 3.10:(see next page for the legend)

Behavior of various statistical quantifiers of the dynamics of the CML (3.8) in dimension 2, with $N \times N$ elements and periodic boundary conditions ($N = 200$), and with R of equation (3.10) being 3. In all panels, the parameters are : $a = 0.65$, $b = 2.15$ $n = 45$. (a) Evolution of the Boltzmann-Gibbs entropy of the density f_t^c displayed in (c) and defined implicitly in (3.5). (b) behavior of the temporal autocorrelation function (3.6) at a "typical site" on the lattice. (c) The distribution of activity f_t^c across the lattice at equilibrium; this probability density is time invariant and probably reflects the existence of an invariant measure. It's invariance does not rigorously imply, but strongly indicates invariance of the measure in $\mathbb{R}^{N^2}$. (d) Spatial correlation function for the left panel of Figure 3.11.

In the first phase, as shown in Figure 3.10, the statistical quantifiers of the motion relax to steady states which reflect the probable existence of an invariant measure describing the equilibrium thermodynamic properties of the lattice. In this case, the activity of the lattice (*cf.* Figure 3.11) is spatially disordered as well as temporally chaotic (we use the term "spatial disorder", rather than spatial chaos, since the lattices described here are finite). The resulting behavior is reminiscent of that observed previously in lattices of tent and logistic maps, where it has been described as "spatiotemporal chaos" (*cf.* Section 3.2.1).

Grey Scale: White $\Leftrightarrow$ N_t^j is 0, Black $\Leftrightarrow$ N_t^j is 1.8.

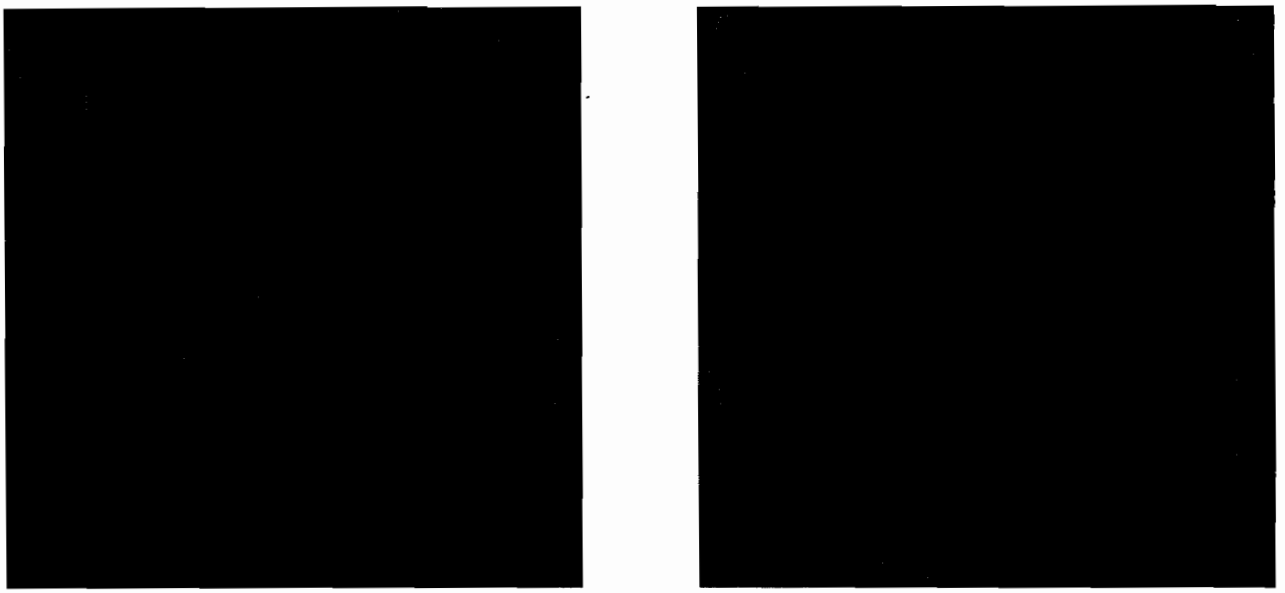

FIGURE 3.11:
These two panels are snapshots of the activity of a 200×200-element lattice with periodic boundary conditions at times $t = 10^3$ (left panel) and $t = 10^3 + 1$ (right panel). They display spatiotemporal chaos in the CML (3.8) with 200×200 sites. The parameters are as in Figure 3.10. The initial distribution of sites was uniform over $[0.5, 1.5]$.

The second of the two phases mentioned above is, as in the cases of tent and logistic maps, characterized by the cyclical statistical behavior displayed in Figures 3.12 and 3.13 and the possible formation of large scale patterns, examples of which are given in Figure 3.14. The formation of large scale patterns occurred only in the statistically cycling regime. However, there is still no clear understanding of the possible link between statistical instability in this system and the formation of patterns (*cf.* Section 3.8).

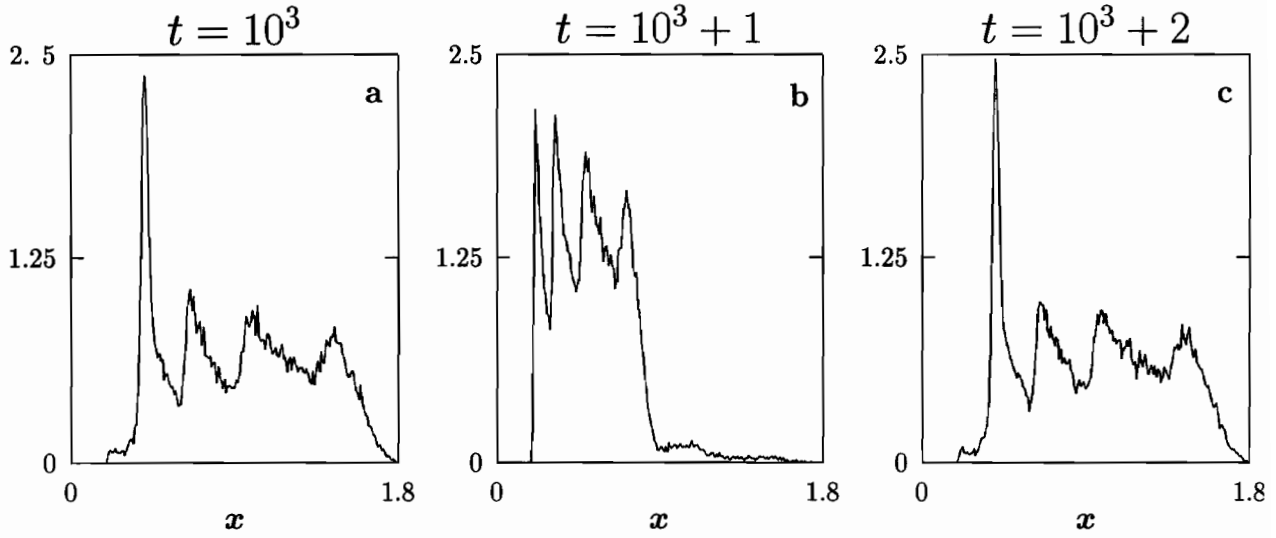

FIGURE 3.12:
Illustration of statistical cycling in the CML (3.8). The three panels display the distribution of activity defined implicitly in (3.5) across a lattice at three consecutive times, when the lattice is composed of 200×200 sites, and the parameters are: $a = 0.5$, $b = 2.5$, $n = 18$. The initial distribution was uniform over $[0.5, 1.5]$. The exact asymptotic cycle (in density space) depends on the initial preparation.

When patterns appear, two scenarios can be observed: 1) synchronized clusters can grow in a relatively short time (less than 10^3 iteration for a lattice of $\mathcal{O}(10^4)$ elements) until they cover the entire lattice (as in the top panels of Figure 3.14): The statistical cycling is then temporal rather than spatial [the synchronization within each cluster is not deterministic: all the sites within one cluster are contained within a small region of the real line referred to as a *band*]; and 2) the expansion of the clusters is very slow, and during a very long transient, macroscopic clusters appear to be metastable. In this case, (bottom panels of Figure 3.14), the statistical cycling is both temporal and spatial (the spatial cycling reflecting the presence of correlated and anticorrelated clusters of activity). In other words, the main difference between the situations which give rise to the formation of large clusters

of correlated activity, and the situations which give rise to the synchronization of the entire lattice seems to be the length of transients: It appears that the patterns of Figure 3.14 (bottom panels) eventually synchronize and look like those of Figure 3.14 (top panels), but the transients are, as expected [100], extremely long.

Figures 3.11 and 3.14 display snapshots of the activities of 200×200 lattices of maps of the form (3.8) coupled together according to (3.9) with (3.10), with periodic boundary conditions and for different values of the radius R and control parameters. In Figures 3.10, 3.12 and 3.13, some of the standard statistical quantifiers of chaotic motion are displayed when the lattice is either in the statistically stable or the statistically periodic phase. It is important to realize that the regions of parameter space in which both statistical stability and statistical cycling are observed are "large" in the sense that they are easily located during preliminary numerical trials.

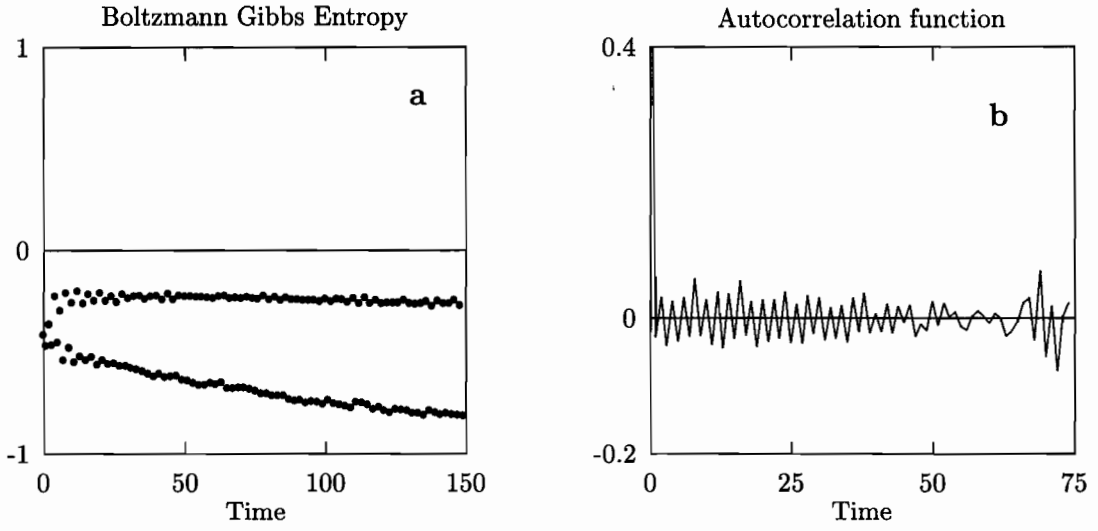

FIGURE 3.13:
The temporal correlation function (3.6) and Boltzmann-Gibbs entropy of f_t^c for the CML (3.8) when the parameters are the same as in Figure 3.12. The thermodynamic "equilibrium" for this system consists in two metastable states visited alternatively in time.

3.4 Summary of the numerical investigations

In summary, the numerical descriptions of Sections 3.2 and 3.3.2 indicate that:

1) An initially featureless excitable CML can spontaneously organize itself into large clusters of correlated and anti-correlated activity (*cf.* Figure 3.14).

2) The formation of large scale patterns occurs only when the statistical behavior of the lattice is nontrivial. In this case the lattice does not relax to statistical equilibrium but it evolves to a statistically periodic state. This implies that the CML under consideration possesses a thermodynamic equilibrium unlike those described in classical statistical mechanics. This equilibrium consists in a sequence of states visited periodically in time. We will come back to the implications of this observation in the discussion.

Grey Scale: White $\Leftrightarrow$ N_t^j is 0, Black $\Leftrightarrow$ N_t^j is 1.8.

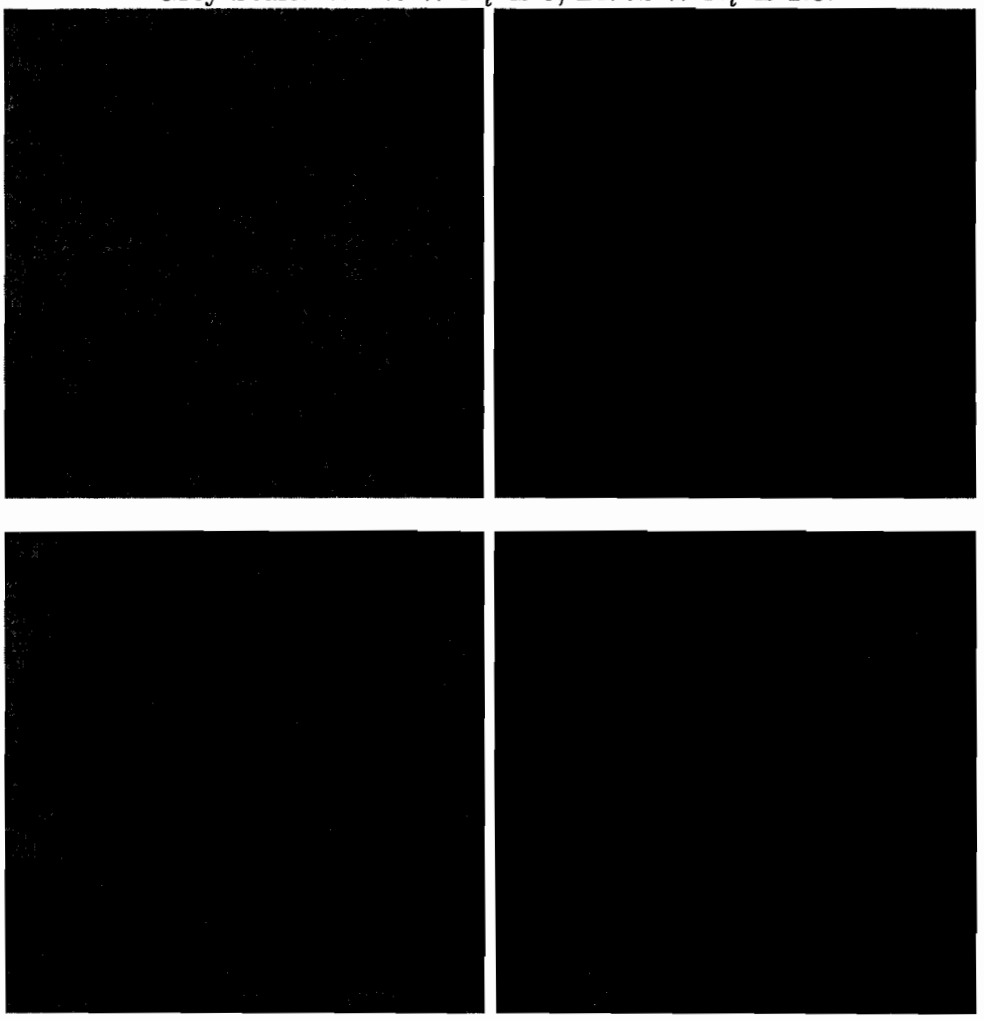

FIGURE 3.14

Snapshots of the activity of a 200×200-site CML (3.8) when it is in the statistically cycling regime. Left panels: $t = 10^3$; Right panels: $t = 10^3 + 1$. The top panels illustrate the formation of correlated clusters of activity which cover the entire lattice. The parameters in this case are as in Figures 3.12 and 3.13 with 82 nearest neighbors ($R = 5$) included in the neighbourhood. The bottom panels display the formation of patterns for the same parameter values but only 28

nearest neighbors ($R = 3$) influencing the activity of a given site. The initial preparations of the lattices were featureless, and the initial condition for each site was a random number picked from a density uniform on $[0.5, 1.5]$.

Given the paucity of rigorous results concerning the dynamics of large chaotic CML's, it is of great interest to describe this behavior analytically. Unfortunately, the map (3.8) cannot at present be dealt with in such a manner because it is not expanding everywhere. We propose in Section 3.7 a nonlinear CML which accounts for much of the complexity described here, while remaining amenable to analytic treatment. This analysis makes use of a conceptual tool-box which is introduced in the next section.

3.5 Mathematical preliminaries

The transfer operators induced by the nonsingular CML's considered here act on functions which are elements of normed linear spaces (*cf.* Appendix 3C for related definitions). The metric properties of these spaces depend on the choice of the norm. For reasons which will become clear in the next section, two natural norms arise in the descriptions of CML's: The familiar L^1 norm, and the so-called *bounded variation* norm. To introduce the latter, it is necessary to recall the definition of the variation of a high dimensional function. The short discussion given here is based on the presentations of [64, 109, 227].

3.5.1 Functions of bounded variation

First, we define the gradient in the distributional sense $\nabla_{\rm d}$. Let $\mathbf{f}$ be a real-valued function defined on an open set $\mathbb{X} \subset \mathbb{R}^N$, and $\mathcal{C}^1(\mathbb{X})$ denote the space of differentiable functions from $\mathbb{X}$ to $\mathbb{X}$ having compact support. Then the operator $\nabla_{\rm d}$ is the vector valued measure defined by

$$\nabla_{\rm d}\mathbf{f} \equiv (\frac{\partial \mathbf{f}}{\partial x_1}, \cdots, \frac{\partial \mathbf{f}}{\partial x_N}).$$

With this definition, it is possible to define the *variation* of $\mathbf{f}$:

$$\bigvee(\mathbf{f}) = \|\nabla_{\rm d}\mathbf{f}\| \tag{3.12}$$

where

$$\|\nabla_{\rm d}\mathbf{f}\| \equiv \sup\left\{\int_{\mathbf{X}} \mathbf{f}\frac{\partial \mathbf{h}}{\partial x_i} d\mu_{\rm L}^{\mathbf{X}} : \mathbf{h} \in \mathcal{C}^1(\mathbb{X}), |\mathbf{h}| \leq 1\right\}, \quad \mathbf{h} = (h^{(1)}, \cdots, h^{(N)}),$$

and $\mu_L^{\mathbb{X}}$ denotes the Lebesgue measure on $\mathbb{X}$. A more detailed presentation is given in Chapter 5 of [227], and in [64, 109].

With the definition (3.12), it is possible to introduce the bounded variation norm:

$$\| \cdot \|_{BV} \equiv \bigvee(\cdot) + \| \cdot \|_{L^1}. \tag{3.13}$$

The space of functions of bounded variation defined on $\mathbb{X}$ is a Banach space (*cf.* [64]) denoted $BV(\mathbb{X})$.

The rationale for introducing the notion of variation, and the associated norm for the probabilistic description of CML dynamics, is that it allows us to use the following result from the theory of linear operators due to Ionescu Tulcea and Marinescu.

3.5.2 The result of Ionescu Tulcea and Marinescu

This result was originally published in [206], and is of fundamental importance for our analytic description of the probabilistic properties of deterministic CML's. We do not state the original form of the theorem here, since it is much too general from our point of view. Our presentation is inspired by the descriptions of Loviscach [139].

Theorem 3.1: (Adapted from Ionescu Tulcea and Marinescu [206])
Consider two Banach spaces

$$(\mathbb{A}, \| \ \|_{\mathbb{A}}) \subset (\mathbb{Y}, \| \ \|_{\mathbb{Y}})$$

with the properties:

a) If $\{\mathbf{f}_n\}$ *is a bounded sequence of elements of* $\mathbb{A}$ *such that*

$$\lim_{n \longrightarrow \infty} \| \mathbf{f}_n - \mathbf{f} \|_{\mathbb{Y}} = 0$$

where $\mathbf{f} \in \mathbb{Y}$, *then* $\mathbf{f}$ *is also an element of* $\mathbb{A}$, *and* $\| \mathbf{f} \|_{\mathbb{A}} \leq \sup_n \| \mathbf{f}_n \|_{\mathbb{A}}$.

b) Let $\mathcal{P} : (\mathbb{A}, \| \ \|_{\mathbb{A}}) \longmapsto (\mathbb{A}, \| \ \|_{\mathbb{A}})$, *be a bounded operator which can be extended to a bounded operator in* $(\mathbb{Y}, \| \ \|_{\mathbb{Y}})$.

c) Suppose that there is an integer n *such that*

c1. If X *is a* $\| \ \|_{\mathbb{A}}$*-bounded subset, then* $\mathcal{P}^n X$ *is compact in* $\mathbb{Y}$.

c2. $\sup_n \| \mathcal{P}^n \|_{\mathbb{Y}} < \infty$

c3. There exists $\omega \in (0,1)$ *and* $\Omega \geq 0$ *such that*

$$\| \mathcal{P}^n \mathbf{f} \|_{\mathbb{A}} \leq \omega \| \mathbf{f} \|_{\mathbb{A}} + \Omega \| \mathbf{f} \|_{\mathbb{Y}}, \quad \textit{for all } \mathbf{f} \in \mathbb{A}. \tag{3.14}$$

If conditions (a)-(c) are satisfied, then the operator $\mathcal{P}$ is asymptotically periodic, and admits the spectral decomposition (1.21).

For the sake of completeness, we mention that the original version of Theorem 3.1 does not directly discuss asymptotic periodicity, but Rychlik showed that the properties implied by the theorem in turn imply asymptotic periodicity (*cf.* Theorems 1-3 of [187]) when the embedding space $(\mathbb{Y}, \| \|_{\mathbb{Y}})$ is $(L^1(\mathbb{X}), \| \|_{L^1})$. In order to apply this theorem to the study of CML's, we follow Gorá and Boyarski [66] in choosing $(\mathbb{A}, \| \|_{\mathbb{A}}) = (BV(\mathbb{X}), \| \|_{BV})$ included in $(\mathbb{Y}, \| \|_{\mathbb{Y}}) = (L^1(\mathbb{X}), \| \|_{L^1})$.

• Verifying a)

By Theorem 1.9 of [64], if $\{\mathbf{f}_n\} \in BV(\mathbb{X})$, $\| \mathbf{f}_n \|_{BV} \leq K$ for $n = 1, 2 \cdots$ and $\mathbf{f}_n \to \mathbf{f}$ in L^1, then $\mathbf{f} \in BV(\mathbb{X})$ and $\| \mathbf{f}_n \|_{BV} \leq K$.

• Verifying b) and c2)

The operators under consideration here (*i.e.* Perron-Frobenius operators) are Markov [122, 134], and their operator norm is 1, hence b) and c2) are both verified.

• Verifying c1)

This property follows from the compactness Theorem 1.19 of [64].

Hence, the theorem of Ionescu Tulcea and Marinescu guarantees that the transfer operators associated with CML's admits the spectral decomposition (1.21) if the condition c3) is satisfied. By focusing our attention on restrictions of $(BV(\mathbb{X}), \| \|_{BV})$ and $(L^1(\mathbb{X}), \| \|_{L^1})$ to the corresponding linear subspaces of normalized probability densities, and remembering the definition (3.13) of the bounded variation norm, the inequality in c3) becomes, for $n = 1$,

$$\bigvee(\mathcal{P}\mathbf{f}) \leq \omega \bigvee(\mathbf{f}) + \tilde{\Omega}, \qquad \tilde{\Omega} > 0 \tag{3.15}$$

where $\tilde{\Omega} = \Omega + \omega$. In concrete examples, we study specific CML's and obtain conditions on their control parameters such that the inequality (3.15) holds.

3.5.3 Sufficient conditions for statistical cycling

Here we derive a sufficient condition for the asymptotic periodicity of the Perron-Frobenius operator $\mathcal{P}_\Phi$ for coupled map lattices composed of piecewise expanding mappings. Our approach, inspired by the work of Góra and Boyarski [66], involves placing bounds on the variation of $\mathcal{P}_\Phi \mathbf{f}$, by using essentially geometrical arguments, and then using these bounds to invoke the result of Ionescu Tulcea and Marinescu discussed above. It should be noted that our analysis provides a sufficient condition for the spectral decomposition (1.21), and

that when condition (3.15) is not satisfied, we are not in a position to discuss the density evolution associated with chaotic CML's.

For typical CML's, the requirement that (3.15) be satisfied places natural constraints on the control parameters of Φ. To proceed, note that since Φ is a piecewise monotone mapping we have from (1.8)

$$\begin{aligned} \bigvee(\mathcal{P}_\Phi \mathbf{f}) &= \bigvee\left(\sum_{i=1}^{s(\Pi)} \frac{\mathbf{f}(\Phi_{|\pi_i}^{-1}(\mathbf{x}))}{\mathcal{J}_i^{-1}(\mathbf{x}))}\chi_{\tilde{\pi}_i}(\mathbf{x})\right) \\ &\leq \sum_{i=1}^{s(\Pi)} \bigvee\left(\frac{\mathbf{f}(\Phi_{|\pi_i}^{-1}(\mathbf{x}))}{\mathcal{J}_i^{-1}(\mathbf{x}))}\chi_{\tilde{\pi}_i}(\mathbf{x})\right) \\ &\leq \mathcal{Q}\sum_{i=1}^{s(\Pi)} \bigvee\left(\mathbf{f}(\Phi_{|\pi_i}^{-1}(\mathbf{x}))\chi_{\tilde{\pi}_i}(\mathbf{x})\right) \end{aligned} \tag{3.16}$$

where $\mathcal{Q} \in \mathbb{R}^+$ satisfies

$$\frac{1}{\max_{\pi_i \in \Pi} \mathcal{J}_i^{-1}(\mathbf{x})} \ll \mathcal{Q} \ll \frac{1}{\min_{\pi_i \in \Pi} \mathcal{J}_i^{-1}(\mathbf{x})} \tag{3.17}$$

and depends on the transformation under consideration. Each term in the sum on the right hand side of (3.16) can now be evaluated explicitly. From the definition (3.12),

$$\begin{aligned} \bigvee\left(\mathbf{f}(\Phi_{|_i}^{-1}(\mathbf{x}))\chi_{\tilde{\pi}_i}(\mathbf{x})\right) &= \left\|\nabla_{\mathrm{d}}\left[\mathbf{f}(\Phi_{|_i}^{-1}(\mathbf{x}))\chi_{\tilde{\pi}_i}(\mathbf{x})\right]\right\|_{L^1} \\ &= \int_{\mathbb{X}} \left|\nabla_{\mathrm{d}}\left[\mathbf{f}(\Phi_{|_i}^{-1}(\mathbf{x}))\right]\chi_{\tilde{\pi}_i}(\mathbf{x})\right| d\mu_{\mathrm{L}}^{\mathbb{X}} + \int_{\mathbb{R}^N} \left|\mathbf{f}(\Phi_{|_i}^{-1}(\mathbf{x}))\nabla_{\mathrm{d}}\left[\chi_{\tilde{\pi}_i}(\mathbf{x})\right]\right| d\mu_{\mathrm{L}}^{\mathbb{X}} \\ &= \bigvee\left(\mathbf{f}(\Phi_{|_i}^{-1}(\mathbf{x}))\right)\Big|_{\mathbf{x}\in\tilde{\pi}_i} + \int_{\mathbb{R}^N} \left|\mathbf{f}(\Phi_{|_i}^{-1}(\mathbf{x}))\nabla_{\mathrm{d}}\left[\chi_{\tilde{\pi}_i}(\mathbf{x})\right]\right| d\mu_{\mathrm{L}}^{\mathbb{R}^N}. \end{aligned} \tag{3.18}$$

Since $\mathcal{Q} > \mathcal{J}$, a simple change of variables yields

$$\bigvee\left(\mathbf{f}(\Phi_{|\pi_i}^{-1}(\mathbf{x}))\right)\Big|_{\mathbf{x}\in\tilde{\pi}_i} < \mathcal{Q}\bigvee(\mathbf{f}(\mathbf{x}))\Big|_{\mathbf{x}\in\pi_i}. \tag{3.19}$$

The integral in the right hand side of equation (3.18) can be simplified using example 1.4 of [64], which states that for any $\mathbf{u} \in BV(\mathbb{X})$, and $\mathbb{A} \subset \mathbb{X}$ with piecewise C^2 boundaries of finite $(N-1)$-dimensional measure,

$$\int_{\mathbb{X}} |\mathbf{u}(\mathbf{x})\nabla_{\mathrm{d}}[\chi_{\mathbb{A}}(\mathbf{x})]|\, d\mu_{\mathrm{L}}^{\mathbb{R}^N} = \int_{\partial\mathbb{A}} |\mathbf{u}(\mathbf{x})|\, d\mu_{\mathrm{L}}^{\mathbb{R}^{N-1}}.$$

Choosing $\mathbf{u}(\mathbf{x}) = \mathbf{f}(\Phi_{|_i}^{-1}(\mathbf{x}))$, and $\mathbb{A} = \tilde{\pi}_i$, one obtains

$$\int_{\mathbb{X}} |\mathbf{f}(\Phi_{|_i}^{-1}(\mathbf{x}))\nabla_{\mathrm{d}}[\chi_{\tilde{\pi}_i}(\mathbf{x})]\, d\mu_{\mathrm{L}}^{\mathbb{R}^N} = \int_{\partial\tilde{\pi}_i} |\mathbf{f}(\Phi_{|_i}^{-1}(\mathbf{x}))|\, d\mu_{\mathrm{L}}^{\mathbb{R}^{N-1}}. \tag{3.20}$$

Furthermore, for any $\mathbf{u} \in BV(\mathbb{X})$, and any $\mathbb{A}$ as specified above, we have from Lemma 3 of [66]

$$\int_{\partial \mathbf{A}} \mathbf{u}(\mathbf{x}) d\mu_{\mathrm{L}}^{\mathbb{R}^{N-1}} \leq \frac{1}{\sin\theta(\mathbb{A})} \bigvee (\mathbf{u}(\mathbf{x}))\Big|_{\mathbf{x}\in\mathbf{A}} + \mathcal{K}_{\mathbf{A}} \tag{3.21}$$

where $\mathcal{K}_{\mathbf{A}} > 0$ is bounded and $\sin\theta(\mathbb{A})$ depends on the smallest angle subtended by intersecting edges of the set $\mathbb{A}$. Letting $\mathbf{u}(\mathbf{x}) = \mathbf{f}(\Phi_{|_i}^{-1}(\mathbf{x}))$ and $\mathbb{A} = \tilde{\pi}_i$ as before, and recalling identity (3.19), the integral in (3.18) satisfies

$$\begin{aligned} \int_{\mathbb{X}} |\mathbf{f}(\Phi_{|_i}^{-1}(\mathbf{x})) \nabla_{\mathrm{d}} [\chi_{\tilde{\pi}_i}(\mathbf{x})]| \, d\mu_{\mathrm{L}}^{\mathbb{R}^N} &\leq \frac{1}{\sin\theta(\tilde{\pi}_i)} \bigvee \left(\mathbf{f}(\Phi_{|_i}^{-1}(\mathbf{x}))\right)\Big|_{\mathbf{x}\in\tilde{\pi}_i} + \mathcal{K}_i \\ &< \frac{\mathcal{Q}}{\sin\theta(\tilde{\pi}_i)} \bigvee (\mathbf{f}(\mathbf{x}))\Big|_{\mathbf{x}\in\pi_i} + \mathcal{K}_i. \end{aligned} \tag{3.22}$$

Letting $\sin\theta(\tilde{\pi}) \equiv \min_i \sin\theta(\tilde{\pi}_i)$, and using (3.18), (3.19), and (3.22), (3.16) becomes

$$\begin{aligned} \bigvee(\mathcal{P}_\Phi \mathbf{f}) &\leq \mathcal{Q} \sum_{i=1}^{s(\Pi)} \left[\mathcal{Q} \bigvee (\mathbf{f}(\mathbf{x}))\Big|_{\mathbf{x}\in\pi_i} + \frac{\mathcal{Q}}{\sin\theta(\tilde{\pi}_i)} \bigvee (\mathbf{f}(\mathbf{x}))\Big|_{\mathbf{x}\in\pi_i} + \mathcal{K}_i \right] \\ &\leq \mathcal{Q}^2 \bigvee (\mathbf{f}) \left[1 + \frac{1}{\sin\theta(\tilde{\pi})} \right] + s(\Pi) \max_i \mathcal{K}_i. \end{aligned} \tag{3.23}$$

Therefore, comparing (3.23) with (3.15), the theorem of Ionescu Tulcea and Marinescu guarantees the asymptotic periodicity of the Perron-Frobenius operator when

$$\mathcal{Q}^2 \left[1 + \frac{1}{\sin\theta(\tilde{\pi})} \right] < 1. \tag{3.24}$$

The explicit form of the CML Φ enters in the calculations of $\mathcal{Q}$ and $\sin\theta(\tilde{\pi})$, and we therefore restrict our attention to specific models in order to complete the analysis.

3.6 Lattices of tent maps

The association of large scale patterns and asymptotic periodicity in CML's was first observed for the case of a diffusively coupled CML in which the local transformation, S, is the generalized tent map. Hence we consider (1.2) with S given by the tent map, for various coupling architectures. This study is facilitated by the fact that for this choice of S, $\sin\theta(\tilde{\pi})$, and $\mathcal{Q}$ of condition (3.24) can be readily calculated.

3.6.1 Calculating $\sin\theta(\tilde{\pi})$

The phase space $\mathbb{X}$ of the transformation Φ is the direct product $\mathbb{X} = [0,1]^{N^2} \subset \mathbb{R}^{N^2}$ if there are N^2 sites on the lattice. Note that each of the elements of this product can be divided into two subintervals $I_1 = [0, 1/2)$, $I_2 = [1/2, 1]$ such that on each of these, S is monotone. Therefore the partition Π on which Φ is piecewise monotone contains 2^{N^2} sets, each one of which is of the form: $\pi_i = I_1^i I_2^{N^2-i}$, where $i = 1, \cdots, 2^{N^2}$. In addition, note that Π is a rectangular partition since I_1 and I_2 are the same for all sites on the lattice.

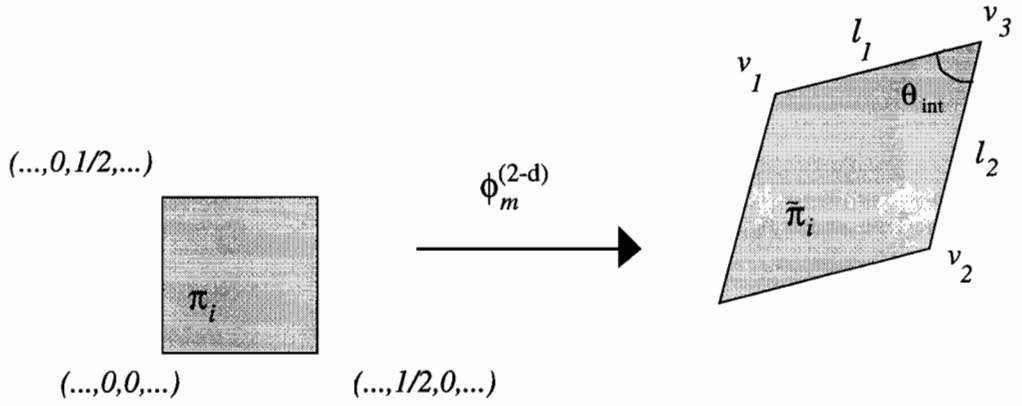

FIGURE 3.15:
Schematic diagram of the evolution of one of the hyperplanes bounding the set π_i under the action of the CML transformation Φ. As in the text, $\tilde{\pi}_i = \Phi_{|\pi_i}(\pi_i)$.

As illustrated in Figure 3.15, the "image sets" denoted $\tilde{\pi}_i$ $(i = 1, \cdots, s(\Pi))$ are rhomboids whose edges subtend angles which are bounded away from 0. The smallest of these angles is denoted θ_{int}, and can be calculated explicitly by noting that the two dimensional restriction of the CML transformation Φ to the plane (x^i, x^j) (x^i and x^j belonging to the same p-neighbourhood) is

$$\Phi^{(2-d)}(\mathbf{x}_t) = \begin{cases} x_{t+1}^i = (1-\varepsilon)S(x_t^i) + \frac{\varepsilon}{p}S(x_t^j) + C_1 \\ x_{t+1}^j = (1-\varepsilon)S(x_t^j) + \frac{\varepsilon a}{p}S(x_t^i) + C_2, \end{cases}$$

where C_1 and C_2 depend only on the activity in the p-neighbourhood of the sites i and j (excluding x^i and x^j themselves). Hence,

$$\begin{aligned} \Phi^{(2-d)}(\cdots, 0, 1/2, \cdots) &= \left(\cdots, \frac{\varepsilon a}{2p} + C_1, (1-\varepsilon)\frac{a}{2} + C_2, \cdots\right) \equiv v_1 \\ \Phi^{(2-d)}(\cdots, 1/2, 0, \cdots) &= \left(\cdots, (1-\varepsilon)\frac{a}{2} + C_1, \frac{\varepsilon a}{2p} + C_2, \cdots\right) \equiv v_2 \end{aligned}$$

$$\Phi^{(2-d)}(\cdots, 1/2, 1/2, \cdots) = \left(\cdots, \frac{a}{2} + \frac{a\varepsilon}{2}\left(\frac{1-p}{p}\right) + C_1, \frac{a}{2} + \frac{a\varepsilon}{2}\left(\frac{1-p}{p}\right) + C_2, \cdots\right) \equiv v_3$$

Denote by ℓ_1 the edge linking v_1 to v_3 and ℓ_2 the edge linking v_2 to v_3. The slope of ℓ_1 is therefore $\varepsilon/p(1-\varepsilon)$, and the angle θ_{int} of intersection of ℓ_1 and ℓ_2 satisfies

$$\tan\theta_{\text{int}} = \frac{p(1-\varepsilon)[\varepsilon^2 - p^2(1-\varepsilon)^2]}{\varepsilon[\varepsilon^2 + p^2(1-\varepsilon)^2]}. \tag{3.25}$$

Using the results of Appendix 3A, since we consider a lattice with N^2 elements we obtain

$$\sin\theta(\tilde{\pi}) = \sqrt{\frac{1-\cos\theta_{\text{int}}}{N^2[1+(N^2-2)\cos\theta_{\text{int}}]}}. \tag{3.26}$$

3.6.2 Calculating $\mathcal{Q}$

To facilitate the presentation, we explicitly write the matrix form of the CML acting on the state vector $\mathbf{x}_t$ in two spatial dimensions when the coupling between the elements is diffusive:
$\mathbf{x}_t$: $\Phi(\mathbf{x}_t) = \mathbf{x}_{t+1}$ where
$\Phi(\mathbf{x}_t) =$

$$\begin{pmatrix}
(1-\varepsilon)S(x_t^1) & \frac{\varepsilon}{4}S(x_t^2) & \overset{0}{\cdots} & \frac{\varepsilon}{4}S(x_t^N) & \overset{0}{\cdots}\ \frac{\varepsilon}{4}S(x_t^{N^2-N}) & \overset{0}{\cdots} & \frac{\varepsilon}{4}S(x_t^{N^2}) \\
\frac{\varepsilon}{4}S(x_t^1) & (1-\varepsilon)S(x_t^2) & \frac{\varepsilon}{4}S(x_t^3) & \cdots & \frac{\varepsilon}{4}S(x_t^{N+1})\ \overset{0}{\cdots} & \frac{\varepsilon}{4}S(x_t^{N^2-N+1}) & \cdots \\
\ddots & \ddots & \ddots & \ddots & \ddots & \ddots & \ddots \\
\frac{\varepsilon}{4}S(x_t^1) & \overset{0}{\cdots} & \frac{\varepsilon}{4}S(x_t^N) & \overset{0}{\cdots} & \frac{\varepsilon}{4}S(x_t^{N^2-N})\ \overset{0}{\cdots} & \frac{\varepsilon}{4}S(x_t^{N^2-1}) & (1-\varepsilon)S(x_t^{N^2})
\end{pmatrix} \tag{3.27}$$

with

$$\mathbf{x}_t \equiv \begin{pmatrix} x_t^1 \\ x_t^2 \\ \vdots \\ x_t^{N^2} \end{pmatrix}.$$

As an aside, this representation of the lattice activity highlights the fact that local coupling in two dimensions is equivalent to long range coupling in one. More importantly, it allows us to calculate the absolute value of the Jacobian of Φ when the slope of S is constant over the phase space, and this quantity will be shown below to provide a good lower bound for $\mathcal{Q}$. The absolute value of the derivative matrix $|D\Phi|$ is given by:

$$|D\Phi| = \begin{pmatrix}
(1-\varepsilon)a & \frac{\varepsilon}{4}a & \overset{0}{\cdots} & \frac{\varepsilon}{4}a & \overset{0}{\cdots}\ \frac{\varepsilon}{4}a & \overset{0}{\cdots} & \frac{\varepsilon}{4}a \\
\frac{\varepsilon}{4}a & (1-\varepsilon)a & \frac{\varepsilon}{4}a & \overset{0}{\cdots} & \frac{\varepsilon}{4}a\ \overset{0}{\cdots} & \frac{\varepsilon}{4}a & \overset{0}{\cdots} \\
 & & & \ddots & & & \\
\frac{\varepsilon}{4}a & \overset{0}{\cdots} & \frac{\varepsilon}{4}a & \overset{0}{\cdots} & \frac{\varepsilon}{4}a\ \overset{0}{\cdots} & \frac{\varepsilon}{4}a & (1-\varepsilon)a
\end{pmatrix}.$$

If the coupling is not diffusive, but contains an arbitrary number of neighbours, the number of off-diagonal entries in the matrix change, but the structure of the matrix will remain essentially the same for all linear coupling architectures. In general, if the tent maps (3.1) are coupled as in (1.2), the possible entries in the derivative matrix $D\Phi_{|\pi_i}$, are,

	$x^{kl} \in I_1$	$x^{kl} \in I_2$
$\phi'_{i,kk}(\mathbf{x})$	$(1-\varepsilon)a$	$-(1-\varepsilon)a$
$\phi'_{i,kl}(\mathbf{x})$	$(\varepsilon/p)a$	$-(\varepsilon/p)a.$

The absolute value of the determinant of this matrix remains unchanged when entire columns are multiplied by -1, and so

$$\mathcal{J}_i(\mathbf{x}) \equiv |\det D\Phi_{|\pi_i}| = \det|D\Phi_{|\pi_i}| = \det|D\Phi|,$$

where $|D\Phi|$ is a real matrix, whose diagonal entries are $(1-\varepsilon)a$, and nonzero off-diagonal entries are $(\varepsilon/p)a$. Since periodic boundary conditions are assumed, $|D\Phi|$ is also symmetric, and hence diagonalizable, and

$$\det|D\Phi| = \prod_{k=0}^{N^2-1} \lambda_k$$

where the λ_k's are the eigenvalues of $|D\Phi|$. Although these eigenvalues depend on the coupling architecture, they are independent of both i and $\mathbf{x}$ when the map is piecewise linear with a slope whose absolute value is constant on the phase space. Therefore $\det|D\Phi_{|\pi_i}|$ is also independent of $\mathbf{x}$ and i, and if there are N^2 elements on the lattice

$$\mathcal{J}_i^{-1}(\mathbf{x}) = \prod_{k=0}^{N^2-1} \lambda_k^{-1}, \quad \forall i = 1, \cdots, 2^{N^2}, \qquad \forall \mathbf{x} \in \mathbb{X} \tag{3.28}$$

where the expressions for the λ_k's for several coupling schemes are listed in Table 3.1 below. Recall that $\mathcal{Q}$ was defined implicitly in (3.16) by the requirement

$$\sum_{i=1}^{s(\Pi)} \bigvee \left(\frac{f(\Phi_{i|\pi_i}^{-1}(\mathbf{x}))}{\mathcal{J}_i^{-1}(\mathbf{x}))} \chi_{\tilde{\pi}_i}(\mathbf{x}) \right) \leq \mathcal{Q} \sum_{i=1}^{s(\Pi)} \bigvee \left(f(\Phi_{|\pi_i}^{-1}(\mathbf{x})) \chi_{\tilde{\pi}_i}(\mathbf{x}) \right).$$

It is clear from (3.28) that

$$\sum_{i=1}^{s(\Pi)} \bigvee \left(\frac{f(\Phi_{i|\pi_i}^{-1}(\mathbf{x}))}{\mathcal{J}_i^{-1}(\mathbf{x}))} \chi_{\tilde{\pi}_i}(\mathbf{x}) \right) = \frac{1}{\prod_{k=0}^{N^2-1} \lambda_k^{-1}} \sum_{i=1}^{s(\Pi)} \bigvee \left(f(\Phi_{|\pi_i}^{-1}(\mathbf{x})) \chi_{\tilde{\pi}_i}(\mathbf{x}) \right),$$

so it is natural to pick

$$\mathcal{Q} = \prod_{k=0}^{N^2-1} \lambda_k. \tag{3.29}$$

As a result, condition (3.24) for asymptotic periodicity, applied to a lattice of generalized tent maps (3.1) coupled linearly as in (1.2) becomes

$$\left[\prod_{k=0}^{N^2-1} \lambda_k^2\right] \left[1 + \frac{1}{\sin\theta(\tilde{\pi})}\right] < 1, \tag{3.30}$$

where $\sin\theta(\tilde{\pi})$ is given by (3.26) and (3.25). Exact expressions for the eigenvalues are necessary to obtain concrete conditions on the parameters a, p and ε such that (3.30) holds. The periodic boundary conditions we have chosen are helpful in this regard since they ensure that the matrix $|D\Phi|$ is circular: the second row is obtained by shifting all the elements of the first row to the right by one position, so that if the entries of the matrix $|D\Phi|$ are denoted ϕ'_{kl} $(k, l = 1, \cdots, N^2)$ $\phi'_{kl} = \phi'_{(k+1)(l+1) \bmod N^2}$ (the modulo operator is a consequence of the periodic boundary conditions). For such matrices, it is well known [158] that

$$\lambda_k = \sum_{m=1}^{N^2} \phi'_{1m} e^{\frac{2\pi k m}{N^2}}, \qquad k = 0, \cdots, N^2 - 1. \tag{3.31}$$

Table 3.1 below gives explicit formulae for (3.31) for an $N \times N$ lattice of tent maps with several coupling architectures discussed in the literature. The sum in the p nearest neighbors case is over half the sites which are included in the neighbourhood because each term in the sum arises from the contribution of two sites: x^m and its mirror image relative to the center of the neighbourhood. The exact expressions for the bounds of this sum are easily derivable, but cumbersome, and therefore not shown here explicitly (the sum is evaluated below, in equation (3.36) for the $p = 28$ case).

Until now, no claim has been made concerning the period of the density cycle resulting from the cyclical spectral decomposition (1.21): there are no general results available to determine the quantity r in (1.21) (indicating the number of disjoint supports of the invariant density) and therefore providing a lower bound on the period of the density cycle (the upper bound being naturally $r!$). However, it is well established [*cf.* (3.2)] that the tent map (3.1) displays a period doubling scenario in the evolution of densities, and it is of interest to understand how this picture survives in arbitrarily large lattices of tent maps coupled together through various coupling schemes.

Coupling	λ_k
Diffusive	$(1-\varepsilon)a + \frac{\varepsilon a}{4}\left[\cos\left(\frac{2\pi k}{N^2}\right) + \cos\left(\frac{2\pi k}{N}\right)\right]$
p nearest neighbors	$(1-\varepsilon)a + \frac{2a\varepsilon}{p}\left[\sum_{m\,:\,p/2\text{sites}} \cos\left(\frac{2\pi k}{N^2}m\right)\right]$
Mean Field	$(1-\frac{N^2\varepsilon}{N^2-1})a$

TABLE 3.1:
Table of the eigenvalues of the derivative matrix $D\Phi$ associated with a square lattice of tent maps for various coupling architectures.

To carry out this analysis, we apply the formalism presented in Section 3.5.3 to compositions of the lattice transformation Φ with itself. Denote by Φ^n the transformation Φ composed n times with itself (*i.e.* $\Phi^2 = \Phi \circ \Phi$). If the spectral decomposition (1.21) applies to Φ^2 with $r = r_2 \neq 1$, then it necessarily applies to Φ with $r = r_1$, where $r_1 = 2r_2$. The same reasoning holds for higher order iterates of Φ and yields $r_1 = nr_n$ for Φ^n. We therefore investigate the spectral characteristics of the Perron-Frobenius operator associated with Φ^2, Φ^4 *etc...*

3.6.3 Diffusive coupling: phase diagram

Note that if λ_k is an eigenvalue of the transformation Φ, then λ_k^n is an eigenvalue of Φ^n, and so condition (3.30) for asymptotic periodicity in a lattice with N^2 sites takes the form

$$\left[\prod_{k=0}^{N^2-1} \lambda_k^{2n}\right]\left[1 + \frac{1}{\sin\theta(\tilde{\pi})}\right] < 1 \tag{3.32}$$

with $\sin\theta(\tilde{\pi})$ given by (3.26), with (3.25) calculated with $p = 2$ if the CML is a chain, or $p = 4$, if the CML has two spatial dimensions.

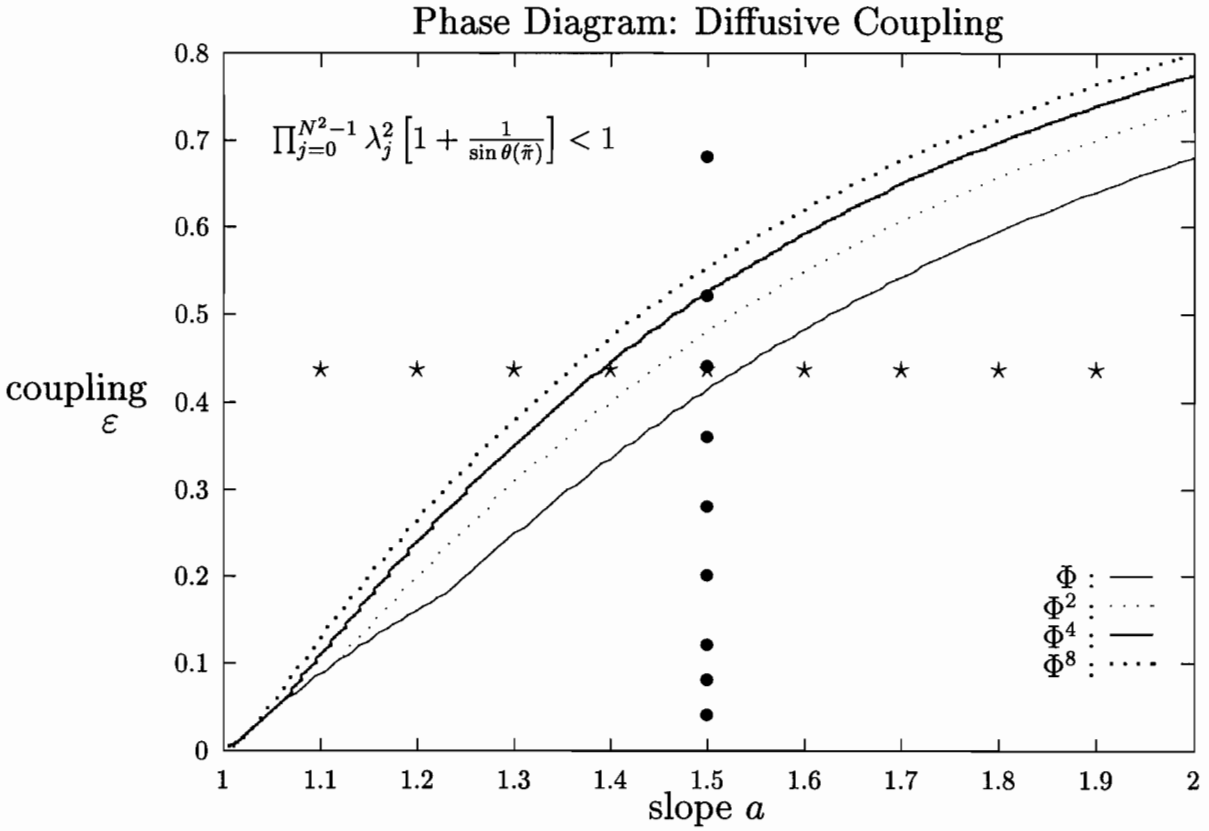

FIGURE 3.16:
Phase diagram for the diffusively coupled tent map with periodic boundary conditions. This figure was obtained from the condition (3.30) for a lattice of 200×200 elements, and the eigenvalues of Table 3.1 corresponding to diffusive coupling for corresponding to Φ, Φ^2, *etc....* The stars indicate the positions of the nine panels of Figure 3.1, full circles, those of the nine panels of Figure 3.3. Compare this diagram with the corresponding activity Figures (3.1 and 3.3).

Figure 3.16 examines the behavior of condition (3.32) for various iterates of $\Phi : \Phi^2$, Φ^4 and Φ^8. For clarity, Figure 3.16 does not display the results of our analysis applied to Φ^n for $n > 8$, because the subsequent curves behave as expected. This phase diagram therefore generalizes previously published results [136] on two diffusively coupled tent maps to N dimensions. It should be clear that the curves displayed in Figure 3.16 do not indicate precisely the location in the (a, ε) plane at which the spectral decomposition of the Perron-Frobenius operator changes. Instead, these curves indicate locations in parameter space at which *sufficient conditions* for a given spectral decomposition of $\mathcal{P}_\Phi$ change. This "onion" like structure is consistent with numerical investigations of diffusively coupled tent map lattices reported in [135], and indicates that the one-dimensional picture (3.2) essentially survives

diffusive coupling, modulo some expected dependence on the coupling strength between the elements.

3.6.4 Mean field coupling: phase diagram

In this case, the evolution of every local site is influenced by the mean activity of the entire lattice. This coupling is of interest because it is a limiting case of long range couplings which are known to arise in optics [101], in the study of evolutionary dynamics [51], and in many physical models of spatially extended systems [150] (see also Section 3.6.4 of Chapter 1). The eigenvalues of the derivative matrix in this case are given in Table 3.1, and the condition (3.30) can again be evaluated explicitly. In this case, the simplicity of the eigenvalues (*cf.* Table 3.1) allows to go one step further since if N is large, we have

$$\lambda_k \sim (1-\varepsilon)a.$$

In addition, if there are N^2 sites on a lattice of globally coupled tent maps, and N is large, the results of Appendix 3A, in conjunction with those of Section 3.6.1 (*cf.* (3.26)) indicate that

$$\sin\theta(\tilde{\pi}) \sim N^{-2}.$$

Hence, condition (3.30) becomes

$$[1+N^2]\left[(1-\varepsilon)^2a^2\right]^{N^2} < 1,$$

which can be written, when N is large

$$(1-\varepsilon)a \lesssim N^{(-1/N^2)}.$$

But $\lim_{N\to\infty} N^{(-1/N^2)} = 1$ (if $N = 200$ for example, $N^{(-1/N^2)} \simeq .9998675505$), so the condition (3.30) for a large lattice becomes effectively

$$(1-\varepsilon)a < 1.$$

Note also that $\lim_{N\to\infty} N^{(-1/nN^2)} = 1$ if $n > 1$, so that we expect the condition (3.30) applied to Φ^n to yield the same condition, for N large enough as the condition for Φ, so that the "onion-like" structure of Figure 3.16 should disappear for global coupling. This is indeed the case. Figure 3.17 displays the phase diagrams for the globally coupled tent map lattice.

This phase diagram is the analytic version of some early numerical results published by Kaneko on a similar model [101]. The overall shape of the transition curve published in that reference separating "spatiotemporal chaos" (or turbulence) and statistical cycling is in agreement with our analytic result, although systematic shifts in parameter space are clearly present. This shift is most important for low values of the coupling ($\varepsilon \lesssim 0.3$) because in these cases, our estimates of the quantity $\mathcal{Q}$ are too conservative. The smaller shifts observed for high coupling values are probably due to a combination of transient effects (which render accurate numerical simulations computationally costly) and inaccuracies in the various bounds of condition (3.24). In any case, the presence of such discrepancies is not surprising given the fact that the estimates given here for the phase transition curves correspond to changes in *sufficient* conditions for asymptotic periodicity, rather than changes in necessary *and* sufficient conditions.

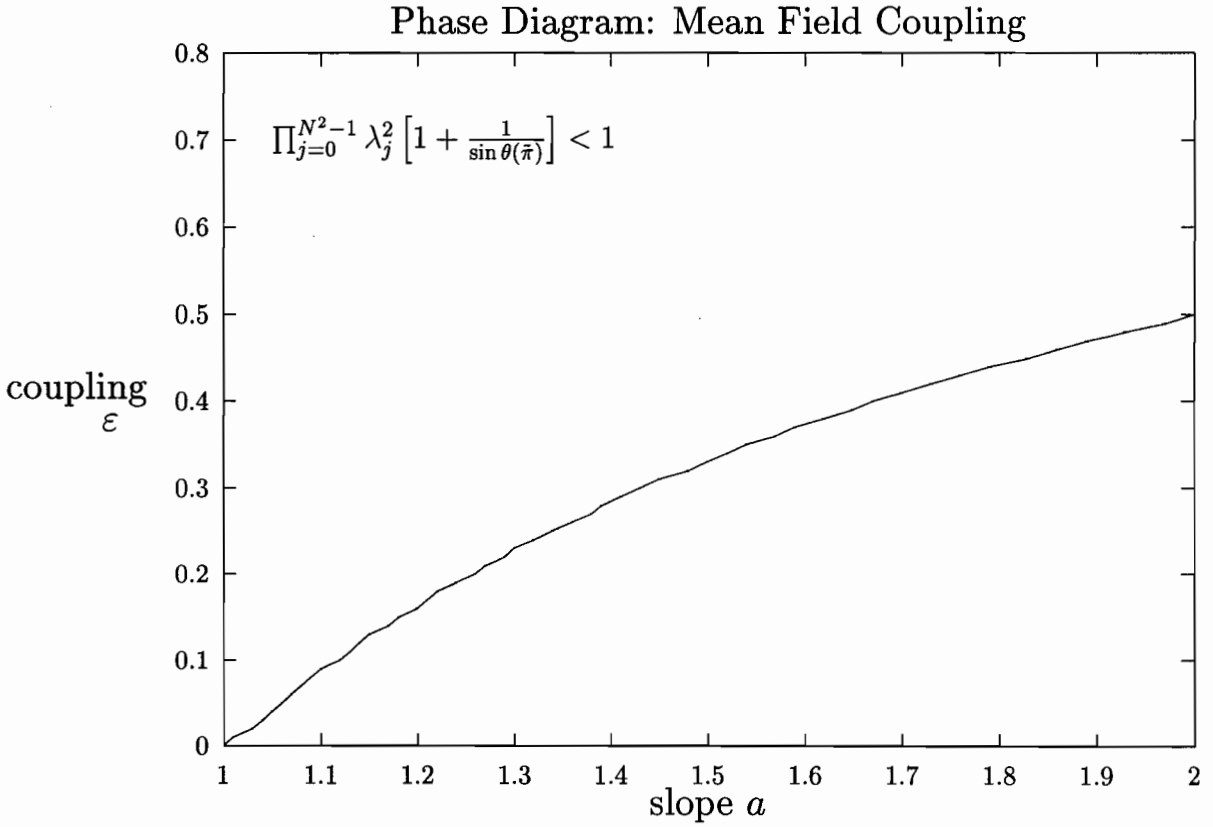

FIGURE 3.17:
Phase diagram for the globally coupled tent map lattice. The diagram is obtained by applying condition (3.30) with the eigenvalues of Table 3.1 corresponding to mean field coupling. It should be noted that the diagrams for Φ^n, $n = 2, 4, \cdots$ yield the *same* curve as the one displayed here.

As explained in the text, this curve is accurately described by the function $\varepsilon = 1 - 1/a$ for all $n \geq 1$.

The most common linear coupling architectures discussed in the literature, diffusive and mean field coupling, have now been treated analytically in a lattice of tent maps. We next investigate a coupling which is closer in nature to the competing populations model presented in Section 3.3.1.

3.7 Lattices of bimodal maps

The methods of Section 3.6 can be extended to more general systems in which the the neighbourhood of a given site acts on its evolution *via* a nonlinear coupling mechanism. Such mechanisms were illustrated in Section 3.3 when considering a generic model of excitable media with inter-element inhibition. We now construct similar CML's which remain analytically tractable.

3.7.1 Presentation of the model

As an example, consider a lattice transformation of piecewise linear maps coupled in a nonlinear fashion to mimic the inter-element inhibition of the excitable CML of Section 3.3.1:

$$\Phi^{(i)}(\mathbf{x}_t) = (1-\varepsilon)S^{(i)}(\mathbf{x}_t) + \frac{\varepsilon}{p} \sum_{\substack{p \text{ nearest} \\ \text{neighbors}}} S^{(j)}(\mathbf{x}_t). \tag{3.33}$$

In this Section, p is chosen so that the inter-element coupling is diffusive; *i.e.* $p = 2$ in dimension 1, $p = 4$ in dimension 2, *etc...*] The inhibitory effect of the neighbourhood is modeled by the local transformation:

$$S^{(i)}(\mathbf{x}_t) = \begin{cases} a x_t^{(i)} & \text{if } x_t^{(i)} \in [0, \tau_t^{(i)}) \\ a(2\tau_t^{(i)} - x_t^{(i)}) & \text{if } x_t^{(i)} \in [\tau_t^{(i)}, 2\tau_t^{(i)}) \\ a(-2\tau_t^{(i)} + x_t^{(i)}) & \text{if } x_t^{(i)} \in [2\tau_t^{(i)}, \tau_t^{(i)} + 1/2) \\ a(1 - x_t^{(i)}) & \text{if } x_t^{(i)} \in [\tau_t^{(i)} + 1/2, 1] \end{cases} \tag{3.34}$$

where $\tau_t^{(i)} \in [1/4, 1/2]$ depends on the mean activity $\xi_t^{(i)}$ in a neighbourhood of $x_t^{(i)}$:

$$\tau_t^{(i)} \equiv \frac{1}{2} - \frac{1}{4d} \sum_{\substack{d \text{ nearest} \\ \text{neighbors}}} x_t^{(j)}. \tag{3.35}$$

This nonlinear coupling is chosen so an increase in the sum over the d neighbors has an inhibitory effect on $x_{t+1}^{(i)}$. When S of CML (3.33) is given by (3.34), the transformation possesses two statistical regimes like the excitable CML discussed in Section 3.3.1. In one phase, the system seems to be ergodic, possessing a unique invariant measure, a one dimensional projection of which is observed numerically. In the other, the statistical quantifiers oscillate periodically in time, indicating that the Perron-Frobenius operator might be asymptotically periodic.

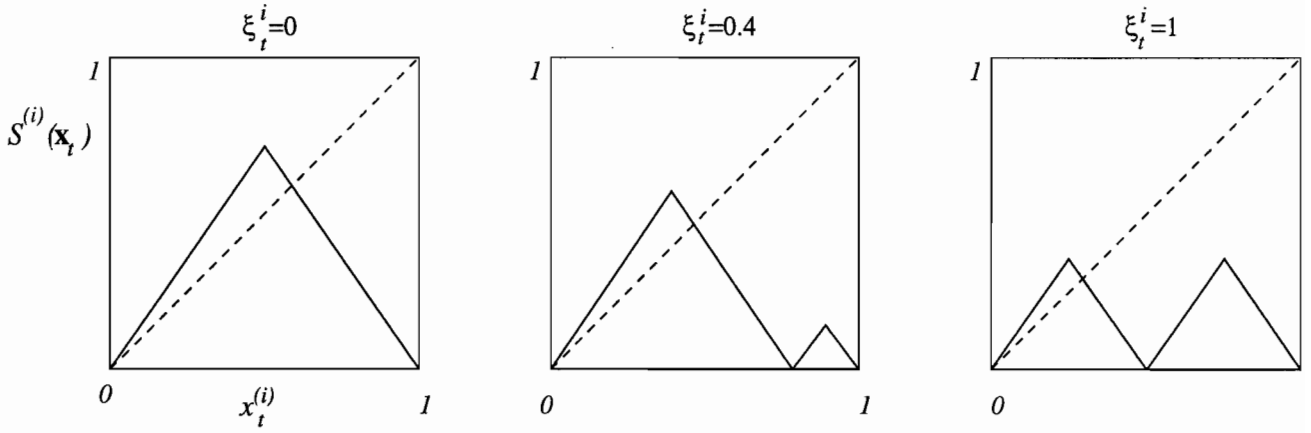

FIGURE 3.18:
Schematic diagram of the bimodal tent map (3.34). The maximum activity of the map decreases if the mean activity of the neighbourhood ξ increases. This inter-element inhibition is meant to mimic the same feature in the more realistic model of Section 3.3.1.

The qualitative observations made concerning the two possible statistical evolutions (to a steady state, or to a limit cycle) of the excitable CML (3.8) hold for the system (3.33) with (3.34). The details of the density cycles are obviously not the same for the two systems, and the structure of the maps is also very different. However, they have similar nonlinear inter-element coupling, and since we have only analytically investigated the behavior of CML's in which the coupling was linear, it is of interest to generalize this analysis to nonlinearly coupled CML's.

The analysis of the previous section can be completely carried out to yield conditions on the parameters of (3.34) sufficient for the cyclical spectral representation of the Perron-Frobenius operator. The eigenvalues of its derivative matrix cannot be evaluated explicitly as a function of the slope a and the number of neighbors p and d included in the two relevant neighborhoods. However, it it possible to derive upper and lower bounds on the quantity $\mathcal{Q}$ of condition (3.24) for (3.34).

3.7.2 Calculating $\mathcal{Q}$

If the d-neighbourhood includes all the sites located within euclidean distance 3 of the site $x_t^{(i)}$ (there are 28 such neighbors in dimension 2), $\mathcal{Q}$ satisfies:

$$\min(\mathcal{Q}_1, \mathcal{Q}_2) \leq \mathcal{Q} \leq \max(\mathcal{Q}_1, \mathcal{Q}_2)$$

where $\mathcal{Q}_1$ and $\mathcal{Q}_2$ are given by

$$\mathcal{Q}_1 = \prod_{k=0}^{N^2-1} \left\{ (1-\varepsilon)a + a\left(\varepsilon - \frac{1}{28}\right)\left[\cos\left(\frac{2\pi k}{N^2}\right) + \cos\left(\frac{2\pi k}{N}\right)\right] - \frac{a}{28}\left[\begin{array}{lll} \cos\left(\frac{4\pi k}{N}\right) & + \cos\left(\frac{6\pi k}{N}\right) & + \cos\left(\frac{4\pi k}{N^2}\right) \\ + \cos\left(\frac{6\pi k}{N^2}\right) & + \cos\left(\frac{2\pi k(N+1)}{N^2}\right) & + \cos\left(\frac{2\pi k(N+2)}{N^2}\right) \\ + \cos\left(\frac{2\pi k(N-1)}{N^2}\right) & + \cos\left(\frac{2\pi k(N-2)}{N^2}\right) & + \cos\left(\frac{2\pi k(2N+1)}{N^2}\right) \\ + \cos\left(\frac{2\pi k(2N+2)}{N^2}\right) & + \cos\left(\frac{2\pi k(2N-1)}{N^2}\right) & + \cos\left(\frac{2\pi k(2N-2)}{N^2}\right) \end{array}\right] \right\} \tag{3.36}$$

and

$$\mathcal{Q}_2 = \prod_{k=0}^{N^2-1} \left\{ a(1-\varepsilon) + a\varepsilon\left[\cos\left(\frac{2\pi k}{N^2}\right) + \cos\left(\frac{2\pi k}{N}\right)\right]\right\}. \tag{3.37}$$

These two quantities allow us to delimit a region in the (a, ε) plane in which the Perron-Frobenius operator admits the cyclical spectral decomposition of Section 4.1. This region is obtained by applying the criterion (3.30) to the system (3.34) with $\mathcal{Q} = \mathcal{Q}_1$ and $\mathcal{Q} = \mathcal{Q}_2$. Define

$$\mathcal{Q}_u = \prod_{k=0}^{N^2-1} \lambda_k^{(u)}, \quad u = 1, 2$$

where the $\lambda_k^{(u)}$ are given implicitly in equations (3.36) and (3.37).

3.7.3 Calculating $\sin\theta(\tilde{\pi})$

To determine the quantity $\sin\theta(\tilde{\pi})$, note that the phase space $\mathbb{X}$ of the transformation Φ defined in (3.34) is again the direct product $[0,1]^{N^2}$ if there are N^2 elements on the lattice. On each of the intervals in $\mathbb{X}$, the transformation $S^{(i)}$ is strictly monotone on four segments $I_1 = [0, \tau_t^{(i)})$, $I_2 = [\tau_t^{(i)}, 2\tau_t^{(i)})$, $I_3 = [2\tau_t^{(i)}, \tau_t^{(i)} + 1/2)$, $I_4 = [\tau_t^{(i)} + 1/2, 1]$, and each of the 4^{N^2} elements of Π is of the form $\pi_{\vec{k}}(i) = I_1^{k_1}(i) \times I_2^{k_2}(i) \times I_3^{k_3}(i) \times I_4^{k_4}(i)$ where $\sum_j k_j = N^2$ (again "i" is the index denoting spatial position on the lattice). Clearly, this partition is no longer rectangular (*cf.* Figure (3B-1)). Using the definition of the thresholds $\tau_t^{(i)}$ given by

equation (3.35), when $p = 4$ (*i.e.* the coupling is diffusive in dimension two), and $d = 28$, the minimum angle of intersection of two edges of the elements of the image partition is, from (3B-2) (*cf.* Appendix 3B)

$$\theta_{\text{int}} = \tan^{-1}\left[-\frac{1}{2}\left(\frac{12543[16(1+2\varepsilon)-15\varepsilon^2]}{1792-53764\varepsilon+50740\varepsilon}\right)\right]. \tag{3.38}$$

From Appendix 3A, $\sin\theta(\tilde{\pi})$ can then be computed as in the linear coupling case of Section 3.6. Hence, for the nonlinearly coupled CML (3.34), the condition (3.24) yields two criteria which give an estimate for the parameter space location of the transition from statistical stability to statistical periodicity:

$$\mathcal{Q}_u^2\left[1+\frac{1}{\sin\theta(\tilde{\pi})}\right] < 1, \quad u = 1, 2. \tag{3.39}$$

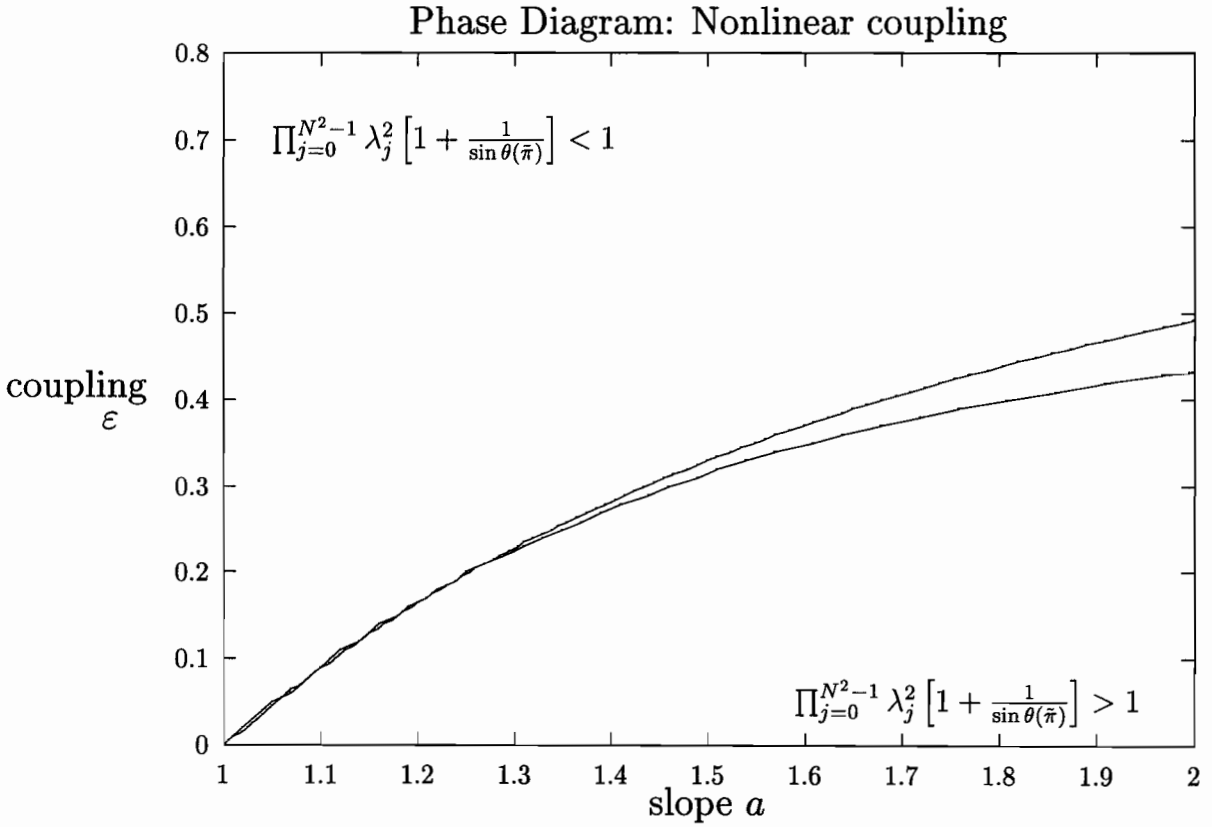

Figure 3.19:
Phase diagram for the nonlinearly coupled CML (3.34). The two curves displayed here are each obtained from (3.39) and they delimit a region which separates the (a, ε) plane in two: Above this region (in the upper left corner) the Perron-Frobenius operator for the CML admits a cyclical spectral decomposition as in (1.21). See text for details.

The two conditions in (3.39) delimit a transition region in the (a, ε) plane which separates two "phases". In one of them, there are sufficient conditions to guarantee a cyclical spectral decomposition of the Perron-Frobenius operator. Figure 3.19 displays the "fuzzy" phase diagram resulting from the application of the two conditions in (3.39) to the system (3.33) with (3.34).

3.8 AP and the formation of patterns

The numerical investigations of Sections 3.2.1 and 3.3.2 indicate that the presence of asymptotic periodicity facilitates the formation of large scale patterns in certain regions of parameter space. To understand the connection between asymptotic periodicity and pattern formation, note that asymptotically periodic systems only occupy small regions of their phase spaces determined by the support of the various v_i's of equation (1.21). For a lattice of N^2 elements, the support of each v_i is a product of N^2 intervals: $\text{support}(v_i) = \mathbb{I}_1 \times \cdots \times \mathbb{I}_N$ where there are r distinct $\mathbb{I}_k \subset [0,1]$ if i also runs from 1 to r (think of the situation for a lattice of tent maps when $r = 2$, and each site belongs to one of two subintervals of $[0,1]$). Denote the r distinct attractive subsets of $[0,1]$ by the symbols $\mathbb{D}_1, \cdots, \mathbb{D}_r$. Hence,

$$\text{support}(v_i) = \prod_{k=1}^{N^2} \mathbb{I}_k = \prod_{j=1}^{r} \left[\prod_{k=1}^{N_j} \mathbb{D}_j \right], \quad \sum_{j=1}^{r} N_j = N^2.$$

The exact form of the $\mathbb{D}_j$'s depends on S and the coupling architecture. If the inter-element coupling in the lattice tends to correlate the activity of neighbouring sites (as is the case for diffusive-like couplings), the evolution of the lattice will be accompanied by the formation of clusters of sites whose values will tend to belong to the same $\mathbb{D}_j$. If the diffusive effects are too strong, all sites will eventually belong to the same $\mathbb{D}_j$ at the same time, and there will be no pattern formation. On the other hand, if the diffusive effects are too weak, neighbouring sites will not tend to belong to the same $\mathbb{D}_j$, and the lack of correlation between nearby elements will be reflected in the lack of large scale patterns. Thus, the appearance of large scale patterns would appear to be the result of a balance between: 1) a coupling induced tendency to synchronize neighbouring sites; and 2) a tendency (due to the asymptotic periodicity) of all site activities to belong to a small number of disjoint subsets of the phase space. If there is only one attractive $\mathbb{D}_j$ (*i.e.* $r = 1$), so the system is statisticaly stable, patterns should not form spontaneously. This is numerically observed to be the case in all the systems we have investigated. We are therefore lead to interpret the effective segregation of regions of

phase space due to asymptotic periodicity as a "reactive" mechanism, which in the presence of diffusive-like couplings, facilitates the appearance of patterns.

3.9 Discussion

The probabilistic description of CML's presented here is a first step towards a more complete understanding of the nonequilibrium thermodynamics and statistical mechanics of these models. For example, comparing Figures 3.16 and 3.17 confirms (for tent maps) the intuitive notion that systems with mean field coupling tend to order more easily than systems with short range interactions.

The importance of the possible presence of statistical cycling in CML's and in more general spatially extended systems lies in its implications for the proper interpretation of the behavior of statistical descriptors of the motion: The notion of thermodynamic equilibrium for these objects must be extended to include a set of states visited sequentially in time.

The cycling of $\mathbf{f}_t$ observed for asymptotically periodic systems is an *ensemble property* and the classical statistical mechanics paradigm which associates a single invariant measure with the state of thermodynamic equilibrium does not apply here. Instead, the thermodynamic equilibrium of the asymptotically periodic CML consists in a sequence of states visited periodically in time. As demonstrated here, the CML's which possess this type of equilibrium are not "pathological" in the sense that they arise in the modeling of many physical and biological systems.

The presence of statistical cycling also implies a type of dependence on the initial conditions which is much stronger than that usually discussed in reference to chaotic dynamical systems. Here the ensemble statistics depend on the initial ensemble. This is a consequence of the dependence of the functionals Γ_i on the initial density $\mathbf{f}_0$ in equation (1.21) (*cf.* Remark 1 of Section 1.4.3).

The regions of parameter space in which asymptotic periodicity occur are large for all the systems discussed here. Therefore, the observation that the statistical quantifiers of the motion cannot be effectively calculated with respect to an invariant measure which exists, but which is almost never observed experimentally, is ubiquitous for these CML's and not the result of very special circumstances. This ubiquity is reflected by the relative frequency of reports discussing supposed violations of the law of large numbers [70, 99, 164, 166] (*cf.* also Section 1.4.5.1 of the Introduction). The present analysis indicates that the one-

dimensional arguments of Pikovsky and Kurths [166] can indeed be extended to arbitrary large dimensional systems which are not necessarily globally coupled.

Since most realistic models of biological or physical relevance must include stochastic perturbations, we conclude by pointing out that analytic investigations of the transfer operator $\mathcal{P}_\Phi$ for stochastically perturbed CML's using appropriate techniques should generalize the approach presented here to a much broader class of spatially extended systems. This motivates the next chapter, in which we consider the behavior of large coupled map lattices perturbed by noise. The investigations are both numerical and analytical, and they lead to the rather surprising conclusion that the presence of noise in CML's will almost always imply the presence of statistical cycling, even when the noiseless system is not asymptotically periodic.

Appendix 3A

In this Appendix, we rigorously define and calculate the quantity $\sin\theta(\tilde{\pi})$ which appears in condition (3.24).

Since the partition $\Pi = \{\pi_i\}_{i=1}^{s}(\Pi)$ of $\mathbb{X} \subset \mathbb{R}^N$ is defined such that the restriction of Φ to π_i, denoted $\Phi_{|\pi_i}$, is differentiable and the π_i's are closed bounded (*i.e.* compact) domains having piecewise hyperplanar boundaries of finite $N-1$-dimensional measure, the angle at which edges of the π_i's intersect is bounded away from zero. In all the cases considered analytically, Φ is also piecewise linear. Hence the edges of the sets $\tilde{\pi}_i$ of the image partition $\tilde{\Pi}$ which are of positive measure also intersect at angles bounded away from zero, because the images of a hyperplane under the action of a piecewise linear Φ are (piecewise) hyperplanar.

Before proceeding with the analysis, it is useful to remind the reader with the concept of a regular cone in $\mathbb{R}^N$:

Definition 4: Regular Cone A regular cone in $\mathbb{R}^N$ is a cone whose base is a $N-1$ dimensional disk d and such that the line joining the center of d to the apex V (not to be confused with the symbol $\bigvee$ used in Section 3.5 to denote the variation) of the cone is perpendicular to d. The angle between this central axis and any segment linking the apex of the cone to d's boundary is called the *summit angle.* ■

The apex of the cone V occurs at the singularities of derivative of Φ. Let SP_i be the set of all singular points of $\partial\pi_i$; hence if $\mathbf{x} \in SP_i$,

$$\frac{\partial(\partial\pi_i(\mathbf{x}))}{\partial x_k} \quad \text{is not defined for some } k. \quad \blacksquare$$

Construct at any $\mathsf{V}_i \in SP_i$ the largest possible regular cone having its apex at V_i and lying completely in π_i. Denote the summit angle of this cone by $\alpha(\mathsf{V}_i)$. Now let

$$\alpha(\theta_{\pi_i}) = \min_{\mathsf{V}_i \in SP_i} \alpha(\mathsf{V}_i) = \alpha(\mathsf{V})$$

and define

$$\sin\theta(\tilde{\pi}_i) = \mid \sin(\alpha(\pi_i)) \mid .$$

Finally, let

$$\sin\theta(\tilde{\pi}) \equiv \min_{\pi_i \in \Pi} \sin\theta(\tilde{\pi}_i).$$

Calculating $\sin\theta(\tilde{\pi})$ turns out to be straightforward when the π_i's are bounded by hyperplanes such that the edges of $\partial\pi_i$ intersecting at V_i do so with angle θ_{int}. To illustrate the procedure, consider Figure (3A-1) which illustrates the situation in $\mathbb{R}^2$ and $\mathbb{R}^3$. If dist(**x**,**y**) denotes the Euclidean distance between points **x** and **y**,

$$\sin\theta(\tilde{\pi}) = \frac{\text{dist}(C_s, C_e)}{\text{dist}(V, C_e)} \tag{3A-1}$$

where Cs is the center of the shaded circle, Ce the middle of one (and any) of the edges of the base of the "pyramid", and V is the apex of the regular cone. Note that if $\theta(\tilde{\pi}) = \pi/2$, then it is straighhtforward from the right of Figure 3A-1 that $\sin\theta(\tilde{\pi}) = 1/\sqrt{3}$ in $\mathbb{R}^3$.

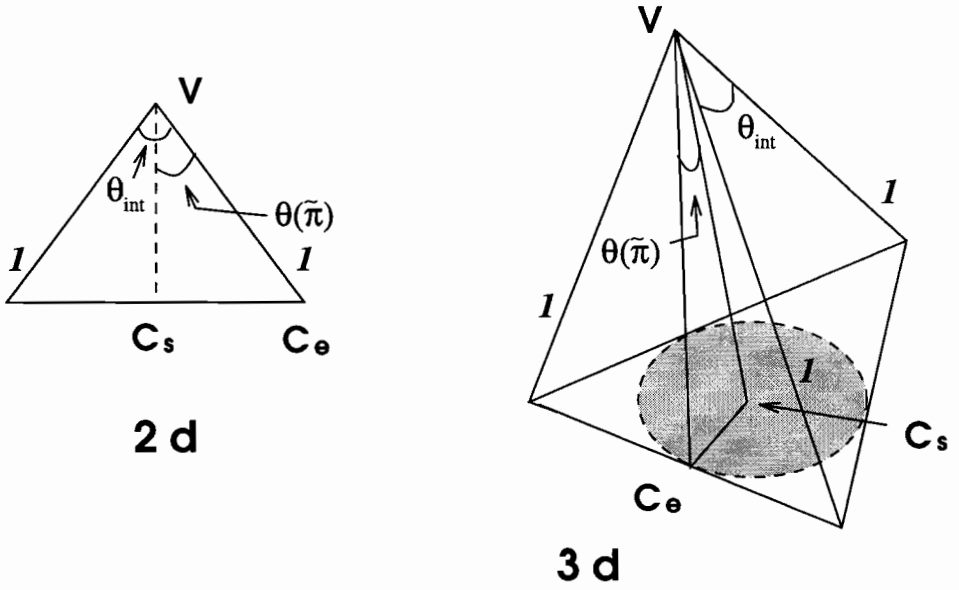

FIGURE 3A-1:
Illustration when $N = 2$ and $N = 3$ of the embedding of a $(N-1)$-sphere in a regular $(N-1)$-simplex (which is one face of a regular N-simplex). Cs denotes the centroid of the $(N-1)$-sphere, Ce denotes the centroid of one edge of the $(N-1)$-simplex containing the $(N-1)$-sphere. V denotes the vertex of the N-simplex not contained in the $(N-1)$-simplex.

In $\mathbb{R}^N$, (3A-1) holds when Cs is the centroid of the $(N-1)$-sphere embedded in one face of the regular N-simplex (which is a regular $(N-1)$-simplex), and Ce is the center of one of the edges of that $(N-1)$-simplex. Although it is not possible to draw the higher dimensional simpleces and spheres, it is easy to embed them in an orthonormal reference frame and proceed with the analysis. For clarity, a simple case is considered before the more general result is given.

Case 1: $\tilde{\Pi}$ is a rectangular partition: $\theta_{\text{int}} = 90^0$ (Warm up)

In this case, any two adjacent edges of the N-simplex intersect at V with angle $\theta_{\text{int}} = \pi/2$. It is easy to show that in $\mathbb{R}^N$, if V is placed at the origin

$$\mathsf{Cs} = \left(\frac{1}{N}, \cdots, \frac{1}{N}\right) \ , \ \mathsf{Ce} = \left(0, \frac{1}{N-1}, \cdots, \frac{1}{N-1}\right)$$

and therefore

$$\text{dist}(\mathsf{Cs}, \mathsf{Ce}) = \frac{1}{\sqrt{N(N-1)}} \ , \ \text{dist}(\mathsf{V}, \mathsf{Ce}) = \frac{1}{\sqrt{(N-1)}}$$

which implies that for a rectangular partition in $\mathbb{R}^N$,

$$\sin\theta(\tilde{\pi}) = \frac{1}{\sqrt{N}} \quad . \quad \blacksquare \tag{3A-2}$$

Case 2: $\tilde{\Pi}$ is not a rectangular partition: θ_{int} arbitrary

In this case we still assume that any two adjacent edges of the N-simplex intersect at V with an arbitrary angle $\theta_{\text{int}} < \pi/2$, where θ_{int} is the same for all angles. The N vertices $v_1, \cdots, v_N$ of the $(N-1)$-simplex forming the base of the N-simplex having apex V at the origin have coordinates which are cyclical permutations of each other. Thus, if $v_1 : (\kappa_1, \cdots, \kappa_N)$, then $v_i : (\text{Per}^i\{\kappa_1, \cdots, \kappa_N\})$ where $\text{Per}\{\kappa_1, \cdots, \kappa_N\} = \{\kappa_N, \kappa_1, \cdots, \kappa_{N-1}\}$. Therefore,

$$\mathsf{Cs} = \left(\frac{\sum_{i=1}^N \kappa_i}{N}, \cdots, \frac{\sum_{i=1}^N \kappa_i}{N}\right) \ , \ \mathsf{Ce} = \left(\frac{\sum_{i=2}^N \kappa_i}{N-1}, \cdots, \frac{\sum_{\substack{i=1 \\ i\neq j}}^N \kappa_i}{N-1}, \cdots, \frac{\sum_{i=1}^{N-1} \kappa_i}{N-1}\right)$$

which implies

$$\sin\theta(\tilde{\pi}) = \frac{1}{N}\sqrt{\frac{\sum_{j=1}^N \left(N\kappa_j - \sum_{i=1}^N \kappa_i\right)^2}{\sum_{j=1}^N \left(\sum_{\substack{i=1 \\ i\neq j}}^N \kappa_i\right)^2}}. \tag{3A-3}$$

Note that if all but one of the κ_i's are zero, and the nonzero κ_i is 1, the vertices v_i all lie on the N dimensional hypercube, and therefore the edges which bound $\partial\pi_i$ intersect at right angles: Π is rectangular as in case 1, and (3A-3) yields $\sin\theta(\tilde{\pi}) = 1/\sqrt{N}$ as expected.

From a practical point of view, given an N dimensional lattice transformation, it is easy to construct the partition Π, but it can be time consuming to obtain the κ_i's used in (3A-3). On the other hand, it is usually straightforward to compute, in terms of the parameters of the transformation, the smallest angle θ_{int} subtended by the edges of the π_i's. It is therefore useful to express $\sin\theta(\tilde{\pi})$ in terms of this θ_{int}. To do so, note that the N apexes v_i (with coordinates $\{\kappa_i\}$) of a N-simplex whose summit V is placed at the origin, and whose edges

intersect there at angles θ_{int} all lie on lines which link the centroid Cs to the apexes of the N-simplex whose edges intersect at the origin at an angle $\pi/2$ (think of the 2 and 3 dimensional situations). The equation of one of these lines is, from our discussion of *Case 1*,

$$-\frac{\kappa_1 - 1}{1 - 1/N} = N\kappa_2 = \cdots = N\kappa_N, \tag{3A-4}$$

and the equations for the $(N-1)$ other lines are obtained by permuting x_1 with the remaining $(N-1)$ coordinates in (3A-4). In addition, all of the v_i's have to be equidistant from Cs. Therefore, we obtain a second set of constraints which must be satisfied by the κ_i's:

$$\left(\kappa_1 - \frac{1}{N}\right)^2 + \sum_{i=2}^{N}\left(\kappa_i - \frac{1}{N}\right)^2 = d_{\text{Cs}v}^2$$

or

$$\left(\kappa_1 - \frac{1}{N}\right)^2 + (N-1)\left(\frac{\kappa_1 - 1}{N-1} + \frac{1}{N}\right)^2 = d_{\text{Cs}v}^2, \tag{3A-5}$$

where $d_{\text{Cs}v}$ is the distance between Cs and the v_i's. Solving these equation yields, for apexes v_1 and v_2 for example,

$$v_1 = \left(\frac{1}{N} + d_{\text{Cs}v}\sqrt{\frac{N-1}{N}}, \frac{1}{N} - \frac{d_{\text{Cs}v}}{\sqrt{N(N-1)}}, \cdots, \frac{1}{N} - \frac{d_{\text{Cs}v}}{\sqrt{N(N-1)}}\right) \tag{3A-6}$$

$$v_2 = \left(\frac{1}{N} - \frac{d_{\text{Cs}v}}{\sqrt{N(N-1)}}, \frac{1}{N} + d_{\text{Cs}v}\sqrt{\frac{N-1}{N}}, \cdots, \frac{1}{N} - \frac{d_{\text{Cs}v}}{\sqrt{N(N-1)}}\right). \tag{3A-7}$$

Now consider vectors $\vec{\text{V}v_i}$ and $\vec{\text{V}v_j}$ where $i \neq j$. The angle subtended by these two vectors is θ_{int} by definition. Therefore,

$$\cos(\theta_{\text{int}}) = \frac{\vec{\text{V}v_i} \cdot \vec{\text{V}v_j}}{|\,\text{V}v_i\,||\,\text{V}v_j\,|}$$

from which it is easy to obtain

$$d_{\text{Cs}v} = \sqrt{\frac{[1 - \cos\theta_{\text{int}}](N-1)}{N[(N-1)\cos\theta_{\text{int}} + 1]}}. \tag{3A-8}$$

Replacing (3A-8) in (3A-7) yields the coordinates of the v_i's as a function of the angle θ_{int}:

$$\kappa_1 = \frac{1}{N} + \frac{N}{N-1}\sqrt{\frac{1 - \cos\theta_{\text{int}}}{(N-1)\cos\theta_{\text{int}} + 1}},\ \kappa_i = \frac{1}{N} - \frac{1}{N}\sqrt{\frac{1 - \cos\theta_{\text{int}}}{(N-1)\cos\theta_{\text{int}} + 1}} \text{ if } i = 2, \cdots, N. \tag{3A-9}$$

Using these expressions in (3A-3) yields, for a lattice of N elements

$$\sin\theta(\tilde{\pi}) = \sqrt{\frac{1-\cos\theta_{\text{int}}}{N[1+(N-2)\cos\theta_{\text{int}}]}}. \quad \blacksquare \tag{3A-10}$$

Note that if $N = 3$ (3A-10) reduces to

$$\sin\theta(\tilde{\pi}) = \frac{1}{\sqrt{3}}\tan\left(\frac{\theta_{\text{int}}}{2}\right)$$

which can be easily derived directly from Figure (3A-1) using simple geometrical arguments.

Appendix 3B

In this Appendix, the angle θ_{int} and the quantity $\sin\theta(\tilde{\pi})$ are computed explicitly for the coupled bimodal maps of Section 3.7. Figure (3B-1) schematically illustrates the evolution of the unit square under the action of the transformation Φ defined in 5.1. Before proceeding, we introduce the following notation:

$$\begin{aligned}
\bar{\tau}_t^i &= \frac{1}{4p}\sum_{k\neq i,j} x_t^{(k)}, \quad k,j \in p-\text{neighbourhood of } i \\
\bar{x}_t^i &= \frac{1}{d}\sum_{k\neq i,j} x_t^{(k)}, \quad k,j \in d-\text{neighbourhood of } i
\end{aligned}$$

Hence the two dimensional restriction $\Phi^{(2\text{-d})}$ of the transformation Φ, which describes the evolution of one face of the hypercube $\mathbb{X}$ is given by:

$$\begin{aligned}
\Phi^{(2\text{-d})(i)}(\mathbf{x}_t) &= (1-\varepsilon)S^{(i)}(\mathbf{x}_t) + \frac{\varepsilon}{p}S^{(j)}(\mathbf{x}_t) + \bar{x}_t^i \\
\Phi^{(2\text{-d})(j)}(\mathbf{x}_t) &= (1-\varepsilon)S^{(j)}(\mathbf{x}_t) + \frac{\varepsilon}{p}S^{(i)}(\mathbf{x}_t) + \bar{x}_t^j
\end{aligned} \tag{3B-1}$$

where the local transformation is again given by (3.34).

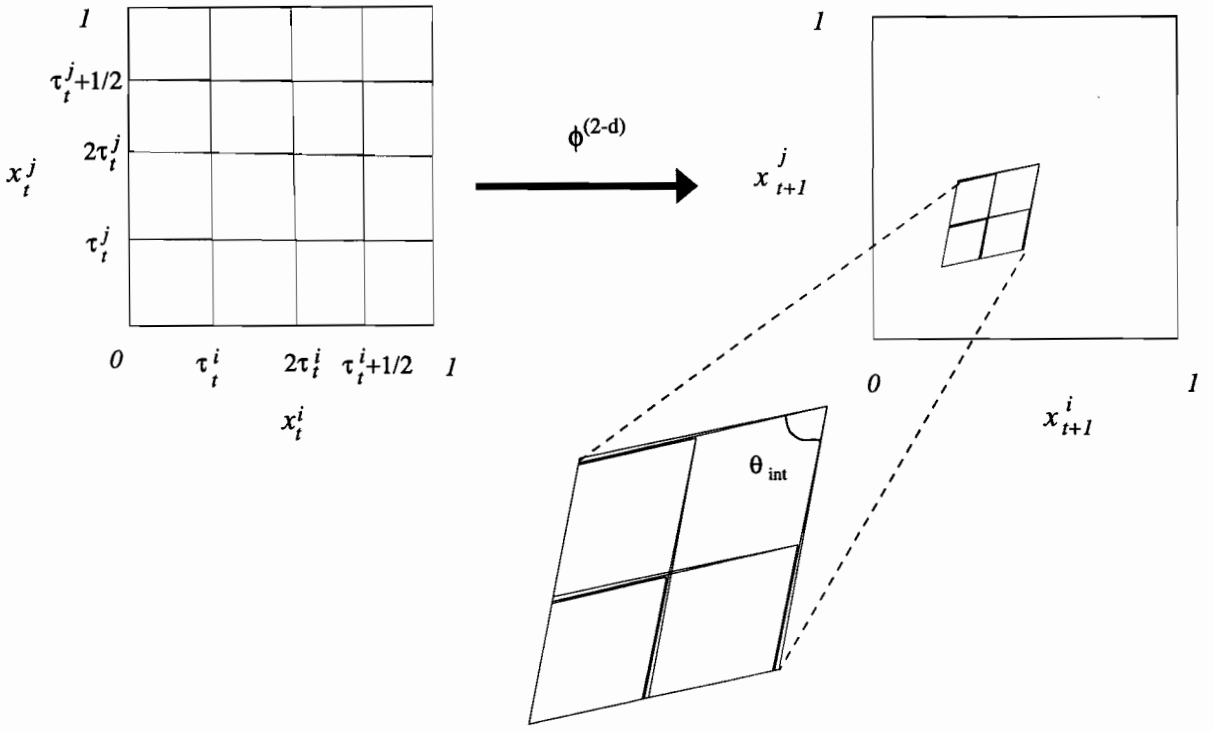

FIGURE 3B-1:
Illustration of the evolution of one face of the hypercube $\mathbb{X} = [0,1]^N$. On each of the rhomboids on the left panel, the transformation Φ is linear with slope $\pm a$. The panel on the right displays the images of these rhomboids. θ_{int} is the smallest angle formed by the edges of the "image rhomboids". In this figure, parameters are $a = 1.4$, $\varepsilon = 0.45$, $p = 28$, $d = 4, \bar{\tau}_t^i = \bar{\tau}_t^j = 0.15, \bar{x}_t^i = \bar{x}_t^j = 0.225$ (the symmetry was chosen for pedagogical purposes; it is in general not present for random initial conditions).This figure was computed with the symbolic manipulator MAPLE.

Determining θ_{int} is straightforward but lengthy, and we have relied heavily on the use of a symbolic manipulator to carry out the explicit calculations. The plan of the algorithm to compute θ_{int} is as follows

1) Using the definition of $\Phi^{(2\text{-d})}$, obtain the coordinates of the 25 vertices of the 16 rhomboids on which $\Phi^{(2\text{-d})}$ is linear (these are displayed on the left panel of Figure (3B-1)).

2) Iterate each of these points, so as to obtain 16 "image rhomboids" (displayed on the right of Figure (3B-1)).

3) Using these coordinates, find the angles of intersection of the edges of these image rhomboids, and find the smallest one, which is by definition θ_{int}. Though the problem seems intractable at first glance, the task is greatly simplified by the many symmetries in the

coordinates of the image rhombs, so that it is not necessary to perform a time-consuming minimization problem.

The analytic expression for θ_{int} is, as expected, independent of the slope a. It is given implicitly by

$$\tan\theta_{\text{int}} = -\frac{1}{2}\left\{\frac{(1-16d^2)[p^2(1-2\varepsilon)+\varepsilon^2(1-p^2)]}{4dp^2-\varepsilon p[1+8d(p+2d)]+\varepsilon^2[4d(1+p(1+4d))+p]}\right\}. \tag{3B-2}$$

This expression can then be used in (3A-10) of the previous appendix, to obtain an expression for the quantity $\sin\theta(\tilde{\pi})$ in terms of the control parameters of the CML of Section 3.7.

Appendix 3C

In this appendix we recall a few concepts from real analysis which are constantly referred to in the treatment of the Perron-Frobenius operator given in this chapter. We included this list of definitions because they do not belong to the standard conceptual toolbox of statistical mechanics. It is obviously not meant as an exhaustive introduction to real analysis.

We start with a few basic definitions which are necessary to clarify the notion of a Banach space. These are important because the phase space probability densities which are induced by nonlinear coupled map lattices are themselves elements of Banach spaces.

1. Linear spaces

A set $\mathbb{X}$ of elements is called a *linear space* if we have a function $+$ on $\mathbb{X}\times\mathbb{X}$ to $\mathbb{X}$ and a function $\cdot$ on $\mathbb{R}\times\mathbb{X}$ to $\mathbb{X}$ which satisfy, for x and y in $\mathbb{X}$

i. $x+y=y+x$;

ii. $(x+y)+z=x+(y+z)$;

iii. There is a unique ϑ in $\mathbb{X}$ such that $x+\vartheta=x$, for all x.

iv. $a(x+y)=ax+ay$ for $a\in\mathbb{R}$.

v. $(a+b)x=ax+bx$ for $a,b\in\mathbb{R}$.

vi. $a(b)x=(ab)x$ for $a,b\in\mathbb{R}$.

vii. $0\cdot x=\vartheta$ and $1\cdot x=x$.

Clearly, $+$ and $\cdot$ are the familiar addition and multiplication by scalars.

2. Norms

A nonnegative real-valued function $\|\|\|$ defined on a linear space $\mathbb{X}$ is called a *norm* if, for $x, y \in \mathbb{X}$,

i. $\| x \| = 0 \Leftrightarrow x = \vartheta$.

ii. $\| x + y \| \leq \| x \| + \| y \|$.

iii. $\| ax \| = |a| \, \| x \|$, $a \in \mathbb{R}$.

Rigorously, a normed linear space is the pair $(\mathbb{X}, \|\|\|)$. When there can be no ambiguity about the norm, the pair is often denoted $\mathbb{X}$. An important family of norms which are frequently used are the so-called L_p norms: the L_p norm of a real valued measurable function f defined on the real interval I, is given by

$$\| f \|_{L_p} \equiv \left[\int_I |f(x)|^p \, dx \right]^{1/p}. \tag{3C-1}$$

3. Metric spaces

A metric space $(\mathbb{X}, \rho)$ is a nonempty set $\mathbb{X}$ of elements together with a real-valued function ρ defined on $\mathbb{X} \times \mathbb{X}$ such that for all x, y and z in $\mathbb{X}$,

i. $\rho(x, y) \geq 0$;

ii. $\rho(x, y) = 0$ if and only if $x = y$.

iii. $\rho(x, y) = \rho(y, x)$.

iv. $\rho(x, y) \leq \rho(x, z) + \rho(z, y)$.

The function ρ is called a *metric*. Normed linear spaces in which the distance between two elements x and y is given by the metric $\rho(x, y) = \| x - y \|_{L_p}$ are known as L_p-spaces.

To introduce the notion of a Banach space, it is useful to describe two more concepts, associated with the behavior of sequences of functions belonging to a metric space.

4. Convergence of sequences; Cauchy sequences

A sequence $\{f_n\}$ in a normed linear space is said to converge to an element f of this space if, given $\epsilon > 0$, there is an N such that for all $n > N$, $\| f - f_n \| < \epsilon$. The sequence $\{f_n\}$ is a *Cauchy sequence* if, given $\epsilon > 0$, there is an N such that for all $n > N$ and $m > N$, $\| f_m - f_n \| < \epsilon$. Each convergent sequence is a Cauchy sequence.

5. Banach spaces

A normed linear space is called a *Banach space* if every Cauchy sequence in the space converges. The property that all Cauchy sequences converge is known as *completeness*. In the remainder of this thesis, the standard notation for a Banach space will be $(\mathbb{X}, \|\|\|)$, where again $\mathbb{X}$ denotes a set of functions, and $\|\|\|$ the norm which endows it. An example of a

Banach space which will be used in the following section, is the space of real valued bounded measurable functions defined on a subset I^n of $\mathbb{R}^n$, endowed with the L_1 norm $(\mathcal{C}[I^n], \|\|_{L_1})$.

We now review some basic properties of linear operators.

6. Bounded linear operators

A mapping M of a linear space $\mathbb{X}$ into a linear space $\mathbb{Y}$ is called a *linear operator* if

$$M(ax_1 + bx_2) = aMx_1 + bMx_2 \tag{3C-2}$$

for all $x_1,\ x_2 \in \mathbb{X}$ and all real $a,\ b$. If $\mathbb{X}$ and $\mathbb{Y}$ are normed, and if there is a constant n such that

$$\| Mx \| \leq \mathsf{n} \| x \| \tag{3C-3}$$

for all x, then M is said to be *bounded.* The least such n is called the norm of operator M. As a consequence of the definition (3C-3), it is straightforward to show that if a linear operator is bounded, it is also continuous and *vice-versa* (*cf.* Chapter 10 of [182]).

7. Spectrum of an operator

Denote by I the identity operator in a space $\mathbb{X}$. The *spectrum* of a bounded operator M is the set $\sigma(M)$ of complex numbers λ such that $(M - \lambda I)^{-1}$ does not exist as a bounded operator in $\mathbb{X}$. The functions which satisfy

$$M\phi_i = \lambda_i \phi \tag{3C-4}$$

are known as the eigenfunctions of the operator M. The quantity

$$\mathsf{R}(M) = \lim_{n \longrightarrow \infty} |M^n|^{1/n} \tag{3C-5}$$

is called the *spectral radius* of M. A simpler but equivalent definition of the spectral radius of M is: $\mathsf{R}(M) = |\lambda_{max}|$ where $|\lambda_{max}|$ is the modulus of the largest eigenvalue.

Chapter 4

The evolution of probability densities in stochastic coupled map lattices

ABSTRACT

This chapter describes the statistical properties of coupled map lattices subjected to the influence of stochastic perturbations. The stochastic analogue of the Perron-Frobenius operator is derived for various types of noise. When the local dynamics satisfy rather mild conditions, the corresponding evolution equation is shown to possess either stable steady state solutions (*i.e* a stable invariant density) or density limit cycles. Convergence to these limit cycle solutions explains the nonstationary behavior of statistical quantifiers at equilibrium. These results are used to explain the numerically observed phase transitions in various lattices of stochastic maps with short range inter-element coupling architectures.

Le hasard est le plus grand romancier du monde:
pour être fécond, il n'y a qu'à l'étudier.

Honoré de Balzac, *La Comédie Humaine, Avant-Propos*

4.1 Introduction

To this point, the systems investigated in this thesis have all been deterministic. Given an initial preparation, there was no uncertainty concerning the eventual state of the model. Determinism is useful, but randomness is often unavoidable, whether it is of natural origin or due to incomplete knowledge. When random fluctuations are an integral part of the situation under study, models which can incorporate some level of uncertainty are also unavoidable. The literature dealing with the influences of noise on deterministic dynamical systems is too vast to be given justice in the scope of this chapter. We refer the interested reader to the work of Horsthemke and Lefever [81] for an extensive description of the qualitative dynamical changes which can result from stochastic perturbations. A more recent overview of related problems, complete with many experimental investigations, is given in [156]. Although investigations of ODE's and one dimensional maps perturbed by noise are numerous, there are still few descriptions of the influence of noise on the evolution of high dimensional dynamical systems. This should not be too surprising, since the noise in many stochastic models is thought to describe the collective behavior of those degrees of freedom which are not the focus of the investigation. When this is the case, a system with a large number of degrees of freedom is sometimes modeled by a small number of effective degrees of freedom perturbed by noise.

This description is not always appropriate, and sometimes it is useful to keep a high dimensional model and study its evolution under the action of noisy perturbations. In this spirit, a few numerical investigations of stochastic CML's have been presented recently [149, 216, 160, 164]. These investigations focus on the probabilistic properties of the stochastic CML's for obvious reasons, and they all point to the general lack of a framework within which such a description should take place. We propose in this chapter to extend the presentation of Chapter 3 to stochastic CML's by investigating the stochastic analogue of the Perron-Frobenius operator, referred to throughout this chapter as the transfer operator.

We reported in Chapter 3 that when the local map S was unimodal on the interval $[0, 1]$, many CML' possessed two distinct phases. In one, the statistical quantifiers of the

motion relaxed to a state of equilibrium. Mathematically, this phase was formally described by an absolutely continuous invariant measure associated with a fixed point of the Perron-Frobenius operator. The other phase was associated with a periodic cycling of the statistical quantifiers of the motion, and reflected the cyclical spectral decomposition (1.21) of the Perron-Frobenius operator. The approach presented here rests on the observation that the transfer operator induced by noisy CML's is a Markov operator defined by a stochastic kernel. We can therefore apply results available concerning these objects to the statistical description of stochastic coupled map lattices.

The types of models investigated here are introduced in Section 4.2, where we also discuss the two most important kinds of stochastic perturbations, additive *vs.* multiplicative (or parametric). Their behavior is discussed numerically in Section 4.3, when the local transformation is either the tent map, the logistic map, or a piecewise linear map known as the "Keener map". The main analytic results are presented in Section 4.4, where the transfer operators for various types of noise are derived explicitly. Implications for the proper construction of the thermodynamics of stochastically perturbed high dimensional dynamical systems are discussed in Section 4.5.

4.2 Stochastic CML's

To introduce stochastic coupled map lattices, recall that in its most general form, a deterministic coupled map lattice is a mapping $\Phi : \mathbb{R}^N \longmapsto \mathbb{R}^N$ governing the evolution of a state vector $\mathbf{x}_t$

$$\mathbf{x}_{t+1} = \Phi(\mathbf{x}_t), \quad t = 0, 1, \cdots. \tag{4.1}$$

In this chapter, we will consider cases where the phase space $\mathbb{X}$ of Φ is a restriction of $\mathbb{R}^N$ to the N-dimensional hypercube: $\mathbb{X} = [0,1] \times \cdots \times [0,1]$. In two spatial dimensions, the evolution of each site of a deterministic coupled map lattice with linear interelement coupling is given by

$$x_{t+1}^{(kl)} = \Phi^{(kl)}(\mathbf{x}_t) = (1-\varepsilon)S(x_t^{(kl)}) + \frac{\varepsilon}{p} \sum_{\substack{p \text{ nearest} \\ \text{neighbours}}} S(x_t^{(ij)}), \quad \varepsilon \in (0,1), \tag{4.2}$$

where $S : [0,1] \longmapsto [0,1]$ describes the local dynamics. The perturbations considered here are random vectors of N numbers (for an N element CML), whose components are independent of one another, each being distributed according to a one dimensional probability density

g. The density $\mathbf{g} = (g^{(1)}, \cdots, g^{(N)})$ of the vector random variable $\boldsymbol{\xi} = (\xi^{(1)}, \cdots, \xi^{(N)})$ will therefore be constructed as the product of its components:

$$\mathbf{g}(\boldsymbol{\xi}) = \prod_{i=1}^{N} g^{(i)}(\xi^{(i)}) = \prod_{i=1}^{N} g(\xi^{(i)}), \quad i = 1, 2, \cdots, N. \tag{4.3}$$

There are various ways in which a stochastic perturbation can influence the evolution of a coupled map lattice: the perturbation can be additive or multiplicative, and it can be applied constantly or randomly. The influence of the noise on the dynamics depends on which of these is considered.

4.2.1 Additive and multiplicative perturbations

These are perturbations applied at each iteration step. When the stochastic perturbation is constantly applied, it can be either added to, or multiply, the original transformation Φ. In the former case, the evolution of a lattice site is given by a relation of the form

$$x_{t+1}^{(kl)} = \Phi^{(kl)}(\mathbf{x}_t) + \xi_t^{(kl)} \equiv \Phi_{\text{add}}^{(kl)}(\mathbf{x}_t) \tag{4.4}$$

and $\boldsymbol{\xi}$ is then referred to as *additive* noise. In the latter, we have

$$x_{t+1}^{(kl)} = \Phi^{(kl)}(\mathbf{x}_t) \times \xi_t^{(kl)} \equiv \Phi_{\text{mul}}^{(kl)}(\mathbf{x}_t) \tag{4.5}$$

and $\boldsymbol{\xi}$ is then referred to as *multiplicative* or *parametric noise.* In general, the effects of additive and multiplicative noise on CML's can be different, since they model different perturbing mechanisms. For example, it is well established that the influence of both types of noise can induce different behavior if the system is close to a Hopf bifurcation [81].

The noise density (4.3) of the perturbations present in (4.4) and (4.5) is always defined so that the phase space of the perturbed tranformations remains the N dimensional hypercube $\mathbb{X}$ defined above. In other words, $\Phi_{\text{add}} : \mathbb{X} \longmapsto \mathbb{X}$ and $\Phi_{\text{mul}} : \mathbb{X} \longmapsto \mathbb{X}$.

Before analytically discussing the dynamics of stochastic CML's, we numerically illustrate typical behaviors using several transformations which have been introduced in the literature.

4.3 Numerical investigations of stochastic CML's

This section illustrates with simple toy models that the presence of noise in CML's can sometimes have trivial consequences, which are expected on the basis of intuition, and sometimes

not-so-trivial consequences, which tend to go against our common expectations of the influence of noise in dynamical systems. In order to keep with what is becoming tradition, we will consider again systems of tent maps, and logistic maps, and we will in addition consider the dynamics of a CML in which the local map belongs to a class of systems introduced by Keener [108], which we refer to as the Keener map lattice.

The statistical descriptors used here to characterize the evolution of the various CML's are the temporal and spatial correlation functions, the Boltzmann-Gibbs entropy and the density of activity on the lattices. These are all defined in the previous chapters.

4.3.1 The tent map and logistic map lattices with noise

These CML's are of the form (4.2), with $p = 4$ in dimensionality 2, and the local map S is either the generalized tent map or the logistic maps discussed in the previous chapters.

4.3.1.1 The tent map lattice

The behavior of the CML (4.2), with S given by the tent map (??), perturbed as in (4.4) remains qualitatively similar to that of the unperturbed system. As the local slope a is decreased from 2 to 1, for a given ε and a given noise amplitude, the period of the banded chaotic behavior doubles successively from period 1 to period 2 to period 4 *etc....* As the period increases, the separation between different bands in the deterministic system diminishes without bound away from 0. As expected, in the stochastic system, the doubling stops when the amplitude of the noise becomes larger than this band separation. Figure 4.1 illustrates this noise induced band merging, when two bands merge into a single one, under the action of additive perturbations. Numerical investigations of this and other CML's indicate that in certain regions of parameter space, the systems are more sensitive to the action of parametric noise than to that of additive noise. This is striking for example, in the case of the lattices of tent maps when the parameters are such that the deterministic lattice is in the period two regime. In this case the transition between period two and period one (stability) behavior is induced for additive perturbations which have an amplitude of about 1/10, or multiplicative perturbations which have an amplitude of about 1/100 (*i.e.* in this case the variable ξ is uniformly supported on $[0.995, 1.005]$). High sensitivity to multiplicative noise is also observed in lattices of logistic maps, and lattices of piecewise linear maps introduced in Section 4.3.2. Investigations of the CML introduced in Section 3.3.1, where S is smooth

and the inter-element coupling is nonlinear show that this system is also more "sensitive" to multiplicative than to additive noise. We should point out, however, that this apparent greater susceptibility to parametric noise is not observed everywhere in the parameter space.

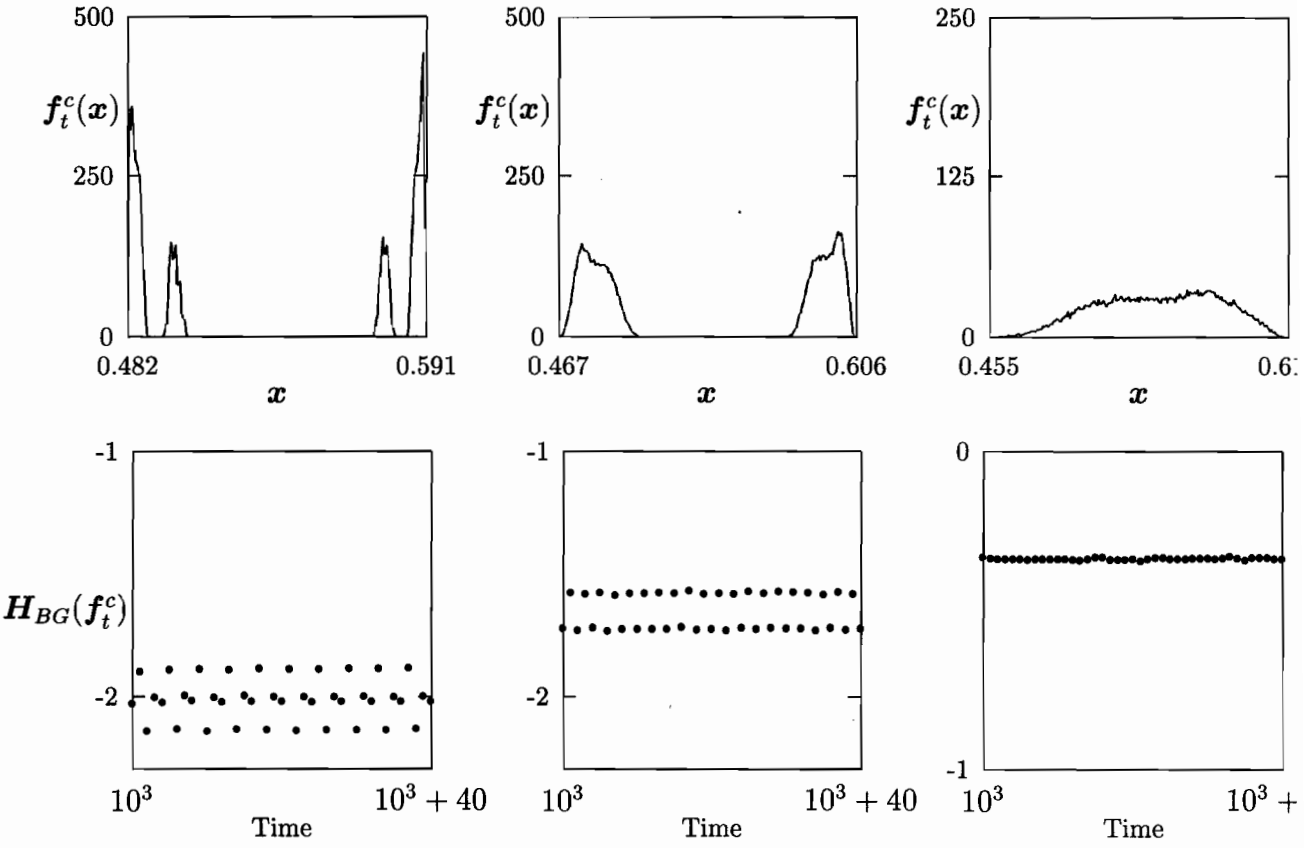

FIGURE 4.1:
Noise induced band merging in a lattice of 200×200 tent maps coupled diffusively, with $a = 1.175$ and $\varepsilon = 0.1$. Top row: Left, the distribution of activity across a deterministic lattice at time $t = 10^3$; center, same distribution when the lattice is perturbed by additive noise uniformly supported on $[0, 0.003]$; right, additive noise supported on $[0, 0.03]$. Bottom row: From left to right, the panels display the temporal behavior of the Boltzmann-Gibbs entropy associated with the densities displayed in the top row. As expected, the lattices are statistically stabilized as the noise amplitude increases.

A surprising effect of the perturbation of a system by noise is the resulting "statistical hysteresis" shown in Figure 4.2, which displays a bifurcation diagram for the Boltzmann-Gibbs entropy of the collapsed density of various lattices subjected to noise. As explained in Section ?? the changes in the behavior of H_{BG} as the control parameters are varied are signatures of phase transitions in the corresponding lattice. When H_{BG} asymptotically reaches a

periodic cycle, reflected by the cycling of ensemble densities, the statistical quantifiers of the motion are also time periodic. This cycling is the same as the behavior reported in Chapter 3 on deterministic lattices. Note that the bifurcation diagram of Figure 4.2 depends, in certain regions of parameter space, on whether the parameter is being increased or decreased. This indicates that the ensemble properties of the CML depend on the initial ensemble density. We will come back in Section 4.4 to an explanation of this phenomenon, which is expected in large classes of stochastic CML's (including the systems whose behavior is displayed in Figure 4.2), on the basis of the spectral properties of the transfer operator.

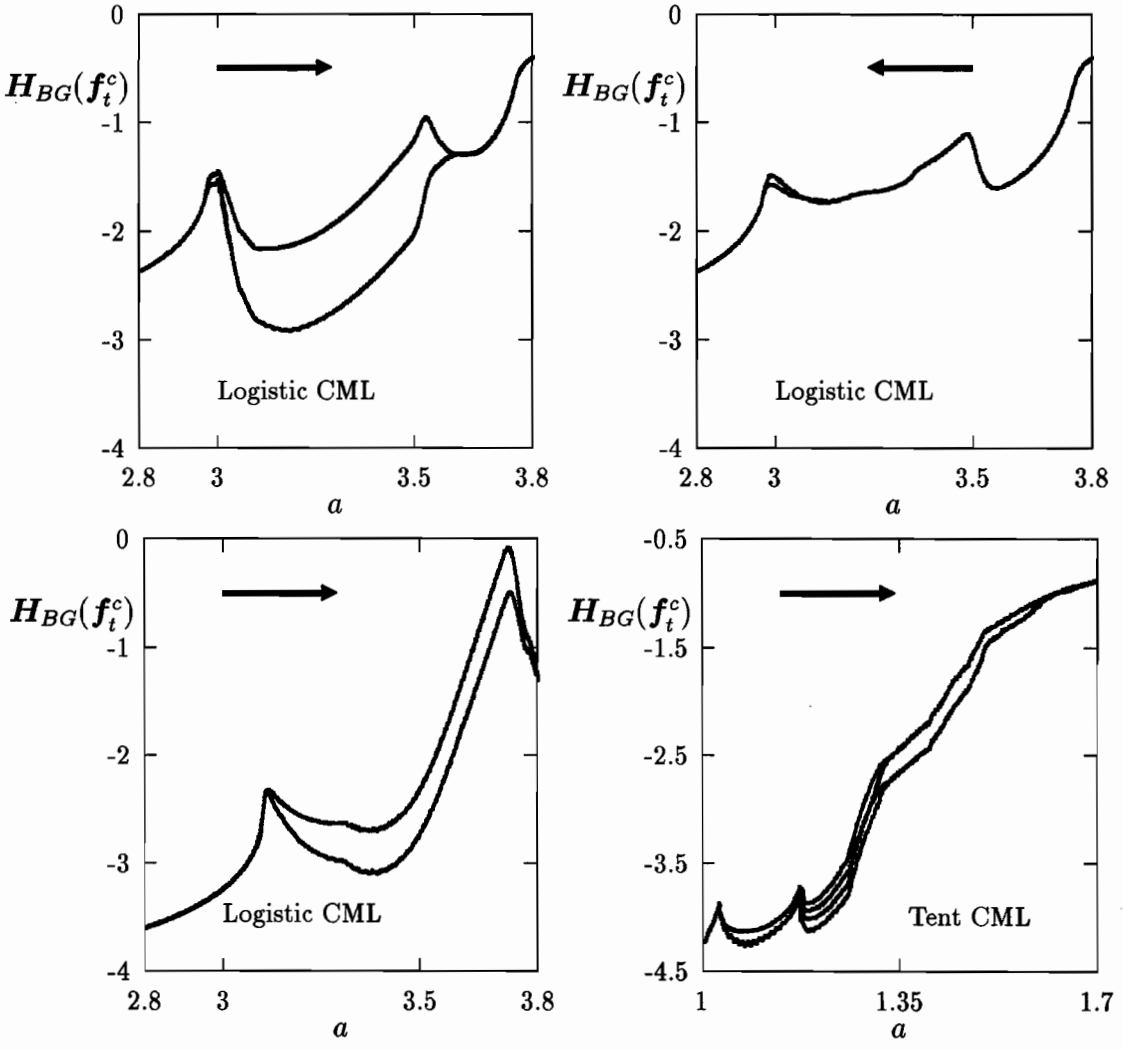

FIGURE 4.2:
"Adiabatic" bifurcation diagrams for the Boltzmann-Gibbs entropy of the distribution of activity in lattices of diffusively coupled tent and logistic maps. For each value of a, the CML's were iterated

10^3 times, with an initial condition given by the last one of the 10^3 iterations corresponding to the previous a value (the increment $\Delta a = 0.002$). *Top row*: lattice of logistic maps, with $\varepsilon = 0.1$, and additive noise supported uniformly on $[0, 0.05]$ (for $a = 2.8$, the initial condition was spatially isotropic, and uniform on $[0.5, 1]$). Note the hysteresis in the behavior of the entropy, which is shown in Section 4.4 to reflect the asymptotic periodicity of the transfer operator (*cf.* also Definition 1). *Bottom left:* same parameters as above, with multiplicative noise supported uniformly on $[0.95, 1]$. *Bottom right:* Diagram for a diffusively coupled tent map lattice, with $\varepsilon = 0.45$, (as in Figure 4.3), and additive noise supported on $[0, 0.01]$. The rest of the parameters are as above. The hysteresis observed in the top row is also observed in tent map lattices, and when the noise is multiplicative.

Pattern formation in the tent map lattice is illustrated in Figure 4.3. As expected, as the noise amplitude is increased, patterns gradually disappear. Numerical observations indicate that pattern formation coincides with statistical cycling in this system (this is clearly illustrated by the top panels of Figure 4.1 and those of Figure 4.3). To understand this connection, note that when the lattice cycles statistically, the density of activity is supported on disjoint supports (as in Figure 4.1 for example). The diffusive-like effect of the coupling in equation (1.2) ensures that nearby sites tend to belong to the same "band" (or support of the distribution), and if this coupling is not strong enough to force all sites into the same band, the state of the lattice at time t consists of clusters of sites which belong to the different bands [strictly speaking, the discretization of the diffusion operator yields a coupling of the form (4.2) where the p-neighbourhood includes only the nearest neighbours, but when more neighbours are taken into account, the coupling still mimics the effect of diffusion in a system with a large diffusion coefficient]. If there is only one support of the collapsed density f_t (*cf.* rightmost panel of Figures 4.1 and 4.3), no discernable patterns occur since the entire attracting interval is occupied with nonzero probability, irrespective of the coupling strength.

As expected [100], the transients leading to the various states of equilibria can be extremely long. The length of those transients is determined by the specificities of the local map, the inter-element coupling and the size of the lattice.

FIGURE 4.3:
Three snapshots of the activity of a 200×200 lattice of diffusively coupled tent maps. Grey scale with 256 levels: 0 is black, 1 is white. The control parameters of the CML are $a = 1.175$ and $\varepsilon = 0.45$ in all three panels. From left to right the support of the additive noise is widened as in Figure 4.1. Here, 10^3 transients were discarded, and for each panel the initial preparation of the lattice was featureless: The initial value for every site was a random variable distributed uniformly on $[0.5, 1]$.

4.3.1.2 The logistic map lattice

The effects of the noise on the dynamics of the logistic map lattice depends to a large extent on whether the unperturbed CML is periodic in time and/or space, or chaotic.

An overview of the dynamics of system (4.2) with S given by (??) which complements the descriptions of Chapter 3 is presented in [31]. When noise is present and the quadatic map is periodic the system can either become statistically periodic, or statistically stable, depending on the strength of the perturbation. In the case of additive noise, when the perturbation is small compared to the amplitude of the periodic cycle, the solutions are statistically periodic, and are reminiscent of the banded chaotic trajectories.

If the amplitude of the perturbation is increased, possibly preexisting spatiotemporal structures are gradually lost, and eventually the CML's are seen to be spatiotemporally chaotic in the sense of Keller and Künzle [109], and Bunimovich and Sinai [21]. Correlations in time and space decay exponentially.

When the unperturbed CML is chaotic, the influence of additive noise is exactly as for the coupled tent map lattices discussed above, and the resulting system is again either statistically periodic or statistically stable. It is of interest to note that the evolution of the statistical quantifiers of the motion in the deterministic case has been conjectured to be

quasiperiodic or chaotic (see for example the discussion surrounding Figures. 19 and 20 of [31]). We do not observe such statistical evolutions when the transients are long enough. The linearity of the Perron-Frobenius operator for the deterministic lattices [135] implies that statistics in these CML's asymptotically reach either stable steady states, or periodic in time. The results of Section 4.4 (and more specifically the linearity of the transfer operators for stochastic CML's) imply the same conclusion in the presence of noise, and indicate that the fluctuations observed by Chaté and Manneville are due to finite-size effects.

The influence of parametric noise on the evolution of the logistic map lattices is qualitatively the same as the influence of additive perturbations, but as with tent map lattices, in some regions of parameter space it is observed that the amplitude of parametric noise needed to statistically stabilize the lattices is much smaller than the additive noise amplitude required to produce the same effect.

We now discuss the influence of noise on a CML which possesses chaotic regimes which cannot be described by probability densities in the absence of noise.

4.3.2 The "Keener map" lattices

Here the local transformation is a piecewise linear map with constant slope on $[0,1]$ which was first considered by Keener [108]:

$$S(x) = (ax + b) \bmod 1 \qquad a, b \in (0,1), \quad x \in [0,1]. \tag{4.6}$$

There exists a range of values for the parameters a and b such that the trajectories are chaotic in the sense that they are attracted to a subset of $[0,1]$ of zero measure (a Cantor set) [108]. Numerically, this is reflected by the fact that if the histogram along a trajectory is constructed, the number of histogram peaks will increase as the bin size decreases (of course the binned trajectory must be sufficiently long for this observation to be of any interest).

For this type of system the Perron-Frobenius operator does not possess a fixed point in the space of probability densities. In fact, it asymptotically transforms almost all initial probability densities into generalized functions. A rigorous treatment of such operators is possible, and studying the nonequilibrium statistical properties of the corresponding CML's involves the reformulation of the problem in terms of the evolution of measures. However this picture is simplified by the presence of noise in the map (4.6) because under the influence of noise, the map induces a transfer operator acting on well defined densities [123]. Furthermore,

the ensemble densities asymptotically reach a limit cycle in density space (as in Figure 4.1) which reflects the underlying asymptotic periodicity of the transfer operator.

This description of the single map's behavior holds for the stochastic CML (4.4) with S given by (4.6): The CML is also statistically periodic. Figure 4.4 shows that the fractal nature of the attractor of the single map survives linear coupling. The effects of adding noise in the system are shown in Figure 4.5, and it is clear that the activity of the lattice is no longer supported on a Cantor set (in $\mathbb{R}^N$).

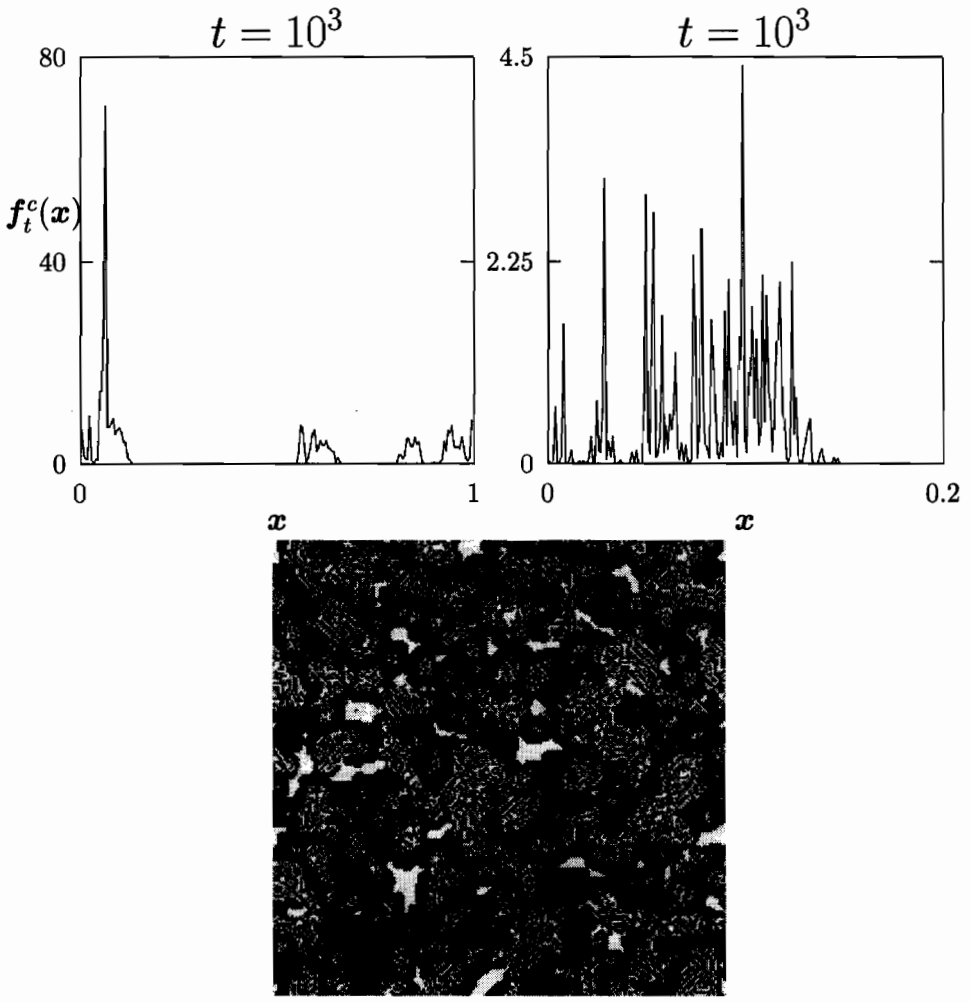

FIGURE 4.4:
Top Right panel displays the distribution of the activity displayed on the bottom panel. The fractal nature of the support of this distribution is suggested by the right panel. *Bottom*: activity of a 200×200 lattice of diffusively coupled Keener maps (4.6) without noise, with $a = 0.5$, $b = 0.571$ and $\varepsilon = 0.45$.

In addition, the temporal evolution of densities is reminiscent of the statistical cycling described above for the tent and logistic map lattices. Figure 4.5 provides a clear illustration of period 3 statistical cycling (also described as "quasiperiodicity"). It has been proposed (Section 3.2.2 of [31]) that deterministic CML's do not display such behavior. Figure 4.5 demonstrates that this observation does not hold for noisy CML's. In addition, the fact that we have not found period 3 cycling in the absence of noise in the tent and logistic map lattices is probably due to the absence of statistical period 3 in the local transformations (2.2) and (2.4) for the parameters used here in the simulations. It is likely that when the local map does possess period 3 statistical cycling, the CML will display the same behavior (at least for small enough values of the coupling). An example of noisy period 3 in the logistic map is given by Lorenz [131]. Lukin and Shestopalov illustrate the same behavior in a map relevant to the modeling of resonant electromagnetic cavities with nonlinearly reflecting boundaries [140].

Note also that the stochastic perturbation of system (4.2) with (4.6) yields a (mathematically) simpler system than in the absence of noise. As mentioned above, the Perron-Frobenius operator associated with the deterministic map acts on (noncontinuous) measures, whereas the transfer operator associated with the stochastic map acts on densities. The results describing the dynamical properties of operators acting on densities are more numerous than those associated with measure evolving operators and, consequently, analytic investigations of the stochastic CML's are more straightforward than those of their deterministic counterparts (for a discussion of the evolution of measures under the action of linear operators, refer to Chapter 12 of [122]). Before proceeding, we briefly summarize our numerical experiments.

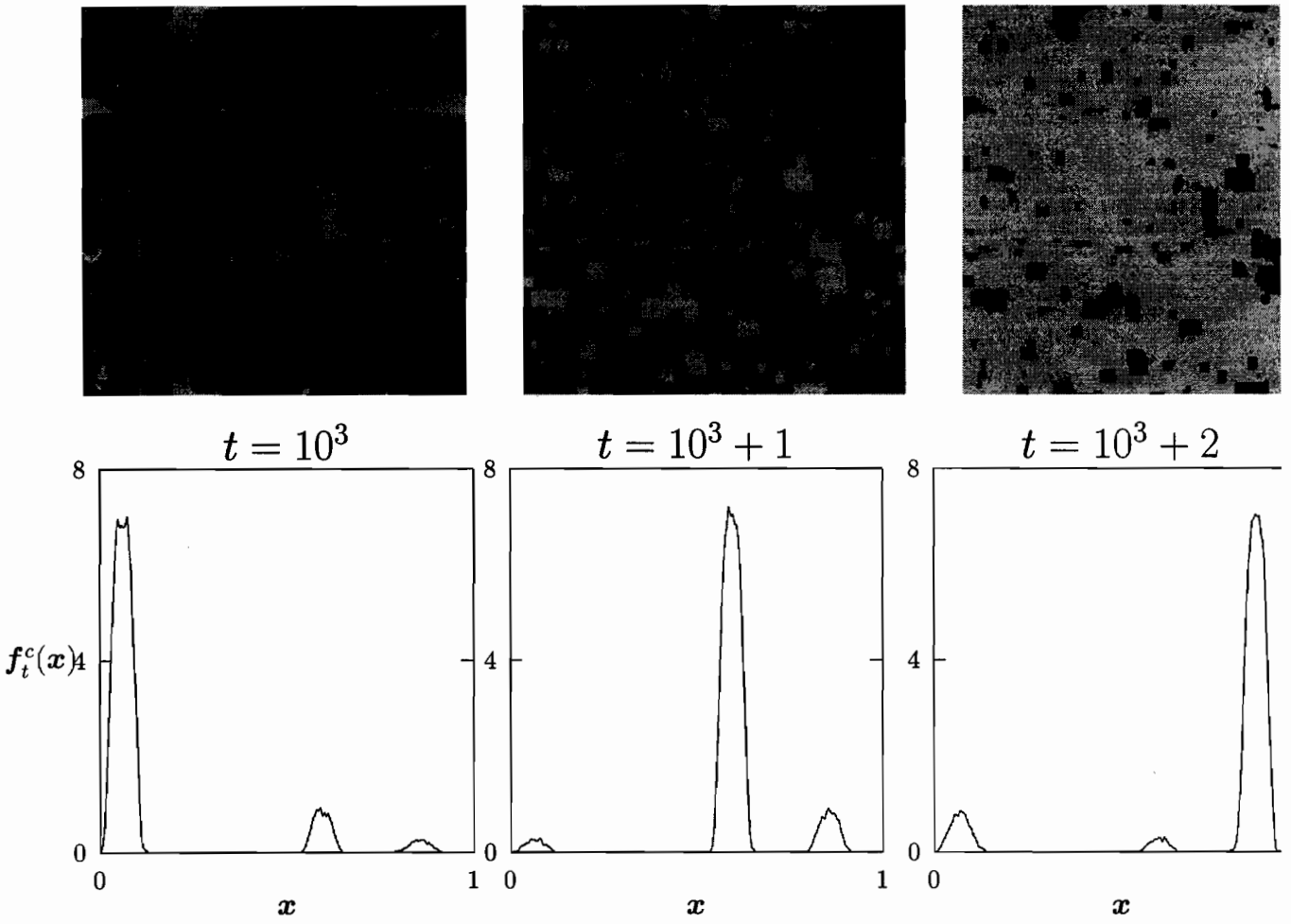

FIGURE 4.5:
Noise induced statistical cycling in a lattice of 200×200 "Keener maps" (4.6), with $a = 0.5$, $b = 0.571$, $\varepsilon = 0.1$ and additive noise uniformly supported on $[0, 0.05]$. The top panels display three successive iterations, and the bottom panels display the corresponding distributions of activity across the lattices. The grey scale for the top row is the same as in Figures 4.1 and 4.3.

4.3.3 Summary of the numerical experiments

Deterministic CML's undergo the following, changes when subjected to stochastic perturbations:

1) Not surprisingly, addition (multiplication) of noise to (by) a system generating a deterministic periodic cycle yields a statistically periodic system if the noise amplitude is small, and a statistically stable one if the noise is large enough to "wash out" the underlying

periodicity. Similarly, addition (multiplication) of noise to (by) a system generating a chaotic trajectory associated with a probability density, yields a system which is either statistically periodic or statistically stable at equilibrium. Again, temporal periodicities in this case survive only small perturbations, and disappear when the noise is sufficiently strong.

2) Perhaps less intuitive is the observation that stochastic perturbations (no matter how minute) of CML's can result in fundamental qualitative changes in both the topology of the attracting sets, and the statistical evolution of the model. Section 4.3.2 illustrates this using a CML of Keener maps which possesses a Cantor set as an attractor in the absence of noise, and which cycles statistically (with period 3) in the presence of noise.

3) CML's which display quasiperiodicity when they are subjected to stochastic perturbations, are also likely to display statistical hysteresis displayed in Figure 4.2. In this case, the asymptotic value of the statistical quantifiers of the motion are seen to depend on the initial preparation of the system (this property is explained analytically in Section 4.4).

In general, dynamical systems need not possess stable equilibrium states, and it is therefore interesting to note that perturbation by noise of all three CML's discussed here yields models which always eventually reach equilibrium conditions, even if the notion of equilibrium must be extended to include statistical periodic cycles.

In the next section, we examine these numerical observations analytically using the theory of Markov operators defined by stochastic kernels.

4.4 Analytic results

Section 4.3 numerically illustrated the influence of noise on the evolution of several CML's. The numerics demonstrated the ubiquity of statistical cycling, and that of the statistical hysteresis displayed in Figure 4.2.

In this section, these results are examined in light of a theoretical framework based on the properties of the transfer operator which describes stochastic maps like the Perron-Frobenius operator describes deterministic ones. Using basic results from the theory of functions of bounded variation, the Perron-Frobenius operator associated with certain deterministic chaotic CML's was shown in the previous chapter to be asymptotically periodic. The approach presented here to determine the spectral characteristics of the Perron-Frobenius operator associated with stochastic CML's is somewhat more "indirect" since it relies on proving a property, known as *constrictiveness* (defined in the proof of Theorem 4.2 in Sec-

tion 4.4.2.2) which, by a theorem due to Komornik [112], implies asymptotic periodicity and the decomposition (1.21).

First, we derive the evolution equation for the phase space density $\mathbf{f}_t$, for CML's perturbed by various types of noise. This evolution equation implicitly defines the transfer operator. Second, it is shown that the transfer operator is linear, Markov and that it is defined by a stochastic kernel. These results are then used to investigate the convergence properties of the sequence $\{\mathbf{f}_t\}$. The relation between these properties and the numerical results of Section 4.3 is then discussed.

Before proceeding, we remind the reader that a function $\mathbf{K} : \mathbb{X} \times \mathbb{X} \longmapsto \mathbb{R}$ is a stochastic kernel if it satisfies

$$\mathbf{K}(\mathbf{x}, \mathbf{y}) \geq 0, \qquad \text{and} \qquad \int_{\mathbf{X}} \mathbf{K}(\mathbf{x}, \mathbf{y})\, d\mathbf{x} = 1.$$

[The integral is understood as a Lebesgue integral with respect to the Lebesgue measure, but in general the measure of integration can be different. Consult [122] for details]. To simplify the algebra the model (4.2) is replaced by a one dimensional version so that the double superscripts of (4.2) and (4.4) are replaced by a single space index denoted i:

$$x_{t+1}^{(i)} = \Phi^{(i)}(\mathbf{x}_t) + \xi_t^{(i)} = (1-\varepsilon) S(x_t^{(i)}) + \frac{\varepsilon}{p} \sum_{\substack{p \text{ nearest} \\ \text{neighbours}}} S(x_t^{(j)}) + \xi_t^{(i)}, \quad \varepsilon \in (0,1). \tag{4.7}$$

The boundary conditions need not be specified explicitly. The only requirement they must meet is that the evolution of the elements on the boundaries be well defined (the frequently encountered periodic and no-flux boundary conditions obviously satisfy this requirement).

4.4.1 Additive noise

In this case, the lattice transformation is (4.4). Consider an initial density $\mathbf{f}_0 : \mathbb{X} \longmapsto \mathbb{X}$ which describes an ensemble of initial lattices. If the noise perturbation is distributed according to density $\mathbf{g}$ (*cf.* (4.3)) the evolution equation for this density is known to be [123]:

$$\mathbf{f}_{t+1}(\mathbf{x}) = \int_{\mathbf{X}} \mathbf{f}_t(\mathbf{y}) \mathbf{g}(\mathbf{x} - \Phi(\mathbf{y}))\, d\mathbf{y}, \quad n = 0, 1, \cdots \tag{4.8}$$

which also defines the transfer operator $\mathcal{P}_{\Phi_{\text{add}}}$ for CML's perturbed as in (4.4) since $\mathcal{P}_{\Phi_{\text{add}}} \mathbf{f}_t(\mathbf{x}) = \mathbf{f}_{t+1}(\mathbf{x})$. Without loss of generality, in the remainder of this section we will assume that the density associated with the stochastic perturbation is piecewise constant and given by

$$\mathbf{g}(\boldsymbol{\xi}) = \prod_{i=1}^{N} \chi_{[a,b]}(\xi^{(i)}), \quad 0 \leq a < b \leq 1, \tag{4.9}$$

where the indicator function χ is defined by $\chi_{[a,b]}(x) = (b-a)^{-1}$ if $x \in [a,b]$ and $\chi_{[a,b]}(x) = 0$ otherwise.

4.4.1.1 Sufficient conditions for statistical cycling

If the CML Φ_{add} is written in the form (4.4), where the density of the perturbation $\boldsymbol{\xi}$ is given by (4.9), and the local map S of (4.2) is bounded and nonsingular then $\mathcal{P}_{\Phi_{\text{add}}}$ defined by (4.8) is asymptotically periodic.

This is is a consequence of the following theorem:

Theorem 4.1 (Lasota and Mackey [122]): Let $\mathbf{K} : \mathbb{X} \times \mathbb{X} \longmapsto \mathbb{R}$ *be a stochastic kernel, and* $\mathcal{P}$ *a Markov operator defined by*

$$\mathcal{P}\mathbf{f}(\mathbf{x}) = \int_{\mathbb{X}} \mathbf{K}(\mathbf{x},\mathbf{y})\mathbf{f}(\mathbf{y})\, d\mathbf{y}. \tag{4.10}$$

Assume that there is a nonnegative $\lambda < 1$ *such that for every bounded* $\mathbb{B} \subset \mathbb{X}$ *there is a* $\delta = \delta(\mathbb{B}) > 0$ *for which*

$$\int_{\mathbb{A}} \mathbf{K}(\mathbf{x},\mathbf{y})\, d\mathbf{x} \leq \lambda \qquad \text{for } \mu(\mathbb{A}) < \delta, \quad y \in \mathbb{B}, \quad \mathbb{A} \subset \mathbb{B}. \tag{4.11}$$

Assume further there exists a Lyapunov function $V : \mathbb{X} \longmapsto \mathbb{R}$ *such that*

$$\int_{\mathbb{X}} V(\mathbf{x})\mathcal{P}\mathbf{f}(\mathbf{x})\, d\mathbf{x} \leq \alpha \int_{\mathbb{X}} V(\mathbf{x})\mathbf{f}(\mathbf{x})\, d\mathbf{x} + \beta, \quad \alpha \in [0,1),\ \beta > 0 \tag{4.12}$$

for every density $\mathbf{f}$. *Then* $\mathcal{P}$ *is asymptotically periodic, and therefore admits the representation (1.21).* [Recall that a nonnegative function $V : \mathbb{X} \longmapsto \mathbb{R}$ is known as a *Lyapunov function* if it satisfies $\lim_{|\mathbf{x}|\to\infty} V(\mathbf{x}) = \infty$.] ■

To show that the operator $\mathcal{P}_{\Phi_{\text{add}}}$ defined in (4.8) satisfies the conditions of Theorem 4.1, note that (4.8) can be written in the form (4.10) with

$$\mathbf{K}(\mathbf{x},\mathbf{y}) = \mathbf{g}(\mathbf{x} - \Phi(\mathbf{y})). \tag{4.13}$$

Clearly $\mathbf{g} > 0$, and since it is a normalized probability density, $\int_{\mathbb{X}} \mathbf{K}(\mathbf{x},\mathbf{y})d\mathbf{x} = 1$, so (4.13) defines a stochastic kernel. In addition, it is straightforward to show that $\mathcal{P}_{\Phi_{\text{add}}}$ is a Markov operator. To verify that (4.11) holds when $\mathbf{K}$ is given by (4.13), remember since $\mathbf{g}$ is integrable, for every $\lambda > 0$, there is a $\delta > 0$ such that

$$\int_{\mathbb{A}} \mathbf{g}(\mathbf{x})\, d\mathbf{x} < \lambda \qquad \text{for } \mu(\mathbb{A}) < \delta.$$

Hence,

$$\int_{\mathbb{A}} \mathbf{K}(\mathbf{x},\mathbf{y})\, d\mathbf{x} = \int_{\mathbb{A}} \mathbf{g}(\mathbf{x}-\Phi(\mathbf{y}))\, d\mathbf{x} = \int_{\mathbb{A}-\Phi(\mathbf{y})} \mathbf{g}(\mathbf{x})\, d\mathbf{x} < \lambda$$

for $\mu(\mathbb{A}-\Phi(\mathbf{y})) = \mu(\mathbb{A}) < \delta$. Thus (4.11) holds for all bounded sets $\mathbb{B}$.

We now check that when S is bounded, (4.12) holds. To do this we pick

$$V(\mathbf{x}) = \prod_{i=1}^{N} \exp|x^{(i)}|. \tag{4.14}$$

Using (4.9), (4.14) and (4.7) , one obtains

$$\begin{aligned}
\int_{\mathbb{X}} \mathbf{g}(\mathbf{x}-\Phi(\mathbf{y}))V(\mathbf{x})\, d\mathbf{x} &= \int_{\mathbb{X}} \prod_{i=1}^{N} \chi_{[a,b]}(x^{(i)}-\Phi^{(i)}(\mathbf{y}))V(\mathbf{x})\, d\mathbf{x} \\
&= (b-a)^{-N} \prod_{i=1}^{N} \int_{a+\Phi^{(i)}(\mathbf{y})}^{b+\Phi^{(i)}(\mathbf{y})} V(x^{(i)})dx^{(i)} \\
&= \left(\frac{e^b-e^a}{b-a}\right)^N \prod_{i=1}^{N} \left[\exp|\Phi^{(i)}(\mathbf{y})|\right] \\
&= \left(\frac{e^b-e^a}{b-a}\right)^N \prod_{i=1}^{N} \left[\exp|S(y^{(i)})|\right]. \qquad (4.15)
\end{aligned}$$

By definition, S is bounded, so $\prod_{i=1}^{N}\left[\exp|S(y^{(i)})|\right]$ is finite. As a result, it is always possible to choose $\alpha \in (0,1)$ and a finite but arbitrarily large β such that

$$\left(\frac{e^b-e^a}{b-a}\right)^N \prod_{i=1}^{N} \left[\exp|S(y^{(i)})|\right] \leq \alpha \prod_{i=1}^{N} \left[\exp|y^{(i)}|\right] + \beta.$$

Thus we have

$$\int_{\mathbb{X}} \mathbf{g}(\mathbf{x}-\Phi(\mathbf{y}))V(\mathbf{x})\, d\mathbf{x} \leq \alpha V(\mathbf{y}) + \beta, \quad \alpha \in (0,1), \quad \beta > 0, \tag{4.16}$$

which implies (4.12). Hence all conditions of Theorem 4.1 are met and $\mathcal{P}_{\Phi_{\text{add}}}$ is asymptotically periodic.

This is a general result. The two main assumptions which are necessary for its derivation are that S be nonsingular and bounded. In light of this result, the numerics of Section 4.3 on the dynamics of the tent, logistic and Keener map lattices are seen to reflect the cyclical spectral decomposition (1.21) of the transfer operator associated with these CML's. In particular, the statistical hysteresis of Figure 4.2 is a consequence of the dependence in (1.21) of the functionals Γ_i on the initial density $\mathbf{f}_0$.

As in Chapter 3, the presence of asymptotic periodicity in systems of the form (4.4) also has important consequences for the proper interpretation of the behavior of their statistical quantifiers. Before discussing these consequences in detail, we consider the behavior of CML's perturbed by multiplicative noise.

4.4.2 Multiplicative noise

Here the transformation Φ_{mul} is given by (4.5). In this section it is proved that the effects of multiplicative noise on CML dynamics are usually similar to the effects of additive noise discussed above. However, the formalism describing these two situations is different, since the mechanisms by which additive and multiplicative perturbations operate are themselves different. Our discussion is inspired by the treatment of the effects of parametric noise on one dimensional maps given by Horbacz [80].

4.4.2.1 Derivation of the transfer operator

To derive the expression for the operator which governs the evolution of ensemble densities, we introduce an arbitrary bounded measurable function $\boldsymbol{h} : \mathbb{X} \longmapsto \mathbb{R}$ which can be written

$$\boldsymbol{h}(\mathbf{x}) = \prod_{i=1}^{N} h^{(i)}(x^{(i)}).$$

The expectation value of $\boldsymbol{h}(\mathbf{x}_{t+1})$ is given by

$$E(\boldsymbol{h}(\mathbf{x}_{t+1})) = \int_{\mathbf{X}} \boldsymbol{h}(\mathbf{x}) \mathbf{f}_{t+1}(\mathbf{x})\, d\mathbf{x} \tag{4.17}$$

However, from (4.5), we have

$$\begin{aligned} E(\boldsymbol{h}(\mathbf{x}_{t+1})) &= E(\boldsymbol{h}(\Phi_{\text{mul}}(\mathbf{x}_t))) \\ &= \int_{\mathbf{X}} \int_{\mathbf{X}} \mathbf{f}_t(\mathbf{y}) \prod_{i=1}^{N} h^{(i)}(z^{(i)} \Phi^{(i)}(\mathbf{y})) g(z^{(i)})\, d\mathbf{z} d\mathbf{y} \end{aligned} \tag{4.18}$$

The preceding equation can be simplified by recalling the following identity. Let $\Phi : \mathbb{X} \longmapsto \mathbb{X}$ be a nonsingular dynamical system which induces the Perron-Frobenius operator $\mathcal{P}_\Phi$. Then for all L^1 function $u : \mathbb{X} \longmapsto \mathbb{X}$, and an L^∞ function $v : \mathbb{X} \longmapsto \mathbb{X}$, we have

$$\int_{\mathbf{X}} \mathcal{P}_\Phi u(x) v(x)\, dx = \int_{\mathbf{X}} u(x) v(\Phi(x))\, dx. \tag{4.19}$$

The operator $\mathcal{K}_\Phi$ such that

$$\mathcal{K}_\Phi v(x) = v(\Phi(x)), \quad \text{for all } x \in \mathbb{X}, \text{ and all } v \in L^\infty$$

is called the *Koopman* operator induced by Φ. Equation (4.19) expresses the fact that $\mathcal{P}_\Phi$ and $\mathcal{K}_\Phi$ are adjoint, and is written

$$\langle \mathcal{P}_\Phi u, v \rangle = \langle u, \mathcal{K}_\Phi v \rangle.$$

where $\langle , \rangle$ denotes the scalar product between two functions.

Applying this identity to equation (4.18) yields

$$E(\boldsymbol{h}(\mathbf{x}_{t+1}) \;=\; \int_{\mathbb{X}} \int_{\mathbb{X}} \mathcal{P}_\Phi \mathbf{f}_t(\mathbf{y}) \prod_{i=1}^{N} h^{(i)}(z^{(i)} y^{(i)}) g(z^{(i)})\, d\mathbf{z} d\mathbf{y} \tag{4.20}$$

where $\mathcal{P}_\Phi$ denotes the Perron-Frobenius operator induced by the deterministic CML Φ. Now let

$$z^{(i)} y^{(i)} = x^{(i)} \Longleftrightarrow dz^{(i)} = \frac{dx^{(i)}}{y^{(i)}}.$$

Using this change of variables, (4.20) becomes

$$E(\boldsymbol{h}(\mathbf{x}_{t+1})) = \int_{\mathbb{X}} \int_{\mathbb{X}'} \mathcal{P}_\Phi \mathbf{f}_t(\mathbf{y}) \prod_{i=1}^{N} \left[h^{(i)}(x^{(i)}) g\left(\frac{x^{(i)}}{y^{(i)}}\right) \frac{1}{y^{(i)}} \right] d\mathbf{x} d\mathbf{y} \tag{4.21}$$

where $\mathbb{X}' = X_1' \times \cdots \times X_N'$ is a product space with each interval in the product defined to be $I_i \equiv [0, y^{(i)}]$. Changing the order of integration in (4.21) yields

$$E(\boldsymbol{h}(\mathbf{x}_{t+1})) = \int_{\mathbb{X}} \int_{\mathbb{Y}'} \mathcal{P}_\Phi \mathbf{f}_t(\mathbf{y}) \prod_{i=1}^{N} \left[h^{(i)}(x^{(i)}) g\left(\frac{x^{(i)}}{y^{(i)}}\right) \frac{1}{y^{(i)}} \right] d\mathbf{y} d\mathbf{x} \tag{4.22}$$

where $\mathbb{Y}'$ is a product space of intervals $Y_i' \equiv [x^{(i)}, 1]$. By assumption $\boldsymbol{h}$ is arbitrary. Therefore, comparing (4.22) with (4.17) and (4.20), we obtain

$$\mathbf{f}_{t+1}(\mathbf{x}) \equiv \mathcal{P}_{\Phi_{\text{mul}}} \mathbf{f}_t(\mathbf{x}) \;=\; \int_{x^{(N)}}^{1} \cdots \int_{x^{(1)}}^{1} \mathcal{P}_\Phi \mathbf{f}_t(\mathbf{y}) \prod_{i=1}^{N} \left[g\left(\frac{x^{(i)}}{y^{(i)}}\right) \frac{1}{y^{(i)}} \right] d\mathbf{y} \tag{4.23}$$

$$= \int_{x^{(N)}}^{1} \cdots \int_{x^{(1)}}^{1} \mathbf{f}_t(\mathbf{y}) \prod_{i=1}^{N} \left[g\left(\frac{x^{(i)}}{\Phi^{(i)}(\mathbf{y})}\right) \frac{1}{\Phi^{(i)}(\mathbf{y})} \right] d\mathbf{y} \tag{4.24}$$

which is the expression for the Perron-Frobenius operator induced by the stochastic CML (4.5). We are now in a position to discuss the asymptotic properties of the iterates of $\mathcal{P}_{\Phi_{\text{mul}}}$.

4.4.2.2 Sufficient conditions for statistical cycling

A CML of the form (4.5), perturbed by the noise term $\boldsymbol{\xi}_t$ distributed with density (4.3) will induce a transfer operator $\mathcal{P}_{\Phi_{\text{mul}}}$ defined by (4.24). If the deterministic part of the transformation (denoted Φ) is bounded and nonsingular, then $\mathcal{P}_{\Phi_{\text{mul}}}$ is asymptotically periodic.

This result follows from the application of the following theorem:

Theorem 4.2: Let $\mathbf{K} : \mathbb{X} \times \mathbb{X} \longmapsto \mathbb{R}$ *be a stochastic kernel and* $\mathcal{P}$ *be the Markov operator defined by*

$$\mathcal{P}\mathbf{f}(\mathbf{x}) = \int_{x^{(N)}}^{1} \cdots \int_{x^{(1)}}^{1} \mathbf{K}(\mathbf{x}, \mathbf{y}) \mathbf{f}(\mathbf{y})\, d\mathbf{y}, \tag{4.25}$$

and assume that inequalities (4.11) and (4.12) are satisfied. Then $\mathcal{P}$ *is asymptotically periodic.*

Proof: This proof rests on a result, originally published by Komornik, which states that a Markov operator $\mathcal{P}$ is asymptotically periodic if and only if it is constrictive. We therefore show here that an operator $\mathcal{P}$ satisfying the conditions of Theorem 4.2 is constrictive, and then invoke the Komornik result. The proof of the theorem is inspired by similar proofs given in Chapter 5 of [122]. Before proceeding, we introduce the notion of constrictiveness.

> *Definition of Constrictiveness:* Let $(\mathbb{X}, \mathcal{B}, \mu)$ be a finite measure space. A Markov operator $\mathcal{P}$ is said to be constrictive if there exists a $\delta > 0$ and $\kappa < 1$ such that for every density f, there is an integer $n_0(f)$ for which
>
> $$\int_{\mathbb{E}} \mathcal{P}f(x)\, \mu(dx) \leq \kappa \quad \text{for} \quad n \geq n_0(f) \quad \text{and} \quad \mu(\mathbb{E}) \leq \delta. \tag{4.26}$$
>
> This property ensures that the iterates $\mathcal{P}^n f$ of any initial density f are not eventually concentrated on a set of small or zero measure. If the space $\mathbb{X}$ is not finite [as would be the case for CML's with a local transformation defined on $\mathbb{R}$ rather than $[0, 1]$], a slight generalization of this definition is desired to rule out the possibility that $\mathcal{P}^n f$ be dispersed throughout the entire space. In this case, $\mathcal{P}$ is said to be constrictive if there is a measurable set $\mathbb{B}$ of finite measure such that for every density f there is an integer $n_0(f)$ for which
>
> $$\int_{\mathbb{X} \setminus \mathbb{B} \bigcup \mathbb{E}} \mathcal{P}f(x)\, \mu(dx) \leq \kappa \quad \text{for} \quad n \geq n_0(f) \quad \text{and} \quad \mu(\mathbb{E}) \leq \delta. \tag{4.27}$$
>
> If $\mathbb{X}$ is finite and $\mathbb{B} = \mathbb{X}$, (4.27) reduces to (4.26). ■

Next, we recall the Chebyshev inequality. Let $(\mathbb{X}, \mathcal{B}, \mu)$ be a measure space, $V : \mathbb{X} \longmapsto \mathbb{R}$ a nonnegative measurable function, and for all densities f set

$$E(V|f) = \int_{\mathbb{X}} V(x) f(x) \mu(dx).$$

If $G_a = \{x : V(x) < a\}$, then

$$\int_{G_a} f(x)\mu(dx) \geq 1 - \frac{E(V|f)}{a} \quad \text{(The Chebyshev inequality).}$$

The proof is given in [122]. For future reference, we define

$$E_n(V|\mathbf{f}) = \int_{\mathbf{X}} V(\mathbf{x}) \mathcal{P}^n_{\Phi_{\text{mul}}} \mathbf{f}(\mathbf{x}) d\mathbf{x}.$$

From (4.12),

$$E_n(V|\mathbf{f}) \leq \alpha E_{n-1}(V|\mathbf{f}) + \beta.$$

By induction,

$$E_n(V|\mathbf{f}) \leq \beta \sum_{i=1}^{n} \alpha^{i-1} + \alpha^n E_0(V|\mathbf{f}) < \frac{\beta}{1-\alpha} + \alpha^n E_0(V|\mathbf{f}).$$

Recall that $\alpha \in [0, 1)$ and that $E_0(V|\mathbf{f})$ is finite for all $\mathbf{f}$, so that there is a $n_0 = n_0(\mathbf{f})$ such that

$$E_n(V|\mathbf{f}) \leq \frac{\beta}{1-\alpha} + 1, \quad \text{for all } n \geq n_0(\mathbf{f}).$$

Hence, using G_a defined as in the Chebyshev inequality, one finds

$$\begin{aligned} \int_{\mathbf{X}\setminus G_a} \mathcal{P}^n_{\Phi_{\text{mul}}} \mathbf{f}(\mathbf{x})\, d\mathbf{x} &= 1 - \int_{G_a} \mathcal{P}^n_{\Phi_{\text{mul}}} \mathbf{f}(\mathbf{x})\, d\mathbf{x} \leq \frac{E_n(V|\mathbf{f})}{a} \\ &\leq \frac{1}{a}\left(1 + \frac{\beta}{1-\alpha}\right) \quad \text{for all } n \geq n_0(\mathbf{f}). \end{aligned} \tag{4.28}$$

Let $\varepsilon = \frac{1}{3}(1-\lambda)$. If we choose a such that

$$a \geq \frac{1}{\varepsilon}\left(1 + \frac{\beta}{1-\alpha}\right), \tag{4.29}$$

we have

$$\int_{\mathbf{X}\setminus G_a} \mathcal{P}_{\Phi_{\text{mul}}} \mathbf{f}(\mathbf{x})\, d\mathbf{x} \leq \varepsilon \quad \text{for } n \geq n_0(\mathbf{f}).$$

Hence, using (4.25), for $n \geq n_0(\mathbf{f})$,

$$\begin{aligned} \int_{\mathbf{X}\setminus G_a \bigcup \mathbf{A}} \mathcal{P}_{\Phi_{\text{mul}}} \mathbf{f}(\mathbf{x})\, d\mathbf{x} &\leq \int_{\mathbf{X}\setminus G_a} \mathcal{P}_{\Phi_{\text{mul}}} \mathbf{f}(\mathbf{x})\, d\mathbf{x} + \int_{\mathbf{A}} \mathcal{P}_{\Phi_{\text{mul}}} \mathbf{f}(\mathbf{x})\, d\mathbf{x} \\ &\leq \varepsilon + \int_{\mathbf{A}} \mathcal{P}_{\Phi_{\text{mul}}} \mathbf{f}(\mathbf{x})\, d\mathbf{x} \\ &\leq \varepsilon + \int_{\mathbf{A}} \int_{x^{(N)}}^{1} \cdots \int_{x^{(1)}}^{1} K(\mathbf{x}, \mathbf{y}) \mathcal{P}^{n-1}_{\Phi_{\text{mul}}} \mathbf{f}(\mathbf{y})\, d\mathbf{y} d\mathbf{x} \end{aligned}$$

$$
\begin{aligned}
&\leq \varepsilon + \int_{\mathbb{A}} \int_0^1 \cdots \int_0^1 K(\mathbf{x},\mathbf{y}) \mathcal{P}_{\Phi_{\text{mul}}}^{n-1} \mathbf{f}(\mathbf{y})\, d\mathbf{y} d\mathbf{x} \\
&\leq \varepsilon + \int_{\mathbb{X}} \mathcal{P}_{\Phi_{\text{mul}}}^{n-1} \mathbf{f}(\mathbf{y})\, d\mathbf{y} \int_{\mathbb{A}} K(\mathbf{x},\mathbf{y})\, d\mathbf{x} \\
&\leq \varepsilon + \int_{\mathbb{X}\setminus G_a} \mathcal{P}_{\Phi_{\text{mul}}}^{n-1} \mathbf{f}(\mathbf{y})\, d\mathbf{y} \int_{\mathbb{A}} K(\mathbf{x},\mathbf{y})\, d\mathbf{x} \\
&\quad + \int_{G_a} \mathcal{P}_{\Phi_{\text{mul}}}^{n-1} \mathbf{f}(\mathbf{y})\, d\mathbf{y} \int_{\mathbb{A}} K(\mathbf{x},\mathbf{y})\, d\mathbf{x}. \qquad (4.30)
\end{aligned}
$$

From (4.11), the integrals over $\mathbb{A}$ in (4.30) are bounded above by λ; the integral over $\mathbb{X} \setminus G_a$ is bounded above by ε, and the integral over G_a is bounded above by 1, so we have

$$
\int_{\mathbb{X}\setminus G_a \bigcup \mathbb{A}} \mathcal{P}_{\Phi_{\text{mul}}} \mathbf{f}(\mathbf{x})\, d\mathbf{x} \leq 2\varepsilon + \lambda = 1 - \varepsilon \quad \text{for } n \geq n_0(\mathbf{f}) + 1
$$

which is the definition of constrictiveness when $\mathbb{X}$ is infinite. However, in our case, $\mathbb{X}$ is the N-dimensional hypercube, so it is not infinite, and the definition of constrictiveness is given by (4.26). To obtain this inequality, note that a as defined in (4.29) is arbitrary, and we can choose it to be large enough so that $G_a = \mathbb{X}$. If we do so, the previous inequality becomes

$$
\int_{\mathbb{A}} \mathcal{P}_{\Phi_{\text{mul}}} \mathbf{f}(\mathbf{x})\, d\mathbf{x} \leq 2\varepsilon + \lambda = 1 - \varepsilon \quad \text{for } n \geq n_0(\mathbf{f}) + 1
$$

which is equivalent to (4.26). Hence, $\mathcal{P}_{\Phi_{\text{mul}}}$ is constrictive. Since it is a Markov operator (we show this below), it is also asymptotically periodic [112]. **Q.E.D**

In the remainder of this section, it is shown that $\mathcal{P}_{\Phi_{\text{mul}}}$ defined in (4.24) is of the form (4.25), that the corresponding kernel satisfies (4.11), and that inequality (4.12) holds if Φ is bounded.

To see that $\mathcal{P}_{\Phi_{\text{mul}}}$ is a Markov operator, note first that from (4.24)

$$
\begin{aligned}
\int_{\mathbb{X}} \mathcal{P}_{\Phi_{\text{mul}}} \mathbf{f}(\mathbf{x})\, d\mathbf{x} &= \int_{\mathbb{X}} \int_{x^{(N)}}^1 \cdots \int_{x^{(1)}}^1 \mathcal{P}_{\Phi} \mathbf{f}(\mathbf{y}) \prod_{i=1}^N \left[g\left(\frac{x^{(i)}}{y^{(i)}}\right) \frac{1}{y^{(i)}} \right] d\mathbf{y} d\mathbf{x} \\
&= \int_{\mathbb{X}} \int_0^{y^{(N)}} \cdots \int_0^{y^{(1)}} \mathcal{P}_{\Phi} \mathbf{f}(\mathbf{y}) \prod_{i=1}^N \left[g\left(\frac{x^{(i)}}{y^{(i)}}\right) \frac{1}{y^{(i)}} \right] d\mathbf{x} d\mathbf{y} \\
&= \int_{\mathbb{X}} \mathcal{P}_{\Phi} \mathbf{f}(\mathbf{y}) \left\{ \int_0^{y^{(N)}} \cdots \int_0^{y^{(1)}} \prod_{i=1}^N \left[g\left(\frac{x^{(i)}}{y^{(i)}}\right) \frac{1}{y^{(i)}} \right] d\mathbf{x} \right\} d\mathbf{y} \\
&= \int_{\mathbb{X}} \mathcal{P}_{\Phi} \mathbf{f}(\mathbf{y}) \left\{ \int_0^1 \cdots \int_0^1 \prod_{i=1}^N \left[g\left(z^{(i)}\right) \right] d\mathbf{z} \right\} d\mathbf{y} \\
&= \int_{\mathbb{X}} \mathcal{P}_{\Phi} \mathbf{f}(\mathbf{y}) d\mathbf{y} \\
&= \int_{\mathbb{X}} \mathbf{f}(\mathbf{y}) d\mathbf{y} = 1 \qquad (4.31)
\end{aligned}
$$

since $\mathcal{P}_\Phi$ is itself a Markov operator. Clearly $\mathcal{P}_{\Phi_{\text{mul}}}$ is linear and this completes the demonstration that it is Markov. Furthermore, from (4.24), $\mathcal{P}_{\Phi_{\text{mul}}}$ can be written as in (4.25) with the kernel given by

$$\mathbf{K}(\mathbf{x},\mathbf{y}) = \prod_{i=1}^{N} \left[g\left(\frac{x^{(i)}}{\Phi^{(i)}(\mathbf{y})} \right) \frac{1}{\Phi^{(i)}(\mathbf{y})} \right]. \tag{4.32}$$

Since $\mathbf{g}$ is a normalized probability density on $\mathbb{X}$, $\mathbf{K}(\mathbf{x},\mathbf{y}) \geq 0$ and $\int_{\mathbb{X}} \mathbf{K}(\mathbf{x},\mathbf{y})d\mathbf{x} = 1$, and therefore $\mathbf{K}$ is a stochastic kernel.

To verify that inequality (4.11) holds when $\mathbf{K}(\mathbf{x},\mathbf{y})$ is given by (4.32), fix an arbitrary $\lambda < 1$. Choose $\mathbb{B} \subset \mathbb{X}$, bounded, and $\mathbb{A} \subset \mathbb{B}$. The function $\mathbf{g}$ is integrable, and so there must be $\delta_1 > 0$ such that

$$\int_{\mathbb{A}} \mathbf{g}(\mathbf{x})\, d\mathbf{x} \leq \lambda \quad \text{for } \mu(\mathbb{A}) < \delta_1, \quad \mathbb{A} \subset \mathbb{B}. \tag{4.33}$$

Define

$$\delta = \delta_1 \inf_{\substack{\mathbf{y}\in\mathbb{B} \\ i=1,\cdots,N}} \Phi^{(i)}(\mathbf{y}).$$

Since $\mathbb{X} \subset \mathbb{R}^N$ is finite, the set $\mathbb{A}$ is a direct product of the form $\mathbb{A} = \prod_{i=1}^N A_i$, where each $A_i \subset \mathbb{R}$ is also finite. Denote by $\mathbb{A} - \Phi(\mathbf{y})$ the direct product $\prod_{i=1}^N A_i/\Phi^{(i)}(\mathbf{y})$. If $\mu(\mathbb{A}) < \delta$, $\mu(\mathbb{A}/\Phi(\mathbf{y})) < \delta_1$ and therefore

$$\begin{aligned} \int_{\mathbb{A}} \mathbf{K}(\mathbf{x},\mathbf{y})d\mathbf{x} &= \int_{\mathbb{A}} \prod_{i=1}^{N} \left[g^{(i)}\left(\frac{x^{(i)}}{\Phi^{(i)}(\mathbf{y})} \right) \frac{1}{\Phi^{(i)}(\mathbf{y})} \right] d\mathbf{x} \\ &= \int_{\mathbb{A}-\Phi(\mathbf{y})} \mathbf{g}(\mathbf{x})\, d\mathbf{x} \\ &\leq \lambda \end{aligned}$$

by (4.33). This verifies inequality (4.11).

If Φ is bounded, it is possible to choose $\alpha_1 \in (0,1)$ and $\beta_1 > 0$ such that

$$0 < \prod_{i=1}^{N} \Phi^{(i)}(\mathbf{x}) \leq \alpha_1 \prod_{i=1}^{N} x^{(i)} + \beta_1 \quad \text{for } x^{(i)} \in [0,1] \text{ and all } i. \tag{4.34}$$

We now show that when Φ satisfies (4.34) the inequality (4.12) is valid. Choose a Lyapunov function $V(x) = \prod_{i=1}^N x^{(i)}$. From (4.24),

$$\begin{aligned} \int_{\mathbb{X}} V(\mathbf{x}) \mathcal{P}_{\Phi_{\text{mul}}} \mathbf{f}(\mathbf{x})\, d\mathbf{x} &= \int_{\mathbb{X}} \prod_{i=1}^{N} x^{(i)} \int_{x^{(N)}}^{1} \cdots \int_{x^{(1)}}^{1} \mathbf{f}(\mathbf{y}) \prod_{i=1}^{N} \left[g\left(\frac{x^{(i)}}{\Phi^{(i)}(\mathbf{y})} \right) \frac{1}{\Phi^{(i)}(\mathbf{y})} \right] d\mathbf{y}d\mathbf{x} \\ &= \int_{\mathbb{X}} \int_{x^{(N)}}^{1} \cdots \int_{x^{(1)}}^{1} \mathcal{P}_\Phi \mathbf{f}(\mathbf{y}) \prod_{i=1}^{N} \left[g\left(\frac{x^{(i)}}{y^{(i)}} \right) \frac{x^{(i)}}{y^{(i)}} \right] d\mathbf{y}d\mathbf{x} \end{aligned}$$

$$
\begin{aligned}
&= \int_{\mathbb{X}} \int_0^{y^{(N)}} \cdots \int_0^{y^{(1)}} \mathcal{P}_\Phi \mathbf{f}(\mathbf{y}) \prod_{i=1}^{N} \left[g\left(\frac{x^{(i)}}{y^{(i)}}\right) \frac{x^{(i)}}{y^{(i)}} \right] \, d\mathbf{x} d\mathbf{y} \\
&= \int_{\mathbb{X}} \mathcal{P}_\Phi \mathbf{f}(\mathbf{y}) \prod_{i=1}^{N} y^{(i)} \int_0^1 \cdots \int_0^1 \prod_{i=1}^{N} \left[g\left(z^{(i)}\right) z^{(i)} \right] \, d\mathbf{z} d\mathbf{y} \\
&= \int_{\mathbb{X}} \mathbf{f}(\mathbf{y}) \prod_{i=1}^{N} \Phi^{(i)}(\mathbf{y}) \int_{\mathbb{X}} \prod_{i=1}^{N} \left[g\left(z^{(i)}\right) z^{(i)} \right] \, d\mathbf{z} d\mathbf{y} \qquad (4.35)
\end{aligned}
$$

where the change of variables $z^{(i)} = x^{(i)}/y^{(i)}$ was used between the third and fourth equalities. Since $\mathbb{X}$ is the N-dimensional unit hypercube,

$$
\langle \mathbf{z} \rangle = \int_{\mathbb{X}} \prod_{i=1}^{N} \left[g\left(z^{(i)}\right) z^{(i)} \right] \, d\mathbf{z} < 1.
$$

Therefore, from (4.34)

$$
\langle \mathbf{z} \rangle \int_{\mathbb{X}} \mathbf{f}(\mathbf{y}) \prod_{i=1}^{N} \Phi^{(i)}(\mathbf{y}) \leq \langle \mathbf{z} \rangle \alpha_1 \int_{\mathbb{X}} \mathbf{f}(\mathbf{y}) V(\mathbf{y}) \, d\mathbf{y} + \langle \mathbf{z} \rangle \beta_1
$$

and as a consequence, there is a $\alpha = \alpha_1 \langle \mathbf{z} \rangle \in [0, 1)$ and a $\beta = \beta_1 \langle \mathbf{z} \rangle > 0$ such that

$$
\int_{\mathbb{X}} V(\mathbf{x}) \mathcal{P}_{\Phi_{\text{mul}}} \mathbf{f}(\mathbf{x}) \, d\mathbf{x} \leq \alpha \int_{\mathbb{X}} V(\mathbf{x}) \mathbf{f}(\mathbf{x}) \, d\mathbf{x} + \beta
$$

thus proving that (4.12) is satisfied.

To summarize, all the conditions of Theorem 4.2 are met by the transfer operator associated with the stochastic coupled map lattice (4.5) and it is therefore asymptotically periodic when the deterministic part of this CML satisfies condition (4.34).

So far, we have considered the statistical behavior of CML's perturbed by noise at each and every time step. As mentioned in Section 4.2.1, these perturbations are known as "constantly applied perturbations". There is another class of perturbations, known as "randomly applied", which were considered in [122]. These results are briefly reviewed in the next section.

4.4.3 Randomly applied perturbations

These perturbations are "strong" in the sense that when they are applied at a time t_*, the value $x_{t_*+1}^{(kl)}$ becomes independent of its preimages. Mathematically, a CML Φ with randomly applied perturbations is written

$$
x_{t+1}^{kl} = \Phi_{\text{ran}}^{(kl)}(\mathbf{x}_t) = \nu_t^{(kl)} \Phi(\mathbf{x}_t) + (1 - \nu_t^{(kl)}) \xi_t^{(kl)} \qquad (4.36)
$$

where $\nu_t^{(kl)}$ is a random variable which takes the two values 0 or 1 with the following probabilities

$$\text{prob}(\nu_t^{(kl)} = 1) = (1 - q), \quad \text{prob}(\nu_t^{(kl)} = 0) = q,$$

where $q \in (0, 1]$ is a control parameter, which is itself distributed with density $\mathbf{g}$. Randomly applied perturbations are in a category which is apart from the (more familiar) constant perturbations of Section 4.2.1. However, their influence on CML dynamics can be investigated using analytical tools related to those presented in the previous sections. In fact, there are strong results concerning the behavior of the iterates of the transfer operator for these systems [122].

Systems of the form (4.2) with randomly applied perturbations are *always* asymptotically stable. To see this, note that the transfer operator for (4.36) is [122]

$$\mathcal{P}_{\Phi_{\text{ran}}}\mathbf{f} = (1 - q)\mathcal{P}_{\Phi}\mathbf{f} + q\mathbf{g}. \tag{4.37}$$

Clearly, $\mathcal{P}_{\Phi_{\text{ran}}}\mathbf{f} > q\mathbf{g}$, which implies that $q\mathbf{g}$ is a nontrivial lower bound function for $\mathcal{P}_{\Phi_{\text{ran}}}\mathbf{f}$ (since $q > 0$), and this in turn implies [122] that there exists a unique density $\mathbf{f}_*$ such that $\mathcal{P}_{\Phi_{\text{ran}}}\mathbf{f}_* = \mathbf{f}_*$, and

$$\lim_{n\to\infty} \left\| \mathcal{P}^n_{\Phi_{\text{ran}}}\mathbf{f} - \mathbf{f}_* \right\|_{L^1} = 0 \qquad \text{for every density } \mathbf{f}. \tag{4.38}$$

This property (exactness, sometimes referred to as asymptotic periodicity) implies mixing (which in turn implies ergodicity) of the CML. Hence we have the rather general result that the slightest perturbation of any nonsingular CML by a stochastic term as in (4.36) yields a system which is always exact, irrespective of the statistical properties of the original lattice transformation.

It is possible to go one step further in our discussion of randomly perturbed CML's, and give an exact expression for the invariant density $\mathbf{f}_*$ of the operator $\mathcal{P}_{\Phi_{\text{ran}}}$. Recall that if $\mathcal{P}$ is a Markov operator, it satisfies

$$\|\mathcal{P}\mathbf{f}\|_{L^1} \leq \|\mathbf{f}\|_{L^1}, \qquad \text{for all } \mathbf{f} \in L^1 \tag{4.39}$$

(this property is known as the *contractiveness* of Markov operators, not to be confused with *constrictiveness* defined in Section 4.4.2.2 in the proof of Theorem 2). Applying (4.39) to the Perron-Frobenius operator $\mathcal{P}_{\Phi}$ associated with the deterministic transformation gives $\|(1-q)^k\mathcal{P}^k_{\Phi}\mathbf{g}\|_{L^1} \leq (1-q)^k\|\mathbf{g}\|_{L^1}$. Hence the series $\sum_{k=0}^{\infty}(1-q)^k\mathcal{P}^k_{\Phi}\mathbf{g}$ is absolutely convergent.

Substituting this series into the expression (4.37) yields

$$\begin{aligned}\mathcal{P}_{\Phi_{\rm ran}} q\sum_{k=0}^{\infty}(1-q)^k\mathcal{P}_\Phi^k\mathbf{g} &= (1-q)\mathcal{P}_\Phi\left[q\sum_{k=0}^{\infty}(1-q)^k\mathcal{P}_\Phi^k\mathbf{g}\right]+q\mathbf{g}\\ &= q\left[\sum_{k=0}^{\infty}(1-q)^k\mathcal{P}_\Phi^k\mathbf{g}-\mathbf{g}\right]+q\mathbf{g}\\ &= q\sum_{k=0}^{\infty}(1-q)^k\mathcal{P}_\Phi^k\mathbf{g}. \qquad (4.40)\end{aligned}$$

In other words, if $\mathbf{f}_* = \sum_{k=0}^{\infty}(1-q)^k\mathcal{P}_\Phi^k\mathbf{g}$ we have $\mathcal{P}_{\Phi_{\rm ran}}\mathbf{f}_* = \mathbf{f}_*$, and $\mathbf{f}_*$ describes the state of thermodynamic equilibrium of the CML (4.36).

4.5 Summary and conjectures

The most surprising conclusion of the analysis presented here is the ubiquity of asymptotic periodicity in stochastic CML's. While our discussions of deterministic lattices in Chapter 3 were model dependent, the statements proven here are rather general. Roughly speaking, as long as the local map S in a system of the form (4.4) or (4.5) is bounded, one expects asymptotic periodicity. We still have no way of determining the period r of the density cycle, and this period could be 1. The results of this chapter remain surprisingly general even in this case because exactness (*i.e.* asymptotic periodicity with $r = 1$) is a property which implies mixing. Proving mixing is usually difficult, and our considerations of the transfer operator therefore provide us with such a result if $r = 1$. Although r cannot be determined analytically, it is important to note that it can be determined numerically with great certainty since the period of the cycle for f_t^c always (with probability 1) equals r (*cf.* the discussion of Section 3.2.1.1).

As discussed in Chapter 1, the notion of equilibrium is usually associated in statistical mechanics with that of an invariant density $\mathbf{f}_*$ which describes the ensemble properties of a given physical system. We know from Chapter 3 that this paradigm is too restrictive and needs to be extended for the proper description of the thermodynamics of nonlinear spatially extended systems modeled by deterministic coupled map lattices. The results presented here lead to the extension of this conclusion to stochastic models

In addition, the considerations of Section 1.4 show that asymptotic periodicity of the transfer operator provides a mechanism for the presence of phase transitions in stochastic lattices. The period r of the statistical cycle (1.21) depends on the parameters of the

transformation, and when this period changes, the lattice undergoes a phase transition.

Another interesting consequence of asymptotic periodicity comes from the dependence of the Γ_i's of equation (1.21) on the initial density $\mathbf{f}_0$ since it implies a dependence of the statistical behavior of an ensemble of lattices on the initial ensemble. This explains the "statistical hysteresis" demonstrated in the bifurcation diagrams of Figure 4.2, and reported earlier in deterministic lattices of logistic maps (*cf.* Section 3.2.2 of [31]).

Finally, the presence of asymptotic periodicity in spatially extended dynamical systems which can be either deterministic (as in Chapter 3, or stochastically perturbed (as in the present chapter) points to the possibility of this behavior in related continuous time models. For example, there is a strong connection (explored in detail in [53, 88, 140]) between certain differential delay equations and discrete time maps (*cf.* also our derivation of the sigmoidal map in Section 2.2.1). The next chapter applies the techniques developed here and in Chapter 3 to the study of these continuous time functional equations which play a prominant role in various fields of investigations, ranging from nonlinear optics to theoretical population biology.

Chapter 5

Coupled Map Lattices as Models Differential Delay Equations

ABSTRACT

We discuss the probabilistic properties of a class of differential delay equations (DDE's), by first reducing the equations to coupled map lattices (CML's), and then considering the spectral properties of the associated transfer operators. The analysis is carried out for the deterministic case and a stochastic case perturbed by additive or multiplicative white noise. This scheme provides an explicit description of the evolution of phase space densities in DDE's, and yields an evolution equation which approximates the analogue for delay equations of the generalized Liouville and Fokker-Planck equations. It is shown that in many cases of interest, for both stochastic and deterministic delay equations, the phase space densities reach a limit cycle in the asymptotic regime. This statistical cycling is observed numerically, apparently for the first time in unforced deterministic continuous time systems, and discussed in light of our analytical descriptions of the transfer operators.

Les termes qui désignent le temps sont empruntés à la langue de l'espace. Quand nous évoquons le temps, c'est l'espace qui répond à l'appel.

Henri Bergson, *La pensée et le mouvant*

5.1 Introduction

In the absence of non-local effects, the instantaneous transmission of information between two systems is impossible without a violation of the assumption of causality. The delays involved necessarily impose a fundamental constraint on any theory describing physical interactions. If the time scale of the delays is comparable to that of the processes under consideration, a sound model must explicitly take the delays into account.

The idea that the evolution of a system can only be predicted given some knowledge of its past history is not novel. A review of the relevance of time-delays in control theory can be found in [11]. In biological systems, delays arise because of the finite speed at which biochemical and electrochemical signals propagate. Hormones are carried by the blood flow to their targets; action potentials propagate down axons and neuro-transmitters must diffuse across the synaptic cleft between neurons. In the study of population dynamics, delay-dependent models reflect the time lags that always exist between environmental stimuli and adaptive responses.

The use of delay-dependent models is in no way exclusive to theoretical biology and biomathematics. A number of physical systems require their use to understand their behavior: the stability of nuclear reactors [52, 67, 126], neutron shielding [15, 167] and bistable optical devices [63, 87, 86] to name just a few. As early as the 1930's Kalecki [93] proposed delay-differential equations as models of cyclic economic commodity market activity. In recent work, delay dependent models have been used to investigate the dynamics of commodity price fluctuations [10, 141].

When a model is formulated in terms of coupled first-order ordinary differential equations for the vector variable $\mathbf{x}(t) = (x_1(t), \ldots, x_n(t))$:

$$\frac{d\mathbf{x}(t)}{dt} = \mathbf{F}(x_1(t), \ldots, x_n(t)), \quad \mathbf{F} \equiv (F_1, \ldots, F_n), \tag{5.1}$$

the initial values $x_j(0)$ suffice to predict the evolution of $x_j(t)$ for any future time. However as the examples cited above illustrate, it is sometimes necessary to use knowledge of the past

history of at least one of the variables to allow prediction.

If the evolution of the variable $x_k(t)$ depends on some cumulative effect of *all* its earlier values, it should be replaced by some function h, weighted by a suitable factor g, and integrated over all previous times. Then the evolution equation is an integro-differential equation:

$$\frac{d\mathbf{x}(t)}{dt} = \mathbf{F}\left(\ldots, \int_{-\infty}^{t} g(t-t')h(x_k(t'))dt', \ldots\right). \tag{5.2}$$

The kernel g specifies the weight to be attached to the function h of x_k at each point of time in the past. This is an example of a DDE with distributed delays.

If there is a discrete time lag in the action of x_k on some other variable, we speak of a *discrete* delay in the system (1.1) and in that case at least one of the set of ODE's is amended by replacing, for example, $\mathbf{F}(\ldots, x_k(t), \ldots)$ by $\mathbf{F}(\ldots, x_k(t-\tau), \ldots)$. Then the equation of evolution

$$\frac{d\mathbf{x}(t)}{dt} = \mathbf{F}(x_1(t), \ldots, x_k(t-\tau), \ldots) \tag{5.3}$$

is a DDE with discrete delay.

In this chapter, the deterministic models we consider are of the form

$$\frac{dx(t)}{dt} = -\alpha x(t) + F(x(t-1)),$$

and when noise enters the problem, they can be written as

$$dx(t) = [-\alpha x(t) + F(x(t-1))]\,dt + G(x(t))\xi(t)dt$$

where $\alpha > 0$, $\xi(t)dt$ denotes a stochastic process whose characteristics will be discussed in Section 5.2.2 below, and the initial condition for the system in both cases is a function φ defined on $[-1, 0)$ (the delay is taken to be 1 without loss of generality). Similar equations routinely appear as realistic models in mathematical biology [129, 145, 143], in nonlinear optics [62, 87], and in the description of agricultural commodity markets [75, 141] to mention a few applications.

The phase space of these systems is infinite dimensional. The ensemble density, which gives the probability of occupation of phase space is therefore a functional. The evolution equation for similar functionals, known as the Hopf equation [24, 79, 128] cannot be integrated due to the lack of a theory of integration with respect to arbitrary functional measures. We introduce in Chapter 5 this functional equation for DDE's, and use perturbation

theory to examine the solution behavior, but the analysis presented there is hampered by the present limits of the theory of integration.

In this chapter we propose a reduction of the original DDE to a finite dimensional system which is arbitrarily accurate. This approximation is framed in both the stochastic and the deterministic case as a coupled map lattice (CML). The work presented here strongly indicates that in many circumstances of interest (from a modeling perspective) the evolution equation for the density functionals (the Hopf equation of the next chapter) can be approximated by the Perron-Frobenius equation in $\mathbb{R}^N$ (or its stochastic equivalent). The resulting description of delayed dynamics is akin to the description of ODE's given by the generalized Liouville equation, or of the Langevin equation by the Fokker-Planck equation. Once the reduction is completed, the analytical techniques available to describe the probabilistic properties of CML's can then be used to explain the presence of continuous-time statistical cycling numerically observed in the DDE's.

In Section 5.2, the reduction of first order DDE's to CML's is described in both the presence and the absence of noise. Section 5.3 briefly reviews the basic concepts necessary to describe the evolution of ensemble densities in CML's developed in Chapters 3 and 4. In Section 5.4.2, the analysis of deterministic systems is presented. Numerical investigations of a particular model confirm analytical predictions. In Section 5.5, we extend this presentation to stochastic models, and explore the remarkable phenomenon of statistical cycling induced by noise.

5.2 From DDE's to CML's

The link between hereditary dynamical systems (framed as functional or delay differential equations) and spatially extended models (hyperbolic PDE's to be precise) has been discussed extensively (*cf.* [14, 38, 213]). In a rather formal context, Fargue [55, 56] argues that it is possible to interpret hereditary systems as being nonlocal, or extended. This allows the introduction of a field which is intrinsic to the system, and the variable which satisfies the hereditary model is then a functional of this field. In other words, the memory in the system is interpreted as a nonlocality.

At a more applied level, Sharkovskiĭ, Maistrenko and Romanenko [192] have shown that systems of hyperbolic PDE's could, given appropriate boundary condition, be reduced *via* use of the method of characteristics to differential delay equations of the first order. Lukin

and Shestopalov [140] have applied this reduction procedure to investigate the dynamics of electromagnetic fields confined to cavities possessing nonlinear reflection properties which are routinely used in the construction of radio-optical devices.

5.2.1 The deterministic case

The deterministic DDE's considered in this section are of the form

$$\frac{dx(t)}{dt} = -\alpha x(t) + F(x(t-1)) \tag{5.4}$$

with an initial function $\varphi(s)$ defined for $s \in [-1, 0)$. There is a continuous time semidynamical system associated with (5.4), given by

$$\frac{dx_\varphi(t)}{dt} = \begin{cases} \frac{d\varphi(t)}{dt} & \text{if } t \in [-1, 0) \\ -\alpha x_\varphi(t) + F(x_\varphi(t-1)) & \text{if } t \geq 0 \end{cases}$$

so that the DDE (1) defines a continuous time operator $\mathcal{S}_t$ acting on bounded functions defined everywhere on $[-1, 0)$. For example, if φ denotes such an initial function,

$$\mathcal{S}_t\varphi = \{x_\varphi(s) : s \in [t-1, t)\}, 0 \leq t \leq 1 \tag{5.5}$$

(if $t > 1$, the initial function is no longer φ).

The first step in the reduction of (5.4) to a coupled map lattice is to use the Euler approximation to dx/dt and write

$$\lim_{\Delta \to 0} \frac{x_\varphi(t) - x_\varphi(t-\Delta)}{\Delta} = -\alpha x_\varphi(t) + F(x_\varphi(t-1)), \qquad \Delta > 0. \tag{5.6}$$

Removing the limit, (5.6) can be approximated by

$$x_\varphi(t) = \frac{1}{(1+\alpha\Delta)} \left[x_\varphi(t-\Delta) + \Delta F(x_\varphi(t-1))\right] \tag{5.7}$$

where $0 < \Delta \ll 1$.

Before describing the second step of the reduction, recall from (5.5) that equation (5.4) transforms an initial function φ defined on $[-1, 0)$ into another function: the solution x_φ defined on $[-1+t, t)$, where $0 < t \leq 1$ is continuous. Hence, if $t < 1$, there is an overlap between φ and x_φ. It is possible to vary the extent of this overlap by restricting the values which can be assumed by the time t in the definition (5.5). For example, if $t = m\Delta$, with $0 < \Delta \ll 1$ and $m = 1, 2, \cdots$, the continuous time definition (5.5) can be replaced by

$$\mathcal{S}_m\varphi = \{x_\varphi(s) : s \in [m\Delta - 1, m\Delta)\}, \quad 0 \leq m\Delta < 1. \tag{5.8}$$

If $\Delta = 1/N$, where $N \gg 1$, then $m = 1, \cdots, N$.

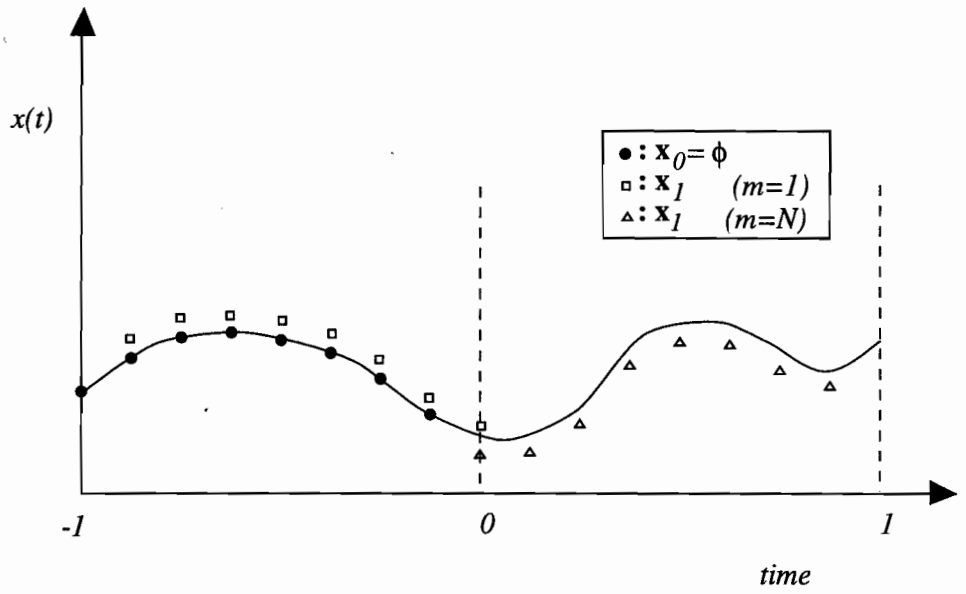

FIGURE 5.1:
Schematic illustration of the approximation of the differential delay equation (5.4) by a coupled map lattice: The initial function is replaced by a set of N points, and these N points form a vector which evolves in time under the action of a N-dimensional discrete time transformation (the coupled map lattice). The parameter $1 \leq m \leq N$ denotes the number of elements of $\mathbf{x}_n$ which are not elements of $\mathbf{x}_{n+1}$. See text for details.

The second step in the reduction consists of approximating the initial function φ by a set of N points (as illustrated in Figure 5.1), and following the evolution of these points approximating the corresponding solution. Hence, if $m = 1$ in (5.8), the initial function φ is replaced by by a vector $\boldsymbol{\varphi} = (\varphi_1, \cdots, \varphi_N)$, and the solution $\{x_\varphi(s) : s \in [\Delta - 1, \Delta)\}$ by a vector $\mathbf{x}_1 = (x_1^1, \cdots, x_1^N)$ (the subscript φ has been dropped to simplify the notation). Now define a discrete time transformation $\Phi_1 : \mathbb{R}^N \longmapsto \mathbb{R}^N$ (the subscript indicates that $m = 1$) such that

$$\Phi_1 \circ \overset{n \text{ times}}{\cdots} \circ \Phi_1 \equiv \Phi_1^n(\mathbf{x}_0) = \mathbf{x}_n, \quad n = 1, 2, \cdots, \qquad \text{where } \mathbf{x}_0 \equiv \boldsymbol{\varphi}.$$

To obtain an explicit expression for Φ_1, let $\Delta \equiv 1/N$, and suppose that $\varphi_j = \varphi(-1 + j\Delta)$, so that in general, x_n^j approximates the value of solution $x(t)$ at time $t = -1 + (n + j)\Delta$. Then, equation (5.7) can be approximated by an N-dimensional difference equation

$$\begin{aligned} x_1^1 &= x_0^2 \\ \vdots &= \vdots \end{aligned}$$

$$
\begin{aligned}
x_1^{j-1} &= x_0^j \\
\vdots &= \vdots \\
x_1^{N-1} &= x_0^N \\
x_1^N &= \frac{1}{(1+\alpha\Delta)}\left[x_0^N + \Delta F(x_0^1)\right].
\end{aligned} \tag{5.9}
$$

In vector notation, the system (6.56) can be written as

$$
\mathbf{x}_{n+1} = \mathbf{A}_1 \circ \mathbf{x}_n, \quad \text{for } n = 0, 1, \cdots \tag{5.10}
$$

where the matrix $\mathbf{A}_1$ is given by

$$
\mathbf{A}_1 = \begin{pmatrix}
0 & 1 & \cdots & 0 & 0 \\
0 & 0 & 1 & \cdots & 0 \\
 & & \ddots & & \\
\frac{\Delta F}{(1+\alpha\Delta)} & 0 & \cdots & 0 & \frac{1}{(1+\alpha\Delta)}
\end{pmatrix}. \tag{5.11}
$$

Equations (5.10) and (5.11) define a transformation Φ_1 which approximates the DDE (5.4). In the limit $N \to \infty$, the solution of the difference equation (5.10) converges to the solution of the DDE (5.4), because x is by definition always differentiable. $\mathbf{x}_n$ approximates the continuous time solution on the time interval $[n\Delta - 1, n\Delta)$, and $\mathbf{x}_{n+1}$ approximates the solution on the time interval $[(n+1)\Delta - 1, (n+1)\Delta)$. As illustrated schematically in Figure 5.1, in general one can approximate the original DDE by a transformation Φ_m such that $\mathbf{x}_{n+1}$ approximates the solution on $[(n+m)\Delta - 1, (n+m)\Delta)$ (with m an integer such that $1 \leq m \leq N$, as in (5.8)).

If $m > 1$ in (5.8), the set of difference equations (6.56) becomes

$$
\begin{aligned}
x_1^1 &= x_0^{1+m} \\
\vdots &= \vdots \\
x_1^j &= x_0^{j+m} \\
\vdots &= \vdots \\
x_1^{N-m+1} &= \frac{1}{(1+\alpha\Delta)}\left[x_0^N + \Delta F(x_0^1)\right] \\
\vdots &= \vdots
\end{aligned}
$$

$$
\begin{aligned}
x_1^i &= \frac{1}{(1+\alpha\Delta)}\left[x_1^{i-1} + \Delta F(x_0^{m+1+(N-i)})\right] \\
\vdots &= \vdots \\
x_1^N &= \frac{1}{(1+\alpha\Delta)}\left[x_1^{N-1} + \Delta F(x_0^{m+1})\right].
\end{aligned} \tag{5.12}
$$

Therefore, in vector notation, the equation which generalizes (5.10) is

$$
\mathbf{x}_{n+1} = \mathbf{B}_m \mathbf{x}_{n+1} + \mathbf{A}_m \circ \mathbf{x}_n, \tag{5.13}
$$

where the $N \times N$ matrices $\mathbf{A}_m$ and $\mathbf{B}_m$ are given by

$$
\mathbf{B}_m = \begin{pmatrix}
0 & \cdots & & & & \cdots & 0 \\
\vdots & & & [N-(m-1)] \text{ Empty rows} & & \vdots & \\
0 & \cdots & & & & \cdots & 0 \\
0 & \overset{(N-m)\ 0's}{\cdots} & 0 & \frac{1}{(1+\alpha\Delta)} & 0 & \cdots & 0 \\
\ddots & & & & & \ddots & \\
0 & \cdots & & 0 & \frac{1}{(1+\alpha\Delta)} & 0 & 0 \\
0 & \cdots & & & 0 & \frac{1}{(1+\alpha\Delta)} & 0
\end{pmatrix} \tag{5.14}
$$

and

$$
\mathbf{A}_m = \begin{pmatrix}
0 & \overset{m\ 0's}{\cdots} & & 0 & 1 & 0 & \cdots & \\
0 & \cdots & & & 0 & 1 & 0 & \cdots \\
\ddots & & & \ddots & & & & \\
0 & \cdots & & & & & 0 & 1 \\
\frac{\Delta F}{(1+\alpha\Delta)} & 0 & \cdots & & & & 0 & \frac{1}{(1+\alpha\Delta)} \\
0 & \frac{\Delta F}{(1+\alpha\Delta)} & 0 & \cdots & & & & 0 \\
\ddots & & & \ddots & & & & \\
0 & \cdots & 0 & \frac{\Delta F}{(1+\alpha\Delta)} & 0 & \cdots & & 0
\end{pmatrix}. \tag{5.15}
$$

In the case where $\mathbf{x}_n$ and $\mathbf{x}_{n+1}$ have no overlap, which corresponds to choosing $m = N$, these matrices become:

$$
\mathbf{B}_N = \begin{pmatrix}
0 & \cdots & & 0 \\
\frac{1}{(1+\alpha\Delta)} & 0 \cdots & 0 & \\
\ddots & & & \ddots \\
0 & \cdots & \frac{1}{(1+\alpha\Delta)} & 0
\end{pmatrix}, \quad
\mathbf{A}_N = \begin{pmatrix}
\frac{\Delta F}{(1+\alpha\Delta)} & 0 & \cdots & 0 & \frac{1}{(1+\alpha\Delta)} \\
0 & \frac{\Delta F}{(1+\alpha\Delta)} & 0 & \cdots & 0 \\
\ddots & & & \ddots & \\
0 & \cdots & & 0 & \frac{\Delta F}{(1+\alpha\Delta)}
\end{pmatrix} \tag{5.16}
$$

Given the form of the matrix $\mathbf{B}_m$, it is possible to write

$$
\mathbf{x}_{n+1} = (\mathbf{I} - \mathbf{B}_m)^{-1} \mathbf{A}_m \circ \mathbf{x}_n \equiv \Phi_m(\mathbf{x}_n). \tag{5.17}
$$

We will assume from now on that F is piecewise linear, because when this is the case, (5.13) can be simplified by replacing composition in the right hand side by a simple multiplication:

$$\mathbf{x}_{n+1} = (\mathbf{I} - \mathbf{B}_m)^{-1}\mathbf{A}_m\mathbf{x}_n \equiv \Phi_m(\mathbf{x}_n). \tag{5.18}$$

We have therefore reduced the differential delay equation (5.4) with a piecewise linear F to a piecewise linear CML Φ_m which can be analyzed from a probabilistic point of view.

This probabilistic analysis is done *via* an investigation of the spectral properties of the Perron-Frobenius operator associated with Φ_m. Before considering the Perron-Frobenius operator, we extend the reduction of deterministic DDE's to CML's to the case where the DDE's are subjected to stochastic perturbations.

5.2.2 The stochastic case

In this section, we explore the approximation of various stochastic DDE's by stochastic CML's. The stochastic DDE's we are concerned with are of the form

$$dx(t) = [-\alpha x(t) + F(x(t-1))]\,dt + G(x(t))\xi(t)dt \tag{5.19}$$

where the stochastic process $\xi(t)dt$ will be either a δ-correlated stationary white noise process, or an Ornstein-Uhlenbeck process [81]. For both types of noise, the stochastic process $x(t)$ is called a solution of the differential equation (5.19) when it satisfies, with probability 1, the integral equation

$$x(t) = x(t_*) + \int_{t_*}^{t}[-\alpha x(s) + F(x(s-1))]ds + \int_{t_*}^{t} G(x(s))d\xi(s) \tag{5.20}$$

where $0 < t_* < t$ and the second integral is a stochastic integral interpreted in either the Itô or the Stratonovich sense [81].

Define a partition of (t_*, t) by $t_* = s_0 < s_1 < \cdots < s_i < \cdots < s_k = t$. In the Stratonovich calculus, the stochastic integral in (5.20) is defined as the limit

$$\int_{t_*}^{t} G(x(s))d\xi(s) = \lim_{k\to\infty}\sum_{i=1}^{k} G\left(\frac{x(s_{i-1}) - x(s_i)}{2}\right)[\xi(s_i) - \xi(s_{i-1})]. \tag{5.21}$$

Similarly, the Itô stochastic integral is defined to be

$$\int_{t_*}^{t} G(x(s))d\xi(s) = \lim_{k\to\infty}\sum_{i=1}^{k} G\left(x(s_{i-1})\right)[\xi(s_i) - \xi(s_{i-1})]. \tag{5.22}$$

Both definitions are clearly not equivalent. Unlike the usual Riemann or Lebesgue integrals which yield the same results when the integrand is such that both are defined, the Itô and Stratonovich integrals of the same function can differ. The choice of either definition must be motivated by careful analysis of the physical situation under consideration [111, 196, 208]. The exact formulation of CML which results from a discrete time approximation depends on whether the stochastic integral in (5.20) is interpreted in the Itô or Stratonovich sense. However, as the reduction schemes for both cases are similar, we will illustrate it with the Itô interpretation of (5.20), which yields a more concise expression for the resulting CML.

The first step in the reduction procedure involves replacing the integrals in (5.20) by the appropriate sums:

$$x(t) = x(t_*) + \lim_{k\to\infty} \sum_{i=1}^{k} \Delta[-\alpha x(s_i) + F(x(s_i - 1))] + \lim_{k\to\infty} \sum_{i=1}^{k} Q\left(x(s_{i-1})\right)[\xi(s_i) - \xi(s_{i-1})], \quad (5.23)$$

where by definition of the Riemann integral $\Delta \equiv (s_i - s_{i-1}) > 0$. The precise value of Δ depends on the difference $t - t_*$ and will be given below.

The sums in (5.23) are over a partition of the interval (t_*, t). Hence by chosing $k = 1$, $t_* = s_0 \simeq t - \Delta$, and $s_1 \simeq t$, we obtain

$$\begin{aligned} \sum_{i=1}^{k} \Delta[-\alpha x(s_i) + F(x(s_i - 1))] &\longrightarrow \Delta[-\alpha x(t) + F(x(t-1))] \\ \sum_{i=1}^{k} Q\left(x(s_{i-1})\right)[\xi(s_i) - \xi(s_{i-1})] &\longrightarrow Q\left(x(t_*)\right)[\xi(t) - \xi(t_*)] \end{aligned}$$

Therefore, (5.23) becomes

$$x(t) = x(t_*) + \Delta\left[-\alpha x(t) + F(x(t-1))\right] + Q\left(x(t_*)\right)[\xi(t) - \xi(t_*)]. \quad (5.24)$$

As in the deterministic case, the second step of the reduction consists in approximating the function $\{x(s) : s \in [n\Delta - 1, n\Delta)\}$ by an N-dimensional vector $\mathbf{x}_n$ as illustrated in Figure 5.1. If the time t is discretized as in Section 5.2.1, the approximating solution (5.24) becomes the N-dimensional difference equation

$$\mathbf{x}_{n+1} = \mathbf{B}_m \mathbf{x}_{n+1} + \mathbf{A}_m \mathbf{x}_n + \left[\mathbf{Q}_m^{(1)} \circ \mathbf{x}_n + \mathbf{Q}_m^{(2)} \circ \mathbf{x}_{n+1}\right] \cdot \left[\boldsymbol{\xi}_{n+1} - \boldsymbol{\xi}_n\right] \quad (5.25)$$

where the matrices $\mathbf{A}_m$ and $\mathbf{B}_m$ are given in (5.15) and (5.14) respectively, and the matrices

$\mathbf{Q}_m^{1,2}$ are given by

$$\mathbf{Q}_m^{(1)} = \begin{pmatrix} 0 & \cdots & & & \cdots & 0 \\ \vdots & & \text{[}N-(m-1)\text{] Empty rows} & & \vdots & \\ 0 & \cdots & & & \cdots & 0 \\ 0 & \overset{(N-m)\ 0's}{\cdots} & 0\ Q\ 0 & & \cdots & 0 \\ \ddots & & & & \ddots & \\ 0 & \cdots & & & Q\ 0\ 0 & \\ 0 & \cdots & & & 0\ Q\ 0 & \end{pmatrix}, \tag{5.26}$$

and

$$\mathbf{Q}_m^{(2)} = \begin{pmatrix} 0 & \overset{m\ 0's}{\cdots} & 0 & 1 & 0 & \cdots & \\ 0 & \cdots & & 0 & 1 & 0 & \cdots \\ \ddots & & \ddots & & & & \\ 0 & \cdots & & & & 0 & 1 \\ Q & 0 & \cdots & & & & 0 \\ 0 & Q & 0 & \cdots & & & 0 \\ \ddots & & & \ddots & & & \\ 0 & \cdots & 0 & Q & 0 & \cdots & 0 \end{pmatrix}. \tag{5.27}$$

The entries of the N-dimensional vector $\boldsymbol{\xi}_n$ are random variables which are independent of one another. Hence, we define the density $\mathbf{g}(\boldsymbol{\xi}_n)$ to be

$$\mathbf{g}(\boldsymbol{\xi}_n) \equiv \prod_{i=1}^{N} g^{(i)}(\xi_n^{(i)}) \equiv \prod_{i=1}^{N} g(\xi_n), \quad n = 0, 1, 2, \cdots. \tag{5.28}$$

5.3 The evolution of probability densities in CML's

In this section, we recall some basic definitions associated with the evolution of probability densities under the action of discrete-time transformations in $\mathbb{R}^N$. These were all described in some detail in the previous chapters, and they are given here to simplify our presentation.

5.3.1 The deterministic case

A discrete-time nonsingular transformation $\Phi : \mathbb{X} \longmapsto \mathbb{X}$ $(\mathbb{X} \subset \mathbb{R}^N)$ induces the Perron-Frobenius operator denoted $\mathcal{P}_\Phi$ which acts on phase space probability densities,

$$\int_{\mathbb{A}} \mathcal{P}_\Phi \mathbf{f}(\mathbf{x})\, d\mathbf{x} = \int_{\Phi^{-1}(\mathbb{A})} \mathbf{f}(\mathbf{x})\, d\mathbf{x}, \quad \text{for all } \mathbb{A} \subset \mathbb{X}, \tag{5.29}$$

and all probability densities $\mathbf{f}$. A change of variable yields the more explicit definitions used in Chapter 3.

5.3.2 The stochastic case

In this case, the evolution of probability densities depends both on the deterministic part of the transformation, and on the type of noise present in the system.

5.3.2.1 Additive noise

In this case, the evolution of an element of the lattice transformation is given by a relation of the form

$$x_{n+1}^{(i)} = \Phi^{(i)}(\mathbf{x}_n) + \xi_n^{(i)} \equiv \Phi_{\text{add}}^{(i)}(\mathbf{x}_n), \tag{5.30}$$

where the density $\mathbf{g} = (g^{(1)}, \cdots, g^{(N)})$ of the vector random variable $\boldsymbol{\xi} = (\xi^{(1)}, \cdots, \xi^{(N)})$ is the product of its components as in equation (5.28). The evolution equation for phase space probability densities in this case is written [123]

$$\mathbf{f}_{n+1}(\mathbf{x}) = \int_{\mathbf{X}} \mathbf{f}_n(\mathbf{y}) \mathbf{g}(\mathbf{x} - \Phi(\mathbf{y}))\, d\mathbf{y}, \quad n = 0, 1, \cdots. \tag{5.31}$$

Equation (5.31) implicitly defines the transfer operator $\mathcal{P}_{\Phi_{\text{add}}}$ for CML's perturbed as in (5.30) since $\mathcal{P}_{\Phi_{\text{add}}} \mathbf{f}_n(\mathbf{x}) = \mathbf{f}_{n+1}(\mathbf{x})$. When the noise is multiplicative, this expression must be altered accordingly.

5.3.2.2 Multiplicative noise

In this case, the evolution of a lattice site is given by

$$x_{n+1}^{(i)} = \Phi^{(i)}(\mathbf{x}_n) \times \xi_n^{(i)} \equiv \Phi_{\text{mul}}^{(i)}(\mathbf{x}_n), \tag{5.32}$$

and the transfer operator $\mathcal{P}_{\Phi_{\text{mul}}}$ is given by (*cf.* Chapter 4 and [134])

$$\mathbf{f}_{n+1} = \int_{x^{(N)}}^{1} \cdots \int_{x^{(1)}}^{1} \mathbf{f}_n(\mathbf{y}) \prod_{i=1}^{N} \left[g\left(\frac{x^{(i)}}{\Phi^{(i)}(\mathbf{y})} \right) \frac{1}{\Phi^{(i)}(\mathbf{y})} \right] d\mathbf{y}, \quad n = 0, 1, \cdots. \tag{5.33}$$

It was shown in Chapter 4 that both $\mathcal{P}_{\Phi_{\text{add}}}$ and $\mathcal{P}_{\Phi_{\text{mul}}}$ are Markov operators defined by stochastic kernels. This property was then used to describe the asymptotic behavior of the sequence of densities $\{\mathbf{f}_n\}$ [*i.e* the convergence to a fixed point or to a limit cycle].

5.4 Applications to deterministic DDE's

In this section, we derive conditions on the control parameters of deterministic CML's which guarantee that the associated Perron-Frobenius operator is asymptotically periodic (*i.e* satisfies (1.21)).

5.4.1 Oscillatory solutions and expansion requirements

We say that a DDE possesses nontrivial statistical behavior when its solutions are oscillatory and bounded (whether they are periodic, quasi-periodic or chaotic). Hence, for a given equation, we restrict our attention to the regions of parameter space in which the trajectories are oscillatory. To illustrate this point, we use a model with F given by the tent map (a similar DDE has been considered by Ershov [53]):

$$F(x) = \begin{cases} ax & \text{if } x < 1/2 \\ a(1-x) & \text{if } x \geq 1/2 \end{cases} \qquad a \in (1, 2]. \tag{5.34}$$

The rationale for choosing this nonlinearity is that the resulting DDE displays a wide array of behaviors which is generic in more general (smooth) systems, while remaining amenable to analytic investigations. In addition, since F maps $[0:1]$ into itself, we know (*cf.* Section 2.1 of [53]) that the solutions of the DDE will be bounded if the initial function takes values in $[0, 1]$ and if $a/\alpha \leq 2$. Finally, our in-depth knowledge about the behavior of large CML's in which the local nonlinearity is given by the tent map should give us some insight into the statistical properties of the corresponding DDE with F given by (5.34).

The first fixed point of equation (5.4) with (5.34) is $x_*^{(1)} = 0$. It is locally stable when $a < \alpha$, and unstable when $a > \alpha$. When $a > \alpha$, the equation possesses another fixed point

$$x_*^{(2)} = \frac{a}{a+\alpha}$$

which is linearly stable when

$$2\alpha \geq a > \alpha \quad \text{and} \quad \sqrt{a^2 - \alpha^2} < \cos^{-1}\left(\frac{\alpha}{a}\right).$$

When $\sqrt{a^2 - \alpha^2} = \cos^{-1}\left(\frac{\alpha}{a}\right)$, the fixed point becomes unstable *via* a Hopf bifurcation, and the solutions of the DDE no longer converge to $x_*^{(2)}$. As mentioned above, the solutions must remain bounded when the initial function belongs to the interval $[0, 1]$, and since they do not converge to the fixed point, they must oscillate. We restrict our discussion of the dynamics of (5.4) to regions of parameter space in which the solutions are oscillatory, because stationary solutions are trivial from a statistical perspective. Hence our description of the probabilistic properties of (5.4) with (5.34) holds when the parameters of the equation satisfy

$$2\alpha \geq a > \alpha \quad \text{and} \quad \sqrt{a^2 - \alpha^2} > \cos^{-1}\left(\frac{\alpha}{a}\right). \tag{5.35}$$

When condition (5.35) is satisfied, the corresponding CML Φ_m expands distances in at least one direction. To see this, note that from (5.13) with (5.14) and (5.15), the total derivative of the variable x_{n+1}^{N-m} is given by

$$\begin{aligned} \frac{dx_{n+1}^{N-m}}{d\mathbf{x}_n} &= \frac{\partial x_{n+1}^{N-m}}{\partial x_n^N} + \frac{\partial x_{n+1}^{N-m}}{\partial x_n^1} \\ &= \frac{N+a}{N+\alpha}. \end{aligned}$$

and so $\frac{dx_{n+1}^{N-m}}{d\mathbf{x}_n} > 1$ if and only if $a > \alpha$. If condition (5.35) is satisfed, this is always the case, and therefore when the DDE possesses oscillatory solutions, the corresponding CML is hyperbolic (or expanding if one chooses to define expansion by the requirement that at east one eigendirection be expanding).

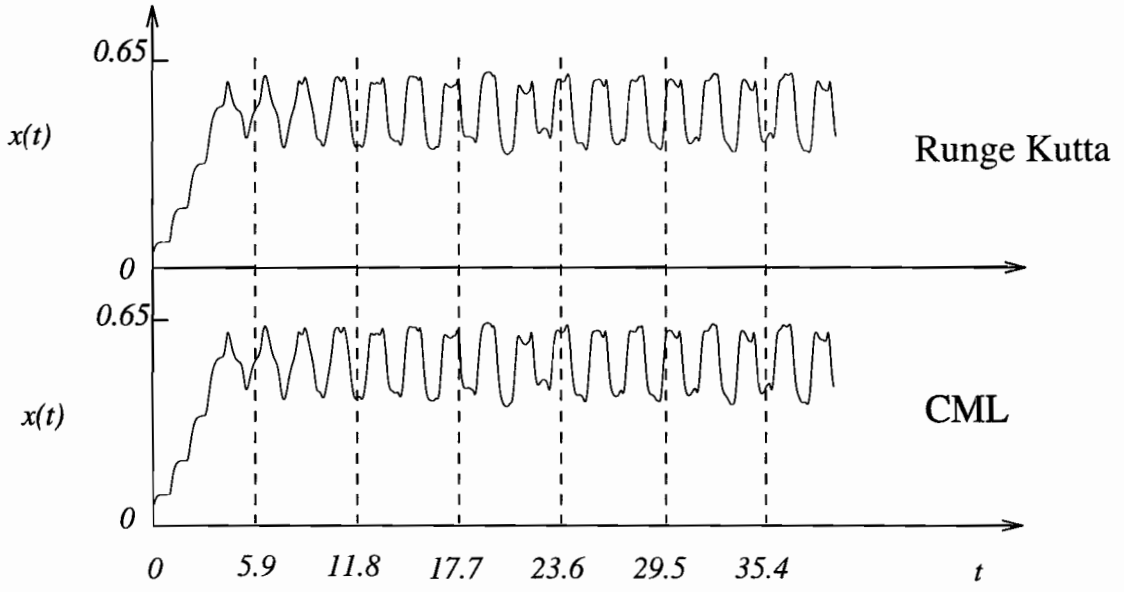

FIGURE 5.2:
Two numerical solutions of the DDE (5.4) with the nonlinearity given by (5.34), when $a = 13$, $\alpha = 10$, and a constant initial function $\varphi(s) = 0.2$ for $s \in [-1, 0)$. *Top:* The solution was produced by a standard adaptation of the fourth order Runge-Kutta method, with 40 points per delay. *Bottom:* The solution was produced by the CML approximation (5.13), with $m = N = 1000$. As expected, although both solutions are in excellent agreement with one another, the Runge-Kutta method is numerically more efficient than the Euler approximation which underlies our derivation of the CML. The motivation for the CML approach is that it yields a system which is amenable to analytic investigations.

Examples of oscillatory solutions of equation (5.4) with F given by (5.34) are shown in Figure 5.2. The parameters used to produce that figure are the same as the ones used to

produce the "ensemble density" results presented in Figure 5.4 below. As expected, the remarkable agreement between the solutions obtained by both methods breaks down when N becomes too small (*i.e.* of order 10^2), and for large times when the solution is chaotic. Having derived the CML approximation to the DDE, we now use this expression to rigorously discuss the thermodynamic (or probabilistic) behavior of the equation.

5.4.2 The result

When the parameters α and a of the DDE (5.4), with nonlinearity F given by (5.34), satisfy (5.35), and the initial function φ for the equation belongs to the interval $[0,1]$, the corresponding CML (5.13) induces a Perron-Frobenius operator which is asymptotically periodic and therefore admits the spectral decomposition (1.21).

We now prove this statement.

Using basic properties of determinants [158], for all $\mathbf{x} \in \mathbb{X}$, and all $i = 1, \cdots, M$ the Jacobian of $\Phi^{-1}(\mathbf{x})$ is

$$\mathcal{J}(\Phi_{|_i}^{-1}(\mathbf{x})) = \mathcal{J}^{-1} = \frac{\det\left(\mathbf{I} - |\mathbf{B}'_m|\right)}{\det|\mathbf{A}_m{}'|} \tag{5.36}$$

where $|\mathbf{A}'_m|$ and $|\mathbf{B}'_m|$ can be obtained by replacing F by a in $\mathbf{A}_m$ (defined in (5.15)) and $\mathbf{B}_m$ (defined in (5.14)) respectively. It is straightforward to verify that

$$\mathcal{J}^{-1} = \left[\frac{(N+\alpha)}{a}\right]^m. \tag{5.37}$$

Therefore, using the definition (1.8), basic properties of the variation and (5.37)

$$\begin{aligned} \bigvee(\mathcal{P}_\Phi \mathbf{f}) &= \bigvee\left(\sum_{i=1}^{s(\Pi)} \frac{\mathbf{f}(\Phi_{|_i}^{-1}(\mathbf{x}))}{\mathcal{J}(\Phi_{|_i}^{-1}(\mathbf{x}))}\chi_{\tilde{\pi}_i}(\mathbf{x})\right) \\ &\leq \sum_{i=1}^{s(\Pi)} \bigvee\left(\frac{\mathbf{f}(\Phi_{|_i}^{-1}(\mathbf{x}))}{\mathcal{J}(\Phi_{|_i}^{-1}(\mathbf{x}))}\chi_{\tilde{\pi}_i}(\mathbf{x})\right) \\ &= \mathcal{J}\sum_{i=1}^{s(\Pi)} \bigvee\left(\mathbf{f}(\Phi_{|_i}^{-1}(\mathbf{x}))\chi_{\tilde{\pi}_i}(\mathbf{x})\right). \end{aligned} \tag{5.38}$$

As in Chapter 3 each term in the sum on the right hand side of (5.38) can now be evaluated explicitly, and resulting bounds can be placed on the left hand side of the equation. The end result is, as in Section 3.5,

$$\bigvee(\mathcal{P}_\Phi \mathbf{f}) \leq \mathcal{J}\sum_{i=1}^{s(\Pi)}\left[\mathcal{J}\bigvee(\mathbf{f}(\mathbf{x}))\Big|_{\mathbf{x}\in\pi_i} + \frac{\mathcal{J}}{\sin\theta(\tilde{\pi}_i)}\bigvee(\mathbf{f}(\mathbf{x}))\Big|_{\mathbf{x}\in\pi_i} + \mathcal{K}_i\right]$$

$$\leq \mathcal{J}^2 \bigvee(\mathbf{f}) \left[1 + \frac{1}{\sin\theta(\tilde{\pi})}\right] + s(\Pi)\, \max_i \mathcal{K}_i. \tag{5.39}$$

Therefore, comparing (5.39) (using (5.37)) with (3.15), the theorem of Ionescu Tulcea and Marinescu (*cf.* Section 3.5) guarantees the asymptotic periodicity of the Perron-Frobenius operator when

$$\left[\frac{a}{(N+\alpha)}\right]^{2m} \left[1 + \frac{1}{\sin\theta(\tilde{\pi})}\right] < 1. \tag{5.40}$$

In order for this inequality to yield precise conditions on the control parameters of the CML, it is necessary to evaluate the quantity $\sin\theta(\tilde{\pi})$ in terms of these parameters. This calculation is straightforward given the analysis of Chapter 3.

If the boundaries of the sets $\tilde{\pi}_i$ intersect at an angle which is bounded below by $\theta_{\text{int}} > 0$ (for all $i = 1, \cdots, s(\Pi)$), then when $\mathbb{X}$, and thus the π_i's, are subsets of $\mathbb{R}^N$, we have from Appendix 3A [138]

$$\sin\theta(\tilde{\pi}) = \sqrt{\frac{1 - \cos\theta_{\text{int}}}{N[1 + (N-2)\cos\theta_{\text{int}}]}}. \tag{5.41}$$

Note that if the boundaries of the image sets intersect at right angles so that $\theta_{\text{int}} = 90^0$, we have $\sin\theta(\tilde{\pi}) = 1/\sqrt{N}$. In general however, the image partition is not rectangular, and the angle θ_{int} must be determined from the definition of the CML under consideration.

Recall that the sets π_i are defined to be the subsets of $\mathbb{X}$ on which the CML given in (5.13) is piecewise linear. If F is given by (5.34), these sets are of the form $\pi_i = [0, 1/2]^i \times (1/2, 1]^{2^N - i}$, since the solution $x(t)$ of the original DDE (5.4) satisfies $0 \leq x(t) \leq 1$ for all $t > 0$ by hypothesis. Hence the π_i's are delimited by 3^N vertices, $\{\mathbf{v}_q = (v_q^{(1)}, \cdots, v_q^{(N)})\}$, $q = 1, \cdots, 3^N$ where each component $v_q^{(k)}$ is either 0, 1/2 or 1 for $k = 1, \cdots, N$. The images $\tilde{\mathbf{v}}_q$ of the $\mathbf{v}_q$'s are the vertices of the image partition whose elements are denoted $\tilde{\pi}_i$.

From equations (5.13), (5.14) and (5.15), we have

$$\begin{aligned}
\tilde{v}_q^{(k)} &= v_q^{(k+m)}, \quad \text{for } k = 1, \cdots, N-m \\
\tilde{v}_q^{(N-m+1)} &= \frac{\Delta F(v_q^{(1)})}{(1+\alpha\Delta)} + \frac{v_q^{(N)}}{(1+\alpha\Delta)} \\
\tilde{v}_q^{(N-m+j)} &= \sum_{p=1}^{j} (-1)^{(p-1)} \left[\frac{\Delta F(v_q^{(j+1-p)})}{(1+\alpha\Delta)}\right]^p \quad \text{for } j = 2, \cdots, m.
\end{aligned} \tag{5.42}$$

Determining the smallest angle θ_{int} which can be subtended by edges of one of the image sets $\tilde{\pi}_i$ is a tedious minimization problem. However, a conservative lower bound for θ_{int} can

be obtained relatively easily. If this lower bound is used in (5.41), we obtain a lower bound for $\sin\theta(\tilde{\pi})$, and the resulting conditions on a, α, m and N obtained from (5.40) will be correspondingly conservative.

The angle $\theta_{\rm int}$ is defined by three points which are images of three of the 3^N vertices delimiting the sets π_i. The lower bound for $\theta_{\rm int}$ is defined by a triplet such that two of the three elements are distinct but as close as (5.42) permits, while being as far from the third as possible. Hence, to determine the lower bound for $\theta_{\rm int}$, two distances must be estimated. The first is the greatest Euclidean distance separating two points belonging to the same face of one of the image sets (which is bounded above by $\sqrt{N}$, the "diameter" of the phase space $\mathbb{X}$). The second is the smallest distance $d_{\tilde{q}\tilde{q}'}$ separating two images $\tilde{\mathbf{v}}_q$ and $\tilde{\mathbf{v}}_{q'}$ $(q \neq q')$,

$$d_{\tilde{q}\tilde{q}'} = \sqrt{\sum_{k=1}^{N} [\tilde{v}_q^{(k)} - \tilde{v}_{q'}^{(k)}]^2}.$$

Minimizing this distance is straightforward since all the terms are positive, so we must first pick $\mathbf{v}_q$ and $\mathbf{v}_{q'}$ such that their images differ in only one of their components, and then try to minimize the resulting difference by choosing this component appropriately.

There are two ways to choose $\mathbf{v}_q$ and $\mathbf{v}_{q'}$ such that $\tilde{\mathbf{v}}_q$ and $\tilde{\mathbf{v}}_{q'}$ differ in a single component.

1) From (5.42), if $\mathbf{v}_q$ and $\mathbf{v}_{q'}$ differ by only one component which belongs to both the preimage $\mathbf{v}_{q,q'}$ and the image $\tilde{\mathbf{v}}_{q,q'}$ (*i.e.* $v_q^{(i)} = v_{q'}^{(i)}$ for all i except for $i = k$, with $m < k < N$), then $d_{\tilde{q}\tilde{q}'}$ must equal the distance separating $\mathbf{v}_q$ and $\mathbf{v}_{q'}$. This nonzero distance is bounded below by $1/2$.

2) It is possible to obtain a more conservative (*i.e.* smaller) estimate for $d_{\tilde{q}\tilde{q}'}$ by noting that in the regions of parameter space which are of interest, from (5.42), Φ_m is a contraction along some directions. If $\mathbf{v}_q$ and $\mathbf{v}_{q'}$ differ in their k^{th} component with $1 \leq k \leq m$, then their images $\tilde{\mathbf{v}}_q$ and $\tilde{\mathbf{v}}_{q'}$ will possess $(k - m + 1)$ different components $\{j = N - (k - m + 1), N - (k - m) + 1, \cdots, N\}$. By choosing $k = m$, $\tilde{\mathbf{v}}_q$ and $\tilde{\mathbf{v}}_{q'}$ differ in a single component.

In the second case, the distance between $\tilde{\mathbf{v}}_q$ and $\tilde{\mathbf{v}}_{q'}$ is minimized, and from (5.42) it is easily shown to be

$$\begin{aligned} d_{\tilde{q}\tilde{q}'} = |\tilde{v}_q^{(N)} - \tilde{v}_{q'}^{(N)}| &= \left| \frac{F(v_q^m) - F(v_{q'}^m)}{(N+\alpha)} \right| \\ &\geq \frac{a}{2(N+\alpha)}, \end{aligned} \tag{5.43}$$

since if $F(v_q^m) - F(v_{q'}^m) \neq 0$, then $F(v_q^m) - F(v_{q'}^m) \geq a/2$.

From plane analytic geometry, θ_{int} is therefore bounded below by the angle subtended by a horizontal line, and a line of slope $\frac{a}{2\sqrt{N}(N+\alpha)}$, so

$$\tan\theta_{\text{int}} = \frac{a}{2\sqrt{N}(N+\alpha)}.$$

Therefore, if N is large we have, using the approximations $\cos\theta_{\text{int}} \simeq 1-\theta_{\text{int}}$, and $\sin\theta_{\text{int}} \simeq \theta_{\text{int}}$ (for small θ_{int})

$$\theta_{\text{int}} \simeq \frac{a}{2\sqrt{N}(N+\alpha)}.$$

Using the same approximations in (5.41), we obtain

$$\sin\theta(\tilde{\pi}) \simeq \sqrt{\frac{a}{2N^{3/2}(N+\alpha)[1+(N-2)]}}.$$

Replacing this conservative estimate in the condition (5.40), we finally obtain an explicit condition on the parameters of the CML which is sufficient to guarantee asymptotic periodicity:

$$\left[\frac{a}{(N+\alpha)}\right]^{2m}\left[1+\sqrt{\frac{2N^{3/2}(N+\alpha)[1+(N-2)]}{a}}\right] < 1. \tag{5.44}$$

If N is large, the left hand side of the preceding inequality behaves like $N^{-2m}N^{7/4}$. Hence the inequality is always satisfied for N large enough, and Theorem 3.1 of Section 3.5 implies that $\mathcal{P}_{\Phi_m}$ is always asymptotically periodic, when Φ_m approximates the DDE (5.4) with F given by (5.34) under the condition (5.35) (though the period could be 1).

Numerically, this result is reflected by the temporally periodic behavior of various statistical descriptors of the motion. As an example, consider the "ensemble sample density" $p(x,t)$. This function is obtained by integrating (5.4) with a large number of different initial functions $\{\varphi_1,\cdots,\varphi_E\}$ (E large) and then, at time t, binning the set of points $\{x_{\varphi_i}(t)\}$, where $x_{\varphi_i}(t)$ denotes the solution of the DDE corresponding to the initial function φ_i. Schematically, Figure 5.3 displays this construction. To establish a parallel with more frequently discussed models, if the equation satisfied by $x(t)$ was an ordinary differential equation (rather than a DDE), the evolution of $p(x,t)$ would be described by the Liouville equation.

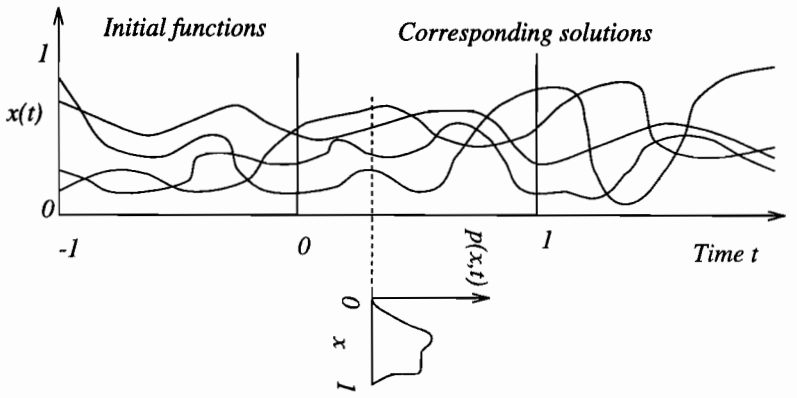

FIGURE 5.3:
Schematic illustration of the construction of the "sample ensemble density" $p(x,t)$. A set of initial conditions $\{\varphi_1, \cdots, \varphi_E\}$ generates a set of solutions $\{x_{\varphi_i}\}_{i=1}^E$, and at time t, the distribution of values $\{x_{\varphi_i}(t)\}_{i=1}^E$ is given by $p(x,t)$.

The statistical cycling predicted by (5.44) can be observed numerically by following the function $p(x,t)$ for successive times. Figure 5.4 displays such a numerical simulation for the DDE (5.4) with F defined in (5.34). The novel feature displayed in Figure 5.4 is the dependence of the asymptotic density cycle on the initial density which describes the set of initial functions used to carry out a set of simulations. This property is not observed in continuous-time systems without delays, and it can be understood in light of the dependence of the functionals $\Gamma_{1,\cdots,r}$ of equation (1.21) on the initial density $\mathbf{f}_0$. This dependence on initial conditions is in a sense much stronger than that usually discussed in relation to chaotic dynamical systems: Here the evolution of an ensemble of DDE's depends on the exact distribution of the initial ensemble.

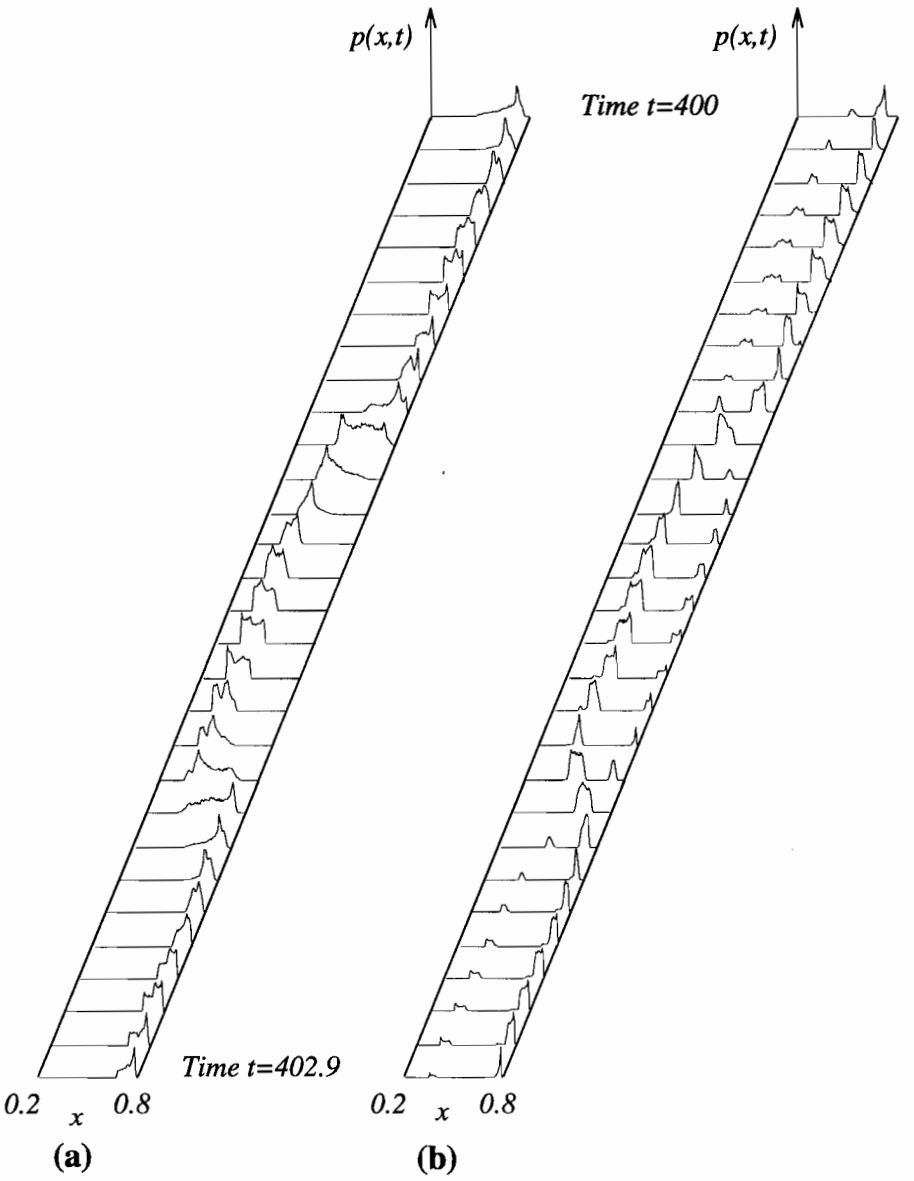

FIGURE 5.4:
Statistical cycling in an ensemble of DDE's of the form (5.4) with nonlinearity F given by (5.34). The parameters in the equation are $a = 13$, $\alpha = 10$, and the CML used for the solution contained $N = 10^3$ sites. Both (a) and (b) were produced with 22500 initial functions. **(a)** Each of the initial functions was a random process supported uniformly on $[0.65, 0.75]$. **(b)** The initial functions were random processes supported either on $[0.65, 0.75]$ (for 17000 cases) or on $[0.35, 0.45]$ (for the remaining 5500 initial functions). The cycling is not transient, and is observed for all times. The dependence of the density cycle on the initial density reflects the dependence of the Γ_i's of (1.21) on $\mathbf{f}_0$.

Since the pioneering work of Ikeda *et al.* [87]), the dynamics of optical bistable devices

have been modelled by equations of the form (5.4). It has been shown that in certain optical bistable devices perturbed by noise, the evolution of $p(x,t)$ may involve a gradual switching from one preferred state to another (known as "noise-induced transient bimodality"), when the system was given an impulse in the form of an instantaneous change in the suitably normalized field strengths (*cf.* [120] and the references therein). If this impulse was replaced by periodic modulation, one would expect to observe the same phenomenology as the statistical cycling of Figure 5.4. In this case, asymptotic periodicity therefore provides a theoretical explanation for a cycling which does not require the introduction of a potential function in the model equation.

Since the presence of stochastic fluctuations in experimental situations is ubiquitous, it is of interest to discuss the presence of statistical cycling and asymptotic periodicity in models which are stochastically perturbed.

5.5 Application to stochastic models

In this section, we investigate the properties of the transfer operators (5.31) and (5.33) induced by the stochastic CML's (5.30) and (5.32). Our discussion is based on the results presented in [134]. In the deterministic case, deriving equation (5.44) required detailed knowledge of the function F. In the stochastic case, our results are, to a large extent, independent of the details of the model, and can be summarized as follows:

If the solution $x(t)$ of the stochastic DDE (5.19) belongs to $[0,1]$ for all $t > 0$, then the CML approximating (5.19) induces an asymptotically periodic transfer operator.

This statement stems from the application to equations (5.31) and (5.33) of Theorem 1 and Theorem 2 of Chapter 4. To apply these results to $\mathcal{P}_{\Phi_{\text{add}}}$ and $\mathcal{P}_{\Phi_{\text{mul}}}$, let

$$\mathbf{K}_{\text{add}}(\mathbf{x},\mathbf{y}) = \mathbf{g}(\mathbf{x}-\Phi)$$

for the additive noise case, and

$$\mathbf{K}_{\text{mul}}(\mathbf{x},\mathbf{y}) = \prod_{i=1}^{N}\left[g\left(\frac{x^{(i)}}{\Phi^{(i)}(\mathbf{y})}\right)\frac{1}{\Phi^{(i)}(\mathbf{y})}\right]$$

for the multiplicative noise case. Hence, from (5.31) and (5.33)

$$\begin{aligned}\mathcal{P}_{\Phi_{\text{add}}}\mathbf{f}(\mathbf{x}) &= \int_{\mathbf{X}}\mathbf{K}_{\text{add}}(\mathbf{x},\mathbf{y})\mathbf{f}(\mathbf{y})\,d\mathbf{y}\\ \mathcal{P}_{\Phi_{\text{mul}}}\mathbf{f}(\mathbf{x}) &= \int_{x^{(N)}}^{1}\cdots\int_{x^{(1)}}^{1}\mathbf{K}_{\text{mul}}(\mathbf{x},\mathbf{y})\mathbf{f}(\mathbf{y})\,d\mathbf{y}.\end{aligned}$$

Since $\mathbf{g}$ is a normalized probability density on $\mathbb{X}$, $\mathbf{K}_{\text{add,mul}}(\mathbf{x},\mathbf{y}) > 0$, and $\int_{\mathbb{X}} \mathbf{K}_{\text{add,mul}}(\mathbf{x},\mathbf{y}) = 1$, so that both $\mathbf{K}_{\text{add,mul}}(\mathbf{x},\mathbf{y})$ are stochastic kernels. In addition, it was shown in Chapter 4 (*cf.* Section 4.4.1.1 and 4.4.2.2) that they both satisfy (4.11) and (4.12). Hence, Theorems 4.1 and 4.2 yield the desired results on the asymptotic periodicity on CML's approximating DDE's perturbed by additive and multiplicative noise.

This result depends on two assumptions: The noise density $\mathbf{g}$ must be normalized on the hypercube $\mathbb{X}$, and the solution $x(t)$ defined in (5.20) must remain in the interval $[0,1]$ for all $t > 0$. One of the intriguing consequences of the ubiquitous presence of asymptotic periodicity in stochastic CML's is explored in the next section.

5.5.1 Noise-induced statistical cycling

The effects of noise on dynamical systems have been the subject of intense investigations (an extensive overview of this literature is given in [156]). It is well understood that the presence of noise in nonlinear models can result in profound qualitative changes of the systems under study. The mechanisms which bring about these changes depend to a large extent on the specificities of the model under consideration. For example, Kapral and Celarier [104] have discussed the influence of additive noise on bistable systems, and showed in this case how the noise-induced transitions reflect a crossing of the basin boundaries. Here we describe a different class of noise-induced transitions in a DDE of the form (5.4) with a nonlinearity F given by

$$F(x) = (ax + b) \bmod 1, \quad 0 < a < 1,\ 0 < b < 1. \tag{5.45}$$

As we will show, these transitions are best understood as resulting from a noise-induced bifurcation in the deterministic part of the model. The motivation for this choice of F is twofold. First, the behavior of the corresponding one dimensional map $x_{n+1} = F(x_n)$ has been well-documented (see Chapter 4, Section 4.3.2). Second, the presence of stochastic perturbations in equation (5.4) with F given by (5.45) can result in qualitative changes in the statistical behavior of the solutions [122, 174]. Before describing the behavior of the DDE, it is helpful to recall several properties of the map $x_{n+1} = F(x_n)$, which are due to Keener [108], and complement our description of Section 4.3.2.

As expected, the map $x_{n+1} = F(x_n)$ with F defined in (5.45) can possess stable limit cycle solutions, when $0 < a < 1,\ 0 < b < 1$. Less expected is the presence in the same region of parameter space (*i.e.* when $0 < a < 1,\ 0 < b < 1$), of aperiodic trajectories which

are attracted to a Cantor set in [0,1]. In either case, the solutions cannot be described by probability densities. Since the trajectories visit only a Cantor set in the asymptotic regime, the probability of occupation of phase space is not a differentiable function. In fact, the probabilistic properties of the map (5.45) are described by the evolution of noncontinuous measures, rather than the more usual probability densities. For fixed $0 < a < 1$, a change in the parameter $0 < b < 1$ can therefore result in a bifurcation from a periodic solution to a chaotic one. A similar behavior is observed when the system is perturbed by noise, such that

$$F(x) = (ax + b + \xi) \bmod 1, \quad 0 < a < 1,\ 0 < b < 1. \tag{5.46}$$

where ξ is a δ-correlated discrete time random process distributed uniformly on subintervals of $[0, 1]$. If ξ has the "right amplitude", the map undergoes noise-induced bifurcations. These cannot be described deterministically however, since the map is then stochastic, but must be described in terms of the evolution of probability densities. Such noise-induced bifurcations have been discussed in the one-dimensional map [174], and in diffusively coupled lattices of the map (5.46) [134]. We now give numerical evidence that similar behavior is expected in the stochastic differential equation (5.4) with F given by (5.46).

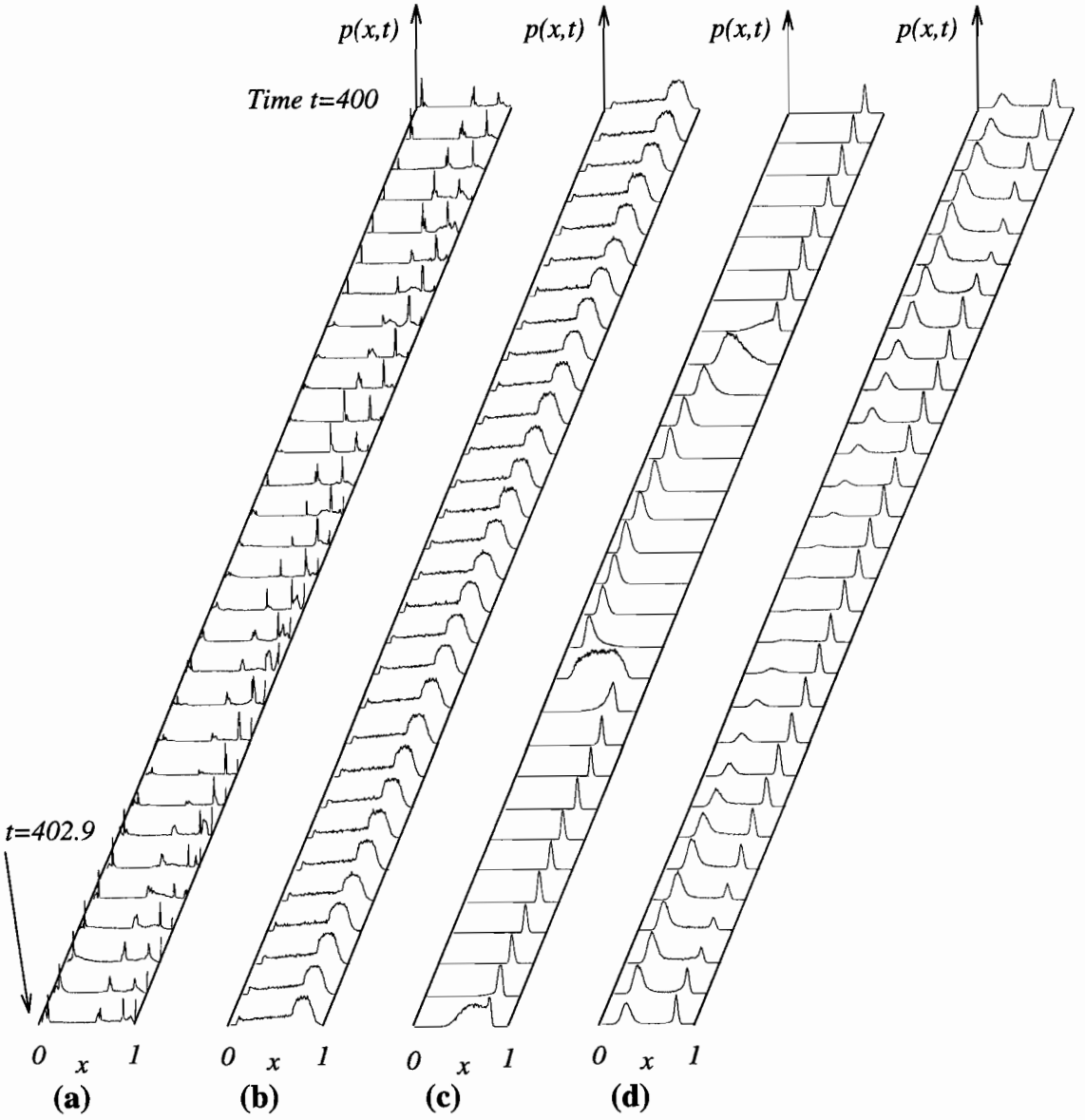

FIGURE 5.5:

Noise induced statistical cycling in (5.4) with F given by (5.34). As in Figure 5.4, each simulation was performed with 22500 random initial functions. In all four panels, the parameters of the equation were $a = 0.5$, $b = 0.567$, $\alpha = 10$. For panels (a)-(c) the initial density was as in Figure 5.4(a). **(a)** No noise in the system: $p(x,t)$ is not a density, but a generalized function (see text for details). **(b)** Noise present as in (5.46), supported uniformly on $[0, 0.1]$. The system is asymptotically stable, and $r = 1$ in (1.21). **(c)** Noise uniformly supported on $[0, 0.2]$, and $r = 2$ in (1.21). **(d)** Same noise as in (b)-(c), with an initial density as in Figure 5.4(b). Here Γ_1 and Γ_2 of equation (1.21) are not the same as in panel (c) because the initial density $\mathbf{f}_0$ has changed.

Figure 5.5 displays the temporal evolution of the ensemble sample density $p(x,t)$ in the absence and the presence of noise, and clearly illustrates the presence of noise-induced statistical cycling in this equation. The behavior displayed in Figure 5.5 can be understood by noting the similarities between one dimensional maps $x_{n+1} = F(x_n)$ and equations of the form (5.4). Ivanov and Sharkovskiĭ [88] have studied the dynamics of the DDE (5.4) by noting that in the limit $\alpha \to \infty$, and $F/\alpha \to \tilde{F}$ in (5.4), and with discrete time, one obtains the one dimensional map $x_{n+1} = \tilde{F}(x_n)$. Although in general the bifurcation structure of the one dimensional map need not survive this singular perturbation [146], Ivanov and Sharkovskiĭ showed that when the function $\tilde{F} : \mathbb{R} \longmapsto \mathbb{R}$ leaves a subset of $\mathbb{R}$ invariant, (in our case, this subset is $[0,1]$), then the solutions of the DDE visit the locations on $[0,1]$ which are visited by the iterates of the map (consult [88] for precise statements). On the basis of their analysis, one therefore expects that the bifurcation structure of the one dimensional map will, in some regions of parameter space, yield information on the bifurcation structure of the corresponding DDE.

Numerically, the bifurcations from chaotic to periodic attractors in the discrete map are also found in the deterministic DDE, and as illustrated in Figure 5.6, they can be induced by the perturbation of the function F as in (5.46).

Hence, the noise-induced statistical cycling displayed in Figure 5.5 probably reflects the presence in the DDE of a noise-induced bifurcation from a chaotic attractor to a periodic one. The presence of noise superimposed on the periodic solution could then explain the cyclical statistical behavior of Figures 5.5c and 5.5d. It is interesting to note that this phenomenon is consistent with the spectral decomposition (1.21) which was obtained using rather general considerations.

The behavior displayed in Figure 5.5, though somewhat counterintuitive at first glance, is therefore not unexpected for systems possessing limit cycles and chaotic attractors which are close in some sense in the space of control parameters.

present work opens the way for a more rigorous study of the present approximations, in the limit where the difference between the DDE and the CML vanishes. From a practical perspective however, the fact that there is no finite limit on the accuracy of our description of DDE's renders the presence of asymptotic periodicity in these systems inevitable. This would in turn imply the existence of semi-groups of operators which would possess the continuous time analogue of the decomposition (1.21), which has only been defined up to now for discrete time dynamical systems. More generally, the strong connection demonstrated here between models framed as delay differential equations and models framed as coupled map lattices opens the way for the cross-applications of techniques which have traditionally been used for the exclusive investigation of one or the other of these classes of models.

We have mentioned in the introduction of this chapter that the proper formulation of the evolution of densities under the action of differential delay equations should be a field theory, since the phase space of the DDE's are infinite dimensional. The next chapter introduces the corresponding formalism.

Chapter 6

The transfer operator for differential delay equations

ABSTRACT

We extend techniques developed for the study of turbulent fluid flows to the statistical study of the dynamics of differential delay equations. Because the phase spaces of differential delay equations are infinite dimensional, phase space densities for these systems are functionals. We derive a Hopf-like functional differential equation governing the evolution of these densities. The functional differential equation is reduced to an infinite chain of linear partial differential equations using perturbation theory. A necessary condition for a measure to be invariant under the action of a nonlinear differential delay equation is given. Finally, we show that the evolution equation for the density functional is the Fourier transform of the infinite dimensional version of the Kramers-Moyal expansion.

Croire tout découvert est une erreur profonde;
C'est prendre l'horizon pour les bornes du monde.

Antoine-Marin Lemierre, *L'Utilité des Découvertes faites dans les Sciences et les Arts sous le Règne de Louis XV*

6.1 Introduction

It is clear from the development of chapter 5 that the statistical properties of certain differential delay equations can be investigated by reducing these functional equations to finite dimensional systems. While that approach is fruitful to understand the numerically and experimentally observed behavior of certain delayed control loops, it is not completely satisfactory from a mathematical point of view, because delay differential equations are infinite dimensional semidynamical systems. This chapter proposes a possible description of the evolution of probability densities under the action of continuous-time DDE's which makes use of conceptual tools originally developped to investigate the probabilistic properties of the Navier-Stokes equations.

More specifically, we derive a functional differential equation for the characteristic functional $\mathcal{Z}_t$ of the measure defined on the phase space of a nonlinear DDE. This functional equation describes the evolution of a density of initial functions We show that the evolution equation for $\mathcal{Z}_t$ (a Hopf-like equation) is the Fourier transform of the infinite dimensional extension of the K-M expansion. This approach to the study of delayed dynamics was inspired by the work of Capiński [24] which extended functional techniques introduced by Hopf [79].

The formalism used throughout this paper is that of probability theory in function spaces. Consequently, there is a strong analogy between our presentation, field theories and the functional description of fluid mechanics. In particular, perturbation theory and the expansion of characteristic functionals in terms of probability moments are applicable to the study of differential delay equations.

The outline of the chapter is as follows. Section 6.2 recalls basic measure-theoretic definitions, introduces the characteristic functional $\mathcal{Z}_t$ and presents the derivation of the Kramers-Moyal equation in N dimensions (N finite). Section 6.3 introduces the characteristic functional appropriate for the discussion of DDE's, and the evolution equation for this functional (the Hopf equation) when the DDE's possess smooth feedback nonlinearities. In Section 6.4, this equation is reduced *via* perturbation theory to a chain of partial differential

equations which are examined in some detail for two examples. In Section 6.4.3 we give some necessary conditions which must be met by the invariant measures, and in Section 6.5 we explain the relation between our Hopf equation and the functional version of the Kramers Moyal equation.

6.2 Preliminaries

The spirit of our approach to the statistical study of DDE's parallels that of classical statistical mechanics in which, since the work of Gibbs and Boltzmann, physicists have grown accustomed to dealing with densities describing the thermodynamic states of a given system (whether it be discrete or continuous in time as in [133]). Here, we are interested here in examining the evolution of a density of functions, which characterizes a family of probability measures defined on a function space. We start by recalling some concepts from measure theory and probability theory.

A density of functions can be described by a measure defined on a function space. A collection $\mathcal{A}$ of subsets of a function space X (here a Banach space) is called a **σ-algebra** if:
1) When $A \in \mathcal{A}$ then $X \backslash A \in \mathcal{A}$;
2) Given a sequence (finite or not) $\{A_k\}$ of subsets of X, $A_k \in \mathcal{A}$, then $\bigcup_k A_k \in \mathcal{A}$; and
3) $X \in \mathcal{A}$.
Further, a real valued set function μ defined on a σ-algebra is called a **measure** if:
1) $\mu(\emptyset) = 0$;
2) $\mu(A) \geq 0$ for all $A \in \mathcal{A}$; and
3) $\mu\left(\bigcup_k A_k\right) = \sum_k \mu(A_k)$ if $\{A_k\}$ is a finite or infinite sequence of pairwise disjoint subsets of $\mathcal{A}$, that is, $A_i \bigcap A_j = \emptyset$ for $i \neq j$.
Finally, if $\mathcal{A}$ is a σ-algebra of subsets of X and if μ is a measure on $\mathcal{A}$, then the triple $(X, \mathcal{A}, \mu)$ is called a **measure space**. The sets belonging to $\mathcal{A}$ are called measurable sets because, for them, the measure is defined.

If X is a finite dimensional space and not a function space, a simple example of a measure space is given by taking X to be the real line, $X = \mathbb{R}$ with the σ-algebra chosen to be a partition of mutually disjoint subsets of X. If the measure μ is defined by ascribing a non-negative number to each element of $\mathcal{A}$, then the measure describes a piecewise constant distribution of points on the real line, each constant segment corresponding to an element of $\mathcal{A}$. This illustrates that distributions can be associated to a measure . The same is true when

the space is infinite dimensional. The *Wiener measure* is an example of such a measure. It has been discussed in detail in the context of stochastic wave propagation [128, 197], and used to study a class of partial differential equations encountered in some cell population dynamics problems [122].

6.2.1 Characteristic functionals

In this section, we introduce the characteristic functional which is the basic tool used to derive the partial differential equations for the moments of the distribution of initial functions.

In probability theory, the moments of all order of a probability distribution W_ξ with density $W(\xi)$ can be obtained from the *characteristic function.* If we have a random vector $(\xi_1, \cdots, \xi_n)$ and a vector $\boldsymbol{a} = (a_1, \cdots, a_n)$, $E(\cdot)$ denotes an expectation, and $\{\cdot, \cdot\}$ a scalar product, then the characteristic function ϕ is defined by (with $i^2 = -1$)

$$\begin{aligned} E\left(e^{i(a_1\xi_1+\cdots+a_n\xi_n)}\right) &= \int_X e^{i(a_1\xi_1+\cdots+a_n\xi_n)}\, W(\xi)d\xi, \\ &= \int_X e^{i\{a,\xi\}}\, dW_\xi \;\equiv\; \phi(\boldsymbol{a}). \end{aligned} \tag{6.1}$$

[The characteristic function ϕ is also known as the *generating function* in the applied mathematics literature]. Differentiation of $\phi(\boldsymbol{a})$ yields

$$\left.\frac{\partial\phi}{\partial \boldsymbol{a}}\right|_{a=0} = i\, E\,(\xi)\,,$$

while in general,

$$\left.\frac{\partial^n\phi}{\partial \boldsymbol{a}^n}\right|_{a=0} = i^n\, E(\xi^n).$$

Thus, differentiation of the characteristic function ϕ yields all the moments of the density $W(\xi)$ when the vectors ξ are finite dimensional.

Now consider the generalization to the situation when ξ is a function f defined on an interval Δ (finite or not). Let f be an element of a function space $\mathcal{C}$ with the topology given by the supremum norm. μ is a probability measure (*i.e.* it is normalized to 1) defined on the space $\mathcal{C}$. If $f(r)$ is defined for all $r \in \Delta$, the **characteristic functional** $\mathcal{Z}$ of the measure μ [sometimes referred to as the *characteristic functional* for the correlation functions associated with the distribution of functions $f(r)$] is defined by

$$\begin{aligned} \mathcal{Z}[J] &= \int_{\mathcal{C}} \exp\left[i\int_\Delta J(r)f(r)\,dr\right]\, d\mu(f) \\ &\equiv \left\langle \exp\left[i\int_\Delta J(r)f(r)\,dr\right]\right\rangle. \end{aligned} \tag{6.2}$$

$J(r)$ is called the *source* of the function $f(r)$. Thus, (6.2) defines the functional analogue of the characteristic function. The first realization of the process will yield one function f, a second realization will yield a second function, *etc.*.

Functionally differentiating $\mathcal{Z}$ with respect to the source $J(r)$ gives:

$$\left.\frac{\delta \mathcal{Z}[J]}{\delta J(r)}\right|_{r=\xi} \equiv \frac{\delta \mathcal{Z}[J]}{\delta J(\xi)} = \left\langle \frac{\delta}{\delta J(\xi)} \exp\left[i \int_\Delta J(r) f(r) dr\right] \right\rangle$$
$$= i \left\langle f(\xi) \exp\left[i \int_\Delta J(r) f(r) dr\right] \right\rangle .$$

In general, we have

$$\left(\frac{1}{i}\frac{\delta}{\delta J(\xi_1)}\right) \cdots \left(\frac{1}{i}\frac{\delta}{\delta J(\xi_n)}\right) \mathcal{Z}[J] =$$
$$\left\langle f(\xi_1) \cdots f(\xi_n) \exp\left[i \int_\Delta J(r) f(r)\, dr\right] \right\rangle ,$$

so

$$\langle f(\xi_1) \cdots f(\xi_n) \rangle = \frac{1}{i^n} \left.\frac{\delta^n \mathcal{Z}[J]}{\delta J(\xi_1) \cdots \delta J(\xi_n)}\right|_{J(\xi)=0} . \tag{6.3}$$

Thus, n-fold functional differentiation of $\mathcal{Z}$ with respect to the sources yields the n-point correlation functions

$$\langle f(\xi_1) \cdots f(\xi_n) \rangle ,$$

giving the complete statistical description of the distribution of functions in the space $\mathcal{C}$ of which f is a fixed but arbitrary element. Remember that this distribution of functions is also described by the probability measure μ defined on $\mathcal{C}$. Hence, $\mathcal{Z}$ is sometimes called the **characteristic functional of the measure μ.** Bochner's theorem (a finite dimensional version of which is presented in [180]) gives conditions on the measure which guarantee the existence of $\mathcal{Z}$, and we will sate without proof that these conditions are met here. As an aside, note that the proof makes use of the techniques of nonstandard analysis, and is not included here because its statement requires the introduction of a number of concepts and definitions which are not relevant to the rest of our discussion. Schematically, the nonstandard analytical methods allow to view real function spaces as hyperfinite spaces, and these can be treated as (finite) Euclidean spaces from a nonstandard perspective. Hence the construction of measures is possible, and a rigorous formulation of the ideas presented here results. The plan of the proof was communicated to us by Cápinski [25]. For an introduction to nonstandard analysis, consult [1, 85].

In conclusion, we extend the characteristic functional definition to a two variable density. The associated measure is defined on a "two-dimensional" function space $\mathcal{C} \times \mathcal{C}$, elements of which are pairs of functions (f_1, f_2). If these functions are defined for $(r_1, r_2) \in \Delta_1 \times \Delta_2$ then the characteristic functional is defined by

$$\mathcal{Z}[J_1, J_2] = \left\langle \exp i \left[\int_{\Delta_1} J_1(r_1) f_1(r_1) dr_1 + \int_{\Delta_2} J_2(r_2) f_2(r_2) dr_2 \right] \right\rangle \tag{6.4}$$

where the brackets indicate integration with respect to the *joint probability measure* [128] of the random field $(f_1(r_1), f_2(r_2))$ (the characteristic functional for a two-variable density is sometimes referred to as a *joint characteristic functional* [128]).

We can generalize these ideas to the case where $\mathcal{Z} = \mathcal{Z}_t$ is time varying, describing an evolving family of measures μ_t. In particular, $\mathcal{Z}_t$ can describe the evolution of a distribution of functions under the action of a given (semi)dynamical system. For example, a DDE will transform a distribution of initial functions with measure μ_0 into a distribution of functions with measure μ_{t_*} at time $t_* > 0$. The functional differential equation derived in Section 2 is the evolution equation for the characteristic functional of the family of measures generated by the action of a DDE on an initial distribution of functions.

Before proceeding to derive this functional equation in the next section, we review how the evolution equation for the densities in a finite dimensional space is obtained from the Kramers-Moyal expansion. The Kramers-Moyal expansion is an important tool of statistical mechanics, and we show in Section 3 that our functional equation (6.81) is the Fourier transform of the functional Kramers-Moyal expansion.

6.2.2 The Kramers-Moyal expansion for N variables

The Kramers-Moyal (K-M) expansion, from which the Liouville and Fokker-Planck equations can be derived, governs the temporal evolution of the density $W(\mathbf{x}, t)$ of the probability of finding the system at location $\mathbf{x}$ in phase space at time t. If the system under consideration is a n dimensional set of ordinary differential equations

$$\frac{d\mathbf{x}}{dt} = \boldsymbol{F}(\mathbf{x})$$

or, alternately,

$$\frac{dx_i}{dt} = F_i(x_1, \cdots, x_n) \;\; i = 1, \cdots, n,$$

the K-M expansion yields the generalized Liouville equation

$$\frac{\partial W(\mathbf{x},t)}{\partial t} = -\sum_{i=1}^{n} \frac{\partial\{W(\mathbf{x},t)\, F_i\}}{\partial x_i}. \tag{6.5}$$

When the system under consideration is a finite dimensional set of stochastic differential equations

$$\frac{dx_i(t)}{dt} = F_i(x_1,\cdots,x_n) + \sigma_{ij}(\mathbf{x})\zeta \quad i = 1,\cdots,n, \tag{6.6}$$

where ζ is a white noise perturbation with zero mean and unit variance and σ_i is the amplitude of the perturbation, the K-M expansion reduces to the Fokker-Planck equation

$$\frac{\partial W(\mathbf{x},t)}{\partial t} = -\sum_{i=1}^{n} \frac{\partial\{W(\mathbf{x},t)\, F_i\}}{\partial x_i} + \frac{1}{2}\sum_{i,j=1}^{n} \frac{\partial^2\{\sigma_{ij}(\mathbf{x})^2 W(\mathbf{x},t)\}}{\partial x_i \partial x_j} \tag{6.7}$$

if the Itô calculus is used to interpret (6.6) [181].

We now derive the Kramers-Moyal expansion in N-dimensions. Consider the N-dimensiona random vector $\boldsymbol{\xi} = (\xi_1,\cdots,\xi_N)$. The probability density $W(\boldsymbol{\xi}, t+t_*)$ of finding the vector with value $\boldsymbol{\xi}$ at time $t+t_*$ and the probability density $W(\boldsymbol{\xi}',t)$ are related by

$$W(\boldsymbol{\xi}, t+t_*) = \int_{\mathbb{R}^N} P(\boldsymbol{\xi}, t+t_*|\boldsymbol{\xi}', t) W(\boldsymbol{\xi}', t)\, d\boldsymbol{\xi}' \tag{6.8}$$

where the *transition probability amplitude* $P(\boldsymbol{\xi}, t+t_*|\boldsymbol{\xi}', t)$ gives the probability that if the system is observed at $(\boldsymbol{\xi}',t)$, it will be observed at $(\boldsymbol{\xi},t+t_*)$. Denoting the N-dimensional Dirac δ function by $\delta(\boldsymbol{\xi}) = \delta(\xi_1)\cdots\delta(\xi_N)$, the transition probability amplitude P satisfies

$$P(\boldsymbol{\xi}, t+t_*|\boldsymbol{\xi}', t) = \int_{\mathbb{R}^N} \delta(\mathbf{u}-\boldsymbol{\xi}) P(\mathbf{u}, t+t_*|\boldsymbol{\xi}', t)\, d\mathbf{u}. \tag{6.9}$$

It is possible to write down a formal Taylor expansion for the δ function about $\boldsymbol{\xi}'$ to give

$$\begin{aligned} \delta(\mathbf{u}-\boldsymbol{\xi}) &= \delta(\boldsymbol{\xi}' - \boldsymbol{\xi} + \mathbf{u} - \boldsymbol{\xi}') \\ &= \sum_{\lambda=0}^{\infty} \frac{1}{\lambda!} \frac{(-\partial)^\lambda}{\partial\xi_{j_1}\cdots\partial\xi_{j_\lambda}} (u_{j_1} - \xi'_{j_1})\cdots(u_{j_\lambda} - \xi'_{j_\lambda})\, \delta(\boldsymbol{\xi}' - \boldsymbol{\xi}), \end{aligned} \tag{6.10}$$

where we use the convention of summing over repeated latin indices (*i.e.* for each "λ-term", we sum over $j_1,\cdots,j_\lambda$). [As it stands, relation (6.10) does not make mathematical sense: to understand its meaning, notice that multiplying (6.10) by a function of $\boldsymbol{u}$ and $\boldsymbol{\xi}'$,

and integrating over these two variables, one recovers a Taylor expansion for this function.] Inserting (6.10) into (6.9), we obtain

$$\begin{aligned} P(\boldsymbol{\xi}, t+t_*|\boldsymbol{\xi}', t) &= \int_{\mathbb{R}^N} \sum_{\lambda=0}^{\infty} \frac{1}{\lambda!} \left(\frac{(-\partial)^\lambda}{\partial \xi'_{j_1} \cdots \partial \xi'_{j_\lambda}} \right) \\ &\quad \times (u_{j_1} - \xi'_{j_1}) \cdots (u_{j_\lambda} - \xi'_{j_\lambda})\, \delta(\boldsymbol{\xi}' - \boldsymbol{\xi}) P(\mathbf{u}, t+t_*|\boldsymbol{\xi}', t)\, d\mathbf{u} \\ &= \sum_{\lambda=0}^{\infty} \frac{1}{\lambda!} \left(\frac{(-\partial)^\lambda}{\partial \xi'_{j_1} \cdots \partial \xi'_{j_\lambda}} \right) \int_{\mathbb{R}^N} (u_{j_1} - \xi'_{j_1}) \cdots (u_{j_\lambda} - \xi'_{j_\lambda}) \\ &\quad \times P(\mathbf{u}, t+t_*|\boldsymbol{\xi}', t)\, d\mathbf{u}\, \delta(\boldsymbol{\xi}' - \boldsymbol{\xi}). \end{aligned} \tag{6.11}$$

The moments M of the probability density W are defined in terms of the corresponding transition probability P by (*cf.* [181])

$$M^{\lambda}_{j_1,\cdots,j_\lambda}(\boldsymbol{\xi}', t, t_*) = \int_{\mathbb{R}^N} (u_{j_1} - \xi'_{j_1}) \cdots (u_{j_\lambda} - \xi'_{j_\lambda}) P(\mathbf{u}, t+t_*|\xi', t)\, d\mathbf{u}, \tag{6.12}$$

so we can write (6.11) in terms of the moments:

$$P(\boldsymbol{\xi}, t+t_*|\boldsymbol{\xi}', t) = \left[\sum_{\lambda=0}^{\infty} \frac{1}{\lambda!} \left(\frac{(-\partial)^\lambda}{\partial \xi'_{j_1} \cdots \partial \xi'_{j_\lambda}} \right) M^{\lambda}_{j_1,\cdots,j_\lambda}(\boldsymbol{\xi}', t, t_*) \right] \delta(\boldsymbol{\xi}' - \boldsymbol{\xi}). \tag{6.13}$$

Assuming that the Fourier transform of the probability W be an analytic function, we can expand the moments in a power series about $t_* = 0$:

$$\frac{1}{\lambda!} M^{\lambda}_{j_1,\cdots,j_\lambda}(\, \boldsymbol{\xi}', t, t_*) = \mathcal{D}^{\lambda}_{j_1,\cdots,j_\lambda}(\boldsymbol{\xi}', t)\, t_* + \mathcal{O}(t_*^2) + \cdots. \tag{6.14}$$

Substituting (6.13) and (6.14) into (6.8) yields, for small t_*,

$$W(\boldsymbol{\xi}, t+t_*) \simeq \int_{\mathbb{R}^N} \left[\sum_{\lambda=0}^{\infty} \left(\frac{(-\partial)^\lambda}{\partial \xi'_{j_1} \cdots \partial \xi'_{j_\lambda}} \right) \mathcal{D}^{\lambda}_{j_1,\cdots,j_\lambda}(\boldsymbol{\xi}', t)\, t_* \right] W(\boldsymbol{\xi}', t) \delta(\boldsymbol{\xi}' - \boldsymbol{\xi})\, d\boldsymbol{\xi}'. \tag{6.15}$$

Dividing (6.15) by t_* and taking the limit $t_* \longrightarrow 0$ we obtain the **Kramers-Moyal expansion**

$$\frac{\partial W(\boldsymbol{\xi}, t)}{\partial t} \simeq \sum_{\lambda=1}^{\infty} \left(\frac{(-\partial)^\lambda}{\partial \xi_{j_1} \cdots \partial \xi_{j_\lambda}} \right) \mathcal{D}^{\lambda}_{j_1,\cdots,j_\lambda}(\boldsymbol{\xi}, t)\, W(\boldsymbol{\xi}, t). \tag{6.16}$$

For an extensive discussion of the Kramers-Moyal expansion and its truncation to yield either the Liouville or the Fokker-Planck equation, see [181].

Before proceeding to derive an infinite dimensional version of the K-M expansion useful for the ivestigation of delayed dynamics, note that equation (6.16) can be derived from the

characteristic function ϕ given by (6.1). To illustrate this, recall that the characteristic function, the conditional probability, and the moments are related by

$$\begin{aligned}\phi(\mathbf{a}) &= \int_{\mathbb{R}^N} e^{i\{\mathbf{a},(\xi-\xi')\}} P(\boldsymbol{\xi}, t+t_*|\boldsymbol{\xi}', t) d\boldsymbol{\xi} \\ &= \sum_{\lambda=0}^{\infty} \frac{(i\mathbf{a})^\lambda}{\lambda!} M^\lambda_{j_1,\cdots,j_\lambda}(\boldsymbol{\xi}', t, t_*). \end{aligned} \tag{6.17}$$

We can rewrite (6.17) as

$$P(\boldsymbol{\xi}, t+t_*|\boldsymbol{\xi}', t) = \frac{1}{(2\pi)^N} \int_{\mathbb{R}^N} e^{-i\{\mathbf{a},(\xi-\xi')\}} \left[\sum_{\lambda=0}^{\infty} \frac{(i\mathbf{a})^\lambda}{\lambda!} M^\lambda_{j_1,\cdots,j_\lambda}(\boldsymbol{\xi}', t, t_*)\right] d\mathbf{a}. \tag{6.18}$$

It is possible to represent the δ function as a Fourier integral, and the derivatives of this integral are then the derivatives of the δ function (see for example Appendix A in [61])

$$\frac{1}{(2\pi)^N} \int_{-\infty}^{\infty} (i\mathbf{a})^N e^{-i\{\mathbf{a},(\xi-\xi')\}} \, d\mathbf{a} = \left(\frac{(-\partial)^N}{\partial\xi_{j_1}\cdots\xi_{j_N}}\right) \delta(\boldsymbol{\xi} - \boldsymbol{\xi}').$$

[In the above, the notation is not rigorously correct, but it is standard in mathematical physics to discuss properties of the δ function without explicitly having it under the necessary integral sign, as long as these properties are then used when the context allows it rigorously.] Therefore, (6.18) becomes

$$P(\boldsymbol{\xi}, t+t_*|\boldsymbol{\xi}', t) = \left[\sum_{\lambda=0}^{\infty} \frac{1}{\lambda!} \left(\frac{(-\partial)^\lambda}{\partial\xi'_{j_1}\cdots\partial\xi'_{j_\lambda}}\right) M^\lambda_{j_1,\cdots,j_\lambda}(\boldsymbol{\xi}', t, t_*)\right] \delta(\boldsymbol{\xi}' - \boldsymbol{\xi}) \tag{6.19}$$

which is just (6.13). Hence (6.16) can be derived directly from the definition (6.17). In Section **??** we use an extension of this formalism to derive the infinite dimensional version of (6.16) directly from the characteristic functional (6.2).

6.3 Characteristic functionals for delay equations

We consider DDE's of the form

$$\frac{du}{ds} = -\alpha u(s) + F(u(s-1)) \text{ for } 1 < s, \tag{6.20a}$$

in which the delay τ is taken to be 1 without loss of generality, with the initial function

$$u(s) = v(s) \text{ if } s \in [0,1]. \tag{6.20b}$$

From now on we write (6.20a)-(6.20b) as the combined system

$$\begin{cases} u(s) &= v(s) & \text{for } s \in [0,1], \\ \frac{du(s)}{ds} &= -\alpha u(s) + F(v(s-1)) & \text{for } 1 < s < 2, \end{cases} \tag{6.21}$$

and denote by $\mathcal{S}_t$ the corresponding semidynamical system $\mathcal{S}_t : \mathcal{C}([0,1]) \longmapsto \mathcal{C}([0,1])$ given by

$$\mathcal{S}_t v(x) = u_v(x+t), \tag{6.22}$$

where u_v denotes the solution of (6.21) corresponding to the initial function v. Equation (6.22) defines a *semidynamical system* because a DDE is **noninvertible**, *i.e.* it cannot be run unambiguously forward and backwards in time.

From (6.22), the system (6.21) is equivalent to considering

$$\frac{\partial}{\partial t}\mathcal{S}_t v(x) = \begin{cases} \frac{\partial}{\partial t} v(x+t) & \text{for } x \in [0, 1-t], \\ -\alpha u(x+t) + F(v(x+t-1)) & \text{for } x \in (1-t, 1]. \end{cases} \tag{6.23}$$

Thus, we consider a segment of a solution of (2) defined on an interval $I_t = [t, t+1]$, as t increases (continuously) [*i.e.* the DDE (6.21) operates on a *buffer* of length 1, "sliding" it along the time axis]. Equation (6.23) states that the contents of this buffer are the initial condition v when the argument $(x+t)$ is less than 1, and the solution u of the equation otherwise.

We next introduce the characteristic functional $\mathcal{Z}_t$ of a family of probability measures evolving from an initial measure. We define the characteristic functional $\mathcal{Z}_t$ for (6.23) by

$$\mathcal{Z}_t[J_1, J_2] = \int_{\mathcal{C}} \exp\left[i \int_0^1 J_1(x) u_v(x+t)\, dx + i \int_0^1 J_2(x) v(x)\, dx \right] d\mu_0(\mathcal{T}_t^{-1}(v, u_v)). \tag{6.24a}$$

The source functions J_1 and J_2 are elements of $\mathcal{C}([0,1])$ and the measure of integration is the initial measure μ_0 (describing the initial distribution of functions) composed with $\mathcal{T}_t^{-1}(v, u_v)$ where $\mathcal{T}_t(v) : \mathcal{C}([0,1]) \longmapsto \mathcal{C} \times \mathcal{C}$ is defined by

$$\mathcal{T}_t(v) = (v, u_v).$$

For simplicity, we will use the notation $\mu_0(\mathcal{T}_t^{-1}(v, u_v)) \equiv \mathcal{W}[v, \mathcal{S}_t(v)]$, so (6.24a) becomes

$$\mathcal{Z}_t[J_1, J_2] = \int_{\mathcal{C}} \exp\left[i \int_0^1 J_1(x) u_v(x+t)\, dx + i \int_0^1 J_2(x) v(x)\, dx \right] d\mathcal{W}[v, \mathcal{S}_t(v)]. \tag{6.24b}$$

When no confusion is posssible, we write $\mathcal{W}_t$ for $\mathcal{W}[v, \mathcal{S}_t(v)]$.

If f and g are two functions defined on an interval I, we denote their scalar product by

$$\{f, g\} \equiv \int_I f(x)g(x)\, dx.$$

To simplify the notation we also write

$$\Upsilon[J_1, J_2; v] = \exp\left[i\{J_1(x), u_v(x+t)\} + i\{J_2(x), v(x)\}\right]. \tag{6.25}$$

Υ is used from now on to denote the function of J_1, J_2 and v defined in (6.25). We begin by noting the following relations

$$\begin{aligned} \frac{\delta^n \mathcal{Z}_t}{\delta J_1^n(\xi)} &= i^n \left\langle \Upsilon u_v^n(\xi + t) \right\rangle, \\ \frac{\delta^n \mathcal{Z}_t}{\delta J_2^n(\xi)} &= i^n \left\langle \Upsilon v^n(\xi) \right\rangle, \end{aligned} \tag{6.26}$$

where it is understood that

$$\left\langle \begin{pmatrix} \vdots \end{pmatrix} \right\rangle = \int_{\mathcal{C}} \begin{pmatrix} \vdots \end{pmatrix} d\mathcal{W}[v, \mathcal{S}_t(v)].$$

Note that if μ_0 is the probability measure on the space of all initial functions v, and A is any subset of $\mathcal{C}([0,1])$, then

$$\mu_t(A) \equiv \mu_0(\mathcal{S}_t^{-1}(A)).$$

In other words, the probability that a randomly chosen function belongs to A at time t equals the probability that the counterimage of that function (under the action of $\mathcal{S}_t$) belonged to the counterimage of the set A. This defines the family of measures characterized by the solutions $\mathcal{Z}_t$ of a functional differential equation which is the Fourier transform of the infinite dimensional version of the K-M expansion. The derivation of such an equation for a DDE was first considered by Capiński [24]. If the semiflow $\mathcal{S}_t$ is measure-preserving with respect to μ_0, then $\mu_0(A) \equiv \mu_0(\mathcal{S}_t^{-1}(A))$. In this case, we alternately say that the measure μ_0 is invariant with respect to $\mathcal{S}_t$.

We are now in a position te derive an evolution equation for the characteristic functional.

6.3.1 A functional differential equation for $\mathcal{Z}_t$

Time differentiation of the characteristic functional $\mathcal{Z}_t$ defined in (6.24b) yields, in conjunction with (6.23),

$$\begin{aligned}
\frac{\partial \mathcal{Z}_t}{\partial t} &= i\left\langle \Upsilon \int_0^1 J_1(x)\frac{\partial u_v(x+t)}{\partial t}\,dx \right\rangle \\
&= i\left\langle \Upsilon \int_0^1 J_1(x)\frac{\partial u_v(x+t)}{\partial x}\,dx \right\rangle \\
&= i\left\langle \Upsilon \int_0^{1-t} J_1(x)\frac{\partial v(x+t)}{\partial x}\,dx - \alpha\Upsilon\int_{1-t}^1 J_1(x)u(x+t)\,dx \right\rangle \\
&\quad + i\left\langle \Upsilon \int_{1-t}^1 J_1(x)F(v(x+t-1))\,dx \right\rangle . \qquad (6.27)
\end{aligned}$$

Therefore, from equation (6.26) and the definition (6.23), we obtain

$$\begin{aligned}
\frac{\partial \mathcal{Z}_t}{\partial t} &= \int_0^{1-t} J_1(x)\frac{\partial}{\partial x}\left(\frac{\delta \mathcal{Z}_t}{\delta J_1(x)}\right)\,dx - \alpha\int_{1-t}^1 J_1(x)\frac{\delta \mathcal{Z}_t}{\delta J_1(x)}\,dx \\
&\quad + i\left\langle \Upsilon \int_{1-t}^1 J_1(x)F(v(x+t-1))\,dx \right\rangle . \qquad (6.28)
\end{aligned}$$

Equation (6.28) is related to the Hopf functional differential equation for the evolution of the characteristic functional $\mathcal{Z}_t$, and contains all the statistical information describing the evolution of a density of initial functions under the action of the differential delay system (6.20a)-(6.20b). An equation similar to (6.28) was first obtained by Capiński for a differential delay equation with a logistic nonlinearity (see Example 1 below).

In order to derive the Hopf equation *per se*, we restrict our attention to situations where the feedback function F in the DDE (6.20a) is a polynomial

$$F(v) = \sum_{k=1}^{n} a_k v^k. \qquad (6.29)$$

With nonlinearity (6.29), equation (6.28) becomes, with identities (6.26),

$$\begin{aligned}
\frac{\partial \mathcal{Z}_t}{\partial t} &= \int_0^{1-t} J_1(x)\frac{\partial}{\partial x}\left(\frac{\delta \mathcal{Z}_t}{\delta J_1(x)}\right)\,dx - \alpha\int_{1-t}^1 J_1(x)\frac{\delta \mathcal{Z}_t}{\delta J_1(x)}\,dx \\
&\quad + \sum_{k=1}^{n} i^{(1-k)}\,a_k \int_{1-t}^1 J_1(x)\frac{\delta^k \mathcal{Z}_t}{\delta J_2^k(x+t-1)}\,dx. \qquad (6.30)
\end{aligned}$$

Analytically solving the Hopf equation (6.30) is not possible at present, though a correct method of solution should make use of integration with respect to measures defined on the space $\mathcal{C}$. Presently, the theory of such integrals only allows their consistent utilization

in solving functional differential equations when the measure of integration is the *Wiener measure* [197].

The lack of a formalism within which to evaluate functional integrals with respect to general measures also poses a problem for the development of field theories in physics where the characteristic and the generating functionals (CF,GF) both play a fundamental role. The *characteristic functional*, presented here, is the *Fourier transform* of a probability distribution (*i.e.* by Bochner's theorem it is the Fourier transform of a measure [180]). The *generating functional*, however, is the Laplace transform of a probability distribution.

In statistical physics, the GF is interpreted as the partition function for systems with an infinite number of degrees of freedom, while in quantum field theory the CF is used to obtain the Green's functions from which the scattering amplitudes for various processes are calculated. In quantum field theory, the measure of integration is the Wiener measure for the free particle problem for which the field equations are Wiener measure preserving; this is not the case when particles interact, and the systems under consideration are no longer Wiener measure preserving. In that case, investigators reduce the functional integral to a countably infinite product of finite dimensional integrals by coarse-graining the phase space (or, in the language of quantum field theory, replacing the continuum by a lattice) [188].

Before proceeding to treat the Hopf equation in a perturbative manner, we illustrate its specific form for a simple nonlinear delay equation.

Example 1. The differential delay equation

$$\frac{du}{ds} = -\alpha u(s) + ru(s-1)[1-u(s-1)], \tag{6.31}$$

can be considered as a continuous analogue of the discrete time logistic map

$$u_{n+1} = ru_n(1-u_n) \tag{6.32}$$

because equation (6.31) is the *singular perturbation* of the logistic map (6.32) as defined in [88]. The characteristic functional is defined by (6.24b), and the functional differential equation corresponding to (6.30) was shown by Capiński [24] to be

$$\begin{aligned}\frac{\partial \mathcal{Z}_t}{\partial t} &= \int_0^{1-t} J_1(x)\frac{\partial}{\partial x}\left(\frac{\delta \mathcal{Z}_t}{\delta J_1(x)}\right)dx - \alpha\int_{1-t}^{1} J_1(x)\frac{\delta \mathcal{Z}_t}{\delta J_1(x)}\,dx \\ &\quad + r\int_{1-t}^{1} J_1(x)\frac{\delta \mathcal{Z}_t}{\delta J_2(x+t-1)}\,dx - ri^{-1}\int_{1-t}^{1} J_1(x)\frac{\delta^2 \mathcal{Z}_t}{\delta J_2^2(x+t-1)}\,dx. \quad \bullet \end{aligned} \tag{6.33}$$

In spite of the fact that we cannot solve the Hopf equation analytically, relatively mild assumptions allow one to gain significant insight into the dynamics of $\mathcal{Z}_t$. More precisely, if $\mathcal{Z}_t$ is analytic we can expand it in a power series and treat the Hopf equation in a perturbative manner. We follow this approach in the next section.

6.4 The moments of the measure $\mathcal{W}_t$

The statistical properties of the random field of functions v and u are described by an infinite hierarchy of moments of the measure $\mathcal{W}_t$. For fixed t, the average value of the contents of the buffer defined on $I_t = [t, t+1]$ (*i.e.* v on $[t,1]$ and u_v on $(1, 1+t]$), which is just the first order moment of the measure $\mathcal{W}_t$, is

$$M_v^1(t,x) \equiv \int_{\mathcal{C}} v(x+t)\, d\mu_0(v) \qquad \text{for } x \in [0, 1-t], \tag{6.34}$$

$$M_u^1(t,x) \equiv \int_{\mathcal{C}} u_v(x+t)\, d\mu_0(v) \qquad \text{for } x \in (1-t, 1]. \tag{6.35}$$

These two equations can be written as one relation:

$$M^1(t,x) \equiv \int_{\mathcal{C}} u_v(x+t)\, d\mathcal{W}_t \qquad \text{for } x \in [0,1].$$

The definition of the second order moment (or covariance function) $M^2(t,x,y)$ is, with the same notation,

$$\begin{aligned}
M^2(t,x,y) &= \int_{\mathcal{C}} v(x+t)v(y+t)\, d\mu_0(v) \equiv M_{vv}^2(t,x,y) \quad \text{for } x,y \in [0,1-t]\times[0,1-t],\\
M^2(t,x,y) &= \int_{\mathcal{C}} u_v(x+t)v(y+t)\, d\mu_0(v) \equiv M_{uv}^2(t,x,y) \quad \text{for } x,y \in (1-t,1]\times[0,1-t],\\
M^2(t,x,y) &= \int_{\mathcal{C}} v(x+t)u_v(y+t)\, d\mu_0(v) \equiv M_{vu}^2(t,x,y) \quad \text{for } x,y \in [0,1-t]\times(1-t,1],\\
M^2(t,x,y) &= \int_{\mathcal{C}} u_v(x+t)u_v(y+t)\, d\mu_0(v) \equiv M_{uu}^2(t,x,y) \quad \text{for } x,y \in (1-t,1]\times(1-t,1].
\end{aligned}$$

The subscripts of the various components of M^2 refer to the segments of the solution whose correlation is given by the particular component. For example, M_{uv}^2 describes the correlation between u and v segments of the solution as is illustrated in Figure 6.1. Remember that the initial function is defined on an interval $[0,1]$, so to complete the description of the statistical dependence of the solution u_v on the initial function it is necessary to introduce the functions M_{ou}^2. M_o^1 is the first order moment of measure μ_0, M_{oo}^2 is the second order moment of μ_0 *etc...* .

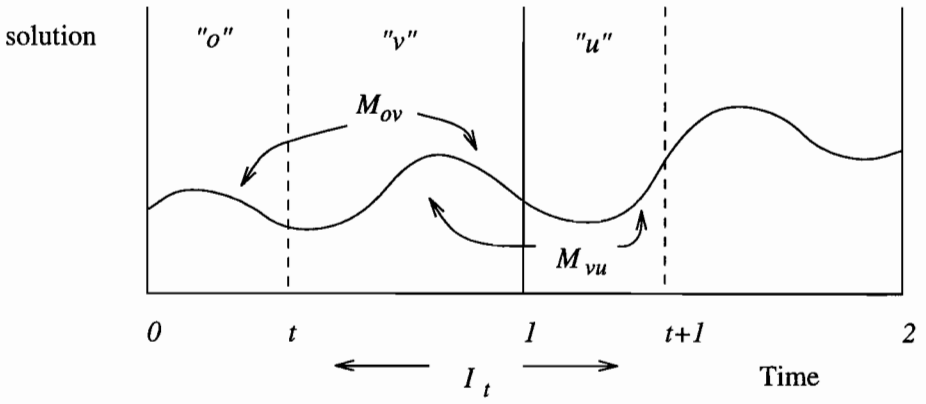

FIGURE 6.1

A DDE transforms a function defined on $[0,1]$ into a function defined on I_t. Illustration of the "o", "v" and "u" segments of the solution.

The moments of the measure $\mathcal{W}_t$ are also given by the power series expansion of the characteristic functional $\mathcal{Z}_t$ as we next discuss.

6.4.1 Taylor series expansion of the functional $\mathcal{Z}_t$

The expression for the series expansion of a functional can be understood with the following argument. Let

$$F(y_1, \cdots, y_k) = F(\mathbf{y})$$

be a function of k variables. The power series expansion of F is

$$F(\mathbf{y}) = \sum_{n=0}^{\infty} \sum_{i_1=0}^{k} \cdots \sum_{i_n=0}^{k} \frac{1}{n!} \mathcal{E}_n(i_1, \cdots, i_n)(y_1, \cdots, y_n), \tag{6.36}$$

where

$$\mathcal{E}_n(i_1, \cdots, i_n) = \left. \frac{\partial^n F(\mathbf{y})}{\partial y_1 \cdots \partial y_n} \right|_{\mathbf{y}=0}.$$

Passing to a continuum in the following sense

$$\begin{aligned} i &\longrightarrow x_i, \\ y_i (i = 1, \cdots, k) &\longrightarrow y(x), \\ -\infty < \quad x \quad &< \infty, \\ \sum_i &\longrightarrow \int_{\mathbb{R}} dx, \end{aligned}$$

we obtain the corresponding series expansion of a *functional* $\mathcal{F}$:

$$\mathcal{F}[y] = \sum_{n=0}^{\infty} \int_{\mathbf{R}^n} dx_1 \cdots dx_n \mathcal{E}_n(x_1, \cdots, x_n) y(x_1) \cdots y(x_n),$$

where

$$\mathcal{E}_n(x_1, \cdots, x_n) = \frac{1}{n!} \frac{\delta^n \mathcal{F}[y]}{\delta y(x_1) \cdots \delta y(x_n)} \bigg|_{y=0}.$$

$\mathcal{F}[y]$ is called the *characteristic functional* of the functions $\mathcal{E}_n$.

With these conventions, the expansion of the characteristic functional (6.24b) is

$$\mathcal{Z}_t[J_1, J_2] = \sum_{p=0}^{\infty} \sum_{q=0}^{p} \int_0^1 \cdots \int_0^1 \mathcal{E}_{pq}(t, x_1, \cdots, x_p) \left(\prod_{j=1}^{q} J_1(x_j)\, dx_j \right) \left(\prod_{j=q+1}^{p} J_2(x_j)\, dx_j \right). \quad (6.37)$$

The kernels $\mathcal{E}_{pq}$ in the expansion are proportional to the moment functions of the measure $\mathcal{W}[v, \mathcal{S}_t v]$. From the relations (6.26) they are given by

$$\begin{aligned} \mathcal{E}_{pq}(t, x_1, \cdots, x_p) = \frac{1}{p!} \frac{\delta^p \mathcal{Z}_t}{\delta J_1^q\, \delta J_2^{p-q}} &= \frac{i^p}{p!} \langle u_v(x_1) \cdots u_v(x_q) v(x_{q+1}) \cdots v(x_p) \rangle \\ &= \frac{i^p}{p!} M^p_{u^q v^{(p-q)}}(t, x_1, \cdots, x_p), \end{aligned} \quad (6.38)$$

where from now on we use the notation $M^p_{u^q v^{(p-q)}}(t, x_1, \cdots, x_p) = M^p_{u^q v^{(p-q)}}(t, \mathbf{x})$. Equation (6.37) is the infinite dimensional generalization of the well known expansion of a characteristic function in terms of the corresponding probability moments (or their Legendre transforms, the cumulants).

6.4.2 PDE's for the moments

The evolution equation of the k^{th} moment is given by substituting the moment in question into (6.30) and then using formula (6.37) to the appropriate order.

Consider the first order moments of the measure $\mathcal{W}_t$. If we substitute the definitions (6.38) and the expansion (6.37) into equation (6.30), we obtain a P.D.E for the moment $M^1(t, x)$:

$$\begin{aligned} \frac{\partial}{\partial t} M^1_v(t, x) &= \frac{\partial}{\partial x} M^1_v(t, x) \quad \text{for } x \in [0, 1-t], \\ \frac{\partial}{\partial t} M^1_u(t, x) &= -\alpha M^1_u(t, x) + \sum_{k=1}^{n} a_k M^k_{o^k}(x + t - 1, .^k., x + t - 1) \\ &\qquad \text{for } x \in (1-t, 1]. \end{aligned} \quad (6.39)$$

Equation (6.39) is simply the Hopf equation (6.30) for the first order moments. In (6.39) the k arguments of $M^k_{o^k}$ indicate that it is the k-point autocorrelation function of the initial function distribution described by μ_0. Moments whose label does not contain u are moments of the initial measure.

The second order moment functions $M^2(t,x)$ are given by the solutions of the four equations:

$$\begin{aligned}
\frac{\partial}{\partial t}M^2_{vv}(t,x,y) &= \frac{\partial}{\partial x}M^2_{vv}(t,x,y)+\frac{\partial}{\partial y}M^2_{vv}(t,x,y) \\
&\qquad \text{for } (x,y)\in[0,1-t)\times[0,1-t), \qquad (6.40)\\
\frac{\partial}{\partial t}M^2_{uv}(t,x,y) &= \frac{\partial}{\partial y}M^2_{uv}(t,x,y)-\alpha M^2_{uv}(t,x,y)+ \\
&\quad +\sum_{k=2}^{n} a_k M^k_{o^{(k-1)}v}(t,x+t-1,\overset{(k-1)}{\dots},x+t-1,y) \\
&\qquad \text{for } (x,y)\in(1-t]\times[0,1-t], \qquad (6.41)\\
\frac{\partial}{\partial t}M^2_{vu}(t,x,y) &= \frac{\partial}{\partial x}M^2_{vu}(t,x,y)-\alpha M^2_{vu}(t,x,y)+ \\
&\quad +\sum_{k=2}^{n} a_k M^k_{vo^{(k-1)}}(t,x,y+t-1,\overset{(k-1)}{\dots},y+t-1) \\
&\qquad \text{for } (x,y)\in[0,1-t]\times(1-t,1], \qquad (6.42)\\
\frac{\partial}{\partial t}M^2_{uu}(t,x,y) &= -2\alpha M^2_{uu}(t,x,y)+ \\
&\quad +\sum_{k=1}^{n} a_k \{\, M^k_{o^{(k-1)}u}(t,x+t-1,\overset{(k-1)}{\dots},x+t-1,y)+ \\
&\quad +M^k_{uo^{(k-1)}}(t,x,y+t-1,\overset{(k-1)}{\dots},y+t-1)\,\}, \\
&\qquad \text{for } (x,y)\in(1-t,1]\times(1-t,1]. \qquad (6.43)
\end{aligned}$$

The functions M^2_{ou} and M^2_{oou} are given by

$$\begin{aligned}
\frac{\partial}{\partial t}M^2_{ou}(t,x,y) &= -\alpha M^2_{ou}+ \\
&\quad +\sum_{k=2}^{n} a_k M^k_{o^k}(x,y+t-1,\overset{k}{\dots},y+t-1), \qquad (6.44)\\
\frac{\partial}{\partial t}M^3_{oou}(t,x,y,z) &= -\alpha M^3_{oou}(t,x,y,z)+ \\
&\quad +\sum_{k=3}^{n} a_k M^k_{o^k}(x,y,z+t-1,\overset{k}{\dots},z+t-1), \qquad (6.45)
\end{aligned}$$

and similar equations give the moments $M^k_{o^{(k-1)}u}$.

A pattern clearly emerges from the preceding analysis: The moment $M^p(t,\mathbf{x})$ is given by 2^p partial differential equations of the same form as (6.41) through (6.43) since $M^p(t,\mathbf{x})$ is a function of p variables, each of which can belong to one of two possible intervals ($[0,1-t]$ or $(1-t,1]$). The first of these equations (when all the x_k's belong to $[0,1-t]$) is

$$\frac{\partial}{\partial t}M^p_{v^p}(t,\mathbf{x}) = \sum_{j=1}^{p}\frac{\partial}{\partial x_j}M^p_{v^p}(t,\mathbf{x}). \tag{6.46}$$

We call the equations which give the moments of the form $M^p_{v^l u^{(p-l)}}$ **mixed** equations because they yield functions which correlate mixed u and v segments of the solution. For the moment of order p, there are (2^p-2) mixed equations and 2 **pure** equations. The pure equations give $M^p_{v^p}$ and $M^p_{u^p}$, the p-point autocorrelation functions of the v and u segments of the solution.

If $x_j \in [0,1-t]$ for $j=1,\cdots,l$ and $x_j \in (1-t,1]$ for $j=l+1,\cdots,p$, then when the forcing term F of equation (6.20a) is the polynomial (6.29), the generic form of the mixed equation for $M_{v^l u^{(p-l)}}$ is

$$\begin{aligned}\frac{\partial}{\partial t}M^p_{v^l\,u^{(p-l)}}(t,\mathbf{x}) &= \sum_{i=1}^{l}\frac{\partial}{\partial x_i}M^p_{v^l\,u^{(p-l)}}(t,\mathbf{x}) - \alpha(p-l)\,M^p_{v^l\,u^{(p-l)}}(t,\mathbf{x}) \\ &\quad + \sum_{j=0}^{n-1} a_j\left\{M^{(p+j)}_{v^l\,o^j\,u^{(p-l)}}(t,\mathbf{x}) + M^{(p+j)}_{v^l\,u^{(p-l)}\,o^j}(t,\mathbf{x})\right\}. \end{aligned}\tag{6.47}$$

Once again, this equation is one representative of the (2^p-2) mixed equations to be solved to obtain the moment of order p. Deriving these equations is tedious, but the task is greatly simplified by the similarity existing between the systems of equations for moments of different orders.

Equation (6.37) presented above is reminiscent of functional expansions in quantum field theory and statistical mechanics which are usually dealt with using Feynman diagrams.

In quantum field theory, Feynman diagrams are used to represent the terms in the expansion of a characteristic functional which describes the distribution of fields (in physics, fields are elements of a function space: they are functions, or *paths* in the phase space.). The evolution equations for these fields are obtained by replacing various Lagrangians in the Euler-Lagrange equations which result from applying the principle of least action [188]. Feynman diagrams are used to represent the moments (or n-point correlation functions) of the distribution of fields. The n^{th} moment of the distribution, (or n-point correlation function) is represented by n diagrams [170]. In our treatment of delayed dynamics, the n^{th} moment can also be represented by graphs. Preliminary studies indicate that a graphical

treatment of (6.37) is possible but we have been unable so far to make significant progress. We leave as an open problem the efficient use of Feynman diagrams for the probabistic description of delayed dynamics.

Before proceeding, we illustrate the ideas presented above and derive the partial differential equations analogous to (6.39) and (6.41) through (6.43) for the nonlinear DDE (6.31) considered in Example 1.

Example 2. When the DDE is

$$\frac{du}{ds} = -\alpha u(s) + ru(s-1) - ru^2(s-1),$$

the first order moment equations are given by

$$\begin{aligned}
\frac{\partial M_v^1(t,x)}{\partial t} &= \frac{\partial M_v^1(t,x)}{\partial x}, \\
\frac{\partial M_u^1(t,x)}{\partial t} &= -\alpha M_u^1(t,x) + rM_o^1(x+t-1) - rM_{oo}^1(x+t-1, x+t-1). \qquad (6.48)
\end{aligned}$$

The four evolution equations for the second order moments are

$$\frac{\partial M_{vv}^2(t,x,y)}{\partial t} = \frac{\partial M_{vv}^2(t,x,y)}{\partial x} + \frac{\partial M_{vv}^2(t,x,y)}{\partial y}, \text{ for } x, y \in [0, 1-t] \qquad (6.49)$$

$$\begin{aligned}
\frac{\partial M_{vu}^2(t,x,y)}{\partial t} &= \frac{\partial M_{vu}^2(t,x,y)}{\partial x} - \alpha M_{vu}^2(t,x,y) + rM_{vo}^2(t,x,y+t-1) \\
&\quad -rM_{voo}^3(t,x,y+t-1,y+t-1), \text{ for } x \in [0,1-t],\ y \in (1-t,1] \qquad (6.50)
\end{aligned}$$

$$\begin{aligned}
\frac{\partial M_{uv}^2(t,x,y)}{\partial t} &= \frac{\partial M_{uv}^2(t,x,y)}{\partial y} - \alpha M_{uv}^2(t,x,y) + rM_{ov}^2(t,x+t-1,y) \\
&\quad -rM_{oov}^3(t,x+t-1,x+t-1,y), \text{ for } x \in (1-t,1],\ y \in [0,1-t] \qquad (6.51)
\end{aligned}$$

$$\begin{aligned}
\frac{\partial M_{uu}^2(t,x,y)}{\partial t} &= -2\alpha M_{uu}^2(t,x,y) + r\left[M_{ou}^2(t,x+t-1,y) + M_{uo}^2(t,x,y+t-1)\right] - \\
&\quad r\left[M_{oou}^3(t,x+t-1,x+t-1,y) + M_{uoo}^3(t,x,y+t-1,y+t-1)\right], \\
&\quad \text{for } x, y \in (1-t,1]. \qquad (6.52)
\end{aligned}$$

To solve these equations, one needs to solve first for the moments M_{ou}^2, M_{uo}^2, and M_{oou}^3 which satisfy equations of the following form

$$\frac{\partial M_{ou}^2(t,x,y)}{\partial t} = -\alpha M_{ou}^2(t,x,y) + \beta M_{oo}^2(t,x,y), \qquad (6.53)$$

$$\begin{aligned}
\frac{\partial M_{oou}^3(t,x,y,z)}{\partial t} &= -\alpha M_{oou}^3(t,x,y,z) + rM_{ooo}^3(x,y,z+t-1) \\
&\quad -rM_{oooo}^4(x,y,z+t-1,z+t-1). \qquad (6.54)
\end{aligned}$$

Hence, the moments can be obtained by successively solving ordinary or hyperbolic partial differential equations. Suppose for illustration that first order moments of the initial measure are real nonnegative constants:

$$M_o^1 = m_1 \tag{6.55}$$

$$M_{oo}^2 = m_2 \tag{6.56}$$

$$M_{ooo}^3 = m_3 \tag{6.57}$$

$$M_{oooo}^4 = m_4. \tag{6.58}$$

First Moment:

For $M_u^1(t,x)$, the evolution equation (6.50) reduces to

$$\frac{\partial M_u^1(t,x)}{\partial t} = -\alpha M_u^1(t,x) + r(m_1 - m_2), \tag{6.59}$$

whose solution is

$$M_u^1(t,x) = \gamma_1 + \left[M_u^1(0,x) - \gamma_1\right] e^{-\alpha t} \quad \text{where } \gamma_1 \equiv \frac{r(m_1 - m_2)}{\alpha}. \tag{6.60}$$

At $t = 0$, from (6.22) and (6.23) we know that $v(1) = u_v(1)$. In addition, $M_o^1(t,x) \equiv M_v^1(t,x)$. Therefore, from (6.34)-(6.35),

$$M_o^1(t=0, x=1) = \int_C v(1) d\mu_0 = \int_C u_v(1) d\mu_0(v) = M_u^1(t=0, x=1)$$

and from the initial condition (6.56) we conclude $M_u^1(t=0,x) = m_1$. Hence

$$M_u^1(t,x) = \gamma_1 + [m_1 - \gamma_1] e^{-\alpha t}. \tag{6.61}$$

Second Moments:

To obtain expressions for M_{uv}^2, M_{vu}^2, M_{uu}^2 we have to solve their respective equations of motion (remember that M_{vv}^2 is given). We first tackle (6.51) (this choice is arbitrary; (6.52) can be dealt with in the same manner):

$$\frac{\partial M_{uv}^2(t,x,y)}{\partial t} = \frac{\partial M_{uv}^2(t,x,y)}{\partial y} - \alpha M_{uv}^2(t,x,y) + r(m_2 - m_3) \tag{6.62}$$

with initial condition $M_{uv}^2(0,x,y) = M_{vv}^2(0,x;y) \equiv m_2$ for all x, y in the domains defined in (6.51). This initial condition is, as for the first moment, obtained from equations (6.34)-(6.35). Equation (6.62) is solved using the method of characteristics, and the solution is

$$M_{uv}^2(t,x,y) = \gamma_2 + [m_2 - \gamma_2] e^{-\alpha t} \quad \text{where } \gamma_2 \equiv \frac{r(m_2 - m_3)}{\alpha}. \tag{6.63}$$

The moment $M^2_{vu}(t,x,y)$ can be obtained in a similar way and the result is

$$M^2_{vu}(t,x,y) = M^2_{uv}(t,x,y). \tag{6.64}$$

This equality is due to the fact that the moments of the initial measure are constant. Finally, it is necessary to solve (6.54) and (6.54) before obtaining M^2_{uu}. Using (6.57)-(6.58),

$$\begin{aligned}
M^2_{ou} &= \gamma_2 + [m_2 + \gamma_2]\, e^{-\alpha t} && (6.65)\\
M^2_{uo} &= \gamma_2 + [m_2 + \gamma_2]\, e^{-\alpha t} && (6.66)\\
M^2_{oou} &= \gamma_3 + [m_3 + \gamma_3]\, e^{-\alpha t} \quad \text{where} \quad \gamma_3 \equiv \frac{r(m_3 - m_4)}{\alpha} && (6.67)\\
M^2_{uoo}(t) &= \gamma_3 + [m_3 + \gamma_3]\, e^{-\alpha t} && (6.68)
\end{aligned}$$

so that (6.52), the evolution equation for M^2_{uu} becomes

$$\frac{\partial M^2_{uu}(t,x,y)}{\partial t} = -2\alpha M^2_{uu}(t,x,y) + 2r\gamma_2 + 2r\gamma_3 + 2re^{\alpha t}\left[m_2 - m_3 + \gamma_2 - \gamma_3\right]. \tag{6.69}$$

The above is a linear first order ODE which can be solved to give

$$M^2_{uu}(t) = \frac{-2re^{-\alpha t}}{3\alpha}\left[m_2 - m_3 + \gamma_2 - \gamma_3\right] - \frac{r}{\alpha}\left[\gamma_2 - \gamma_3\right] + \mathcal{K}e^{2\alpha t}, \tag{6.70}$$

where

$$\mathcal{K} \equiv \frac{2r}{3\alpha}\left(m_2 - m_3 + \frac{1}{2}(\gamma_3 - \gamma_2)\right) + m_2 \quad \bullet$$

This analysis can be carried out in a similar way when the moments are not constants, but such that the equations derived above remain solvable analytically.

6.4.3 Invariant measures

It is of physical interest to investigate the constraint to be satisfied by a measure μ_*, invariant under the action of a differential delay equation. For the nonlinear DDE (6.31), the characteristic functional $\mathcal{Y}$ of such a measure is defined as

$$\mathcal{Y}[J_1] = \int_{\mathcal{C}} \exp\left[i\int_0^1 J_1(x)u_v(x+t)\,dx\right]\, d\mu_*$$

and so we have

$$\mathcal{Y}[J_1] = \mathcal{Z}_t[J_1, 0] \qquad \text{for all } t.$$

where $\mathcal{Z}_t[J_1, J_2]$ is given by (6.24b). The Hopf equation (6.33) becomes

$$\begin{aligned} 0 \;=\; & \int_0^{1-t} J_1(x)\frac{\partial}{\partial x}\left(\frac{\delta \mathcal{Y}}{\delta J_1(x)}\right) dx - \alpha \int_{1-t}^{1} J_1(x)\frac{\delta \mathcal{Y}}{\delta J_1(x)}\, dx \\ & + r\int_{1-t}^{1} J_1(x)\frac{\delta \mathcal{Y}}{\delta J_1(x+t-1)}\, dx - ri^{-1}\int_{1-t}^{1} J_1(x)\frac{\delta^2 \mathcal{Y}}{\delta J_1^2(x+t-1)}\, dx, \quad \text{for all } t. \end{aligned}$$

By choosing $t = 0$, the first integral in the Hopf equation must vanish so that we have,

$$\frac{\partial}{\partial x}\left(\frac{\delta \mathcal{Y}}{\delta J_1(x)}\right) = 0 \quad \text{a.e.}$$

From this relation a **necessary** condition for the invariant measure follows: using (6.38), the moments must satisfy

$$\sum_{k=1}^{n} \frac{\partial}{\partial x_k} M^n_{u^q v^{(n-q)}}(x_1, \cdots, x_k) = 0.$$

6.5 The Hopf equation and the Kramers-Moyal expansion

The treatment of delayed dynamics in this chapter is developed in the spirit of the previous chapters, concerned with dynamics evolving in finite-dimensional spaces. The need for such a treatment presented here arises from the nature of some experimental data available in the biological sciences where large collections of units, whose individual dynamics are given by DDE's, have been considered [46, 48, 47, 148]. For the sake of completeness, it is interesting to formalize the connection between the results presented here, and more usual presentations in finite-dimensional settings.

As illustrated by the rest of this thesis, one of the powerful tools of modern statistical mechanics is the use of equations describing the evolution of densities of initial conditions under the action of a finite dimensional dynamical system. When that system is a set of ODE's the evolution equation is known as the *generalized Liouville equation.* The generalized Liouville equation discussed here does not require the assumption of incompressibility. [When this incompressibility assumption is valid, which is the case when dealing with conservative systems, the *generalized* Liouville equation reduces to the Liouville equation. Therefore, the Liouville equation studied in Hamiltonian mechanics is a special case of a more general equation of evolution for the phase-space densities of dynamical systems.]

When the system is a set of stochastic differential equations perturbed by realizations of a Wiener process, the evolution of densities is given by the *Fokker-Planck equation* [181]. In general, for finite dimensional systems the evolution of densities is governed by the *Kramers-Moyal (K-M) equation.* It is of some interest to understand how the K-M formalism carries over to systems with an infinite number of degrees of freedom such as DDE's.

The Hopf equation is probabilistic in the sense that it describes a set of DDE's in the same way that the Schrödinger equation describes a microscopic physical system (A Schrödinger equation can always be transformed into a Fokker-Planck equation, which is just a truncation of the K-M expansion, but the physical interpretation of the transformation remains unclear [181]). Given that this is precisely the role of the K-M expansion for finite dimensional dynamical systems, it is important to clarify the relation between the functional version of the K-M equation and the Hopf-like equation (6.30) derived here. Our derivation of the functional version of the K-M expansion is inspired by the derivation of the N-dimensional case given by Risken [181].

To make the connection between $\mathcal{Z}_t$ and the K-M expansion more explicit, consider the expansion (6.37) of the characteristic functional $\mathcal{Z}_t$. Using equation (6.38), (6.37) becomes

$$\mathcal{Z}_t[J_1, J_2] = \sum_{p=0}^{\infty} \sum_{q=0}^{p} \int_0^1 \cdots \int_0^1 \frac{i^p}{p!} M^p_{u^q v^{(p-q)}}(t, \mathbf{x}) \left(\prod_{j=1}^{q} J_1(x_j)\, dx_j \right) \left(\prod_{j=q+1}^{p} J_2(x_j)\, dx_j \right). \quad (6.71)$$

Let $\mathcal{P}[G, H|G', H']$ be the transition probability functional that given the pair $(G'(x+t), H'(x+t))$ in $\mathcal{C}\times\mathcal{C}$, with $x \in [0, 1-t]\times(1-t, 1]$ we obtain the pair $(G(x+t+t_*), H(x+t+t_*))$ for $x \in [0, 1-(t+t_*)] \times (1-(t+t_*), 1]$ (*i.e.* G (G') is an initial function which generates a solution H (H')).

$\mathcal{W}[v, \mathcal{S}_{(t+t_*)}v]$ is related to the transition probability functional $\mathcal{P}$ by

$$\mathcal{W}[v, \mathcal{S}_{(t+t_*)}v] = \int_{\mathcal{C}} \mathcal{P}[v, \mathcal{S}_{(t+t_*)}v|v', \mathcal{S}_t v']\mathcal{W}[v', \mathcal{S}_t v']\, d\mu_0(v'). \quad (6.72)$$

In addition, $\mathcal{W}$ is the inverse Fourier transform of the characteristic functional $\mathcal{Z}_t[J_1, J_2]$ introduced in equation (6.24b)

$$\mathcal{W}[v, \mathcal{S}_t v] = \int_{\mathcal{C}} \Upsilon^{-1}\, \mathcal{Z}_t[J_1, J_2]\, d\mathcal{V}[J_1, J_2]. \quad (6.73)$$

Also,

$$\mathcal{Z}_{t+t_*} = \int_{\mathcal{C}} \tilde{\Upsilon}^{-1} \mathcal{P}[v, \mathcal{S}_{(t+t_*)}v|v', \mathcal{S}_t v'] d\mu_0(v'),$$

and therefore,

$$\mathcal{P}[v, \mathcal{S}_{(t+t_*)}v|v', \mathcal{S}_t v'] = \int_{\mathcal{C}} \tilde{\Upsilon} \mathcal{Z}_{t+t_*}[J_1, J_2] d\mathcal{V}[J_1, J_2] \tag{6.74}$$

where

$$\tilde{\Upsilon} = \exp\left\{-i\left[\int_0^1 J_2(x)(v(x) - v'(x))\, dx + \int_0^1 J_1(x)\left(\mathcal{S}_t v'(x) - \mathcal{S}_{(t+t_*)}v(x)\right) dx\right]\right\},$$

and the measure of integration $\mathcal{V}[J_1, J_2]$ is a measure like the one used in the definition (6.24a) of the characteristic functional. More precisely *the measure $\mathcal{W}$ describes the distribution of functions in $\mathcal{C}$ generating pairs $(v, \mathcal{S}_t v)$ under the action of the transformation $\mathcal{T}$ (defined below (6.24a), and the measure $\mathcal{V}[J_1, J_2]$ describes the distribution of functions generating pairs (J_1, J_2) in the same space.* Inserting (6.71) into equation (6.74) we obtain

$$\begin{aligned}\mathcal{P}[v, \mathcal{S}_{(t+t_*)}v|v', \mathcal{S}_t v'] \;=\; & \int_{\mathcal{C}} \tilde{\Upsilon}\left[\sum_{p=0}^{\infty}\sum_{q=0}^{p}\int_0^1 \cdots \int_0^1 \frac{1}{p!} M^p_{u^q v^{(p-q)}}(t + t_*, \mathbf{x})\right. \\ & \left.\times \left(\prod_{j=1}^{q} iJ_1(x_j)\, dx_j\right)\left(\prod_{j=q+1}^{p} iJ_2(x_j)\, dx_j\right)\right] d\mathcal{V}[J_1, J_2]. \end{aligned} \tag{6.75}$$

The Dirac δ functional is a straightforward generalization of the more usual N-dimensional version. It satisfies

$$\int_{\mathcal{C}} \delta[H - G] d\omega = \begin{cases} 1 & \text{if } H = G \text{ almost everywhere} \\ 0 & \text{otherwise,} \end{cases} \tag{6.76}$$

where H and G are elements of $\mathcal{C}$, ω is a measure defined on $\mathcal{C}$ and the result of the integration is a number (not a function). We will use this definition to simplify expansion (6.75). Before doing so, recall the following identity (derived in Appendix 6A):

$$\begin{aligned}&\int_{\mathcal{C}} \left(\prod_{j=1}^{q} iJ_1(x_j)\right)\left(\prod_{j=q+1}^{p} iJ_2(x_j)\right) \tilde{\Upsilon} d\mathcal{V}[J_1, J_2] = \\ &\left(\frac{(-\delta)^p}{\delta u_v(x_1)\cdots\delta u_v(x_q)\delta v(x_{(q+1)})\cdots\delta v(x_p)}\right)\delta[v - v']\delta[\mathcal{S}_{(t+t_*)}v - \mathcal{S}_t v'].\end{aligned} \tag{6.77}$$

Introduce the symbolic differential operator

$$\mathcal{Q}\left(u_v^q, v^{(p-q)}\right) = \frac{(-\delta)^p}{\delta u_v(x_1)\cdots\delta u_v(x_q)\delta v(x_{(q+1)})\cdots\delta v(x_p)}.$$

Using identity (6.77), equation (6.75) reduces to

$$\mathcal{P}[v, \mathcal{S}_{(t+t_*)}v|v', \mathcal{S}_t v'] = \left[\sum_{p=0}^{\infty}\sum_{q=0}^{p}\frac{1}{p!}\int_0^1\cdots\int_0^1 \mathcal{Q}\big(u_v^q, v^{(p-q)}\big)M^p_{u^q v^{(p-q)}}(t+t_*, \mathbf{x})d\mathbf{x}\right] \times\delta[v-v']\,\delta[\mathcal{S}_{(t+t_*)}v - \mathcal{S}_t v']. \tag{6.78}$$

Suppose that the moments $M^p_{u^q v^{(p-q)}}(t+t_*, \mathbf{x})$ can be expanded in a power series about $t_* = 0$:

$$\frac{1}{p!}M^p_{u^q v^{(p-q)}}(t+t_*, \mathbf{x}) = \mathcal{B}^p_{u^q v^{(p-q)}}(t, \mathbf{x})\, t_* + \mathcal{O}(t_*^2) + \cdots. \tag{6.79}$$

Equation (6.78) with expansion (6.79) is inserted in (6.72) to yield

$$\mathcal{W}[v, \mathcal{S}_{(t+t_*)}v] \simeq \int_{\mathcal{C}}\left[\sum_{p=0}^{\infty}\sum_{q=0}^{p}\int_0^1\cdots\int_0^1 \mathcal{Q}\big(u_v^q, v^{(p-q)}\big)\mathcal{B}^p_{u^q v^{(p-q)}}(t, \mathbf{x})t_*\, d\mathbf{x}\right] \times\mathcal{W}[v', \mathcal{S}_t v']\delta[v-v']\,\delta[\mathcal{S}_{(t+t_*)}v - \mathcal{S}_t v']d\mu_0(v') \tag{6.80}$$

where the measure μ_0 is defined on the space of initial functions. Carrying out the functional integration in (74) and dividing by t_* gives

$$\frac{\mathcal{W}[v, \mathcal{S}_{(t+t_*)}v] - \mathcal{W}[v, \mathcal{S}_t v]}{t_*} \simeq \left[\sum_{p=1}^{\infty}\sum_{q=0}^{p}\int_0^1\cdots\int_0^1 \mathcal{Q}\big(u_v^q, v^{(p-q)}\big)\mathcal{B}^p_{u^q v^{(p-q)}}(t, \mathbf{x})d\mathbf{x}\right] \times\mathcal{W}[v, \mathcal{S}_{(t+t_*)}v].$$

Taking the limit $t_* \longrightarrow 0$, we get the **infinite dimensional version of the Kramers-Moyal expansion**:

$$\frac{\partial\mathcal{W}[v, \mathcal{S}_t v]}{\partial t} \simeq \left[\sum_{p=1}^{\infty}\sum_{q=0}^{p}\int_0^1\cdots\int_0^1 \mathcal{Q}\big(u_v^q, v^{(p-q)}\big)\mathcal{B}^p_{u^q v^{(p-q)}}(t, \mathbf{x})d\mathbf{x}\right]\ \mathcal{W}[v, \mathcal{S}_t v]. \tag{6.81}$$

The above analysis is not restricted to delay differential equations of the form (6.20a-6.20b). The only real constraint imposed on the dynamical system under consideration is that its phase-space be a normed set of functions on which probability measures can be defined. Therefore this analysis is also valid for the statistical investigation of partial differential equations. In fact this approach was pioneered by E. Hopf in [79] in which he derived an evolution equation for the characteristic functional describing the solutions of the Navier-Stokes equations statistically.

From (6.80), it is clear that taking the Fourier transform of (6.81) yields the evolution equation for the characteristic functional $\mathcal{Z}_t[J_1, J_2]$. However, in Section 6.3.1, we derived

the Hopf evolution equation (6.30) for $\mathcal{Z}_t[J_1, J_2]$. Thus we conclude that the Hopf equation (6.30) is the Fourier transform of the infinite dimensional extension of the Kramers-Moyal expansion (6.81).

From (6.14), the K-M coefficients are given by solving the partial differential equations presented in Section 6.4.

6.6 Discussion

The introduction of the joint characteristic functional (6.24b) provides a tool for the investigation of differential delay equations from a probabilistic point of view. This approach is meaningful from a physical perspective when dealing with large collections of entities whose dynamics are governed by DDE's. For example, it is well known that certain aspects of neuronal activity can be described with nonlinear DDE's of the type discussed here [143]. In addition physiological evidence suggests that in some cases the functional unit in the brain is not the single neuron, but a collection of neurons. Therefore, it is expected that to analyze physiologically plausible neural networks a probabilistic approach will be more adequate than a purely deterministic one. Moreover, a probabilistic description is clearly needed when the models are formulated as stochastic DDE's. In this case, the characteristic functional (6.24b) is no longer valid, but it can modified in a way similar to that presented in Section 7 of [128] (in the context of stochastic PDE's), and a *three interval generating functional* should then be considered.

As a conclusion, we note that the expansion (6.37) is similar to functional expansions in quantum field theory and statistical mechanics which are treated in a perturbative manner and analyzed with Feynman diagrams. Although the moment PDE's of Section 6.4 might indeed be deduced from a graphical analysis of expansion (6.37), it remains to be seen whether the introduction of proper Feynman diagrams will provide, through graphical manipulations, significant insight into delayed dynamics.

Appendix 6A

Here we derive equation (6.77)

$$\int_{\Xi} \tilde{\Upsilon} \left(\prod_{j=1}^{q} iJ_1(x_j) \right) \left(\prod_{j=q+1}^{p} iJ_2(x_j) \right) d\mathcal{V}[J_1, J_2] = \left(\frac{(-\delta)^p}{\delta u(x_1) \cdots \delta u(x_q) \delta v(x_{(q+1)}) \cdots \delta v(x_p)} \right) \delta[v - v'] \delta[\mathcal{S}_{(t+t_*)} v - \mathcal{S}_t v']. \quad \text{(6A-1)}$$

Recall that the δ functional can be written:

$$\begin{aligned} \delta[G - H] &= \int_{\mathcal{C}} e^{-i \int_0^1 K(r)[G(r) - H(r)]\, dr}\, d\omega, \\ &\equiv \int_{\mathcal{C}} \Upsilon_1\, d\omega \end{aligned} \quad \text{(6A-2)}$$

where the functions H and G, defined on $r \in [0,1]$, are elements of the function space $\mathcal{C}([0,1])$. Functionally differentiating (6A-2) yields

$$\frac{\delta \delta[G - H]}{\delta G} = \int_{\mathcal{C}} (-iK(r))\ \Upsilon_1\, d\omega.$$

More generally,

$$\frac{\delta^q \delta[G - H]}{\delta G(r_1) \cdots \delta G(r_q)} = \int_{\mathcal{C}} (-i)^q \left(\prod_{j=1}^{q} K(r_j) \right) \Upsilon_1\, d\omega. \quad \text{(6A-3)}$$

We can define $\delta[E - F]$, where E and F are elements of $\mathcal{C}[0,1]$, in a fashion analogous to (6A-2):

$$\begin{aligned} \delta[E - F] &= \int_{\mathcal{C}} e^{-i \int_0^1 L(r)[E(r) - F(r)]\, dr}\, d\omega \\ &\equiv \int_{\mathcal{C}} \Upsilon_2\, d\omega. \end{aligned} \quad \text{(6A-4)}$$

From (6A-3), it is clear that if $\delta[G-H]$ is differentiated q times while $\delta[E-F]$ is differentiated $(p-q)$ times, the product of the two quantities will be

$$\begin{aligned} &\frac{\delta^q \delta[G - H]}{\delta G(r_1) \cdots \delta G(r_q)} \times \frac{\delta^{(p-q)} \delta[E - F]}{\delta E(r_{q+1}) \cdots \delta E(r_p)} = \\ &\qquad \frac{\delta^p}{\delta G(r_1) \cdots \delta G(r_q) \delta E(r_{(q+1)}) \cdots \delta E(r_p)} \delta[G - H] \delta[E - F] \\ &= \int_{\Xi} \left(\prod_{j=1}^{q} -iK(r_j)\, dr \right) \left(\prod_{j=q+1}^{p} -iL(r_j) \right) \Upsilon_1\, \Upsilon_2 d\mathcal{V}[J_1, J_2]. \end{aligned} \quad \text{(6A-5)}$$

Replacing $[G-H]$ by $[v-v']$ and $[E-F]$ by $[\mathcal{S}_{(t+t_*)}v-\mathcal{S}_t v']$, identifying the source functions K, L with J_1, J_2, and using the identity $\Upsilon_1\Upsilon_2=\tilde{\Upsilon}$, (6A-5) yields (6.77).

Appendix 6B

The concept of a functional is well known; a functional is a mapping whose arguments are functions and whose values are real numbers. Usually functionals are defined by integrals:

$$\Phi[\lambda] = \int_a^b F[\lambda(r)]\, dr \tag{6B-1}$$

where F is a given function. A variation $\delta\Phi[\lambda]$ of the functional $\Phi[\lambda]$ is defined by:

$$\delta\Phi[\lambda] = \{\Phi[\lambda + \delta\lambda] - \Phi[\lambda]\}$$

where the brackets indicate that we only consider the part of the difference which is linear in $\delta\lambda$, and $\delta\lambda(r)$ is zero everywhere except in a neighbourhood $\Delta(x)$ of some point x lying in the interval $[a, b]$. The **functional derivative** (or **variational** derivative) of the functional $\Phi[\lambda]$ at the point x is defined by

$$\frac{\delta\Phi[\lambda]}{\delta\lambda(x)} = \lim_{\Delta(x)\to 0} \frac{\{\Phi[\lambda + \delta\lambda] - \Phi[\lambda]\}}{\int_{\Delta(x)} \delta\lambda(r)\, dr}.$$

As an example consider the linear functional

$$\Phi[\lambda] = \int_a^b \lambda(r) g(r)\, dr. \tag{6B-2}$$

Its derivative is calculated according to the definition as follows:

$$\Phi[\lambda + \delta\lambda] = \int_a^b \lambda(r) g(r)\, dr + \int_a^b \delta\lambda(r) g(r)\, dr,$$

hence

$$\Phi[\lambda + \delta\lambda] - \Phi[\lambda] = \int_{\Delta(x)} \delta\lambda(r) g(r)\, dr,$$

and we can calculate the functional derivative

$$\frac{\delta\Phi[\lambda]}{\delta\lambda(x)} = \lim_{\Delta\to 0} \frac{\int_{\Delta(x)} \delta\lambda(r) g(r)\, dr}{\int_{\Delta(x)} \delta\lambda(r)\, dr}.$$

If $g(r)$ is continuous, then by virtue of the mean value theorem,

$$\int_{\Delta(x)} \delta\lambda(r) g(r)\, dr = x' \int_{\Delta(x)} \delta\lambda(r)\, dr, \qquad x' \in \Delta(x).$$

Because $x' \to x$ as $\Delta(x) \to 0$, one finally gets, for the functional derivative of (6B-2),

$$\frac{\delta}{\delta\lambda(x)}\left[\int_a^b \lambda(r)g(r)\,dr\right] = g(x).$$

It is possible to define functional derivatives of higher order, in analogy to the finite dimensional situation. In fact, many well known results concerning the differential calculus of finite dimensional objects have analogues in the infinite dimensional case. For a summary of the main results of functional calculus we refer the reader to Sobczyk [197].

Remark. The concept of a functional derivative presented here is a special case of the differentiation of a mapping of a topological space into another. If this space is Banach, then the derivatives can be Fréchet or Gâteaux derivatives. Furthermore, if the mapping under study is a functional whose arguments are elements of the Banach space $\mathcal{C}$, then its Fréchet derivative is the functional derivative defined in this section.

Chapter 7

Conclusion

On peut continuer à tout temps
l'étude, mais non pas l'écolage...

Michel Eyquem de Montaigne, *Essais, II, 28*

The presentation of Chapter 1 concluded with a list of problems which surface repeatedly in the literature dealing with coupled map lattices. These are linked to the absence of a framework within which their statistical properties can be investigated, and therefore to a lack of understanding of the origins of thermodynamic behavior in these systems.

The work presented in Chapters 2, 3 and 4 partially fills this theoretical void. The investigations of Chapter 2 on the simplest possible CML's led us to postulate that the phase transitions observed in larger coupled map systems could be analytically understood by studying the evolution of ensemble probability densities. This evolution is governed by operators, and their spectral characteristics hold the key to the analytical description of coupled map lattices from a statistical point of view. Chapter 3 focuses on the properties of deterministic lattices, and the analysis is presented for simple systems which are piecewise linear. The cornerstone of this approach is a result of Tulcea Ionescu and Marinescu which, loosely speaking, describes the spectral properties of a linear continuous operator by focusing on the behavior a function's norm as it evolves under the action of the operator. This technique yields analytical skeletons of phase diagrams for CML's which have been discussed numerically in the literature (*cf.* Figures 3.16, 3.17 and 3.19). Chapter 4 extends this approach to CML's perturbed by noise. The results obtained in this case are of a general nature, because they are essentially model-independent, and they are in a sense stronger

than those of Chapter 3 because they apply to most CML's likely to be of use in a modeling context (*i.e.* in which the local map is bounded).

Our investigations of CML's lead in a natural fashion to a discussion of related continuous time models, framed as differential delay equations. The strong connection between spatially extended systems and DDE's has been recognized for some time [38, 55, 212, 213], but a number of recent investigations [53, 140, 217] have hinted at the possibility that certain delay differential equations might be studied explicitly by focusing on finite high dimensional coupled map systems. Chapter 5 introduces one reduction from DDE's to CML's, valid for both deterministic and stochastic equations, which allows us to apply the techniques of Chapters 3 and 4 to differential delay equations. This analysis points to the presence of cyclical statistical evolution in these equations (*cf.* Figures 5.4 and 5.5), and provides the first example of such behavior in unforced continuous-time systems. It also calls for experimental verifications of this prediction; we describe below an experimental setup designed for this purpous.

Finally, we conclude the thesis with a rather formal presentation of the "proper" construction of statistical mechanics for the differential delay equations discussed in Chapter 5. The spirit of the approach presented in Chapter 6 is the same as that of the rest of the thesis, but the methods developed are rather dissimilar, because we take the conceptual step from finite dimensional spaces to infinite-dimensional ones. As a result, much of the intuition is lost, and the formalism becomes rather cumbersome. However, this step also permits us to identify some unresolved mathematical problems, whose answers will also be of great use to investigators having to deal with functional integrals in whatever context. For example, some of the current research on the theory of integration with respect to arbitrary functional measures using the methods of nonstandard analysis is motivated by the presence of such integrals in various fields of research, one of which is the probabilistic description of control loops with retarded feedback modeled by DDE's.

The contents of the thesis, summarized above, point to various research avenues, which we now briefly describe.

Further characterization of the statistical cycle

Although asymptotic periodicity, and the presence of phase transitions in arbitrary large coupled map lattices can now be proven rigorously, it is still not possible to give necessary and sufficient conditions on the control parameters of a given model which would locate these transitions unambiguously. In deterministic CML's we give sufficient conditions on

the parameters. This is a significant improvement from the existence results which were available previously [21, 22, 72, 109], but there is room for further determination of the statistical behavior of some of the simpler models.

In addition, we have repeatedly mentioned the unknown (analytical) dependence of the functionals Γ_i in equation (1.21) on the initial ensemble density $\mathbf{f}_0$. This property has intriguing consequences, for it implies that the ensemble behavior of an asymptotically periodic system depends on the initial (out of equilibrium) ensemble considered. Hence the states of thermodynamic equilibria are not unique, and it would be very interesting to understand what the number of possible states of equilibria is (that is the number of density cycles of period r, where r is the number of Γ's in (1.21)) and their relative stability (*i.e.* the size of their basins of attraction).

CML's with an infinite number of elements

One of the original motivations for studying CML's was to increase our understanding of fluid turbulence. The variety of spatial phenomena observed in CML's is staggering, and some systems (such as some of the examples of Figures 3.1, 3.2 and 3.4) display a spatially complex evolution which is reminiscent of developped fluid turbulence. However, spatial chaos is only possible in systems with infinite spatial extension, and so it is of interest to extend at least some of the results presented here to CML's with an infinite number of elements. Keller and Künzle [109] have laid the foundations for such a program by defining the notion of variation for functions of an infinite (but countable) number of variables. However, the techniques presented here are not easily extendable to these situations because of the absence of proper embedding theorems, and their extension to infinite lattices is therefore left as an open problem. We conclude by mentioning that the existing descriptions of infinite lattices do not make use of transfer operator techniques (except [109]), but focus instead on symbolic chains (*cf.* Sections 1.4 and 1.4.4.3) and that the results presented in this thesis might stimulate the search for cyclical density evolutions in such systems using the techniques of the thermodynamic formalism.

Experimental verification of statistical cycling in DDE's

The cycling density behavior discussed in Chapter 5 can be observed numerically (*cf.* Figures 5.4 and 5.5), but it has not yet been described in an experimental setup. However, Prof. Frank Moss (University of Missouri) has completed the design and implementation of a task specific analogue computer to investigate the phenomenon in a model DDE of the

form (5.4). The design of the analogue computer is similar to the one given in [137], and the experimental methods are explicitly described by Moss and McClintock in reference to the analogue simulation of ordinary differential equations [157]. Preliminary results indicate that the tell-tale features of asymptotic periodicity (dependence of the asymptotic cycle on the initial density, change of the period as parameters are varied) are all observed experimentally. These unpublished results are promising because they provide the first experimental evidence of statistical cycling in an unforced, continuous-time autonomous physical system. One of the areas of physics in which delay differential equations arise quite frequently is nonlinear optics, and more specifically the study of resonnant cavities filled with nonlinear media. It is therefore no surprise that continuous time statistical cycling is also expected in these systems.

Statistical cycling in nonlinear optics

This short discussion is based on a review paper by Lange which describes in some detail the phenomenon of noise-induced transient bimodality in nonlinear optical resonnators. [120]. We now describe this experiment schematically, and conclude with admittedly speculative remarks based on intuition rather than experience with optically bistable devices.

The quantity measured in the experiment described by Lange [*ibid.*] is the output intensity of light transmitted by a nonlinear resonnator which is driven by a Dye laser. When the input is switched from a low level to a sufficiently higher one, the output intensity also changes. If the experiments are performed a large number of times, the density of output intensities is seen to change rather abruptly, some time after the step increase of the input light intensity. In the absence of noise, these densities are unimodal, and centered around one of the two bistable attractors. In the presence of noisy fluctuations in the input light levels, the densities are bimodal, with peaks centered around each of the two levels for a transient time until the switch from one output level to the other is completed. Hence in the experiments described by Lange, there is no periodic cycling in the densities because there is no periodic input. We conjecture that periodic cycles in the densities will be observed if the input light intensities are modulated periodically. This observation might seem trivial, but our theoretical description of asymptotic stability implies that the *statistical* properties of a set of experiments will then depend on the distribution of initial conditions. Such dependence is counterintuitive, and can lead to the erroneous conclusion that experimentally observed differences in the ensemble statistics are due to some intrinsic drift in the parameters of the system under consideration, when they are in fact due to a little known, but

fascinating dynamical property known as asymptotic periodicity.

Appendices

A Computer codes

Because of space limitations, most of the computer code developed to obtain the various numerical (and symbolic, using MAPLE) results presented in the thesis cannot be included here. For the sake of completeness, we do include the CML approximation to a differential delay equation used in Chapter 5 (mainly because the code is much shorter than the programs for Chapter 3, and because the "engine" is the same whether the model is a CML or a DDE.

```
/* this program simulates the evolution of
   an ensemble of differential delay equations, approximated by a coupled
   Map lattice, via the Euler approximation of the derivative.
   The state of the equation at any given time is the state
   of a ring of coupled maps at that time.
   Can compute the collapsed densities of the activity of the ring,
   and/or the temporal correlation function at the desired site.

   The feedback functions
   are contained in the functions "mapq,h,m etc..", The connections are
   contained, along with the boundary conditions
   in "iterate". The functions "get_pard" and "get_pari" are used for the
   I/O for this program (they allow the user not to have to specify all parameters
   everytime the program is run).

   The original DDE is:
         dx/dt = -ax(t)+F(x(t-tau))

   and the map is
         x^i_t = (ab+1)^{-1}*x^{i-1}_t+bF(x^{i-1}_{t-1})
   with appropriate boundary conditions and b = 1/N, N is the number of maps.

*/


/*****************************************************/
```

```
#include <stdio.h>
#include <stdlib.h>
#include <math.h>
#include "ddepars.h"


double latto[WIDTH];
double lattn[WIDTH];
double intermed[WIDTH];

int counter;


main()
{
  int x,z,zz,Index,en_num,t,time,length,czort,other,u,k,bufc,buffer_sampled;
  int time1,time2,time3,time4,time5,time6,time7,time8,time9,time10;
  double average,autocor,square,tcor[1000],tcor_buf[1000],xcor_buf[1000];
  double BGE[1000],dumbg;
  int enbinplot[150][10][3];
  double  initialv,activ_for_bin[22500][10][3];
  int ens_counter,ens_size,num_of_buf;

  FILE *para;   FILE *ini;
  FILE *tc;     FILE *bg;
  FILE *acti;   FILE *sol;
  FILE *ens1;   FILE *ens2;
  FILE *ens3;

  tc=fopen("ddetcor.dat", "w");   bg=fopen("ddeBGentropy.dat", "w");
  acti=fopen("ddeactiv.dat", "w");  para=fopen("ddedenpar.dat", "r");
  ini=fopen("ddecodensini.dat", "r");  sol=fopen("solution.dat", "w");
  ens1=fopen("noise1.0.4.dat", "w");  ens2=fopen("noise2.0.4.dat", "w");
  ens3=fopen("noise3.0.4.dat", "w");

    fscanf(para, "%d", &choice);    fscanf(para, "%d", &inichoice);
    fscanf(para, "%d", &duration);     fscanf(para, "%d", &tran);
    fscanf(para, "%d", &tcorchoice);     fscanf(para, "%d", &pikx);
    fscanf(para, "%d", &storechoice);    fscanf(para, "%d", &codenchoice);
```

```
   fscanf(para, "%d", &ens_size);    fscanf(para, "%d", &num_of_colde);
   fscanf(para, "%d", &bgchoice);    fscanf(para, "%lf", &r);
   fscanf(para, "%lf", &beta)    fscanf(para, "%lf", &epsilon);
   fscanf(para, "%lf", &co);    fscanf(para, "%lf", &alpha);
   fscanf(para, "%lf", &inileft);    fscanf(para, "%lf", &iniright);
   fscanf(para, "%d", &seedchoice);    fscanf(para, "%d", &keepchoice);

 fclose(para);

/****The following statements constitute the I/O for the program*******/

 printf("Choose F: Tent (1), quadratic (2), Keener (3): [%d] ", choice);
      choice = get_pari(choice);
 printf("Do you want the initial function to be a constant (0), the final one of the
previous run (1), or a random function (use this in this version) (2) [%d] ", inicho
      inichoice=get_pari(inichoice);
 printf("How many time delays should this simulation last (please use an even integ
[%d] ", duration);
      duration = get_pari(duration);
 printf("How many time delays should be discarded as transients (please use an even
integer)? [%d] ", tran);
      tran = get_pari(tran);
 printf("Do you want to store the activity at one time in each buffer of the last si
of the ensemble(1 for yes, 0 for no)? [%d] ", tcorchoice);
      tcorchoice=get_pari(tcorchoice);
 if(tcorchoice == 1){
      printf("Enter that time (must be an integer in [0,%d]): [%d] ", WIDTH, pikx);
           pikx=get_pari(pikx);}
 printf("Do you want to store x(t), the solution of the last DDE in the ensemble? (1
[%d] ", storechoice);
 storechoice=get_pari(storechoice);

 printf("Do you want to compute ensemble-sample densities (1 for yes, 0 for no)? [%
", codenchoice);
      codenchoice=get_pari(codenchoice);
 printf("Enter number of elements in the ensemble (make sure enbinnum is OK): [%d]
", ens_size);
      ens_size=get_pari(ens_size);
 if(codenchoice == 1){

     printf("Do you want to compute their BG entropy? (1 for yes, 0 for no)? [%d] ", b
```

```
            bgchoice=get_pari(bgchoice);
        printf("This simulation is done on an ensemble of %d elements, so\n", ens_size);
        printf("we use %d bins for the collapsed density.\n", enbinnum);}
  if (choice == 1){
        printf("Enter the value of a for the tent: [%f] ", r);
        r = get_pard(r);
        }
  else if (choice == 2){
        printf("Enter the value of L for the quadratic nonlinearity s(x)=Lx(1-x): [%f
", r);
        r = get_pard(r);}
  else if (choice == 3){
        printf("Enter the value of r for the function s(x)=(rx +b) mod1: [%f] ", r);
        r = get_pard(r);
        printf("Enter the value of b for the same function: [%f] ", beta);
        beta = get_pard(beta);}
  else if (choice == 4){
        printf("Enter the value of c for the Mori function: [%f] ", r);
        r = get_pard(r);}

        printf("Enter alpha, the decay rate in the DDE: [%f] ", alpha);
         alpha=get_pard(alpha);
     if(inichoice == 0){
      printf("Enter the value of the initial function: [%f] ", co);
        co=get_pard(co);}
  if(inichoice == 2){
     printf("Lower bound of the support of the random initial functions (on [0,1])? [
", inileft);
        inileft=get_pard(inileft);
     printf("Upper bound of the support of the random initial functions (on [0,1])? [
", iniright);
        iniright=get_pard(iniright);
     printf("Enter the seed used to get the initial function (must be an integer): [%
", seedchoice);
        seedchoice=get_pari(seedchoice);}
/*  printf("Do you want to store the solution in the last delay for later use as an initial funct
  printf("Enter 1 for yes, 0 for no: [%d] ", keepchoice);
        keepchoice=get_pari(keepchoice);  */

    para=fopen("ddedenpar.dat", "w");
        fprintf(para, "%d\n", choice); fprintf(para, "%d\n", inichoice);
```

```
        fprintf(para, "%d\n", duration);
        fprintf(para, "%d\n", tran);  fprintf(para, "%d\n", tcorchoice);
        fprintf(para, "%d\n", pikx);
        fprintf(para, "%d\n", storechoice); fprintf(para, "%d\n", codenchoice);
        fprintf(para, "%d\n", ens_size);   fprintf(para, "%d\n", num_of_colde);
        fprintf(para, "%d\n", bgchoice);     fprintf(para, "%f\n", r);
        fprintf(para, "%f\n", beta);         fprintf(para, "%f\n", epsilon);
        fprintf(para, "%f\n", co);           fprintf(para, "%f\n", alpha);
        fprintf(para, "%f\n", inileft);      fprintf(para, "%f\n", iniright);
        fprintf(para, "%d\n", seedchoice);   fprintf(para, "%d\n", keepchoice);

 fclose(para);



 time1=0;    time2=100;
 time3=200;  time4=300;
 time5=400;  time6=500;
 time7=600;  time8=700;
 time9=800;  time10=900;
 buffer_sampled=0;   num_of_buf=3;

 srand48(seedchoice);  /*initializes the random generator drand48() */
 ens_counter=0;

    z=0;
    zz=0;

/* START ENSEMBLE LOOP */
 for(ens_counter=0; ens_counter < ens_size; ens_counter++){

    x=0;
 counter=0;
 Index=0;

 /*used for plotting collapsed densities in the proper format for plt*/
  z=0;
  zz=0;
  delta =0.001;    /*delta must be 1/WIDTH, otherwise the CML doesn't approximate the
DDE !!!*/
  t=0;
```

```
    buffer_sampled =0;

/***We can now go through the integration of the CML for as long as specified by the user*

/*********Specify the initial density: It is a linear transformation of a
random variableuniformly distributed on [0,1].                              */

   if (counter == 0){

    if(inichoice == 0){
      Index=0;

   for(x≥0; x<WIDTH; x++){
    Index=Index+1;
    initialv=co;
    if ( inichoice == 0){
      latto[x]=initialv;}
    else if (inichoice == 1){
      fscanf(ini, "%lf", &latto[x]);}
   }

   x=0;}
    else if (inichoice > 0){
     Index=0;
   for(x≥0; x<WIDTH; x++){
    Index=Index+1;
    initialv=drand48();
    initialv=(iniright−inileft)*initialv + inileft;
        if(ens_counter>18000){
        initialv=(0.1)*drand48() + 0.65;}
    if ( inichoice == 2)
      latto[x]=initialv;
    else if (inichoice == 1)
      fscanf(ini, "%lf", &latto[x]);
         }
    x=0;
    }
   }

/*********************************************************/
/**This stage makes the "old" lattice, the "new" one of the previous time step*/
```

```
    if (counter ≥ 1){
     for(x≥0; x <WIDTH; x++){
       latto[x]=lattn[x];
     }
    x=0;
   }

/*****************************************************/
/**The following lines store the activity for the ensemble stats. (Brutish way)**/
 if(counter ≥ duration−num_of_buf){
 if(codenchoice == 1){
              activ_for_bin[ens_counter][0][buffer_sampled] = (latto[time1]−0.4)*4;
              activ_for_bin[ens_counter][1][buffer_sampled] = (latto[time2]−0.4)*4;
              activ_for_bin[ens_counter][2][buffer_sampled] = (latto[time3]−0.4)*4;
              activ_for_bin[ens_counter][3][buffer_sampled] = (latto[time4]−0.4)*4;
              activ_for_bin[ens_counter][4][buffer_sampled] = (latto[time5]−0.4)*4;
              activ_for_bin[ens_counter][5][buffer_sampled] = (latto[time6]−0.4)*4;
              activ_for_bin[ens_counter][6][buffer_sampled] = (latto[time7]−0.4)*4;
              activ_for_bin[ens_counter][7][buffer_sampled] = (latto[time8]−0.4)*4;
              activ_for_bin[ens_counter][8][buffer_sampled] = (latto[time9]−0.4)*4;
              activ_for_bin[ens_counter][9][buffer_sampled] = (latto[time10]−0.4)*4;

        buffer_sampled = buffer_sampled+1;

 }
}



/**  Store the temporal activity at one chosen site: pikx  **/
   if(ens_counter == ens_size−1){
    if(tcorchoice == 1){
      if (counter ≥ tran){
        tcor_buf[t]=latto[pikx];
        fprintf(acti, "%f\n", latto[pikx]);
        t=t+1;} }}

/*****************************************************/
/**** The next loop iterates the activity at each site of the CML. This creates the "new" la

   Index=0;
```

```
    for(x=0; x <WIDTH; x++){
        Index=Index+1;
    iterate(x);
        if(counter ≥ tran && storechoice == 1 && ens_counter == ens_size−1){
        fprintf(sol, "%f\n", latto[x]);}
     }
    x=0;

}

/**********end of the temporal iteration loop ***************/
}

/*******Calculation of the temporal correlation function at site pikx****/
  if(tcorchoice == 1){
     z=0;
     length = (duration−tran)/2;
     autocor=0;
     average=0;
     for(z≥0; z<length; z++){
          average=average+tcor_buf[z];}
          average=average/length;

     z=0;
     time=0;
     czort=0;
     square=0;
     for(time≥0; time < length; time++){
      czort=length−time;
      autocor=0;

      for(z ≥ 0; z < czort; z++){
                other=z+time;
                square = (tcor_buf[z]−average)*(tcor_buf[other]−average);
                autocor = autocor+square;
                if ( z == czort−1){
                    tcor[time] = autocor/czort;
                    tcor[time]=tcor[time]/tcor[0];
                    fprintf(tc, "%d\t%f\n", time, tcor[time]);
                  }
                 }
```

```
                z=0;
              }
    }

if (inichoice == 0){
printf("N.B. The initial density was supported uniformly on [%3.2f,%3.2f] for this
run.\n", inileft, iniright);}

if (keepchoice == 1){
    ini=fopen("ddecodensini.dat", "w");
    x=0;

    for(x≥0; x< WIDTH; x++){
            fprintf(ini, "%f\n", latto[x]);

    }
  }
    x=0;
    z=0;


/*******Calculation of the ensemble densities at 4 different times, for ens_size functions****

     if(codenchoice == 1){
            x=0;
            z=0;
            k=0;
/*****k is the number of samples within one buffer ********/
            bufc =0;
            for(bufc=0; bufc < 3; bufc++){
             for(k=0; k<10; k++){
              for (x=0; x<ens_size;x++){
                  z=floor(activ_for_bin[x][k][bufc]*enbinnum);
                  enbinplot[z][k][bufc]=enbinplot[z][k][bufc]+1;}}}
        x=0;
        z=0;
        k=0;

        for(z≥0; z<enbinnum; z++){
```

```
                fprintf(ens1, "%d %d %d %d %d %d %d %d %d %d\n", z, enbinplot[z][0][0], enbin-
plot[z][1][0], enbinplot[z][2][0], enbinplot[z][3][0], enbinplot[z][4][0], enbinplot[z][5][0], enbinplo
enbinplot[z][7][0], enbinplot[z][8][0], enbinplot[z][9][0]);
        }
  x=0;
  z=0;
        for(z≥0; z<enbinnum; z++){
                fprintf(ens2, "%d %d %d %d %d %d %d %d %d %d\n", z, enbinplot[z][0][1], enbin-
plot[z][1][1], enbinplot[z][2][1], enbinplot[z][3][1], enbinplot[z][4][1], enbinplot[z][5][1], enbinplo
enbinplot[z][7][1], enbinplot[z][8][1], enbinplot[z][9][1]);
        }
  x=0;
  z=0;
        for(z≥0; z<enbinnum; z++){
                fprintf(ens3, "%d %d %d %d %d %d %d %d %d %d\n", z, enbinplot[z][0][2], enbin-
plot[z][1][2], enbinplot[z][2][2], enbinplot[z][3][2], enbinplot[z][4][2], enbinplot[z][5][2], enbinplo
enbinplot[z][7][2], enbinplot[z][8][2], enbinplot[z][9][2]);
        }
  x=0;
  z=0;
       }

printf("Done\n");
/***End of main***/



}



/**********************FUNCTIONS FOLLOW***************/

/********The hat map*************/

double maph(i)
    int i;
{

 if(latto[i] ≤ 0.5)
    intermed[i]=delta*r*latto[i];
```

```
  else if (latto[i] > 0.5)
     intermed[i]=delta*r*(1-latto[i]);

  return(intermed[i]);

}
/********The quadratic map********/
double mapq(i)
     int i;
{
  intermed[i]=delta*r*(latto[i]*(1-latto[i]));

  return(intermed[i]);

}

/********The Keener map********/
double mapk(i)
     int i;
{
  double noise;

/****Include some multiple of noise in the intermed line if you
want to put noise in the equation (i.e the CML) *********/
  noise=drand48();

  intermed[i]=alpha*delta*(r*latto[i]+beta-floor(r*latto[i]+beta));

  return(intermed[i]);

}



/**********The ryadic map**********/

double mapr(i)
     int i;
{
  intermed[i]=r*latto[i]+beta+(drand48()*0.4)-floor(r*latto[i]+beta+(drand48()*0.4));
```

```
  return(intermed[i]);

}

/**********The Mori map**********/

double mapm(i)
    int i;
{

  if (latto[i] ≤ r)
    intermed[i]=((1−r)/r)∗latto[i]+r;
  else if(latto[i] > r)
    intermed[i]=(1/(1−r))−(1/(1−r))∗latto[i];

  return(intermed[i]);

}

double iterate(i)
    int i;
{
  int l;

  l= WIDTH−1;



/**************The following is for the hat map*********/
  if (choice == 1){
    if (i == 0 ){
       lattn[i] = (1/(alpha∗delta+1))∗(latto[l]+maph(i));}
    else if (i == l){
        lattn[i] = (1/(alpha∗delta+1))∗(lattn[i−1]+maph(i−1));}
    else if (i > 0 && i < l){
       lattn[i] = (1/(alpha∗delta+1))∗(lattn[i−1]+maph(i));}

}

/***********The following is for the quadratic map**********/
```

```
if (choice == 2){
    if (i == 0 ){
       lattn[i] = (1/(alpha*delta+1))*(latto[l]+mapq(i));}
    else if (i == l){
        lattn[i] = (1/(alpha*delta+1))*(lattn[i-1]+mapq(i-1));}
    else if (i > 0 && i < l){
       lattn[i] = (1/(alpha*delta+1))*(lattn[i-1]+mapq(i));}

}

/********The following is for the Keener map**************/

if (choice == 3){
    if (i == 0 ){
       lattn[i] = (1/(alpha*delta+1))*(latto[l]+mapk(i));}
    else if (i == l){
        lattn[i] = (1/(alpha*delta+1))*(lattn[i-1]+mapk(i-1));}
    else if (i > 0 && i < l){
       lattn[i] = (1/(alpha*delta+1))*(lattn[i-1]+mapk(i));}

}

  return(lattn[i]);



}
/* The following functions are used in the I/O.  */

double get_pard(par)
double par;
{
   double par1;
   char str[20];
    gets(str);
    if (sscanf(str,"%lf",&par1) == 1) par = par1;

   return(par);

}
```

```
int get_pari(par)
int par;
{
    int par1;
    char str[20];
     gets(str);
     if (sscanf(str,"%d",&par1) == 1) par = par1;

    return(par);

}
```

B Author's contributions to the manuscripts

1. J. Losson and M. C. Mackey, The thermodynamics of coupled map lattices. In S. Verduyn-Lunel, editor *Dynamical Systems and their Applications in Science*, Elsevier, Amsterdam (1995).

1. Review of the literature on coupled map lattices.
2. Description of lattice thermodynamics.
4. Discussion of the "violations" of the law of large numbers.

2. J. Losson and M. C. Mackey, Coupling induced statistical cycling in two diffusively coupled maps, *Physica D* **72**:324-342 (1994)

1. Numerical Simulations (and development of the code in C and MAPLE).
2. Geometrical investigation of the coupled tent maps.
3. Theory.

3. J. Losson and M. C. Mackey, Statistical cycling coupled map lattices, *Phys. Rev. E* **50**:843-856 (1994)

1. Numerical simulations (and again, development of the code in C and MAPLE).
2. Introduction of functions of bounded variation to examine the properties of tent map CML's.
3. Derivation of the phase diagram for tent map lattices.

4. J. Losson, J. G. Milton and M. C. Mackey, Phase transitions in networks of chaotic elements with short and long range interactions, *Physica D* in press (1994)

1. Numerics (as above).
2. Derivation of the conditions for asymptotic periodicity for the iterates of the tent map CML.
3. Derivation of the phase diagrams for the globally coupled lattices.
4. Introduction and analysis of the piecewise linear model of Section 3.7

5. J. Losson and M. C. Mackey, The evolution of probability densities in stochastic coupled map lattices. Submitted to *Phys. Rev. E* (July 1994).

1. Numerical simulations as above.
2. Derivation of the transfer operator for CML's in the presence of multiplicative noise.

3. Proof of the constrictiveness of the operator associated with the additive noise case for a CML defined on $[0,1]^N$.

4. Proof of Theorem 2 of Chapter 4, and of constrictiveness in the multiplicative noise case if the local map is bounded.

6. J. Losson and M. C. Mackey, Coupled map lattices as models of delay differential equations. Submitted to *Phys. Rev. E* (August 1994).

1. Literature review.
2. Numerics.
3. Reduction of the DDE's to CML's.
4. Derivation of the analytical results.

7. J. Losson and M. C. Mackey, Hopf-like equation and perturbation theory for delay differential equations, *J. Stat. Phys.* **69**:1025-1046.

1. Perturbation expansion of the characteristic functional.
2. Solution of the moment equations.
3. Explanation of the connection with the Kramers-Moyal equation.

Bibliography

[1] S. Albeverio, J. E. Fenstad, R. Høeghn-Krohn, and T. L. Linstrøm. *Nonstandard methods in stochastic analysis and mathematical physics.* Academic Press, New York, 1986.

[2] P. Alstrøm and D.Stassinopoulos. Spatiotemporal intermittency in coupled maps. In T. Riste and D. Sherrington, editors, *Spontaneous formation of space-time structures and criticality*, page 313. Kluwer Academic, 1991.

[3] R.E. Amritkar, P.M. Gade, A.D. Gangal, and V.M. Nandkumaran. Stability of periodic orbits of coupled map lattices. *Phys. Rev. Lett.*, **44**:3407–3410, 1991.

[4] P. Andersen and S. A. Andersson. *Physiological basis of the* alpha *rhythm.* Appleton Century Crofts, New York, 1968.

[5] I. Aranson, D. Golomb, and H. Sompolinski. Spatial coherence and temporal chaos in macroscopic systems with asymmetrical coupling. *Phys. Rev. Lett.*, **68**:3495–3498, 1992.

[6] R. Badii. Conservation laws and thermodynamics formalism for dissipative dynamical systems. *Riv. Nuovo Cimento*, **12**:1–72, 1989.

[7] D. Barkley. A model for fast computer simulation of waves in excitable media. *Physica D*, **49**:61–70, 1991.

[8] C. Beck and F. Schlögl. *Thermodynamics of Chaotic Systems.* Cambridge University Press, Cambridge, 1993.

[9] J. R. Beddington. Age distribution and the stability of simple discrete time population models. *J. Theor. Biol.*, **47**:65–74, 1974.

[10] J. Bélair and M. C. Mackey. Consummer memory and price fluctuations in commodity markets: An integro-differential model. *J. Dynam. Diff. Eq.*, **1**:299–325, 1989.

[11] Bellman and Kalaba. *Mathematical trends in control theory.* Dover, New York, 1964.

[12] L. Biferale, A. Crisanti, M. Falcioni, and A. Vulpiani. One-dimensional asymmetrically coupled maps with defects. *J. Phys. A*, **26**:L923–L928, 1993.

[13] P. M. Binder and V. Privman. Collective behavior in one-dimensional locally coupled map lattices. *J. Phys. A: Math. Gen*, **25**:l775–L780, 1992.

[14] S. P. Blythe, R. M. Nisbet, and W. S. Gurney. The dynamics of population models with distributed maturation period. *Theor. Pop. Biol.*, **25**:289–311, 1984.

[15] V. Boffi and R. Scozzafava. A first order linear differential-difference equation with n delays. *J. Math. Anal. Appl.*, **17**:577–601, 1967.

[16] R. Bowen. *Equilibrium states and the ergodic theory of Anosov diffeomorphisms.* Springer, New York, 1975. Lecture notes in mathematics **470**.

[17] A. Boyarsky and M. Scarowsky. On a class of transformation which have unique absolutely continuous invariant measures. *Trans. Amer. Math. Soc.*, **255**:243–262, 1979.

[18] I. N. Bronshteyn and K. A. Semendyayev. *Handbook of mathematics.* Van Nostrand, New York, 1978. *cf.* the discussion of Section 5.1.5 which describes in some detail the various forms of the law of large numbers.

[19] M. J. Brooks and B. K. P. Horn. Shape and source from shading. In *Proc. Int. Joint Conf. Artificial Intel.*, pages 932–936, 1985.

[20] M. J. Brooks and B. K. P. Horn. *Shape from shading.* MIT Press, Cambridge, MA, 1989.

[21] L. A. Bunimovich and Ya G. Sinai. Spacetime chaos in coupled map lattices. *Nonlinearity*, **1**:491–516, 1988.

[22] L. A. Bunimovich and Ya. G. Sinai. Statistical mechanics of coupled map lattices. In K. Kaneko, editor, *Theory and applications of coupled map lattices*, pages 169–189. J. Wiley & Sons, 1993.

[23] E. R. Caianiello. Outline of a theory of thought processes and thinking machines. *J. Theor. Biol.*, **2**:204–235, 1961.

[24] M. Capiński. Hopf equation for some nonlinear differential delay equation and invariant measures for corresponding dynamical system. *Universitatis Jagellonicae Acta Mathematica, Fasciculus XXVIII*:171, 1991.

[25] M. Capiński. Private communication.

[26] F. Chapeau-Blondeau and G. Chauvet. Stable, oscillatory, and chaotic regimes in the dynamics of small neural networks with delay. *Neural Networks*, **5**:735–743, 1992.

[27] H. Chaté and P. Manneville. Transition to turbulence *via* spatiotemporal intermittency. *Phys. Rev. Lett.*, **58**:112–115, 1987.

[28] H. Chaté and P. Manneville. Spatio-temporal intermittency in coupled map lattices. *Physica D*, **32**:409–422, 1988.

[29] H. Chaté and P. Manneville. Structure of clusters generated by spatiotemporal intermittency and directed percolation in two space dimensions. *Phys. Rev. A*, **38**:4351–4354, 1988.

[30] H. Chaté and P. Manneville. Evidence of collective behavior in cellular automata. *Europhys. Lett.*, **14**:409–413, 1991.

[31] H. Chaté and P. Manneville. Collective behaviors in spatially extended systems with local interactions and synchronous updating. *Prog. Theor. Phys.*, **87**:1–60, 1992.

[32] H. Chaté and P. Manneville. Emergence of effective low dimensional dynamics in the macroscopic behavior of coupled map lattices. *Europhys. Lett.*, **17**:291–296, 1992.

[33] C. Clark. *Mathematical bioeconomics: The Optimal management of Renewable Resources.* John Wiley & Sons, Toronto, 1976. *cf. pages* 230-232.

[34] G. Cocho and G. Martínez-Mekler. On a coupled map lattice formulation of the evolution of genetic sequences. *Physica D*, **51**:119–130, 1991.

[35] G. Cocho, A. Gelover Santiago, and G. Martínez-Mekler. An interplay between local and global dynamics in biological networks: The case of genetic sequences. In N. Boccara, E. Goles, S. Martínez, and P. Picco, editors, *NATO ASI Series C (Vol. 396): Cellular Automata and Cooperative Systems*, pages 85–100. Kluwer, 1993.

[36] G. Cocho, A. Gelover Santiago, G. Martínez-Mekler, and A. Rodin. Nonlinear modeling of the AIDS virus genetic sequence evolution. *Int. J. Modern Phys. C*, **5**:321–324, 1994.

[37] W. Cochran. *The dynamics of atoms in crystals.* Crane Russak, NY, 1973.

[38] K. Cooke and D. W. Krumme. Differential-difference equations and nonlinear initial-boundary value problems for linear hyperbolic partial differential equations. *J. Math. Anal. Appl.*, **24**:372–387, 1968.

[39] M. G. Cosenza and R. Kapral. Coupled maps on fractal lattices. *Phys. Rev. A.*, **46**:1850–1858, 1992.

[40] M. G. Cosenza and R. Kapral. Spatiotemporal intermittency on fractal lattices. *CHAOS*, **4**:99–104, 1994.

[41] M.C. Cross and P.C. Hohenberg. Pattern formation outside of equilibrium. *Rev. Mod. Phys.*, **65**:851–1086, 1993. We refer specifically to Section VII-D (pp 950-953) of the review.

[42] J. P. Crutchfield and K. Kaneko. Phenomenology of spatio-temporal chaos. In H. Bai-lin, editor, *Directions in Chaos*, Singapore, 1986. World Scientific.

[43] R. J. Deissler. One dimensional strings, random fluctuations and complex chaotic structures. *Phys. Lett. A*, **100**:451–454, 1984.

[44] R. J. Deissler. Spatially growing waves, intermittency and convective chaos in an open-flow system. *Physica D*, **25**:233–260, 1987.

[45] E. D. Denman. Coupled mode theory. *J. Math. Anal. Appl.*, **21**:242–248, 1968.

[46] A. Destexhe. *Aspect nonlinéaire de l'activité rythmique du cerveau.* PhD thesis, Universié Libre de Bruxelles, March 1992.

[47] A. Destexhe. Oscillations, complex spatiotemporal behavior and information transport in networks of excitatory and inhibitory neurons, 1994. Submitted to Phy. Rev. E.

[48] A. Destexhe. Stability of periodic oscillations in a network of neurons with time-delay, 1994. Submitted to Phys. Lett. A.

[49] E. J. Ding and Y. N. Lu. Universal scaling behavior in the weakly coupled map lattice. *Phys. Lett. A*, **161**:357–359, 1992.

[50] K. Kaneko (Editor), editor. *Theory and applications of coupled map lattices.* John Wiley & Sons, New York, 1993.

[51] M. Eigen and P. Schuster. *The hypercycle.* Springer Verlag, Berlin, 1979.

[52] W. K. Ergen. Kinetics of the circulating fuel nuclear reactor. *J. Appl. Phys.*, **25**:702–711, 1954.

[53] S. A. Ershov. Asymptotic theory of multidimensional chaos. *J. Stat. Phys.*, **69**:781–812, 1992.

[54] L. Fabiny and K. Wiesenfeld. Clustering behavior of oscillator arrays. *Phys. Rev. A*, **43**:2640–2648, 1991.

[55] D. Fargue. Réducibilité des systèmes héréditaires à des systèmes dynamiques. *Comptes Rendus de l'Académie des Sciences*, **277B**:471–473, 1973. (French).

[56] D. Fargue. Réducibilité des systèmes héréditaires. *Int. J. Nonlin. Mech.*, **9**:331–441, 1974. (French).

[57] J. D. Farmer. Sensitive dependence on parameters in nonlinear dynamics. *Phys. Rev. Lett.*, **55**:351–354, 1985.

[58] J.E. Franke and A-A Yakubu. Extinction in systems of bobwhite quail type populations. *Can. Appl. Math. Quart.*, 1994. In press.

[59] J. Froyland. Some symmetric, dissipative, two-dimensional maps. *Physica D*, **8**:423–434, 1983.

[60] J.A.C Gallas, P. Grassberger, H.J. Hermann, and P. Ueberholz. Noisy collective behavior in cellular automata. *Physica A*, **180**:19–41, 1992.

[61] S. Gasiorowicz. *Quantum physics.* John Wiley & Sons, New-York, 1974.

[62] H. M. Gibbs. *Optical bistability: Controling light with light.* Academic Press, Orlando, 1985.

[63] H. M. Gibbs, F. A. Hopf, D. L. Kaplan, and R. L. Shoemaker. Observation of chaos in optical bistability. *Phys. Rev. Lett.*, **46**:474–477, 1981.

[64] E. Giusti. *Minimal Surfaces and Functions of Bounded Variation.* Birkhauser, Berlin, 1984.

[65] D. Golomb and J. Rinzel. Clustering in globally coupled inhibitory neurons. *Physica D*, **72**:259–282, 1994.

[66] P. Góra and A. Boyarski. Absolutely continous invariant measures for piecewise expanding C^2 transformations in $\setminus^n$. *Isr. J. Math.*, **67**:272–285, 1989.

[67] V. D. Gorjačenko. *Methods in the Theory of Stability in Nuclear Reactor Dynamics.* Atomizdat, Moscow, 1971. (Russian).

[68] W. T. Grandy. *Foundations of Statistical Mechanics.* D. Reidel, Dordrecht, 1988.

[69] C. Grebogi, S. W. McDonald, E. Ott, and J. A. Yorke. Final state sensitivity: an obstruction to predictability. *Phys. Lett. A*, **99**:415–418, 1983.

[70] M. Griniasty and V. Hakim. Correlation and dynamics in ensembles of maps: Simple models. *Phys. Rev. E*, **49**:2661–2667, 1994.

[71] S. Grossman and S. Thomae. Correlations and spectra of periodic chaos generated by the logistic parabola. *J. Stat. Phys.*, **26**:485–504, 1981.

[72] V.M. Gundlach and D.A. Rand. Spatio-temporal chaos: 1. Hyperbolicity, structural stability, spatiotemporal shadowing and symbolic dynamics; spatio-temporal chaos: 2. Unique Gibbs state for higher dimensional symbolic system; 3. Natural spatio-temporal measures for coupled circled map lattices. *Nonlinearity*, **6**:165–230, 1993.

[73] P. Hadley and M. R. Beasley. Dynamical states and stability of linear arrays of Josephson junctions. *Appl. Phys. Lett.*, **50**:621–623, 1987.

[74] G. He and J. Li. The mechanism of pattern selection in coupled map lattices. *Phys. Lett. A*, **185**:55–58, 1994.

[75] U. an der Heiden. Periodic, aperiodic and stochastic behavior of differential-difference equation modeling biological and economical processes. In L. Collaty, G. Meinardus, and W. Wetterling, editors, *Differential-Difference Equations: Applications and Numerical Problems Workshop*, Basel, 1983. Birkhäuser Verlag.

[76] U. an der Heiden and M. C. Mackey. The dynamics of production and destruction: Analytic insight into complex behavior. *J. Math. Biol.*, **16**:75–101, 1982.

[77] A. V. M. Herz. Global analysis of recurrent neural networks. In E. Domany, J. L. van Hemmen, and K. Schulten, editors, *Models of Neural Networks,* Volume 3, page 44 pages. To appear in 1994. We refer more specifically to the discussion of Section 3.4.

[78] A. V. Holden, J. V. Tucker, H. Zhang, and M. J. Poole. Coupled map lattices as computational systems. *CHAOS*, **2**:367–376, 1992.

[79] E. Hopf. Statistical hydromechanics and functional calculus. *J. Ratl. Mech. Anal.*, **1**:87–123, 1952.

[80] K. Horbacz. Dynamical systems with multiplicative perturbations. *Ann. Polon. Math.*, **50**:93–102, 1989.

[81] W. Horsthemke and R. Lefever. *Noise-Induced Transitions.* Springer-Verlag, Berlin, 1984.

[82] J. M. Houlrik and I. Webman. Critical behaviour and mean-field theory of coupled map lattices. *Physica Scripta*, **33**:189–192, 1989.

[83] J. M. Houlrik, I. Webman, and M. H. Jensen. Mean-field theory and critical behavior of coupled-map lattices. *Phys. Rev. E*, **41**:4210–4222, 1990.

[84] J.M. Houlrik. Periodic orbits in a two variable coupled map. *CHAOS*, **2**:323–327, 1993.

[85] A. E. Hurd and P. A. Loeb. *An introduction to nonstandard real analysis.* Academic Press, New York, 1985.

[86] K. Ikeda, K. Kondo, and O. Akimoto. Successive higher harmonic bifurcations in systems with delayed feedback. *Phys. Rev. Lett.*, **49**:1467–1470, 1982.

[87] K. Ikeda and K. Matsumoto. High dimensional chaotic behavior in systems with time-delayed feedbak. *Physica D*, **29**:223–235, 1987.

[88] A. F. Ivanov and A. N. Sharkovskiĭ. Oscillations in singularly perturbed delay equations. *Dynamics Reported*, **3**:165, 1991. Springer Verlag (edited by H. O. Walter and U. Kirchgraber).

[89] M. V. Jakobson. Absolutely continuous invariant measures for one-parameter families of maps. *Commun. Math. Phys.*, **81**:39–88, 1981.

[90] G. E. James, E. M. Harrell II, and R. Roy. Intermittency and chaos in intracavity doubled lasers. *Phys. Rev. A*, **41**:2778–2790, 1990.

[91] M. H. Jensen. Boundary layer instability in a coupled map model. *Physica D*, **32**:203–207, 1989.

[92] M. H. Jensen. Fluctuations and scaling in a model of boundary-layer-induced turbulence. *Phys. Rev. Lett.*, **62**:1361–1363, 1989.

[93] M. Kalecki. A macroeconomic theory of business cycles. *Econometrica*, **3**:327–344, 1935.

[94] K. Kaneko. Editor of a CHAOS focus issue on coupled map lattices, **2**:279-367 (1992).

[95] K. Kaneko. Period doubling of kink-antikink patterns, quasiperiodicity of antiferro-like structures and spatial intermittency in coupled logistic lattice - Toward a prelude of a field-theory of chaos. *Prog. Theor. Phys.*, **72**:480–486, 1984.

[96] K. Kaneko. Lyapunov analysis and information flow in coupled map lattices. *Physica D*, **23**:436–447, 1986.

[97] K. Kaneko. Pattern dynamics in spatio-temporal chaos. *Physica D*, **34**:1–41, 1989.

[98] K. Kaneko. Towards a thermodynamics of spatiotemporal chaos. *Prog. Theor. Phys. Supplement*, **99**:263–287, 1989.

[99] K. Kaneko. Globally coupled chaos violates the law of large numbers but not the Central-Limit Theorem. *Phys. Rev. Lett.*, **65**:1391–1394, 1990.

[100] K. Kaneko. Supertransients, spatiotemporal intermittency and stability of spatiotemporal chaos. *Phys. Lett. A*, **149**:105–112, 1990.

[101] K. Kaneko. Mean field fluctuations of a network of chaotic elements. *Physica D*, **55**:368–384, 1992.

[102] K Kaneko and T. Ikegami. Homeochaos: dynamic stability of a symbiotic network with population dynamics and evolving mutation rate. *Physica D*, **56**:406–429, 1992.

[103] R. Kapral. Chemical waves and coupled map lattices. In K. Kaneko, editor, *Theory and applications of coupled map lattices*, pages 135–168. J. Wiley & Sons, 1993.

[104] R. Kapral and E. Celarier. Mechanisms for noise-induced transitions in chemical systems. In F. Moss and P. V. E. McClintock, editors, *Noise in nonlinear dynamical systems: Theory of noise-induced processes in special aplications*, pages 209–250. Cambridge University Press, 1989.

[105] R. Kapral, R. Livi, G. L. Oppo, and A. Politi. Dynamics of complex interfaces. *Phys. Rev. E*, **49**:2009–2022, 1994.

[106] F. Kaspar and H. G. Schuster. Scaling at the onset of spatial disorder in piecewise linear maps. *Phys. Lett. A*, **113**:451–453, 198.

[107] J. D. Keeler and J. D. Farmer. robust space-time intermittency and $1/f$ noise. *Physica D*, **23**:413–435, 1986.

[108] J. P. Keener. Chaotic behavior in piecewise continuous difference equations. *Trans. Amer. Math. Soc.*, **261**:589–604, 1980.

[109] G. Keller and M. Künzle. Transfer operators for coupled map lattices. *Ergod. Theor. Dyn. Sys.*, **12**:297–318, 1992.

[110] I. G. Kevrekidis, R. Rico-Martínez, R. E. Ecke, R. M. Farber, and A. S. Lapedes. Global bifurcations in Rayleigh-Bénard convection. Experiments, empirical maps and numerical bifurcation analysis. *Physica D*, **71**:342–362, 1994.

[111] P. E. Kloeden and E. Platen. *Numerical Solution of Stochastic Differential equations.* Springer Verlag, Berlin, 1992. We refer more specifically to Section 6.1.

[112] J. Komornik. Asymptotic periodicity of the iterates of weakly contrictive Markov operators. *Tohoku Math. J.*, **38**:15–27, 1986.

[113] J. Komornìk and A. Lasota. Asymptotic decomposition of Markov operators. *Bull. Polish Acad. Sci.*, **35**:321–327, 1987.

[114] H. Kook, F.H. Ling, and G. Schmidt. Universal behavior of coupled nonlinear systems. *Phys. Rev. A*, **43**:2700–2708, 1991.

[115] S. P. Kuznetsov. Critical behavior of one dimensional chains. *Pis'ma Zh. Tekh. Fiz.*, **9**:94–98, 1983.

[116] S. P. Kuznetsov. Renormalization group, universality and scaling in dynamics of one-dimensional auto-wave media. *Izvest. Vyss. Ucheb. Zav. Radiof.*, **29**:888–902, 1986.

[117] S. P. Kuznetsov. Renormalization group, universality and scaling in dynamics of coupled map lattices. In K. Kaneko, editor, *Theory and applications of coupled map lattices*, pages 52–94. J. Wiley & Sons, 1993.

[118] S. P. Kuznetsov and A. S. Pikovsky. Universality and scaling of period doubling bifurcations in a dissipative distributed medium. *Physica D*, **19**:384–396, 1986.

[119] Y. C. Lai and R. Winslow. Extreme sensitive dependence on parameters and initial conditions in spatio-temporal chaotic dynamical systems. *Physica D*, **74**:353–371, 1994.

[120] W. Lange. Use of an electronic model as a guideline in experiments on transient optical bistability. In F. Moss and P. V. E. McClintock, editors, *Noise in nonlinear dynamical systems: Experiments and simulations*, pages 159–188. Cambridge University Press, 1989.

[121] A. Lasota, T. Y. Li, and J. A. Yorke. Asymptotic periodicity of the iterates of Markov operators. *Trans. Am. Math. Soc.*, **286**:751–764, 1984.

[122] A. Lasota and M. C. Mackey. *Chaos, Fractals and Noise: Stochastic Aspects of Dynamics.* Springer Verlag, New York, 1994.

[123] A. Lasota and M.C. Mackey. Noise and statistical periodicity. *Physica D*, **28**:143–154, 1987.

[124] A. Lasota and J. Socała. Asymptotic properties of constrictive Markov operators. *Bull. Polish Acad. Sci.*, **35**:71–76, 1987.

[125] A. Lasota and J. A. Yorke. Statistical periodicity of Markov operators. *Časopis pro pěstování matematiky*, **111**:1–11, 1986. February 1986 issue.

[126] J. J. Levin and J. A. Nohel. On a nonlinear delay equation. *J. Math. Anal. Appl.*, **8**:31–44, 1964.

[127] H. Levine and W. N. Reynolds. Coupled map lattice techniques for simulating interfacial phenomena in reaction diffusion systems. *CHAOS*, **2**:337–342, 1992.

[128] R. M. Lewis and R. H. Kraichnan. A space-time functional formalism for turbulence. *Comm. Pure Appl. Math.*, **15**:397–411, 1962.

[129] A. Longtin and J. G. Milton. Modeling autonomous oscillations in the human pupil eye reflex using nonlinear delay differential equations. *Bull. Math. Biol.*, **51**:605, 1989.

[130] E. N. Lorenz. Deterministic non-periodic flow. *J. Atmos. Sci.*, **20**:130–141, 1963.

[131] E.N. Lorenz. Noisy periodicity and reverse bifurcation. *N.Y. Acad. Sci.*, **357**:282–291, 1980.

[132] J. Losson. Bifurcations and chaos in a paradigm equation for delayed mixed feedback. In L. Nadel and D. Stein, editors, *SFI lectures on Complex Systems*, pages 527–533. Addison Wesley, 1991.

[133] J. Losson and M.C. Mackey. Coupled map lattices as models of differential equations. *Phys. Rev. E*, , 1994. submitted.

[134] J. Losson and M.C. Mackey. The evolution of probability densities in stochastic coupled map lattices. *Phys. Rev. E.*, 1994. Submitted.

[135] J. Losson and M.C. Mackey. Statistical cycling in coupled map lattices. *Phys. Rev. E*, **50**:843–856, 1994.

[136] J. Losson and M.C. Mackey. Statistical cyling in two diffusively coupled maps. *Physica D*, **72**:324–342, 1994.

[137] J. Losson, M.C. Mackey, and A. Longtin. solution multistability in first order nonlinear differential delay equations. *CHAOS*, **3**:167–176, 1993.

[138] J. Losson, J.G. Milton, and M.C. Mackey. Phase transitions in networks of chaotic elements with short and long range interactions. *Physica D*, 1994. In press.

[139] J. Loviscach. *Probabilistic models of chaotic maps.* PhD thesis, Universität Bielefeld, July 1993.

[140] K. Lukin and V.P Shestopalov. Electrodynamics of the quasi resonant one dimensional systems with nonlinearly reflecting boundaries. *in* "Proceedings of the 4^{th} International Seminar on Mathematical Methods in Electromagnetic Theory", pp.328-334 September 1991, Alushta, Ukraine.

[141] M. C. Mackey. Commodity price fluctuations: Price dependent delays and nonlinearities as explanatory factors. *J. Econ. Theory*, **48**(2):497–509, 1989.

[142] M. C. Mackey. *Time's Arrow: The Origin of Thermodynamic Behavior.* Springer-Verlag, Berlin, 1992.

[143] M. C. Mackey and U. an der Heiden. The dynamics of recurrent inhibition. *J. Math. Biol*, **19**:211–225, 1982.

[144] M. C. Mackey and L. Glass. Oscillation and chaos in physiological control systems. *Science*, **197**:287–289, 1977.

[145] M. C. Mackey and J. G. Milton. Feedback, delays and the origin of blood cell dynamics. *Comm. Theor. Biol.*, **1**(5):299–327, 1990.

[146] J. Mallet-Paret and R. D. Nussbaum. A bifurcation gap for a singularly perturbed delay equation. In M. F. Barnsley and S. G. Demko, editors, *Chaotic Dynamics and Fractals*, pages 263–286. Academic Press, 1986.

[147] P. Manneville. *Dissipative structures and weak turbulence.* Academic Press, San Diego, CA, 1990.

[148] C. M. Marcus and R. M. Westervelt. Stability of analog neural networks with delay. *Phys. Rev A*, **39**:347–359, 1989.

[149] G. Mayer-Kress and K. Kaneko. Spatiotemporal chaos and noise. *J. Stat. Phys.*, **59**:1489–1508, 1989.

[150] B.M. McCoy and T.T. Wu. *The Two-Dimensional Ising Model.* Harvard University Press, Cambridge, Ma, 1973.

[151] J. Milton, T. Mundel, U. an der Heiden, J. P. Spire, and J. Cowan. Travelling activity waves, 1994. Preprint, University of Chicago.

[152] J. G. Milton. Private communication.

[153] J.G. Milton and J. Bélair. Chaos, noise and extinction in models of population growth. *Theor. Pop. Biol.*, **37**:273–290, 1990.

[154] R. E. Mirollo and S. H. Strogatz. Synchronization of pulse-coupled biological oscillators. *SIAM J. Appl. Math.*, **50**:1645–1662, 1990.

[155] L. Molgedey, J. Schuchhardt, and H. G. Schuster. Suppressing chaos in neural networks by noise. *Phys. Rev. Lett.*, **69**:3717–3719, 1992.

[156] F. Moss and P. V. E. McClintock, editors. *Theory of continuous Fokker-Planck systems; Theory of noise-induced processes in special applications; Experiments and simulations*, volume **1,2,3** of *Noise in Nonlinear Dynamical Systems.* Springer Verlag, Berlin, 1989.

[157] F. Moss and P.V.E McClintock, editors. *Noise in nonlinear dynamical systems*, volume **3**, chapter II. Cambridge University Press, Cambridge, 1989.

[158] T. Muir. *A Treatise on the Theory of Determinants.* Dover, New York, NY, 1960.

[159] J. D. Murray. *Mathematical Biology.* Springer-Verlag, Berlin, 1990.

[160] S. Nichols and K. Wiesenfeld. Mutually destructive fluctuations in globally coupled arrays. *Phys. Rev. E*, **49**:1865–1868, 1994.

[161] H. Nozawa. A neural network model as a globally coupled map and applications based on chaos. *CHAOS*, **2**:377–386, 1992.

[162] Y. Oono and S. Puri. Study of phase separation dynamics by use of cell dynamical systems. 1. Models. *Phys. Rev. A*, **38**:434–453, 1988.

[163] N. Parekh and S. Puri. Velocity selection in coupled-map lattices. *Phys. Rev. E*, **47**:1415–1418, 1993.

[164] G. Perez, S. Sinha, and A. Cerdeira. Order in the turbulent phase of globally coupled maps. *Physica D*, **63**:341–349, 1993.

[165] A. Pikovsky. Do globally coupled maps really violate the law of large numbers. *Phys. Rev. Lett.*, **72**:1644–1646, 1994.

[166] A.S. Pikovsky. A dynamical model for periodic and chaotic oscillations in the Belousov-Zhabotinskii reaction. *Phys. Lett. A*, **85**:13–16, 1981.

[167] G. Placzek. On the theory of the slowing down of neutrons in heavy substances. *Phys. Rev. C*, **69**:423–453, 1946.

[168] A. Politi, R. Livi, G. L. Oppo, and R. Kapral. Unpredictable behavior in stable systems. *Europhys. Lett.*, **22**:571–576, 1993.

[169] Y. Pomeau. Periodic behavior of cellular automata. *J. Stat. Phys.*, **70**:1379–1382, 1993.

[170] V. N. Popov. *Functional integrals and collective excitations.* Cambridge University Press, Cambridge, 1990.

[171] C.B. Price, P. Wambacq, and A. Oosterlinck. The plastic coupled map lattice: A novel image-processing paradigm. *CHAOS*, **2**:351–366, 1992.

[172] G. D. Price and S. C. Parker. The computer simulation of the lattice dynamics of silicates. In *NATO ASI Series B Vol. 225: Physical Properties and Thermodynamic Behavior of Minerals*, pages 591–618. 1988.

[173] N. Provatas and M. C. Mackey. Asymptotic periodicity and banded chaos. *Physica D*, **53**:295–318, 1991.

[174] N. Provatas and M. C. Mackey. Noise-induced asymptotic periodicity in a piecewise linear map. *J. Stat. Phys.*, **63**:585–612, 1991.

[175] S. Puri, R.C. Desay, and R. Kapral. Coupled map model with a conserved order parameter. *Physica D*, **50**:207–230, 1991.

[176] Z. Qu and G. Hu. Spatiotemporally periodic states, periodic windows, and intermittency in coupled map lattices. *Phys. Rev. E*, **49**:1099–1108, 1994.

[177] N.K. Rakhmanova and A.I. Rakhmanov. On a bifurcation of chaotic attractors in the coupled map systems, 1992. Preprint of the Keldysh Institute of Applied Mathematics.

[178] K. R. Rao, S. L. Chaplot, N. Choudhury, S. Ghose, and D. L. Price. Phonon density of states and specific heat of forsterite. *Science*, **236**:64–65, 1987.

[179] R. M. Redheffer. Difference equations and functional equations in transmission line theory. In *Modern mathematics for the engineer (Chapter XII)*. McGraw-Hill, New York, 1961.

[180] C. E. Rickart. *General Theory of Banach Algebras.* Van Nostrand Company, Princeton, N.J, 1960.

[181] H. Risken. *The Fokker-Planck Equation*, volume **18** of *Springer Series in Synergetics.* Springer-Verlag, Berlin, 1984.

[182] H. L. Royden. *Real analysis.* Mcmillan, New York, 1968. Second edition.

[183] D. Ruelle. *Thermodynamic formalism* in Encyclopedia of Mathematics and its Applications. Addison-Wesley, New York, 1978.

[184] D. Ruelle. Measures describing a turbulent flow. *N. Y. Acad. Sci.*, **357**:1–9, 1980.

[185] D. Ruelle and F. Takens. Note concerning "on the nature of turbulence". *Comm. Math. Phys.*, **23**:344–345, 1971. This references only contains a list of relevant Russian work on the topic.

[186] D. Ruelle and F. Takens. On the nature of turbulence. *Comm. Math. Phys.*, **20**:167–192, 1971.

[187] M. Rychlik. Bounded variation and invariant measures. *Studia Math.*, **LXXVI**:69–80, 1983.

[188] L. H. Ryder. *Quantum Field Theory.* Cambridge University Press, Cambridge, 1985.

[189] E. K. H. Salje, editor. *NATO ASI Series C, Vol. 225: Physical properties and thermodynamic behavior of minerals.* D. Reidel, Dordrecht, 1988.

[190] H. G. Schuster. *Deterministic Chaos, an Introduction.* Physik Verlag, Weinheim, 1984.

[191] H. G. Schuster, editor. *Nonlinear dynamics and Neural Networks.* VCH, Weinheim, 1991.

[192] A.N. Sharkovskiĭ, Yu. L. Maistrenko, and E. Yu. Ramanenko. *Raznostnie Uravneniya i ikh Prilozheniya.* Kiev Naukova Dumka, Kiev, 1986. (Russian).

[193] A. Shrier, H. Dubarsky, M. Rosengarten, M. R. Guevarra, S. Nattel, and L. Glass. Prediction of complex atrioventricular conduction rhythms in humans with use of the atrio-ventricular nodal recovery curve. *Circulation*, **76**:1196–1205, 1987.

[194] M. Silber, L. Fabiny, and K. Wiesenfeld. Stability results for in-phase and splay-phase states of solid-state laser arrays. *J. Opt. Soc. Am. B*, **10**:1121–1129, 1993.

[195] Ya. G. Sinai. Construction of Markov partitions. *Funct. Anal. Appl.*, **2**:245–2, 1968.

[196] J. Smythe, F. Moss, P.V.E. McClintock, and D. Clarkson. Ito versus stratonovich revisited. *Phys. Lett. A*, **3**:95–98, 1983.

[197] K. Sobczyk. *Stochastic Wave Propagation.* Elsevier, Amsterdam, 1984.

[198] R. V. Solé, J. Bascompte, and J. Valls. Nonequilibrium dynamics in lattice ecosystems: Chaotic stability and dissipative structures. *CHAOS*, **2**:387–395, 1992.

[199] R. V. Solé and J. Valls. Order and chaos in a 2d Lotka-Volterra coupled map lattice. *Phys. Lett. A*, **153**:330–336, 1991.

[200] H. Sompolinsky, H. J. Sommers, and A. Crisanti. Chaos in random neural networks. *Phys. Rev. Lett.*, **61**:259–262, 1988.

[201] M Steriade and M. Deschênes. The thalamus as a neuronal oscillator. *Brain Res. Rev.*, **8**:1–63, 1984.

[202] J. Swift, S. H. Strogatz, and K. Wiesenfeld. Averaging of globally coupled oscillators. *Physica D*, **55**:239–250, 1992.

[203] P. Szépfalusy and T. Tél. New approach to the problem of chaotic repellers. *Phys. Rev.*, **34A**:2520–2523, 1986.

[204] S. Tandri and Y. H. Yang. Comparison of two shape-from-shading algorithms. *Patt. Recogn. Lett.*, **11**:637–642, 1990.

[205] A. Torcini, A. Politi, G. P. Pucioni, and G. D'Alessandro. Fractal dimension of spatially extended systems. *Physica D*, **53**:85–101, 1991.

[206] C.T. Ionescu Tulcea and G. Marinescu. Théorie ergodique pour des classes d'opérations non complètement continues. *Ann. de Math.*, **52**:140–147, 1950.

[207] A. M. Turing. Chemical basis of morphogenesis. *Phil. Trans. Roy. Soc. Lond. B*, **237**:37–72, 1952.

[208] N.G. van Kampen. Itô versus Stratonovich. *J. Stat. Phys.*, **24**:175–186, 1981.

[209] J. Vandermeer. The qualitative behavior of coupled predator-prey oscillations as deduced from simple circle maps. *Ecological modelling*, **73**:135–148, 1994.

[210] O. E. Vega and Y. H. Yang. Shading logic: A heuristic approach to recover shape from shading. *IEEE Trans. Patt. Anal. Machine Intel.*, **15**:592–597, 1993.

[211] T. Viczek. *Fractal growth phenomena.* World Scientific, Singapore, 1989.

[212] A. A. Vitt. K teorii skripichnoĭ strulni. *Zhurnal Tekhnicheskoĭ Fizikie*, **6**:1459–1475, 1936. (Russian).

[213] T. Vogel. *Théorie des Systèmes Evolutifs.* Gauthiers-Villars, Paris, 1965. (French).

[214] I. Waller and R. Kapral. Spatial and temporal structures in systems of coupled nonlinear oscillators. *Phys. Rev. A*, **30**:2047–2055, 1984.

[215] I. Waller and R. Kapral. Synchronization and chaos in coupled nonlinear oscillators. *Phys. Lett. A*, **105**:163–168, 1984.

[216] K. Wiesenfeld and P. Hadley. Attractor crowding in oscillator arrays. *Phys. Rev. Lett.*, **62**:1335–1338, 1989.

[217] F. H. Willeboordse and K. Kaneko. Bifurcations and spatial chaos in an open flow model. *Phys. Rev. Lett.*, **73**:533–536, 1994.

[218] H. R. Wilson and J. D. Cowan. Excitatory and inhibitory interactions in localized populations of model neurons. *Biophysical J.*, **12**:1–24, 1972.

[219] H. R. Wilson and J. D. Cowan. A theory of the functional dynamics of cortical and thalamic nervous tissue. *Kybernetik*, **13**:55–79, 1973.

[220] A. T. Winfree. *When time breaks down: The three dimensional dynamics of electrochemical waves and cardiac arrythmias.* Princeton University Press, Princeton, NJ, 1987.

[221] J. J. Wright and R. R. Kydd. The electroencephalogram and cortical neural networks. *Network*, **3**:341–362, 1992.

[222] T. Yamada and H. Fujisaka. Effect of inhomogeneity on intermittent chaos in a coupled system. *Phys. Lett. A*, **124**:421–425, 1983.

[223] T. Yanagita. Coupled map lattice model for boiling. *Phys. Lett. A*, **165**:405–408, 1992.

[224] T. Yoshida, H. Mori, and H. Shigematsu. Analytic study of chaos of the tent map: Band structures, power spectra and critical behaviors. *J. Stat. Phys.*, **31**:279, 1983.

[225] N. Yu, R.K. DeFreez, D. J. Bossert, R. A. Elliott, H. G. Winful, and D. F. Welch. Observation of sustained self-pulsation in CW operated flared Y-coupled laser arrays. *Electron. Lett*, **24**:1203–1204, 1988.

[226] J.M. Yuan, M. ung, D.H. Feng, and L.M. Narducci. Instabilities and irregular behavior in coupled logistic equations. *Phys. Rev. A*, **28**:1662–1666, 1983.

[227] W.P. Ziemer. *Weakly differentiable functions.* Springer Verlag, Berlin, 1989.

Appendix 2A

The coordinates of the edges of the set $\mathcal{B}$ of Figures 2.5b and 2.6 were obtained using the MAPLE software. They are

$$\beta_0^x = \frac{(1-2\varepsilon+2\varepsilon^2)}{\varepsilon-1}$$

$$\beta_0^y = 2\varepsilon$$

$$\beta_1^x = \frac{a\,(-1-a-4\,a^2\varepsilon+4\,\varepsilon^2a^2+4\,a\varepsilon+a^2-4\,\varepsilon^2a)\,(1-2\,\varepsilon+2\,\varepsilon^2)}{\varepsilon-1}$$

$$\beta_1^y = -2\,\varepsilon a\left(-1-a-4\,a^2\varepsilon+4\,\varepsilon^2a^2+\text{[illegible]}+a^2-4\,\varepsilon^2a\right)$$

$$\beta_2^x = \frac{-4\,a\varepsilon-2+a+4\,\varepsilon^2a+4\,\varepsilon-2\,\varepsilon}{\varepsilon-1}$$

Do not film X

$$\beta_2^y = 2\varepsilon$$

$$\beta_3^x = -\frac{2+3\,a\varepsilon-2\,\varepsilon^2a-4\,\varepsilon-a-8}{\varepsilon-1}\qquad\frac{2\,\varepsilon^2-a^4\varepsilon-12\,a^4\varepsilon^3+12\,\varepsilon^3a^3-}{}$$

$$-\frac{a^3\varepsilon+8\,a^4\varepsilon^4+6\,a^4\varepsilon^2}{\varepsilon-1}$$

$$\beta_3^y = a-2\,a\varepsilon-a^2+2\,a^2\varepsilon-a^3+6\,\text{[illegible]}\qquad+12\,a^4\varepsilon^2-8\,a^4\varepsilon^3+8\,\varepsilon^3a^3+a^4+$$

$$\beta_4^x = -\frac{3\,a\varepsilon+2-a-2\,\varepsilon^2a-4\,\varepsilon+2\,\varepsilon^2-4\,\varepsilon a+\text{[illegible]}+4\varepsilon^3a^2}{\varepsilon-1}$$

$$\beta_4^y = 2\,a\varepsilon-a-4\,a^2\varepsilon+a^2+4\,\varepsilon^2a^2+2\,\varepsilon$$

$$\beta_5^x = \frac{a(-1-5a\varepsilon+8\varepsilon^2a+4a^2\varepsilon-4a^2\varepsilon^2+5\varepsilon+a-a^2-8\varepsilon^2-4\varepsilon^3a+a^4+16a^4\varepsilon^4-24a^3\varepsilon^2}{\varepsilon-1}$$

$$+\frac{a(32\varepsilon^3a^3+4\varepsilon^3+8a^3\varepsilon-32a^4\varepsilon^3-16\varepsilon^4a^3-a^3-8a^4\varepsilon)}{\varepsilon-1}$$

$$\beta_5^y = a\left(-1-4a\varepsilon+4\varepsilon^2a+4\varepsilon+a-4\varepsilon^2\right)$$

$$\beta_6^x = -\frac{(2\,\varepsilon-1)\,(2\,\varepsilon^2a^2-2\,\varepsilon^2a+a\varepsilon-a^2\varepsilon-1)}{\varepsilon-1}$$

$$\beta_6^y = \left(-1-4\,a\varepsilon+4\,\varepsilon^2a+4\,\varepsilon+a-4\,\varepsilon^2\right)a$$

$$\beta_7^x = -\frac{1-2\,\varepsilon+2\,\varepsilon^2-a\varepsilon+2\,\varepsilon^2a-4\,\varepsilon^2a^2+a^2\varepsilon+4\,\varepsilon^3a^2}{\varepsilon-1}$$

$$\beta_7^y = 2\,a\varepsilon-a-4\,a^2\varepsilon+a^2+4\,\varepsilon^2a^2+2\,\varepsilon$$

These coordinates are obtained by forward iterations of the appropriate points of the unit square under the action of the map Φ.